The role of the cell adhesion molecule CHL1 and its interaction partners in cerebellar development

Dissertation with the aim of achieving a doctoral degree at the Faculty of Mathematics, Informatics and Natural Sciences Department of Biology of Universität Hamburg

Submitted by Jelena Katic

2016 in Hamburg

Day of Oral Defense: August 26th, 2016

The following evaluators recommended the admission of the dissertation:

Prof. Dr. Melitta Schachner

Prof. Dr. Christian Lohr

Universitätsklinikum Hamburg-Eppendorf

Center for Molecular Neurobiology Hamburg

Research Group:
Neuronal Translational Control

Martinistraße 52
20246 Hamburg

Kent Duncan, PhD

Phone: +49(0)40 7410-56274
Fax: +49(0)40 7410-53436
Kent.Duncan@zmnh.uni-hamburg.de
www.zmnh.uni-hamburg.de

Delivery address:
Falkenried 94
20251 Hamburg

Universitätsklinikum Hamburg-Eppendorf Martinistraße 52 20246 Hamburg
Zentrum für Molekulare Neurobiologie - Forschergruppen

May 13, 2016

English language Thesis Certification: Jelena Katic

To whom it may concern:

Jelena Katic, who was born on 26.09.1988 in Trstenik , Serbia is submitting her doctoral dissertation in English. The title of her thesis is: **'The role of the cell adhesion molecule CHL1 and its interaction partners in cerebellar development'**.

I hereby certify as a native speaker and molecular biologist that the English language used in this thesis is sufficiently correct for submission.

Yours truly,

Universität Hamburg
Universitätsklinikum Hamburg-Eppendorf
Zentrum für Molekulare Neurobiologie
AG Duncan
Falkenried 94 · D-20251 Hamburg

Kent Duncan, Ph.D. **May 13, 2016**

Zertifikat Nr. QS-6568HH
und EM-8126HH

GL Systems Certification

FAMILIENFREUNDLICHES UNTERNEHMEN

Universitätsklinikum Hamburg-Eppendorf
Körperschaft des öffentlichen Rechts
Gerichtsstand: Hamburg
USt-ID-Nr.: DE21 8618 948

Vorstandsmitglieder:
Prof. Dr. Burkhard Göke (Vorsitzender)
Prof. Dr. Dr. Uwe Koch-Gromus
Joachim Prölß
Rainer Schoppik

Bankverbindung:
HSH Nordbank
Kto.-Nr.: 104364000; BLZ: 21050000
IBAN-Nr.: DE97210500000104364000
BIC: HSHNDEHH

Eidesstattliche Versicherung

Hiermit erkläre ich an Eides statt, dass ich die vorliegende Dissertationsschrift selbst verlasst und keine anderen als die angegebenen Quellen und Hilfsmittel benutzt habe.

Hamburg, den 10. Mai 2016

Jelena Kabić

Unterschrit

Declaration on oath

I hereby declare, on oath, that I have written the present dissertation by my own and have not used other than the acknowledged resources and aids.

Hamburg, 10. May 2016

Jelena Kats

signature

TABLE OF CONTENT

1 INTRODUCTION 10

1.1 Development of the cerebellum 11

1.1.1 Tissue organization in the adult cerebellar cortex 15

1.2 Cell adhesion molecule close homolog of L1- CHL1 17

1.2.1 The role of CHL1 in the cerebellum 20

1.3 Sonic hedgehog signaling pathway 21

1.4 Extracellular matrix molecules – vitronectin and plasminogen activator inhibitor 2 25

2 AIMS OF THE STUDY 28

3 MATERIALS 29

3.1 Animals 29

3.2 Bacterial strains and cell lines 29

3.3 Plasmid vectors 30

3.4 Primers 31

3.5 Recombinant protein constructs and peptides 32

3.6 Solutions and buffers 34

3.7 Cell culture media, buffers and reagents 41

3.8 Bacterial media and reagents 43

3.9 Antibodies 44

3.10 Chemicals and supplies 46

4 METHODS 47

4.1 Biochemical methods 47

4.1.1 Preparation of cerebellar homogenates and cell lysates 47
4.1.2 Determination of the protein concentration 47
4.1.3 Sodium Dodecyl Sulfate-Polyacrylamide Gel Electrophoresis (SDS-PAGE) 47
4.1.4 Western blot analysis 48
4.1.5 Coomassie staining of polyacrylamide gels 48
4.1.6 Immunoprecipitation 48
4.1.7 RhoA activation assay 49
4.1.8 Caspase-3 assay 49
4.1.9 Caspase-9 assay 50
4.1.10 Enzyme-Linked Immuno-Sorbent Assay (ELISA) 50
4.1.11 Label-free binding assay (BIND assay) 51
4.1.12 RNA isolation from brain homogenates 51
4.1.13 RNA isolation from cell lysates 52

4.2 Molecular biology methods and cloning techniques 53

4.2.1 Reverse transcription 53
4.2.2 PCR primer design and general principles of the In-Fusion cloning technique 53
4.2.3 Polymerase chain reaction (PCR) 53
4.2.4 DNA agarose gel electrophoresis 54
4.2.5 PCR fragment purification 55
4.2.6 DNA fragment extraction from agarose gels 55
4.2.7 Restriction digestion 55
4.2.8 In Fusion cloning reaction 55
4.2.9 Production of competent bacteria 56
4.2.10 Transformation of plasmid DNA into bacteria 56
4.2.11 Small scale plasmid isolation (Miniprep) 57
4.2.12 Large scale plasmid isolation (Maxiprep) 57
4.2.13 Sequencing of DNA 57
4.2.14 Site-directed mutagenesis 57
4.2.15 Expression and purification of recombinant proteins from *E. coli* 58

4.3 Real-time PCR 59

4.4 Histological methods and microscopy 60

4.4.1 Tissue preparation and sectioning 60

4.4.2 Immunohistochemistry 60

4.4.3 Proximity ligation assay 61

4.4.4 *In situ* cell death detection assay (TUNEL assay) 62

4.4.5 Microscopy and image processing 63

4.4.6 Co-localization analysis 63

4.4.7 Stereological analysis 64

4.5 Cell culture methods and assays 64

4.5.1 Primary culture of dissociated cerebellar neurons 64

4.5.2 Neurite outgrowth assay 65

4.5.3 Microexplant culture of cerebellar neurons 66

4.5.4 Maintenance and long-term storage of HEK cells 67

4.5.5 Transient transfection of HEK cells 67

4.5.6 Cell death assay 67

4.6 Organotypic slice culture 68

4.6.1 Isolation and maintenance of cerebellar organotypic slices 68

4.6.2 Immunohistochemistry, TUNEL assay and stereological analysis 69

4.6.3 Cell death assay 70

4.7 Statistical analysis 70

5 RESULTS 71

5.1 Interaction of CHL1 with vitronectin and plasminogen activator inhibitor-2 regulates cerebellar development during the first postnatal week 71

5.1.1 CHL1 binds directly to vitronectin via its extracellular domain 71

5.1.2 CHL1 binds to vitronectin and triggers neurite outgrowth in primary cerebellar neurons 73

5.1.3 CHL1 binds directly to PAI-2 via its extracellular domain 74

5.1.4 The extracellular part of CHL1 binds directly to the N-terminus of vitronectin and to the N- and C-terminus of PAI-2 76

5.1.5 CHL1 binds to vitronectin and PAI-2 and triggers neuronal migration in explant cultures of cerebellar neurons 77

5.1.6 CHL1 co-localizes with vitronectin and PAI-2 during the development of the cerebellar cortex 81

5.1.7 CHL1 and vitronectin prevent proliferation and differentiation but enhance inward radial migration of granule cells at the end of the first postnatal week 85

5.2 The interaction of CHL1 with patched-1 triggers cerebellar neuron migration and neurite outgrowth during the end of the first postnatal week and inhibits apoptosis of granule cells during the second postnatal week of cerebellar development 91

5.2.1 CHL1 binds directly to patched via its extracellular domain 91

5.2.2 CHL1 binds to patched and triggers neurite outgrowth and cerebellar migration *in vitro* in a smoothened dependent manner 96

5.2.3 CHL1 binds to the first extracellular loop of patched and prevents patched-induced cell death in a smoothened dependent manner 99

5.2.4 CHL1 binds to patched and inhibits caspase-3 activity in a smoothened dependent and caspase-9 activity in a smoothened independent manner 106

5.2.5 CHL1-Fc inhibits apoptosis of cerebellar granule and Purkinje cells in cerebellar organotypic slices via smoothened signaling pathways 109

5.2.6 CHL1 triggers cellular responses via “non-canonical” Gli-independent signaling pathways 112

5.2.7 CHL1 triggers neurite outgrowth and cerebellar migration in a RhoA-dependent manner 115

5.2.8 CHL1-Fc inhibits apoptosis of cerebellar neurons in a RhoA-dependent manner 117

5.2.9 CHL1 co-localizes with patched and smoothened within the cerebellar cortex at the first and second postnatal week 122

5.2.10 CHL1 inhibits apoptosis of cerebellar granule cells at the second postnatal week *in vivo* 124

6 DISCUSSION 127

6.1 CHL1 binds directly to vitronectin, plasminogen activator inhibitor 2 and patched via ist extracellular domain 127

6.2 Heterophilic interactions of CHL1 with its novel binding partners enhance granule cell migration and neurite outgrowth during the first postnatal week of cerebellar development 128

6.3 CHL1 and vitronectin regulate the development of granule cells *in vivo* during the first postnatal week of cerebellar development 131

6.4 Interaction of CHL1 with patched inhibits apoptosis of granule cells during the second postnatal week of cerebellar development 133

6.5 Functional consequences of CHL1 ablation in the cerebellum 137

6.6 General conclusions 138

7 REFERENCES 140

8 ABSTRACT 154

9 ZUSAMMENFASSUNG 156

10 STATEMENT OF CONTRIBUTION 158

11 ACKNOWLEDGEMENTS 159

1 INTRODUCTION

Cell adhesion molecules (CAMs) of the immunoglobulin superfamily were discovered almost 40 years ago based on their role in cell-cell adhesion (Brackenbury et al., 1977). Ever since, they have played an important role in developmental neuroscience research. First, CAMs were considered to provide "specific glue" to the segregating cells in the nervous system (Jessell, 1988). Later, it became clear that CAMs have more important roles than simple adhesion. CAM-associated signaling was shown to be involved in promotion of axon growth, regulation of cell migration, proliferation, and differentiation during development of the nervous system (Crossin and Krushel, 2000). More recently, the involvement of CAMs in synapse formation and maintenance has been discovered (for review see, Leshchyns'ka and Sytnyk, 2016). All these developmental steps require specific recognition processes mediated by CAMs expressed on the cell surface, thus they can be considered as cell recognition molecules. CAMs bind to each other in two different modes: two molecules that interact with each other in the plane of the same membrane form a *cis-interaction*, while molecules from two different cell membranes bind each other in a *trans*-interaction. CAMs transform an extracellular interaction to intracellular signaling that includes either the modification of second messenger systems or alterations in gene expression that occur through CAM mediated activation of transcription factors (Crossin and Krushel, 2000).

CAM mediated cell-cell adhesion is important for brain morphology and highly coordinated brain functions such as memory and learning (Sanes and Yamagata, 1999; Yamagata et al., 2003; Washbourne et al., 2004). During early development of the nervous system, neurons elongate their axons towards their targets, establish and maintain cellular connections not just with other neurons but also with astrocytes and oligodendrocytes. Cell-cell contacts link neurons with supporting glial cells, which underpin cell migration during development of the nervous system. Neurons that are born in germinal zones far away from their final position in the mature nervous system undergo a series of migration events during development (Hatten, 1999; Marin and Rubenstein, 2003). Two different modes of cell migration during development have been described: radial and tangential migration. Whereas radial migration depends on a close association of the migrating cells with radial glia cells, tangential migration is either independent of mechanical guidance support or loosely follows axon tracts. Still, both types of migration share the requirement for cell-cell interactions and molecular guidance cues for the navigation of migrating cells to their target (Frotscher, 1998). Cell migration was mostly studied in the cerebral cortex or in the cerebellum. Since the cerebellum develops later than other brain structures with an extension into the postnatal age, it presents a convenient model to study developmental events in general. Numerous authors underline the importance of cell-cell adhesion mediated by CAMs during the development of the cerebellum (Kamiguchi et al.,

1998; Sakurai et al., 2001; Marzban et al., 2004; Ango et al., 2004, 2008; Huang et al., 2007; Jakovcevski 2009).

1.1 Development of the cerebellum

The cerebellum is an evolutionarily conserved structure among vertebrates crucial for motor learning. Motor learning is the process of improving the smoothness, skillfulness and accuracy of movement, which can be either complex such as playing piano or simple movements such as an eye blink reflex. However, recent studies suggest an involvement of the cerebellum in emotional or higher cognitive functions such as proper language formation (Ito, 2008; Gebhart et al., 2002). Cerebellar damage leads to ataxia of the upper and lower extremities, impairment of gait, abnormal eye movements and disturbance in speech (Holmes, 1939; Gilman et al., 1981; Grüsser-Cornehls and Bäurle, 2001). Moreover, interactions of the cerebellum with basal ganglia and the frontal lobe are crucial for procedural learning, which involves acquisition of a skill through repeated performance. Disruptions of cerebellum-basal ganglia interactions have been reported for schizophrenia patients (Bigelow et al., 2006).

The cerebellum consists of two hemispheres united in the midline by a region known as the vermis. Two deep fissures divide the cerebellar cortex into lobes, which are further subdivided into lobules by shallow fissures. The lobules are folded into sub-lobules or folia. According to the classical view, the cerebellar cortex has a simple histological organization based on specific units of a few neuronal cell types that are repeating all along the numerous folia composing the cortex (Altman and Bayer, 1997; Sotelo, 2004; Butts et al., 2011; Hashimoto and Hibi, 2012). Although recent evidence suggests that variations in cerebellar cortical anatomy and physiology take place which implies its regional organization (Cerminara et al., 2015), the classical model of an uniform cytoarchitecture will be used in the following to explain the basic principles of cerebellar cortical organization. The cerebellum develops later than other brain structures do; its development lasts until the end of the third postnatal week with temporal confined cellular events such as proliferation, differentiation, migration and apoptosis.

The cerebellum derives from the dorsal part of the anterior hindbrain. Neurons in the cerebellum are generated from two germinal zones: the ventricular zone located at the roof of the fourth ventricle and the rhombic lip located at the caudal edge of the cerebellar primordium (Figure 1.1; Altman and Bayer, 1997; Wingate, 2001). The ventricular zone gives rise to γ-aminobutyric acid (GABA)-ergic neurons of the cerebellar cortex, such as projection Purkinje neurons and interneurons, such as Golgi, Lugaro, basket, stellate and candelabrum cells (Hashimoto and Hibi, 2012). The rhombic lip gives rise to glutamatergic interneurons of the cerebellar cortex such as granule cells and unipolar brush cells, and projection neurons of the

deep cerebellar nuclei. The upper rhombic lip forms a transient secondary germinal zone, called the external granular layer (EGL), which presents the pool of granule cell precursors. Granule cell precursors start to leave the rhombic lip around embryonic day 13 in the mouse and they migrate tangentially over the surface of the cerebellar primordium to accumulate in the EGL. By embryonic day 13, Purkinje cell precursors have already finished their proliferation and started migration towards the cerebellar plate (Miale and Sidman, 1961; Altman and Bayer, 1978). After they have covered the cerebellar surface, granule cell precursors of the EGL start to proliferate as a response to mitogens secreted by the underlying Purkinje cells (Sotelo, 2004).

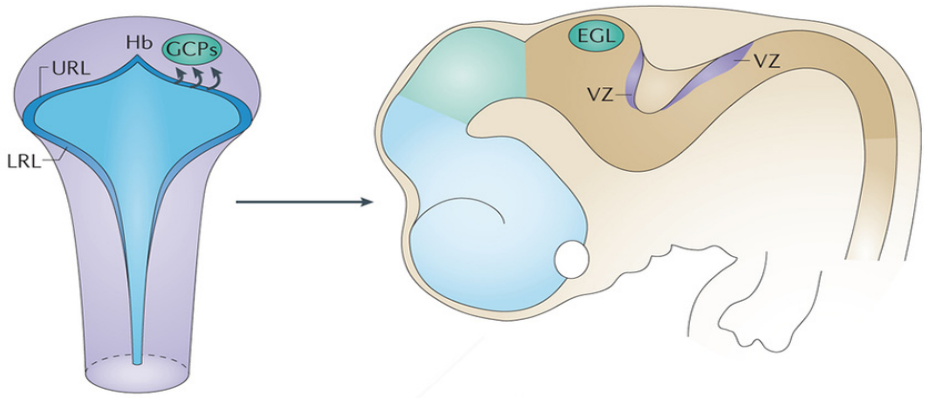

Figure 1.1. The origin of the cerebellum. The upper rhombic lip is a secondary germinal zone where granule cell precursors proliferate and migrate from to form the external granular layer. A second germinal center is the ventricular zone, which gives rise to Purkinje cells and several other types of cerebellar interneurons. Hb: hindbrain; URL: upper rhombic lip; LRL: lateral rhombic lip; GCPs: granule cell precursors; VZ: ventricular zone; EGL: external granule layer. The figure was adapted from Marshall et al., 2014.

The EGL consists of two distinct zones: the superficial (upper) zone, where granule cell precursors actively proliferate, and the inner zone that contains undifferentiated post-mitotic granule cells (Pons et al., 2001). At the end of embryonic development, Purkinje cells secrete the glycoprotein sonic hedgehog, which plays an important role in cell proliferation and fate determination and stimulates proliferation of granule cell precursors within the upper zone of the EGL (Jensen and Wallace, 1997; Roelink et al., 1995; Butts et al., 2011). As a response to sonic hedgehog secretion, granule cell precursors go through a series of symmetrical cell divisions that result in the huge number of granule cells representing about half of the total number of all neurons in the brain (Chédotal, 2010). It is still not clearly understood what terminates proliferation and triggers differentiation of granule cell precursors. Some authors suggest that extracellular matrix proteins such as vitronectin, which is expressed in the inner

zone of the EGL, function as a molecular switch that blocks sonic hedgehog-dependent proliferation and trigger differentiation of granule cells (Pons et al., 2001).

In the inner EGL, post-mitotic granule cells show a unipolar morphology with a single leading process and possess a migration machinery that allows their tangential migration (Figure 1.2). Prior to inward radial migration, post-mitotic granule cells change their morphology from unipolar to bipolar. They extend the second horizontal process on the opposite pole of the cell which elongates parallel to the surface, along the mediolateral axis, and forms the parallel fiber (Figure 1.2). Granule cells extend the third vertical process toward the internal granule layer, which becomes the leading process during inward radial migration across the molecular and Purkinje cell layer. The granule cell body uses radial Bergman glia fibers as a scaffold for the inward migration (Rakic, 1971; Zmuda and Rivas, 1988). Each leading process maintains a close contact with the vertically oriented Bergmann glia fibers through specific cell surface interactions. This concept is known as a glial-guided migration (Rakic, 1971). Some of the cell adhesion molecules, members of the immunoglobulin, integrin and cadherin family, and components of the extracellular matrix were shown to influence neuron-glia interactions leading to proper neuronal migration (Lindner et al., 1983; Chuong et al., 1987; Hack et al., 2002; Saghatelyan et al., 2004).

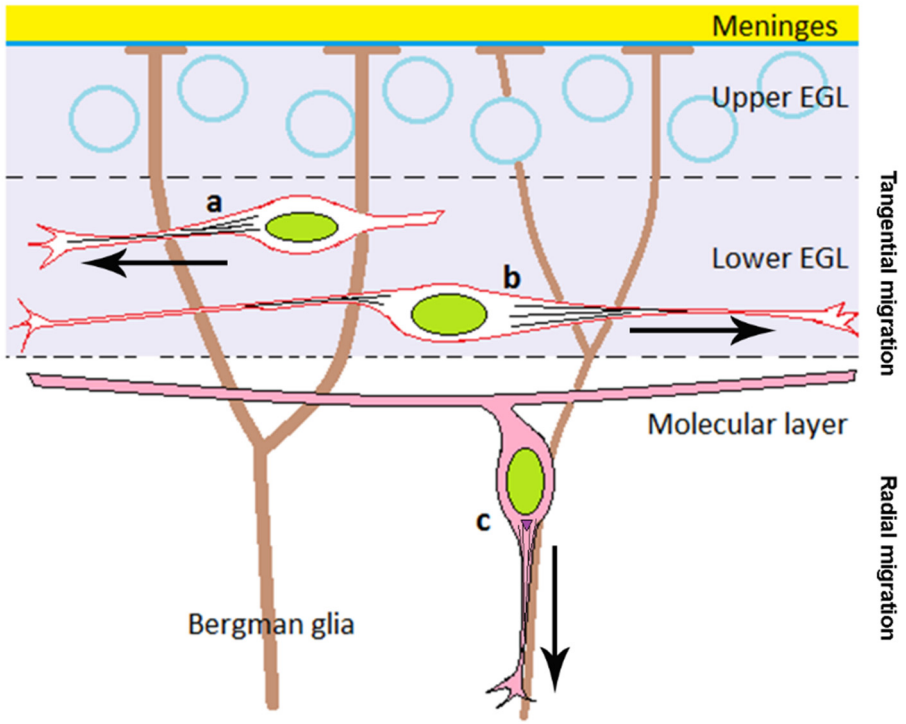

Figure 1.2. Morphological changes of a post-mitotic granule cell that enters the mode of radial migration. (a) In the lower zone of the external granule layer (EGL), granule precursors become unipolar, extend their leading process parallel to the pial surface and migrate tangentially (horizontal arrow). The microtubules (black stripes) reorganize within the leading process and enable its elongation,

while the cell body moves forwards. (b) The granule cell then becomes bipolar with the microtubules relocated at the opposite side of the cell within the second parallel leading process. (c) The granule cell drastically changes its morphology into the characteristic "T-shape", with the third leading process positioned perpendicular to the first two and relocated nucleus. The granule cell switches to radial migration (vertical arrow), sending a third process towards the molecular and internal granule layer and leaves it axon (the parallel fiber) behind. The microtubules are again relocated within the third leading process with the third joined component of the migration machinery - F-actin (violet triangle). The third leading fiber elongates and the cell body moves forwards using the Bergman glia fiber (brown stripes) as a scaffold for its migration.

The internal granule layer (IGL) becomes visible at postnatal day 5 (P5), when the post-mitotic granule cells start their proliferation, and complete their development at around P21 (Altman and Bayer, 1997). The proliferation rate of granule cell precursors in the EGL progressively declines starting from P3. According to the "stacking model", granule cells that differentiate first stack their parallel fiber in the deepest zone of the molecular layer (ML), while those that differentiate at last stack their parallel fiber in the most superficial zone of the ML (Espinosa and Luo., 2008). Granule cell bodies continue migration towards their final destination, the IGL. Parallel fibers of the granule cells form a synaptic contact with the Purkinje cell dendrites, below the ML in the layer known as Purkinje cell layer.

The most numerous neurons in the mammalian brain, granule cells, undergo apoptosis as a part of their normal development, which regulates the final number of granule cells maintained to the adulthood (Wood et al., 1993; Altman and Bayer, 1997; Lossi et al., 1998; Jankowski et al., 2009; Cheng et al., 2011). According to some authors, apoptosis in the EGL eliminates granule cell precursors unable to exit mitosis and to undergo differentiation, while apoptosis of post-mitotic granule cells in the IGL eliminates granule cells that failed to make proper synaptic contacts with Purkinje cell (Lossi et al., 2002). Apoptosis of Purkinje cells might also be a synapse-dependent process, regulated by their connections with climbing fibers (the nature of these connections is described in Chapter 1.1.1). During the first postnatal week one climbing fiber innervates several Purkinje cells, while with the further development the climbing fiber trims its synapse and focusses on a single Purkinje cell: Purkinje cells without connections with climbing fibers are probably also eliminated through apoptosis (Chu et al., 2000; Sugihara, 2006; Cheng et al., 2011). Inhibitory interneurons of the cerebellar cortex also undergo apoptosis during the first two weeks of postnatal development (Yamanaka et al., 2004; Weisheit et al., 2006).

The key period for apoptosis in the mouse cerebellar cortex is between P0 and P14. Because of their earlier development, Purkinje cells undergo apoptosis earlier. Two apoptotic waves have been shown for Purkinje cells: the first one occurs during embryonic development (around E15), while the second apoptotic wave occurs between P0 and P7 with a peak at P3 (Jankowski et al., 2009). Apoptosis in the EGL is prominent between P8 and P12 and gradually

decrease afterwards (Yamanaka et al., 2004, Cheng et al., 2011). In the IGL apoptotic events are prominent in the second postnatal week between P8 and P14 with a peak at P9-P10 (Alavez et al., 2006; Cheng et al., 2011). Figure 1.3 sums up already known facts about the events (proliferation, migration and apoptosis) occurring during the first three postnatal weeks of cerebellar cortex development.

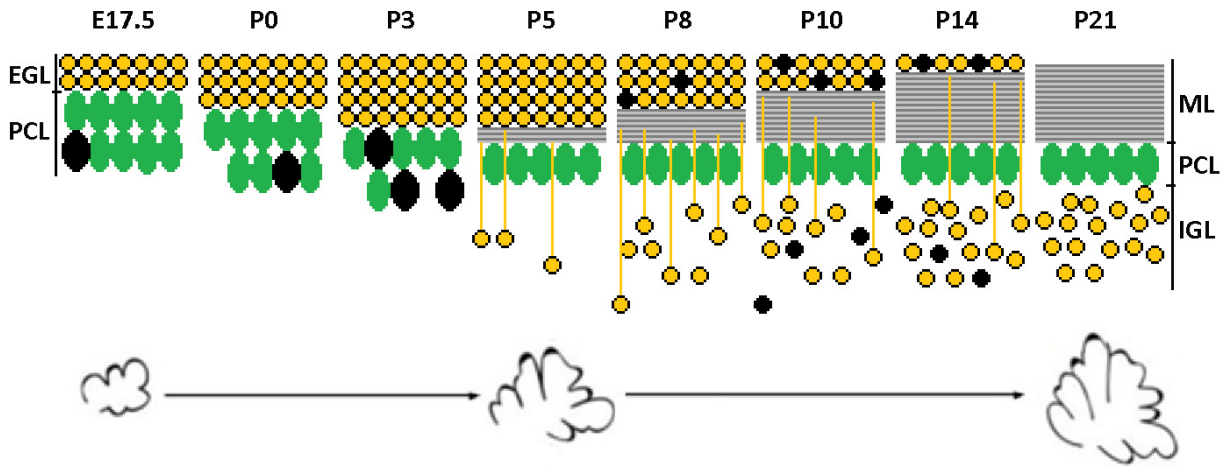

Figure 1.3. Schematic representation of the cerebellar cortex during development of granule and Purkinje cells. During the late embryonic development (E17.5) granule cell precursors (yellow circles) that cover the cerebellar surface start to proliferate. This proliferation lasts until the end of the first postnatal week. Meanwhile, Purkinje cells (green ellipses) that did not manage to exit mitosis undergo apoptosis (black ellipses). Apoptosis of Purkinje cells continues during the first postnatal week. At the end of the first postnatal week (P5), granule cells from the inner EGL that exit mitosis stack their axons in the ML and start inward radial migration through the PCL to form the IGL (the leading processes are presented as vertical yellow stripes). Parallel fibers (gray horizontal lines) that form the ML are detectable at P5. Radial migration continues until the end of the second postnatal week (P14). During the second postnatal week, granule cell precursors from the EGL that did not manage to exit mitosis and post-migrating granule cells from the IGL that failed to establish proper synapses with Purkinje cells undergo apoptosis (black circles). By the end of the third postnatal week (P21), the EGL layer disappears while the IGL is completely established. During postnatal development, the cerebellar volume gradually increases by increasing the number and volume of its lobules. EGL: external granular layer; PCL: Purkinje cell layer; ML: molecular layer; IGL: internal granular layer.

1.1.1 Tissue organization in the adult cerebellar cortex

In adult mammals, the cortex of the cerebellum consists of three main layers: the molecular layer (ML), the Purkinje cell layer (PCL) and the granule layer (GL). The ML is the most superficial layer with a low cellular density and high number of synapses. This characteristic layer consists of millions of parallel fibers (axons of granule cells) that make synapses with the dendritic tree of Purkinje cells. Besides, in the upper part of the ML cell bodies of stellate cells are located, which are small interneurons and selectively innervate Purkinje cell dendrites, while in the inner part of the ML basket cells are situated, which are also interneurons and

make synapses with Purkinje cells in the region of axon initial segment. All dendrites of inhibitory interneurons are found the molecular layer, where they receive synaptic input from the parallel fibers (Figure 1.4). The PCL is a thin region consisting of Purkinje cells bodies that are aligned into a single row and sporadically positioned small candelabrum interneurons. The GL is the layer with the highest cellular density consisting of cell bodies of the most numerous cells, the granule neurons, and other interneurons, such as Golgi, Lugaro and unipolar brush cells (Figure 1.4).

Purkinje cells are the only projection (efferent) neurons of the cerebellum. There are two afferent systems innervating Purkinje cells: climbing and mossy fibers (Sotelo, 2004). Climbing fibers originate from the inferior olivary nucleus and one climbing fiber per one Purkinje cell directly contacts dendrites of one Purkinje cell (Sugihara, 2006). Mossy fibers originate from various nuclei in the spinal cord, brain stem and deep cerebellar nuclei (Gould, 1979; Matsushita et al., 1979; Gould, 1980). They contact Purkinje cells indirectly through granule cells, namely their parallel fibers. One mossy fiber contacts thousands of Purkinje cells through hundreds of parallel fibers, showing a great level of divergence (Sotelo, 2004).

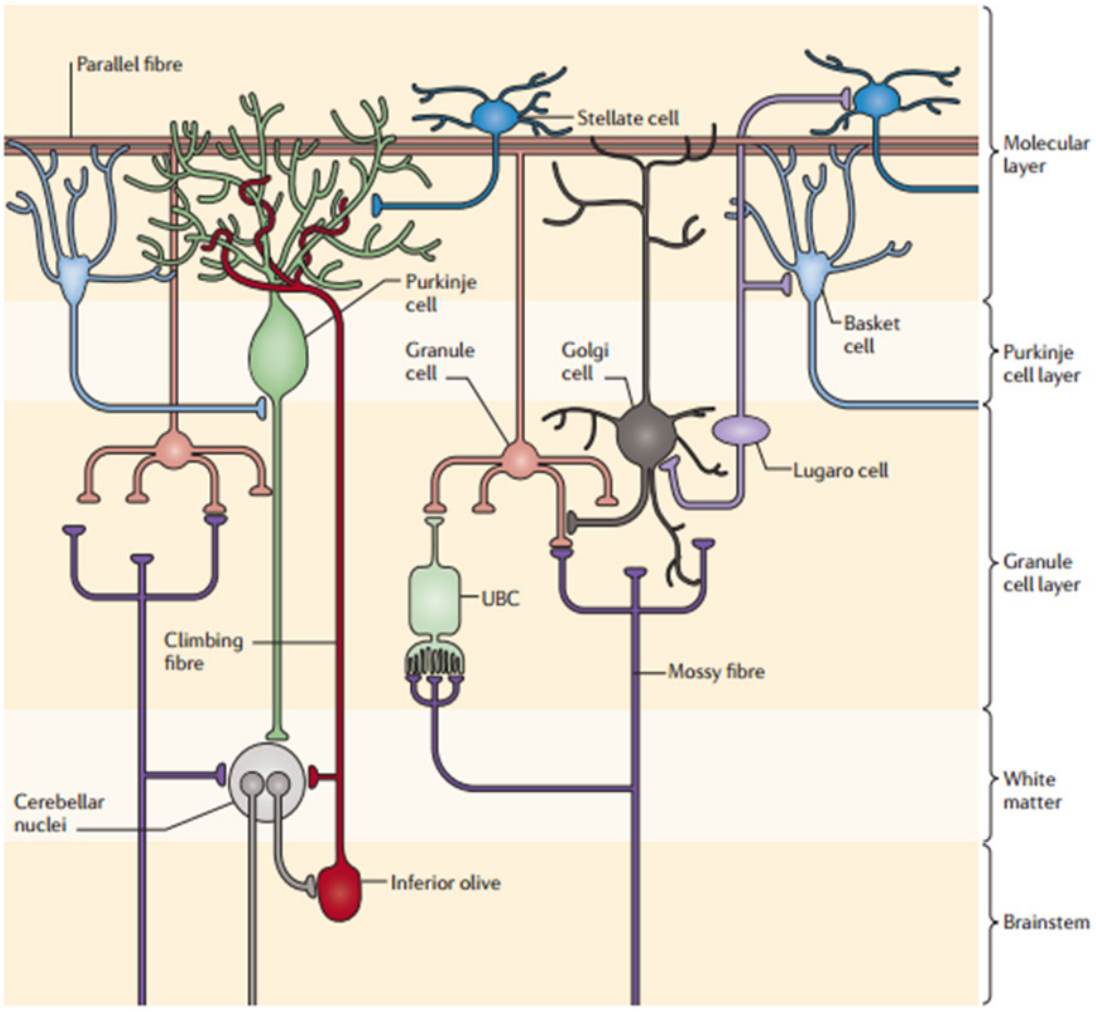

Figure 1.4. Cytoarchitecture of the adult cerebellar cortex. The cerebellar cortex consists of three layers: the most superficial molecular layer (ML), the Purkinje cell layer (PCL), and the deepest granule cell layer (GL). Purkinje cells are the only projection efferents of the cerebellum, with a soma placed in the PCL and a dendritic tree in the ML. The two main types of afferents that project to the cerebellum are climbing fibers from inferior olive, which form synapses directly with Purkinje cells, and mossy fibers from the brainstem, which form synapses indirectly with Purkinje cells through contacting granule cells. The axons of the granule cells, the parallel fibers, ascend to the molecular layer (while their soma is placed in the GL) where they form synapses with the dendritic tree of a Purkinje cell. Stellate interneurons are placed in the upper part of the ML and their axons make synapses with Purkinje cell dendrites. The cell bodies of the basket interneurons are located in the inner part of the ML, while the axons of basket cells extend until the border of PCL/GL to form synapses with the axon initial segment of Purkinje cells. Other interneurons such as Golgi, Lugaro and unipolar brush cells (UBC) are placed in the GL, synapsing either directly or indirectly with granule cells. UBCs are innervated by the mossy fibers. The figure was adapted from Cerminara et al., 2015.

1.2 Cell adhesion molecule close homolog of L1- CHL1

The CHL1 molecule is a member of the immunoglobulin superfamily of neuronal recognition molecules. In general, recognition molecules regulate and modulate cell interactions that occur during development of the nervous system, plasticity in adults, neuronal regeneration after injury and invasion of malignant tumor cells. Recognition molecules include several protein families: adhesion molecules like cadherins, integrins, members of the extracellular matrix (ECM) and proteins belonging to the immunoglobulin superfamily (Williams and Barclay, 1988; Kemler and Ozawa, 1989; Takeichi, 1991; Hynes, 1992; Sanes, 1989; Reichardt and Tomaselli, 1991; Brümmendorf and Lemmon, 2001). The immunoglobulin superfamily consists of several subfamilies that share the same features: immunoglobulin (Ig)-like domains with cysteines that form S-S bridges, fibronectin type III-like repeats, a short domain attached to the cell membrane, the presence of catalytic domains and a high number of glycosylation sites within the extracellular region (Holm et al., 1996). Members of the immunoglobulin superfamily that contain Ig-like domains within their extracellular region are grouped into the family of cell adhesion molecules (Walsh and Doherty, 1997).

Cell adhesion molecules are involved in cell adhesion and establishment of the cyto-architecture of many tissues (Lodish et al., 2000). The majority of cell adhesion molecules are cell-surface proteins that mediate either adhesion between two cells (via homophilic or heterophilic interactions) or interactions between the cell and the ECM molecules. Typical cell adhesion molecules expressed in the CNS are the first discovered neural cell adhesion molecule (NCAM) and the members of L1 subfamily of cell adhesion molecules (Brackenbury et al., 1977; Rathjen and Schachner, 1984; Walsh and Doherty, 1997). All cell adhesion molecules share common features. They are expressed both in the developing nervous system, where they influence migration, axonal pathfinding, neurite outgrowth, proliferation and differentiation of neurons and their precursors (Kamiguchi and Lemmon, 1997;

Brümmendorf et al., 1998), and in the adult nervous system where they influence long-term potentiation, learning, memory consolidation or nerve regeneration after injury (Lüthi et al., 1994; Scholey et al., 1995; Amoureux et al., 2000; Chaisuksunt et al., 2000; Zhang et al., 2000).

The L1 subfamily of cell adhesion molecules was named after the first discovered member, the neural cell adhesion molecule L1 (Rathjen and Schachner, 1984), which plays an important role in the proper development of the nervous system (Fransen et al., 1995; Dahme et al., 1997). Other members of L1 family are: the neuron-glia cell adhesion molecule (NgCAM) and its related cell adhesion molecule (NrCAM) (Grumet et al., 1991), neurofascin (Volkmer et al., 1992), CHL1 (Holm et al., 1996), the two invertebrate cell adhesion molecules such as Drosophila neuroglian and leech tractin (Bieber et al., 1989; Huang et al., 1997), the rat homologue of L1 (NILE) (Prince et al., 1991), the human homologue of CHL1 (CALL) (Wei et al., 1998) and the zebrafish homologues of L1 (L1.1 and L1.2) (Tongiorgi et al., 1995).

CHL1 consist of a N-terminal signal sequence, six immunoglobulin (Ig)-like domains, 4.5 fibronectin type III (FN)-like repeats, a transmembrane domain and a C-terminal intracellular domain (Figure 1.5). Its amino acid sequence is ~60% identical to L1 in the extracellular region and ~40% identical in the intracellular domain (Holm et al., 1996). The four FN-like repeats are highly homologous to the FN-like repeats of other L1 family members, whereas the partial FN-like repeat localized to the membrane-adjacent region of the molecule is the most variable region among L1-related molecules. The intracellular domain is most similar to mouse and chicken Nr-CAM and mouse and rat neurofascin (60% amino acid identity).

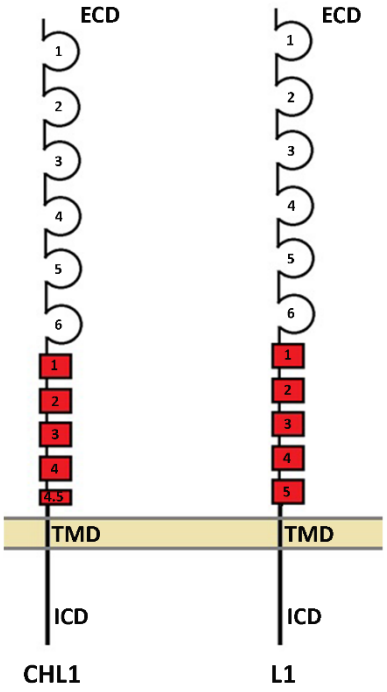

Figure 1.5. The L1 subfamily of cell adhesion molecules expressed in the plasma membrane. Schematic representation of two members of the L1 subfamily, L1 and its close homolog CHL1. Both molecules display a similar structure and common features. They are composed of an extracellular (ECD), a short transmembrane (TMD) and an intracellular domain (ICD). The amino acid sequence of CHL1 is ~60% identical to L1 in the ECD and ~40% identical in the ICD. The ECDs of both molecules consist of six immunoglobulin-like domains (circles) and a varying number of fibronectin type III (FN)-like repeats (red rectangles). L1 has five FN-like repeats, while CHL1 has four complete and one partial FN-like repeat (FN 4.5), which is also the sequence that varies the most between L1 and CHL1 ECDs. The ECDs are known to mediate both heterophilic and homophilic *cis*- and *trans*-interactions.

The CHL1 molecule is present in the tissue in three different molecular weights: the full-length form of 185 kDa, and two fragments of 165 kDa and 125 kDa. The two fragments are released by proteolytic cleavage by a disintegrin and metalloproteinase (ADAM) 8 (Naus et al., 2004). ADAM8 metalloproteinase cleaves within the 2nd and 5th FN domain of CHL1, resulting in 125 and 165 kDa fragments, respectively, that are very potent in stimulating neurite outgrowth and suppressing neuronal cell death in COS-7 cells and cerebellar granule neurons (Naus et al., 2004). Furthermore, the membrane-proximal region of CHL1 contains a cleavage site for the protease BACE1 (β-site amyloid precursor protein-cleaving enzyme-1) (Zhou et al., 2012). BACE1 is responsible for CHL1 processing in the brain and synaptic membranes, within the terminals of hippocampal mossy fibers, olfactory sensory neuron axons, and growth cones of primary hippocampal neurons, which influence proper axon growth and guidance (Hitt et al., 2012).

CHL1 is expressed both by neuronal and glial cells where it regulates numerous developmental events such as neural cell proliferation, migration, differentiation and cell survival (Holm et al., 1996; Hillenbrand et al., 1999). The functions of CHL1 are diverse and sometimes contrary: CHL1 reduces proliferation and differentiation of neural progenitor cells (Huang et al., 2011), but promotes survival and migration of differentiated neural cells (Holm et al., 1996; Chen et al., 1999; Hillenbrand et al., 1999; Buhusi et al., 2003; Jakovcevski et al., 2007, 2009); CHL1 promotes neurite outgrowth by *trans*-interactions with heterophilic binding partners and it inhibits neurite outgrowth by homophilic *trans*-interactions (Chen et al., 1999; Hillenbrand et

al., 1999; Jakovcevski et al., 2007, 2009). CHL1 triggers neurite outgrowth and neuronal survival, when substrate-coated *in vitro* (Chen et al., 1999; Hillenbrand et al., 1999). The extracellular part of CHL1 binds to $\alpha_1\beta_1$ and $\alpha_2\beta_1$ integrins and stimulates migration of HEK 293 cells along collagen I, fibronectin, laminin, and vitronectin, by activating the early integrin signaling intermediates c-sarcoma family kinase (c-Src), phosphatidylinositol 3-kinase (PI3K), and mitogen-activated protein kinase (MAPK). Through its intracellular domain, CHL1 recruits the actin cytoskeletal adapter protein ankyrin to the plasma membrane, which is necessary for promoting integrin-dependent migration on the extracellular matrix proteins (Buhusi et al., 2003). CHL1 is expressed in the presynaptic plasma membrane and synaptic vesicles where it interacts with the 70 kDa heat shock cognate protein (Hsc70) via its intracellular domain and influences proper clathrin-dependent synaptic vesicle recycling (Leshchyns'ka et al., 2006). Via its intracellular domain, CHL1 binds to the constitutively active isoforms of serotonin receptor 2c and modulates signaling pathways in the serotonergic system (Kleene et al., 2015).

CHL1-deficiency in mice results in abnormal brain structure, enlarged ventricles, misguidance of hippocampal mossy fiber projections, improper targeting of olfactory and thalamocortical axons, abnormal positioning of pyramidal cells and their dendrite orientation in the visual cortex, aberrant branching, loss in orientation and targeting of cerebellar stellate cell axons, loss of cerebellar Purkinje and granule cells as well as loss of GABAergic parvalbumin-positive hippocampal interneurons (Montag-Sallaz et al., 2002; Demyanenko et al., 2004, 2011; Nikonenko et al., 2006; Wright et al., 2007; Ango et al., 2008; Jakovcevski et al., 2009; Schmalbach et al., 2015). CHL1-deficient mice show alterations in social and exploratory behavior and the ability to gate sensorimotor information, and in working memory, which leads to serotonin receptor 2c-related reduction in locomotor activity and reactivity to novelty (Montag-Sallaz et al., 2002; Pratte et al., 2003; Irintchev et al., 2004; Morellini et al., 2007; Kolata et al., 2008; Pratte and Jamon, 2009; Kleene et al., 2015). In humans, CHL1 is linked to mental retardation, schizophrenia, major depression, epilepsy, and autism spectrum disorders (Angeloni et al., 1999; Sakurai et al., 2002; Frints et al., 2003; Chen et al., 2005; Chu and Liu, 2010; Tam et al., 2010; Cuoco et al., 2011; Morag et al., 2011; Salyakina et al., 2011; Shoukier et al., 2013). Mental impairment is characteristic of patients with the 3p syndrome, which is associated with a deletion of the CHL1 gene located on chromosome 3 at 3p26.1 (Angeloni et al., 1999; Higgins et al., 2000; Frints et al., 2003; Dijkhuizen et al., 2006).

1.2.1 The role of CHL1 in the cerebellum

The expression of cell adhesion molecules of the L1 subfamily, namely L1, Nr-CAM, neurofascin and CHL1, is important for proper formation of specific cellular circuitries and normal cerebellar functions during cerebellar development (Kamiguchi et al., 1998; Sakurai et

al., 2001; Ango et al., 2004, 2008; Huang et al., 2007). CHL1 is abundantly expressed in the murine cerebellum during postnatal development and throughout adulthood (Holm et al., 1996; Nikonenko et al., 2006). In situ hybridization detects CHL1 mRNA in stellate, basket, and Golgi interneurons and granule cells in the internal granular layer. At the protein level, CHL1 is abundant protein in the molecular layer along the parallel fibers, both in the developing and the adult cerebellum (Jakovcevski et al., 2009). CHL1 is also localized at apical Bergman glia fibers and stellate cells during the development of stellate axon arbors (Ango et al., 2006). The absence of CHL1 causes impaired cerebellar development during the first postnatal week. Stellate axons deviate from Bergman glia fibers and show aberrant branching and orientation; synapse formation between aberrant stellate axons and Purkinje dendrites is reduced leading to progressive atrophy of axon terminals and loss of Purkinje cells, while the inward radial migration of granule cell precursors along the Bergman glia fibers is retarded (Ango et al., 2006; Jakovcevski et al., 2009). A significant loss (20–23%) of Purkinje and granule cells and an abnormally high ratio (+38%) of stellate/basket interneurons to Purkinje cells in 2-month-old CHL1-deficient mice compared with wild-type littermates (Jakovcevski et al., 2009) has been reported. This finding suggests that CHL1 plays a role not only in early postnatal mouse cerebellar development, but also in the adult.

1.3 Sonic hedgehog signaling pathway

Members of the hedgehog family, isolated in early 1990s, are identified to have a central role during embryogenesis, in growth, pattering and morphogenesis of many regions in the body in both vertebrates and invertebrates. Hedgehog signals act as morphogens in a dose-dependent manner to induce cell fate within a target region, as mitogens regulating cell proliferation, and as inducing factors controlling the shape of the developing organ. Signaling can be short- and long-range, direct and indirect (through the activation of a signaling relay), and concentration-dependent (Ingham and McMahon, 2001).

Members of the hedgehog family are secreted peptides that mediate cellular communication in both vertebrates and invertebrates via similar mechanisms. Unlike Drosophila, which has a single hedgehog gene, there are several related genes in vertebrate species. Three hedgehog genes were identified in the mouse: desert hedgehog (DHH), indian hedgehog (IHH), and sonic hedgehog (SHH) (Echelard et al., 1993). DHH is most closely related to the Drosophila hedgehog gene and it is not expressed in the CNS. IHH and SHH are more related to one another, representing a more recent gene duplication event (Robbins et al., 2012). SHH is expressed in three key signaling centers in the vertebrate embryo: the notochord, the floor

plate, and the zone of polarizing activity (ZPA), a population of apical, posterior mesenchyme cells in the limb bud (Ingham and McMahon, 2001).

The sonic hedgehog signals produced in the notochord and floor plate regulate ventral polarity of the developing neural tube (Placzek, 1995). Sonic hedgehog forms an activity gradient over the ventral half of the neural tube coincident with the patterning process and it is both necessary and sufficient for the induction of distinct ventral cell identities in the spinal cord (Marti et al., 1995; Jessell, 2000). Sonic hedgehog specifies the cell fate via its cell-autonomous activation or inhibition, and direct and long-range activity (Hynes et al., 2000; Briscoe et al., 2001). Sonic hedgehog is considered as a morphogen that acts during the early (embryonic) stages of nervous system development. Data that are more recent suggest a role of sonic hedgehog in neurite extension, axon pathfinding, neuron survival and synapse formation during the later stages of CNS development (Harwell et al., 2012; Avilés et al., 2013).

The three mammalian members of the hedgehog family, sonic, desert and indian hedgehog, share the same receptor, the twelve-pass transmembrane protein patched (Jenkins, 2009; Robbins et al., 2012; Briscoe and Thérond, 2013). Patched has two large extracellular loops which interact with hedgehog proteins. In the absence of hedgehog ligands, patched represses the seven-pass transmembrane G protein-coupled receptor smoothened. Binding of hedgehog proteins to patched relief smoothened from repression by patched. In the so-called “canonical” hedgehog signaling pathway, binding of hedgehog ligands to patched activates smoothened, which in turn activates the transcription factors glioma-associated oncogene 1, 2 and 3 (GLI-1, -2, -3). These transcription factors regulate the expression of a number of effector genes, including the patched gene (Goodrich et al., 1997; Robbins et al., 2012; Briscoe and Thérond, 2013). Despite smoothened being an activator of the sonic hedgehog pathway, it does not bind to sonic hedgehog directly (Stone et al., 1996). Smoothened activates all members of the heterotrimeric Gi protein and this activation is suppressed by smoothened antagonists cyclopamine and SANT-1 (Chen et al., 2002; Rominger et al., 2009; Stanton and Peng, 2010). Activation of Gi protein by smoothened is essential in the activation of GLI transcription factors (Riobo et al., 2006).

Recent publications describe other sonic hedgehog signaling pathways independent of transcriptional changes mediated by the GLI family of transcription factors. Those pathways are categorized in the two distinct classes of so-called “non-canonical” hedgehog signaling pathways: “non-canonical” signaling type I works through patched and is smoothened-independent, while “non-canonical” signaling type II operates through smoothened activation (Brennan et al., 2012; Robbins et al., 2012). Hedgehog-induced cell migration, as well as axon guidance and neurite outgrowth, is mediated by the “non-canonical” signaling type II and thus

depends on the activation of smoothened (Kasai et al., 2004; Riobo et al., 2006; Lipinski et al., 2008; Jenkins, 2009; Yam et al., 2009; Polizio et al., 2011a, b; Shen et al., 2013).

In the absence of a sonic hedgehog ligand via "non-canonical" signaling pathway type I, ectopic expression of patched induces apoptosis (Thibert et al., 2003). Patched functions as a so-called "dependence-receptor": in the absence of ligands, patched initiates apoptosis upon cleavage of its C-terminal intracellular domain (at the DXXD site) by caspase-3, followed by recruiting of the pro-apoptotic complex including caspase-9, the caspase associated recruitment domain (CARD) containing protein, the tumor-up-regulated CARD-containing antagonist of caspase-9 (TUCAN-1) and the adaptor protein downregulated in rhabdomyosarcoma LIM-domain protein (DRAL) (Thibert et al., 2003, Mille et al., 2009; Fombonne et al., 2012). In the presence of a sonic hedgehog ligand, patched is unable to recruit the pro-apoptotic complex, which consequentially inhibits apoptosis. Besides, in the absence of sonic hedgehog, patched binds cyclin B1 and inhibits its translocation to the nucleus where it promotes mitosis. Sonic hedgehog stimulation induces a conformational change in patched after which patched loses its affinity for cyclin B1; cyclin B1 dissociates from the patched-cyclin B1 complex and translocates to the nucleus to stimulate proliferation (Brennan et al., 2012; Robbins et al., 2012).

In the type II of "non-canonical" hedgehog signaling, smoothened interacts with heterotrimeric Gi protein and activates Rho family of the small GTPase monomeric G proteins, e.g. RhoA and Rac1. Small GTPases act as molecular switches and rapidly regulate numerous cellular processes (Vetter and Wittinghofer, 2001). After activation by guanine exchange factors, they they bind GTP and interact with their molecular targets. The Rho family was shown to regulate acute cytoskeletal reorganization mediated by smoothened and Gi-protein activation (Riobo et al., 2006; Brennan et al., 2012; Robbins et al., 2012). Besides, smoothened activation triggers the release of the second messenger Ca^{2+} from the endoplasmic reticulum in spinal neurons (Belgacem and Borodinsky, 2011; Brennan et al., 2012; Robbins et al., 2012).

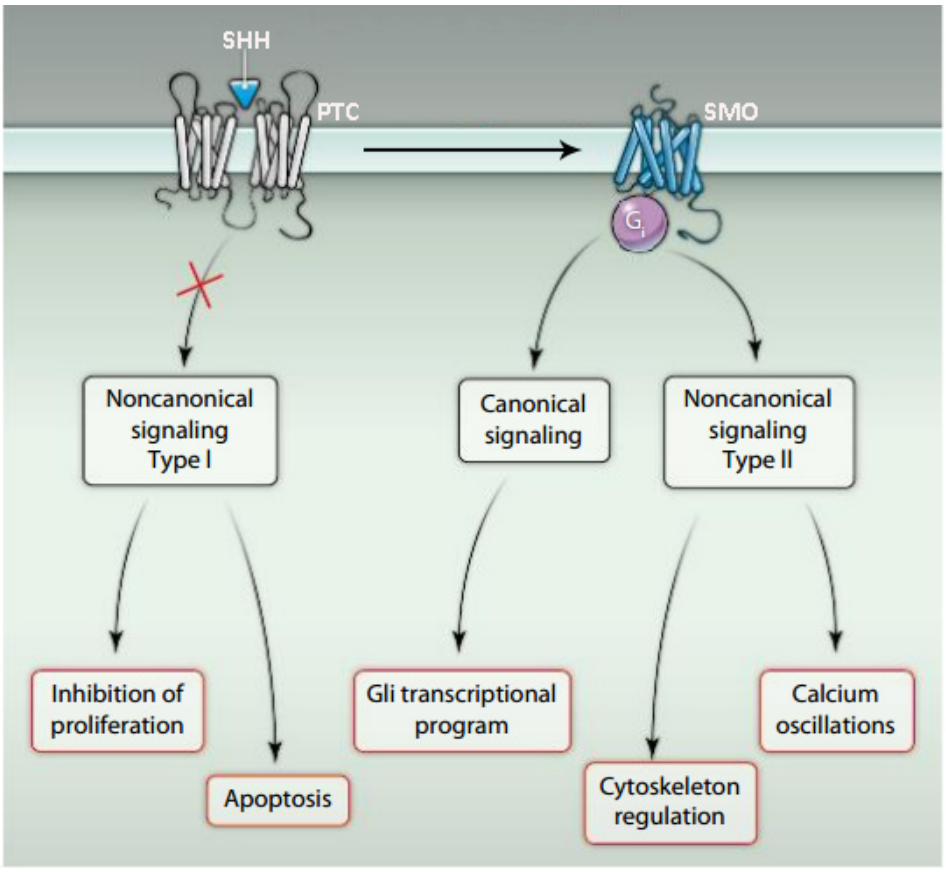

Figure 1.6. Sonic hedgehog signaling network. When sonic hedgehog (SHH) binds its receptor patched (PTC), smoothened (SMO) and PTC dissociate, abrogating SMO repression (vertical arrow). Thereby SMO is activated and able to initiate signal transduction pathways via activation of the heterotrimeric Gi protein. SMO initiates two signaling pathways: the "canonical" pathway including expression of the GLI transcription factors, and the "non-canonical" signaling type II that regulates cytoskeleton motility via activation of Rho GTPases and calcium oscillations. In the absence of the SHH ligand PTC initiates the third "non-canonical" signaling pathway type I: PTC recruits the pro-apoptotic complex that initiates apoptosis and binds cyclin B1, inhibiting its translocation to nucleus that promotes mitosis. Thus, PTC blocks proliferation and initiates apoptosis. Binding of SHH to PTC blocks (red cross) the "non-canonical" signaling pathway type I, inhibiting apoptosis and inducing proliferation. The figure was adapted from Robbins et al., 2012.

Several other binding proteins were shown to function as hedgehog co-receptors. The first one was identified to modulate hedgehog signaling in a *Drosophila* cell line and it was called interference hedgehog (Ihog) (Lum et al., 2003). Ihog is a cell adhesion protein that binds both to patched and hedgehog via its FNIII domains and acts as a positive regulator of hedgehog signaling. Two vertebrate orthologes of Ihog cell adhesion molecule down-regulated by oncogenes (Cdo) and brother of Cdo (Boc), are identified to bind to hedgehog in a similar manner (Tenzen et al., 2006).

That sonic hedgehog is involved in the control of neural cell death was first demonstrated in embryonal tissue: The removal of the notochord leads to massive cell death in the neural tube,

and induction of sonic hedgehog could rescue this phenotype (Charrier et al., 2001). On the other hand, patched was shown to have an intrinsic pro-apoptotic activity both *in vitro* and in the chicken neural tube, which could be rescued by sonic hedgehog stimulation (Thibert et al., 2003). Human patched is a tumor suppressor protein mutated in patients with basal cell nevus syndrome (Johnson et al., 1996) and in cells of various types of sporadic tumors, including those of the skin and brain (Ruiz i Altaba et al., 2002). Mice carrying mutations in the Patched gene also develop medulloblastomas, which are tumors of the cerebellum (Goodrich et al., 1997). Mutations in the Patched gene may be the reason of uncontrolled activation of the sonic hedgehog signaling via GLI transcription factors, which leads to uncontrolled proliferation and tumor formation.

As mentioned before, sonic hedgehog signaling plays a crucial role in the developing cerebellum: sonic hedgehog that is secreted by Purkinje cells acts on granule cell precursors in the external granular layer and triggers their proliferation (Dahmane et al., 1999; Wallace, 1999; Vaillant and Monard, 2009; Hatten and Roussel, 2011; Lewis et al., 2004). However, sonic hedgehog signaling events are not confined to neuronal precursors, they have additional ongoing roles within postmitotic neurons of the developing and adult cerebellum. Patched and smoothened are present in the processes and growth cones of immature neurons in the postnatal developing cerebellum and in the mature cerebellum (Traiffort et al., 1998; Traiffort et al., 1999; Lewis et al., 2004; Varjosalo and Taipale, 2008; Zheng et al., 2010; Petralia et al., 2012). They are expressed by several types of neurons including Purkinje cells, granule cells, and interneurons, and are predominantly localized at the postsynaptic side of the synapses (Petralia et al., 2012).

1.4 Extracellular matrix molecules – vitronectin and plasminogen activator inhibitor 2

The extracellular matrix (ECM) consist of glycoproteins, proteins and polysaccharides secreted by cells, which provides physical support and organization to tissues. Cells contact the ECM via cell membrane receptors such as integrins or cell adhesion molecules. These receptors mediate cell–ECM adhesion and regulate intracellular signaling pathways that control cell proliferation, differentiation, migration and survival during development, contribute to normal tissue functioning, as well as remodeling and repair of tissues during adulthood. Changes in the physical properties and composition of the ECM and altered expression of their receptors occur in many human diseases such as tumor progression. The ECM is both a requirement and a physical barrier for cell movement. Thus, cell migration often involves the coordination of ECM proteolysis, adhesion and signaling (Smith and Marshall, 2010).

The urokinase-type plasminogen activator receptor (uPAR) is an important regulator of ECM proteolysis, cell–ECM interactions and cell signaling. uPAR regulates the activity of the plasminogen activation system, an extracellular proteolytic cascade, by binding the serine protease urokinase-type plasminogen activator (uPA) and its inactive zymogen form, pro-uPA. Activated uPA cleaves the zymogen plasminogen, generating the protease plasmin, which in turn cleaves and activates pro-uPA (Ellis et al., 1991). The plasminogen activation system is negatively regulated by the plasminogen activator inhibitor 1 and 2 (PAI-1 and PAI-2), which bind covalently to their targets and inhibit proteolytic activity of uPA (Ellis et al., 1991; Ye and Goldsmith, 2001). Activation of plasminogen by uPA–uPAR interaction leads to interaction of uPAR with the ECM molecule vitonectin and the integrin cell membrane receptors which facilitates cell migration (Kjoller and Hall, 2001).

Vitronectin is a multifunctional ECM glycoprotein involved in several physiological processes dependent on its localization: in blood it plays a role in the regulation of thrombus formation, coagulation and fibrinolysis, while in the tissue within the extracellular matrix it has an important role in regulating pericellular proteolysis, wound healing, inhibition of the membrane attack complex, cellular adhesion, proliferation, differentiation and migration. It exists as a monomer in the circulation, but the preferred conformation in the ECM is multimeric. Vitronectin interacts with various proteins including the thrombin-antithrombin complex, heparin, PAI-1, collagen, integrins and uPAR (Barnes et al., 1985; Owensby at al., 1991; Kanse et al., 1996; Dahm and Bowers, 1998). Regulation of cellular adhesion and migration depends on the ability of vitronectin to act as a matrix protein that can bind to different cell surface receptors like uPAR and certain subclasses of integrins (Felding-Habermann and Cheresh, 1993; Bae et al., 2013). Interactions between vitronectin and integrin αvβ3, PAI-1, or uPAR can also modulate the clearance of apoptotic cells (Bae et al., 2013).

Vitronectin is involved in the differentiation of diverse cell types in embryonic and adult tissues (Seiffert et al., 1995). In the developing mouse neural tube, vitronectin is expressed in the notochord and in the floor plate, the same place where sonic hedgehog is produced (Martínez-Morales et al., 1997). Previous studies showed that vitronectin promotes the generation of spinal motor neurons and oligodendrocytes by synergistically interacting with sonic hedgehog, both in explants and neuroepithelial cell cultures of chicken embryo spinal cord (Pons and Martí, 2000; Gil et al., 2009).

Vitronectin and its integrin receptor subunit αv are expressed in the postnatal developing cerebellum, namely in the inner part of the external granular layer where granule cell precursors exit mitosis and start to differentiate. In cultures, vitronectin is able to overcome sonic hedgehog-induced proliferation, allowing granule cell differentiation. Vitronectin stimulates phosphorylation of cyclic-AMP responsive element-binding protein (CREB), which

terminates sonic hedgehog-mediated proliferation and induces differentiation of granule cell precursors (Pons et al., 2001). During the first week of cerebellar postnatal development in mice, vitronectin and laminin regulate proper centrosome positioning in the leading process of granule cell precursors, which is required for their inward radial migration. Vitronectin induces integrin-mediated signaling that upregulates phosphoinositide-3 kinase and protein kinase C function and production of phosphatidylinositol 3,4,5-trisphosphate (PIP3) associated with the centrosome (Gupta et al., 2010). Vitronectin is also expressed in the upper molecular layer along parallel fibers, where it stimulates the integrin-dependent elongation of parallel fibers prior to granule cell radial migration (Murase and Hayashi, 1998). In the postnatal cerebellum, Purkinje cells down-regulate sonic hedgehog production, which stimulates the proliferation of oligodendrocyte precursor cells, and upregulates vitronectin production, which inhibits proliferation and stimulates differentiation of oligodendrocytes. Altogether, Purkinje cells control the timing of oligodendrocyte differentiation in the cerebellum through the developmentally regulated expression of sonic hedgehog and vitronectin (Bouslama-Oueghlani et al., 2012).

Plasminogen activator inhibitor type 2 (PAI-2) belongs to the ovalbumin subfamily of serpins. The serpin family comprises a large group of proteins with diverse functions but a common molecular architecture: nine α-helices and three β-sheets with a mobile reactive center loop (Silverman et al., 2001). PAI-2 has an internal signal peptide, which allows synthesis of both intracellular and extracellular forms of the protein (von Heijne et al., 1991). Most of the PAI-2 synthesized remains in the cytosol where its function remains unclear; there are some indications of its involvement in apoptosis. However, in the extracellular matrix, PAI-2 acts an inhibitor of uPA and plays a role in cell migration and tumor metastasis (Jensen, 1997). Recent studies show that vitronectin can form a heterodimer with PAI-2 by making a disulfide bond with the PAI-2 loop connecting helices C and D. PAI-2 remains more stable within the vitronectin-PAI-2 dimer, which enables its longer presence in the ECM where it acts as an inhibitor of uPA (Lobov et al., 2004).

PAI-2 is capable of inhibiting uPA on adherent cells in the presence of vitronectin, influencing cell migration (Lobov and Ranson, 2011). The expression of PAI-2 is upregulated in response to synaptic activity and has a neuroprotective role under stress conditions. The PAI-2 gene has been identified as one of the activity-regulated inhibitors of cell death that occurs in hippocampal neurons (Zhang et al., 2009). The expression of PAI-2 and uPA increases upon excitotoxic kainate treatment, leading to epileptic seizures (Sharon et al., 2002; Iyer et al., 2010; Cho et al., 2012).

2 AIMS OF THE STUDY

In a search for novel binding partners of CHL1, two members of the ECM vitronectin and PAI-2, and the sonic hedgehog receptor patched were identified as potential interaction partners in the research group of Prof. Schachner. The first aim of this study was to confirm these interactions *in vitro* using immunoprecipitation, ELISA and label-free binding assay.

The second aim of this study was to understand the functional implication of the interaction between CHL1 and its newly identified binding partners. For that, functional *in vitro* tests were performed: cell death assay on dissociated cerebellar neurons, cultured HEK 293 cells and organotypic cerebellar slices; migration assay on cerebellar explant cultures and neurite outgrowth assay on dissociated cerebellar neurons.

The third aim of this study was to verify the interaction of CHL1 with vitronectin, PAI-2, patched *in vivo* and to localize the region of this interaction using immunohistochemistry and proximity ligation assay.

Finally, the fourth aim of this study was focused on the role of CHL1 and its binding partners in cerebellar development. It had been shown that CHL1 is expressed in the cerebellum during the late embryonic and the postnatal development, influencing migration of granule cells and Purkinje and granule cell survival. Moreover, vitronectin, sonic hedgehog, patched and smoothened are present in the embryonic and postnatal cerebellum where they synergistically act in developmental processes, such as differentiation and proliferation of granule cell precursors. To understand the role of CHL1 and its newly identified binding partners in cell migration, proliferation, differentiation and apoptosis, specific cell markers were used in stereological analysis of histological sections from CHL1-deficient and wild-type mice of different age.

3 MATERIALS

3.1 Animals

Wild-type C57BL/6J mice were obtained from the central animal facility of the Universitätsklinikum Hamburg-Eppendorf. CHL1-deficient mice were generated by replacement of the exon 1 and the intron 1 of the CHL1 gene with a sequence coding for the herpes simplex virus thymidine kinase gene, an intronic sequence and a PGK-*neo* cassette (Montag-Sallaz et al., 2002). CHL1-deficient mice had been back-crossed onto the C57BL/6J background for more than eight generations. Male and female C57BL/6J mice or CHL1-deficient mice and their age-matched wild-type littermates were used for the experiments.

Vitronectin-deficient mice (B6.129S2 (D2)-Vtn*tm1Dgi*/J) were purchased from Jackson Laboratory (Bar Harbor, ME). Vitronectin-deficient male mice were crossed first to B6D2F1/J female mice, then backcrossed to C57BL/6J mice for twelve generations, and breed in the Department of Medicine, University of Alabama, Birmingham, USA (Bae et al., 2013). Brains from postnatal day five and seven-day old vitronectin-deficient males were a kind gift from a Professor Jaroslaw W. Zmijewski, Department of Medicine, University of Alabama.

All animal experiments were approved by the local authorities of the State of Hamburg (animal permits ORG 535 and G09/098) and confirm to the guidelines set by the European Union.

3.2 Bacterial strains and cell lines

The following bacterial strains and cell lines were used in this study:

Human embryonic kidney cells (HEK293)	ATCC CRL-1573
Escherichia coli M15 (pREP4)	Qiagen *F-, Φ80ΔlacM15, thi, lac-, mtl-, recA+, KmR*
Escherichia coli TOP10 (One Shot Competent cells)	Invitrogen *F-, mcrA, Δ(mrr-hsd RMS-mcrBC), φ80lacZ ΔM15, ΔlacX74, recA1, araD139,Δ(ara-*

	leu)7697, galU, galK, rpsL (Str R), endA1, nupG
Escherichia coli	Clontech
(Stellar Competent)	*F-, endA1, supE44, thi-1, recA1, relA1, gyrA96, phoA, Φ80d lacZΔ M15, Δ (lacZYA - argF) U169, Δ (mrr - hsdRMS - mcrBC), ΔmcrA, λ-*
Escherichia coli	*NEB*
(NEB 5-alpha competent cells)	*fhuA2, Δ(argF-lacZ) U169, phoA, glnV44, Φ80, Δ(lacZ)M15, gyrA96, recA1, relA1, endA1, thi-1, hsdR17*

3.3 Plasmid vectors

The following plasmid vectors were use in this study:

pQE30	Qiagen Prokaryotic expression plasmid designed for recombinant expression of proteins, carrying a RGS-motif followed by a hexahistidine-domain (6xHis) at the 5' end of the multiple cloning site for purification. Amp-resistance.
pRK5-mPTC1-HA	The pRK5-mPTC1-HA construct was a kind gift from Dr. Patrick Mehlen (CNRS, Cancer Research Centre of Lyon, Centre Léon Bérard, Lyon, France). Mouse patched 1 cDNA sequence was cloned in frame with hemagglutinin (HA) into the pRK-5 vector. pRK-5 (BD PharMingen) is a mammalian expression vector designed for high level

expression under the the control of the cytomegalovirus promoter.

3.4 Primers

The following primers were used in this study (Table 3.1):

Table 3.1. List of primers. VT-N, N terminal fragment of vitronectin; PAI2-N, N terminal fragment of plasminogen activator inhibitor 2 (PAI2); PAI2-C, C terminal fragment of PAI2; PQE 30, pQE 30 plasmid; PTC LP1, first extracellular loop of patched; PTC, patched; GLI1, GLI family zinc finger 1; GLI3, GLI family zinc finger 3; R, right; L, left.

Primer name	Sequence	Comment
InF VT-N fw	TCA CCA TCA CGG ATC ATG GCA CCC CTG AGG CCC	In Fusion cloning
InF VT-N rev	GCT CGC ATG CGG ATC AAT GCC CCA GAC ATC TTG G	In Fusion cloning
InF PAI2-N fw	TCA CCA TCA CGG ATC ATG GAA GAA CTT TCC ATG GC	In Fusion cloning
InF PAI2-N rev	GCT CGC ATG CGG ATC GAC AGC ATT CAC CAG CAC	In Fusion cloning
InF PAI2-C fw	TCA CCA TCA CGG ATC TCC TTG AAT GTG CTG AAG AA	In Fusion cloning
InF PAI2-C rev	GCT CGC ATG CGG ATC TTA GGG TGA GGA GAA TCT AC	In Fusion cloning
InF PQE 30 fw	GGA GAA ATT AAC TAT GAG AGG	In Fusion cloning
InF PQE 30 rev	GTT CTG AGG TCA TTA CTG G	In Fusion cloning
Q5 PTC-LP1 fw	GTC AGT GTC ATC CGA GTG	Site-directed mutagenesis with Q5 kit

Q5 PTC-LP1 rev	GAG ATT AGC TGC CTT TAA TC	Site-directed mutagenesis
qPTC R	AAT TCT CGA CTC ACT CGT CCA	qPCR analysis
qPTC L	CTC CTC ATA TTT GGG GCC TT	qPCR analysis
qGLI1 R	ATT GGA TTG AAC ATG GCG TC	qPCR analysis
qGLI1 L	GGA TGA AGA AGC AGT TGG GA	qPCR analysis
qGLI3 R	TGC GTT TCT TCT CTC TCG GT	qPCR analysis
qGLI3 L	ACG AGA ACA GAT GTC AGC GA	qPCR analysis

3.5 Recombinant protein constructs and peptides

The following recombinant protein constructs, peptides and protein inhibitors were used in this study:

active smoothened antagonist SANT-1	Merck Millipore (#559303)
CHL1 P1 peptide: H-EEGATLGEGSKGIRKITEGVN-OH	Schafer-N
CHL1 P2 peptide: H-TKNWGDNDSIFQDVIETRGRE-OH	Schafer-N
CHL1 P3 peptide: H-KTKSLLDGRTHPKEVNILRFSGQR-OH	Schafer-N

CHL1-Fc fusion protein	The extracellular domain of murine CHL1 was fused with the Fc part of human IgG and produced in CHO cells (InVivo)
Fc fragment, human IgG	Dianova (#009-000-008)
His-tagged Pai2 N-terminus (amino acids 1-203)	Produced in *E.coli*
His-tagged Pai2, C-terminus (amino acids 1-200)	Produced in *E.coli*
His-tagged vitronectin, N-terminus (amino acids 160-415)	Produced in *E.coli*
inactive smoothened antagonist Tomatidine	Merck Millipore (#614350)
L1-Fc fusion protein	The extracellular domain of murine L1 was fused with the Fc part of human IgG and produced in CHO cells (InVivo)
NCAM-Fc fusion protein	The extracellular domain of murine NCAM was fused with the Fc part of human IgG and produced in CHO cells (InVivo)
Patched-1 recombinant protein	Biozol (#MBS2011579)
PTC peptide: H-RGYDYVSHINWNEDR-OH	Schafer-N

PTC scrambled peptide: H-YIDRSGWDHNYRVEN-OH	Schafer-N
Rho inhibitor II, Y16	Merck Chemicals (#5040430001)
ROCK inhibitor, Y-27632	Tebu (#10-2301)

3.6 Solutions and buffers

The following solutions and buffers were used in this study:

Protease inhibitor solution (Complete, EDTA free tablets, Roche) – cerebellar homogenates and cell lysates	1 Tablet in 2 ml PBS results in a 25 x stock solution
RIPA buffer – cerebellar homogenates and cell lysates	50 mM Tris-HCl pH 7.4 150 mM NaCl 1 mM EGTA 10 mM NaF 2 mM Na_3VO_4 1% Triton X-100 1 x Protease inhibitor solution
TE buffer – cerebellar homogenates and cell lysates	50 mM Tris pH 8.0 5 mM EDTA 1 x Protease inhibitor solution

BCA Protein Assay solution – determination of the protein concentration	Reagent A: Reagent B (50:1)
10% SDS running gel – SDS-PAGE	1.7 ml dH_2O 2.3 ml 1 M Tris pH 8.8 2 ml 30% acrylamide – bisacrylamide (29:1) 60 µl 10% SDS 15 µl 10% APS 6 µl TEMED
12% SDS running gel – SDS-PAGE	1.3 ml dH_2O 2.3 ml 1 M Tris pH 8.8 2.4 ml 30% acrylamide – bisacrylamide (29:1) 60 µl 10% SDS 15 µl 10% APS 6 µl TEMED
Running buffer – SDS-PAGE	0.25 M Tris-HCl 1.92 M glycine 1 M SDS pH 8.3
Sample buffer – SDS-PAGE	0.4 M Tris-HCl 10% (w/v) SDS 50% (v/v) glycerol

	0.13 % (w/v) bromphenol blue
	2.5% (w/v) β-mercaptoethanol
	pH 6.8
Stacking gel	1.6 ml dH_2O
– SDS-PAGE	0.3 ml 1 M Tris pH 6.8
	0.4 ml 30% acrylamide – aisacrylamide (29:1)
	30 µl 10% SDS
	15 µl 10% APS
	6 µl TEMED
Staining solutions	20% (v/v) methanol
– Coomassie staining of gels	80% (v/v) Roti-Blue (Carl Roth)
Antibody dilution buffer	4% nonfat dry milk powder in 1x TBS
– Western blot analysis	
Blocking buffer	4% nonfat dry milk powder in 1x TBS-T
– Western blot anaylsis	
Blotting buffer	25 mM Tris
– Western blot analysis	192 mM glycine
	0.01% SDS
	10% methanol
Tris-buffered saline (TBS) 10 x	10 mM Tris HCl

– Western blot analysis	150 mM NaCl pH 8.0
TBS-T 1 x – Western blot analysis	0.1% Tween-20 in 1 x TBS
IP lysis buffer – immunoprecipitation	20 mM Tris-HCl 150 mM NaCl 2.5 mM $Na_4P_2O_7$ 1 mM EGTA 1 mM EDTA 1 mM NaF 1 mM PMSF 1 mM Na_3VO_4 1 mM β-glycerolphosphate 1% Triton X-100 1 x protease inhibitor solution pH 7.5
Phosphate buffered saline (PBS) 10 x – ELISA	150 mM NaCl 20 mM Na_3PO_4 pH 7.4
PBS with Ca^{2+} and Mg^{2+} (PBS^{+}) – ELISA	0.2 mM $CaCl_2$ 1 mM $MgCl_2$ 1 x PBS

PBS-T – ELISA	0.1% Tween-20 in 1 x PBS
Blocking solution – ELISA	1% BSA in PBS^+
OPD substrate – ELISA	5 mg OPD (Thermo Fisher Scientific) was mixed with 9 ml dH_2O and 1 ml Stable Peroxide Buffer (10X, Thermo Fisher Scientific)
DNA-sample buffer (5x) – DNA agarose gel electrophoresis	20 % glycerol in TAE buffer 0.025 % Orange G
50 x TAE – DNA agarose gel electrophoresis	2 M Tris/acetat, 100 mM EDTA pH 8.0
TBF1 buffer – production of competent bacteria	100 mM RbCl 50 mM $MnCl_2$ 30 mM potassium acetate 10 mM $CaCl_2$ 15% (v/v) glycerol pH 5.8
TBF2 buffer – production of competent bacteria	10 mM MOPS 10 mM RbCl

	75 mM $CaCl_2$
	15% (v/v) glycerol
	pH 8.0 (adjusted with KOH)
Lysis buffer	50 mM NaH_2PO_4
– expression and purification of recombinant proteins from *E. coli*	300 mM NaCl
	10 mM imidazole
	pH 8.0
	1 x Potease inhibitor solution
Washing buffer 1	50 mM NaH_2PO_4
– expression and purification of recombinant proteins from *E. coli*	600 mM NaCl
	10 mM imidazole
	pH 8.0
Washing buffer 2	50 mM NaH_2PO_4
– expression and purification of recombinant proteins from *E. coli*	300 mM NaCl
	20 mM Imidazole
	pH 8.0
Washing buffer 3	50 mM NaH_2PO_4
– expression and purification of recombinant proteins from *E. coli*	300 mM NaCl
	40 mM imidazole
	pH 8.0
Washing buffer 4	50 mM NaH_2PO_4

– expression and purification of recombinant proteins from *E. coli*	300 mM NaCl 60 mM imidazole pH 8.0
Elution buffer – expression and purification of recombinant proteins from *E. coli*	50 mM NaH_2PO_4 300 mM NaCl 250 mM imidazole pH 8.0
Cacodylate buffer – tissue preparation and sectioning	0.2 M sodium cacodylate in dH_2O pH 7.3 (adjusted with 0.2 M HCl)
4% paraformaldehyde solution (PFA) – tissue preparation and sectioning	400 ml dH_2O was added to 40 g paraformaldehyde and heated with constant stirring under the laminar flow. 1 M NaOH was added until the milky suspension became clear. 500 ml 0.2 M sodium cacodylate and 1 g anhydrous $CaCl_2$ was added and the pH was adjusted to 7.3 with 0.2 M HCl. The volume was adjusted to 1 l. The solution was filtered using a Whatman filter.
Blocking buffer with normal donkey serum – immunohistochemistry	5% normal donkey serum in PBS 0.2% Triton X-100 0.02 % NaN_3

Antibody dilution buffer – immunohistochemistry	0.5 g lambda-carrageenan and 0.02 g NaN_3 were added in 100 ml PBS and heated under constant stirring. The solution was filtered using a Whatman filter.

3.7 Cell culture media, buffers and reagents

All media, buffers and supplements used in this study were filtered prior to use and stred and used under sterile conditions.

HBSS buffer	PAN Biotech (#P04-33500) Hanks´ balanced salt solution without Ca^{2+} and Mg^{2+} containing 0,35 g/l NaHCO4 and phenol red
Medium X-1 – cerebellar neuron culture	1 x Neurobasal A, Invitrogen (#10888022) 1 x penicillin/streptomycin, PAN Biotech (#P06-07100) 0.1 % BSA, PAA laboratories (#K35-002) 10 µg/ml insulin, Sigma-Aldrich (#I6634-250MG) 4 nM L-thyroxine, Sigma-Aldrich (#T2376) 100 µg/ml transferrin holo, Merck Chemicals (#616420) 30 nM Na-selenite, Sigma-Aldrich (#S5261) 1 x Na-pyruvate, PAN Biotech (#P04-43100) 1 x L-glutamine, PAN Biotech (#P04-80100) 1 x B27 supplement, Invitrogen (#17504-044)
Medium X-1 with serum	92.5 % X-1 medium

– cerebellar neuron culture	7.5 % Fetal Horse Serum, VWR (#S0960-500)
Trypsin/DNase solution	0.2 g trypsin, Sigma-Aldrich (#T9935)
– cerebellar neuron culture	20 mg DNase I, Sigma-Aldrich (#D-5025)
	200 µl 80 mM MgCl
	20 ml HBSS
	pH 7.8
DNase I solution	10 mg DNase I
– cerebellar neuron culture	50 mg glucose
	20 ml Neurobasal A
Medium DMEM	Dulbecco's modified Eagle Medium (DMEM) with L-glutamine, sodium pyruvate, high glucose (4.5 g/l), PAA (#P04-04510)
– HEK cell culture	10% Fetal Calf Serum, PAA laboratories (#A15-151-1)
	1 x penicillin/streptomycin
	0.2 mg/ml geneticin, Invitrogen (#10131019)
DMEM freezing medium	70% DMEM
– HEK cell culture	20% FCS
	10% DMSO
Preparation medium	HBSS
– organotypic slice culture	1 mM $CaCl_2$
	4 mM KCl
	5 mM $MgCl_2$

	10 mM glucose
	Adjust pH 7.3 with 1M NaOH
Incubation medium	1 x MEM, Invitrogen (#22561021)
– organotypic slice culture	25% Fetal Horse Serum, VWR (#S0960-500)
	25 mM HEPES, Invitrogen (#15630106)
	1 mM L-glutamine
	100 U/ml penicillin/streptomycin
	1 mg/ml glucose

3.8 Bacterial media and reagents

Listed are bacterial media and reagents used in this study. Media were autoclaved prior to use.

LB-medium	10 g/l bacto-tryptone pH 7.4
	10 g/l NaCl
	5 g/l yeast extract
LB/Amp-medium	100 mg/l ampicillin in LB-Medium
LB/Amp-plates	20 g/l agar in LB-Medium
	100 mg/l ampicillin
LB/Kan-medium	25 mg/l kanamycin in LB-Medium

LB/Kan-plates	20 g/l agar in LB-Medium 25 mg/l kanamycin
IPTG – protein expression in bacteria	1 M IPTG; 238 mg/ml results in 1000x stock

3.9 Antibodies

Commercial antibodies against specific proteins and cell marker antigens were used for immunohistochemistry, proximity ligation assay, immunoprecipitation and Western blot analysis (Table 3.2). Secondary antibodies conjugated either to the cyanine fluorescent dyes (Cy2, 3 or 5) or to the horseradish peroxidase (HRP) were used in immunohistochemistry and Western blot analysis, respectively (Table 3.3).

Table 3.2. List of primary antibodies used in this study. IHC - immunohistochemistry, PLA - proximity ligation assay, IP- immunoprecipitation, and WB - Western blot analysis. Goat and rabbit antibodies were polyclonal if not indicated otherwise; rat and mouse antibodies were monoclonal.

Antigen	Host	Company	Catalog number	Dilution
Calbindin	Mouse	Sigma-Aldrich	C9848	IHC 1:1,000
Calbindin	Rabbit	Sigma-Aldrich	C2724	IHC 1:1,000
Caspase-3 active	Rabbit	R&D Systems	AF835	IHC 1:1,000
CHL1 (extracellular domain)	Goat	R&D Systems	AF2147	IHC 1:100, PLA 1:100, WB 1:1,000
Doublecortin	Goat	Santa Cruz Biotechnology	sc-8066	IHC 1:150

Ki67	Rabbit	Abcam	AB15580	IHC 1:500
NeuN	Mouse	Millipore	MAB377	IHC 1:500
PAI-2 (amino acids 61-130)	Rabbit	Santa Cruz Biotechnology	sc-25746	IHC 1:100
Patched (amino acids 108-422)	Rat	R&D Systems	MAB41051	IHC 1:100, IP: 5 µg/ml
Patched (first extracellular loop)	Rabbit	Acris	17520-1-AP	PLA 1:100
PAX6	Rabbit	Millipore	AB2237	IHC 1:1,000
RhoA	Rabbit, monoclonal	Cytoskeleton	ARH04	WB 1:500
Smoothened	Rabbit	Biozol	GTX60154	IP 5 µg/ml
Smoothened (amino acids 190-240)	Rabbit	Thermo Scientific	PA1-41500	IHC 1:100, PLA 1:100
Vitronectin (amino acids 1-270)	Rabbit	Santa Cruz Biotechnology	sc-15332	IHC 1:100

Table 3.3. List of secondary antibodies used in this study.

Conjugate	Host	Specificity	Company	Dilution
Cy3	donkey	anti-goat	Dianova	1:200
Cy3	donkey	anti-rabbit	Dianova	1:200
Cy2	donkey	anti-rabbit	Dianova	1:200
Cy2	donkey	anti-mouse	Dianova	1:200
Cy5	donkey	anti-rabbit	Dianova	1:200

Cy2	donkey	anti-goat	Dianova	1:200
HRP	donkey	anti-goat	Dianova	1:15,000
HRP	goat	anti-rabbit	Dianova	1:20,000

3.10 Chemicals and supplies

All chemicals, reagents and kits were purchased from the following companies: Abcam (Cambridge, UK); Bayer (Leverkusen, Germany); Acris (Herford, Germany); Bio-Rad Laboratories (Munich, Germany); BioCat (Heidelberg, Germany); BioVision (Milpitas, CA, USA); Biozol (Eching, Germany); Calbiochem-Novabiochem (Bad Soden, Germany); Carl Roth (Karlsruhe, Germany); Chemicon via Millipore; Clontech (Heidelberg, Germany); Corning (Wiesbaden, Germany); Covance (Princeton, NJ, USA); Cytoskeleton (Denver, CO, USA); Dianova (Hamburg, Germany); Eppendorf (Hamburg, Germany); Eurogentec (Saint Jean, Belgium); Fluka (Deisenhofen, Germany); GE Healthcare (Braunschweig, Germany); GeneTex (Irvine, CA, USA); Life Technologies (Darmstadt, Germany); Greiner Bio-One (Solingen, Germany); Hassa (Lübeck, Germany); Macherey-Nagel (Düren, Germany); Merck Chemicals (Darmstadt, Germany); Metabion (Munich, Germany); Millipore (Schwalbach, Germany); NEB (Frankfurt am Main, Germany); PAN-Biotech (Aidenbach, Germany); Pineda (Berlin, Germany); Promega (Mannheim, Germany); Qiagen (Hilden, Germany); Roche Diagnostics (Mannheim, Germany); R&D Systems (Wiesbaden, Germany); Sarstedt (Nümbrecht, Germany); Serva (Heidelberg, Germany); Santa Cruz Biotechnologies (Dallas, USA); Schafer-N (Copenhagen, Denmark); Sigma-Aldrich (Deisenhofen, Germany); SRU Biosystems (Woburn, MA, USA); Synaptic Systems (Göttingen, Germany); Tebu (Offenbach, Germany); Thermo Fisher Scientific (Ulm, Germany); VWR International GmbH (Darmstadt, Germany); Wako Chemicals (Neuss, Germany).

4 METHODS

4.1 Biochemical methods

4.1.1 Preparation of cerebellar homogenates and cell lysates

Cerebella from C57BL/6J mice of different ages were homogenized in ice-cold RIPA or TE buffer (1 ml of buffer per one brain) containing protease inhibitor cocktail (Roche Diagnostics) using a Dounce homogenizer (Wheaton, Millwille, USA). Homogenates were cleared by centrifugation (1,000 g, 10 min, 4˚C). Postnuclear fractions were further pelleted (17,000 g, 20 min, 4˚C) and resuspended in a small volume of homogenization buffer.

Cell cultures were placed on ice, cell culture medium was removed and cells were lysed in ice-cold RIPA buffer containing protease inhibitor cocktail (480 µl per one 6-well plate) and scraped off with cell scrapers (Sarstedt). The cell lysates were collected and cleared and membrane fractions were separated from cytosolic fractions as described above.

4.1.2 Determination of the protein concentration

The protein concentration was determined using the Bicinchoninic acid (BCA) Protein Assay Reagent Kit (Thermo Fisher Scientific). 10 µl of the samples (diluted 5 and 10 times) were placed in a microtiter plate and incubated for 30 min at 37°C with 200 µl of the Solution A and B mixed in a ratio of 1:50. Bovine serum albumin (BSA) solutions ranging from 50 µg/ml to 2 mg/ml were used as standards. The absorbance was measured at 562 nm using the µQuantTM microplate spectrophotometer (Bio-Tek Instruments., Bad Friedrichshall, Germany). The protein concentrations were determined from the calibration absorbance curve of the BSA standards.

4.1.3 Sodium Dodecyl Sulfate-Polyacrylamide Gel Electrophoresis (SDS-PAGE)

Separation of proteins was performed by sodium dodecyl sulfate-polyacrylamide gel electrophoresis (SDS-PAGE) using the Mini-Protean II system (Bio-Rad). Protein samples were diluted in ddH_2O to reach the same concentration (1 mg/ml) and mixed with SDS-sample buffer. Proteins were then denatured at 95°C for 5 min and loaded on Tris-glycine SDS polyacrylamide gels (20 µg of diluted protein sample per lane). Gel concentrations were between 10-12 %, depending on the molecular weight of the protein of interest. Gel runs were performed using running buffer at a constant voltage of 80 V until the bromphenol blue dye

reached the border between stacking and running gel and then at 140 V until the bromphenol blue front reached the bottom of the running gel. The Precision Plus Protein All Blue Standard was used as molecular weight standard (BioRad). Gels were either subjected to Western Blot or stained with Coomassie Brilliant Blue.

4.1.4 Western blot analysis

Proteins were transferred from the SDS-PAGE gel either onto 0.45 µm nitrocellulose (GE Healthcare) or 0.45 µm polyvinylidene difluoride (PVDF, Millipore) membrane using the Mini-Protean II blotting system (Bio-Rad). The blotting sandwich was assembled as described in the manufacturer's protocol. In case of polyvinylidene difluoride membranes, membranes were incubated in methanol for 5 min prior to use. Proteins were transferred electrophoretically in blotting buffer at a constant voltage of 90 V for 2 hours at 4°C.

After electrophoretic transfer, the membranes were placed in glass vessels facing the protein-binding side up and blocked with 4% nonfat milk powder in TBS-T for 1 h at room temperature. The membranes were washed once with TBS-T and incubated overnight at 4°C with appropriate primary antibodies diluted to their optimal/recommended concentration. Next day, membranes were washed 3 times for 5 min in PBST or TBST and incubated with HRP-coupled secondary antibodies (Dianova) for 2 h at room temperature. After washing 3 times for 10 min, proteins were visualized using ECL select or ECL prime reagents (Amersham, GE Healthcare) and the LAS 4000 Mini camera (GE Healthcare, Freiburg, Germany).

4.1.5 Coomassie staining of polyacrylamide gels

To visualize the proteins separated by the PAGE, gels were stained with the colloidal Coomassie staining using the RotiBlue kit (Carl Roth). After the electrophoresis, gels were incubated with Roti-Blue staining solution for 15 h with constant agitation. The gels were then washed 5x with ddH_2O to reduce the background and visualize the stained protein bands.

4.1.6 Immunoprecipitation

Cerebellar homogenates (500 µg of total protein) were incubated with protein A/G-agarose beads (Santa Cruz Biotechnology) for 2 h at 4°C with constant shaking. Beads were pelleted at 1,000 x g and supernatants were incubated with antibodies of interest or control Ig overnight

at 4°C with constant rocking. Next day, samples were incubated with 50 µl protein A/G-agarose beads for 1 h at room temperature. The beads were pelleted at 1,000 x g and washed 4 times with IP lysis buffer containing protease inhibitor cocktails by centrifugation at 1,000 x g for 30 s. The beads were boiled in SDS-PAGE sample buffer at 95°C for 5 min to elute bound proteins. Eluted proteins were then subjected to Western blot analysis.

4.1.7 RhoA activation assay

To estimate the activation of RhoA in cerebellar cells after different treatments, the RhoA activation assay kit (Cytoskeleton) was used. Dissociated cerebellar neurons were cultured for the first two days in X-1 medium containing 7.5 % fetal horse serum (VWR) and for the following three days in serum-free X-1 medium. Cells were treated with 20 µg/ml CHL1-Fc or 20 nM SANT-1 for 20 min, after which they were lysed with ice-cold lysis buffer provided in the kit, scraped and centrifuged (10,000 x g, 2 min, and 4°C). Supernatants were either directly used or snap frozen in liquid nitrogen. To pull-down RhoA protein, 1 mg of the supernatants was incubated with 50 µg of Rhotekin-RBD beads for 1 h at 4°C with gentle rocking. Rhotekin – the Rho effector protein – shows a high affinity to bind GTP-Rho via its Rho binding domain (RBD); that allows only active Rho protein to be precipitated from the cell lysate. After incubation, beads were pelleted (5,000 x g, 3 min and 4°C), washed with the washing buffer provided in the kit and pelleted again. Bound proteins were eluted by boiling the beads in SDS-PAGE sample buffer at 95°C for 5 min; eluted proteins were subjected to the Western blot analysis.

4.1.8 Caspase-3 assay

A colorimetric assay caspase-3 assay kit (BioVision) was used to determine the activity of caspase-3. The assay is based on a caspase-3 substrate comprising the DEVD sequence and the chromophore p-nitroaniline which is detected only after cleavage of the substrate. Dissociated cerebellar neuron cultures or transfected HEK cells were cultured for 6 days in X-1 medium containing 7.5 % fetal horse serum (VWR), or for 24h in DMEM supplemented with 10% fetal calf serum (PAA Laboratories), respectively. After 6 days in culture the medium was exchanged by serum-free X-1 medium containing 20 µg/ml CHL1-Fc, 20 µg/ml L1-Fc, 20 nM SANT-1 or 20 nM tomatidine. HEK cells were transfected as described in the Chapter 4.5.5; after 6 h medium was changed and different treatments were applied directly into the medium. After treatment, both dissociated neurons and HEK cells were cultured for additional 24 h, then lysed for 10 min with the ice-cold lysis buffer provided in the Caspase-3 assay kit, scraped off and centrifuged at 10,000 x g for 3 min and 4°C. Protein concentrations of the supernatants

were measured and samples were diluted in lysis buffer to reach a concentration of 1 µg/µl. 2x Reaction buffer and 5 µl of labeled substrate were added to each sample and incubated 1 h at 37°C. Samples were transferred to a 96-well plate and the absorbance was measured using a spectrophotometer (Bio-Tek Instruments) at 405 nm wavelength.

4.1.9 Caspase-9 assay

To measure the activation of caspase-9 in cells, luminescence Caspase-Glo® 9 Assay (Promega) was used. The assay is based on caspase-9 cleavage of the luminogenic substrate containing the specific LEHD sequence and releasing of luciferase substrate aminoluciferin resulting in luciferase reaction and the production of light. The light emission was quantified using a luminometer (VICTOR³, PerkinElmer, Waltham, USA).

Dissociated cerebellar neurons were seeded on 96-well plates (Greiner), cultured and treated as described in Chapter 4.1.9. After the treatment cells were cultured for additional 24 h at 37°C and 5% CO_2. Prior to starting the assay, the 96-well plates and assay reagents were adjusted to room temperature. Caspase-Glo 9 reagent was added directly to the cells (ratio cell medium: reagent was 1:1) and incubated for 45 min at room temperature. The total reaction was transferred to a plate with white bottom (96-well plate; Corning) and the placed in the luminometer.

4.1.10 Enzyme-Linked Immuno-Sorbent Assay (ELISA)

Recombinant peptides or proteins (10 µg/ml) were immobilized on 384-well high-binding polystyrene plates (Corning), by overnight incubation at 4°C. Plates were rinsed with PBS^+ (PBS containing Ca^{2+} and Mg^{2+}) and incubated for 1 h at room temperature with PBS^+ containing 1% BSA to block unspecific binding. After a washing step with PBST, plates were incubated with the binding proteins diluted in PBS to reach a molar access to immobilized proteins in a range from 0.125 to 5 (1 h at room temperature). Plates were washeds five times for 5 min with PBST; and incubated with primary antibodies and HPR-conjugated secondary antibodies (both 1 h at room temperature). After washing five times for 5 min, wells were shortly incubated with the HRP substrate ortho-phenylenediamine dihydrochloride (OPD; Thermo Fisher). Color reaction was stopped with 2.4 M sulfuric acid and the absorbance was measured at 492 nm using a spectrophotometer.

4.1.11 Label-free binding assay (BIND assay)

To confirm a direct interaction between the extracellular domain of CHL1 present n the CHL1-Fc recombinant protein and specific domains of PAI-2, vitronectin and patched, a BIND assay was performed. The BIND assay (SRU Biosystems) is a label-free assay technology that detects direct protein-protein, protein-peptide, protein-compound, cell-cell or cell-compound interactions. BIND uses optical biosensors based on photonic crystals to measure the kinetic adsorption of biomolecular materials through their greater dielectric permittivity at optical wavelengths compared to water. With these sensors it is possible to determine the affinity and kinetics of a wide variety of molecular interactions without the need for a molecular tag or label (Cooper, 2002; Cunningham et al., 2004).

384-well microplates with a nanostructured optical grid (narrowband guided-mode resonance reflectance filter) are used as biosensor. Upon illumination with broadband light the optical grid reflects only a narrow range of wavelengths of light - Peak Wavelength Value (PWV). After immobilizing the biomolecule on the optical grid, the PWV increases. If the immobilized molecule binds an added ligand a shift in the PWV is detected. Thus, measurement of the PWV shift over time is directly proportional to the mass of the bound molecule (Cunningham et al., 2004).

384-well plates with titan oxide (TiO_2) surface (SRU Biosystems) were rinsed three times with PBS^+. Plates were then coated either with CHL1-Fc or with patched, vitronectin or PAI2 recombinant proteins (overnight at 4°C). Wells were rinsed three times with PBS^+ and PWV shift was measured on the BIND PROFILER reader (SRU Biosystems). Wells were then blocked with 2% BSA in PBS^+ (3 h at room temperature), rinsed three times and PWV shift was measured. Different concentrations of ligands were added to the wells and binding of ligands to the immobilized proteins was measured every 30 s for 1 h at room temperature. PWV shifts determined from wells without ligands were taken as background value and subtracted from values determined after addition of the ligands.

4.1.12 RNA isolation from brain homogenates

Brains from 2-day-old mice were homogenized in 200 µl RIPA buffer and the volume was adjusted to 0.25 ml by adding RNase-free water (QIAGEN). 750 µl of Trizol (TRIzol LS Reagent, Invitrogen) was slowly added to the samples and samples were homogenized with a power homogenizer (Wheaton, Millwille, USA) and centrifuged at 12,000 x g for 10 min at 4°C. The supernatants were transferred to a new tube, and incubated for 5 min at the room

temperature; 0.2 ml chloroform was added and the samples were mixed by inverting the tube 10 times and centrifuged at 12,000 x g for 15 min at 4°C. The clear aqueous upper phases containing RNA were carefully collected without touching the interface and added into a new tube. 0.5 ml isopropanol was added to the samples, incubated at the room temperature for 10 min and centrifuged at 12,000 x g for 10 min at 4°C. Supernatants were discarded and pelleted RNA was dissolved in 100 µl of RNase-free water and incubated in a thermo-mixer (Eppendorf, Hamburg, Germany) at 55°C for 25 min.

RNA was further purified using the RNA cleanup protocol (RNeasy Mini Kit, Qiagen). 100 µl RNA was mixed thoroughly with 350 µl RLT buffer (with β-mercaptoethanol) and then diluted with 250 µl ethanol by pipetting up and down. 700 µl sample was applied to an RNeasy mini column in a 2 ml collection tube and centrifuged at 8,000 x g for 15 seconds at room temperature. RNA bound to the membrane of the column and the flow-through was discarded. This step was repeated by adding 350 µl of RW1 buffer onto the column. To digest remaining DNA, 80 µl DNase I incubation mix was added onto the column and the column was incubated at room temperature for 15 min. 350 µl of RW1 buffer was again added onto the column and the column was centrifuged as indicated before. RPE buffer containing ethanol was added to the column and the column was centrifuged (at 8,000 x g for 15 seconds); this cleaning step was repeated twice. To elute RNA from the column, the column was transferred to a new collection tube, 30 µl of RNase-free water was added directly onto the column and the column was centrifuged at 8,000 x g for 1 min. The RNA concentration in the eluate was determined at 260 nm using the NanoDrop 1000 spectrophotometer (Thermo Fisher Scientific). Purity of the sample was determined by the ratio between absorbance at 260 nm and 280 nm and the ratio between absorbance at 260 nm and 230 nm. A 260/280 ratio of ~2 is considered as pure for RNA. A 260/230 ratio may indicate the presence of co-purified contaminants and the excepted value is in the range from 2.0-2.2. RNA was either frozen at -80°C or directly used in reverse transcription.

4.1.13 RNA isolation from cell lysates

Cells were seeded at 1.5 x 10^6 cells/ml in 6-well plates and cultured in X-1 medium without serum in the incubator for 48 h (37° C, 5% CO_2 and 90% relative humidity). Different treatments were applied directly to the medium and cells were incubated for additional 24 h. The cells were rinsed with HBSS and RNA was isolated using the RNeasy Plus Mini Kit, (Qiagen). 600 µl RLT Plus Buffer containing β-mercaptoethanol (Sigma-Aldrich) were used to lyse the cells. Lysed cells were collected with a rubber cell scraper (Sarstedt) into an Eppendorf tube, pipetted up and down and vortexed to homogenize the lysates. Homogenized cell lysates were

transferred to DNA Eliminator spin columns, placed in a collection tube, and centrifuged at 8,000x g for 15 seconds. All following steps were conducted as described in Chapter 4.1.12, according to the RNeasy Plus Mini Kit protocol. The RNA was eluted with 30 µl of RNase-free water, and the concentration was measured and the reverse transcription was directly run after RNA isolation.

4.2 Molecular biology methods and cloning techniques

4.2.1 Reverse transcription

For first-strand cDNA synthesis 2 µg of the RNA template was mixed with 500 µg/ml oligo dT and dNTPs (10 mM each), and probes were heated at 65°C for 5 min. The mix was then chilled on ice for 2 min. 5 x First-Strand Buffer (SuperScript II kit), RNaseOUT (Invitrogen) and 0.1 M DTT (SuperScript II kit) were added to the mix and incubated for 2 min at 42°C. Finally, reverse transcriptase was added and the mixtures were incubated at 42°C for 50 min. The reaction was terminated by incubation at 70°C for 15 min. Samples were stored at -20°C.

4.2.2 PCR primer design and general principles of the In-Fusion cloning technique

The principle of the In-Fusion cloning technique is based on the property of the In-Fusion enzyme to fuse a PCR-generated insert and any linearized vector by recognizing 15 base pair (bp) homologous sequences at their ends. For that purpose, the In-Fusion HD Cloning Kit (Clontech) was used. PCR-generated inserts should include 15 base pair (bp) long extensions, both on their 5' and 3' ends, which are homologous to the 5' and 3' ends of the linearized vector. Therefore, to generate a PCR insert with 15 bp overhangs, special primers must be constructed so to include: 15 bp overhang on its 5' end that is homologous to 15 bp at one end of the linearized vector, followed with the 18-25 bp long sequence specific to the target PCR insert. Primers were design using the Clontech online In-Fusion tool. Primer melting temperature (Tm) was calculated as the Tm of the part of the primer including only target PCR insert, not the length of the whole primer. The Tm differences between forward and reverse primer were not more than 4°C.

4.2.3 Polymerase chain reaction (PCR)

The *in-vitro* amplification of DNA fragments using the PCR reaction was performed in the *SimpliAmp* Thermal Cycler (Life Technologies). To increase the fidelity and efficiency of the

PCR reaction, CloneAmp HiFi DNA Polymerase (Clontech) was used. Every PCR reaction contains: template DNA obtained from a plasmid or a first strand cDNA (less than 100 ng of DNA template per reaction), In-Fusion forward and reverse primers (10 µM concentration each), CloneAmp HiFi PCR premix and sterilized distilled water. 25 µl reactions were performed in 0.2 ml thin-walled tubes (Biozym). PCR cycling parameters are listed in Table 4.1.

Table 4.1. PCR conditions

Cycle step	Temperature	Time	Number of cycles
Initial denaturation	98°C	5 min	1
Denaturation	98°C	10 s	
Annealing	55°C	15 s	30
Extension	72°C	10 s/kb	
Final Extension	72°C	10 min	1
Cooling	4°C	Hold	

To detect amplified products, 5 µl aliquots of the PCR reaction were analyzed by agarose gel electrophoresis.

4.2.4 DNA agarose gel electrophoresis

Amplified PCR fragments were subjected to an agarose gel placed in a horizontal electrophoresis chamber (BioRad) and separated by application of a constant voltage (10 V/cm gel length). Agarose gels were prepared by heating the agarose (Invitrogen) in the 1x Tris-acetate-EDTA (TAE) buffer. Depending on the size of the expected PCR fragment, gels with a different concentration of agarose were prepared. PCR fragments up to 1 kb in length were separated with gels containing 2.5% agarose in 1 x TAE buffer, whereas PCR fragments longer than 1 kb and linearized plasmids were separated with gels containing 1% agarose in 1 x TAE buffer. To detect double-stranded DNA, Roti-Safe GelStain (Carl Roth) was mixed directly into the boiled agarose solution (5 µl Roti-Safe/100 ml agarose). Polymerized agarose gels were covered with 1 x TAE buffer and PCR fragments were added into the sample pockets. To

detect the size of the PCR products, GeneRuler 1 kb DNA Ladder (Thermo Fisher) was pipetted into one of the gel pockets. DNA sample buffer with the orange G dye was added to the DNA probes and the gel was run until the dye had reached the end of the gel. Gels were recorded with the E.A.S.Y. UV-light documentation system (Herolab, Wiesloch, Germany).

4.2.5 PCR fragment purification

For purification of DNA fragments from a PCR reaction, NucleoSpin® Gel columns or PCR Clean-up columns (Machery-Nagel) in the presence of chaotropic salt was used according to the manufacturer's protocol. The DNA was eluted with 30 µl elution buffer. The DNA concentration was determined using the NanoDrop 1000 Spectrophotometer (Thermo Fisher). The concentration of an 1 µl aliquot of purified DNA sample was calculated by measuring the absorbance at 260 nm. Purity of the sample was determined by a ratio between the absorbance at 260 nm and 280 nm and the ratio between the absorbance at 260 nm and 230 nm.

4.2.6 DNA fragment extraction from agarose gels

DNA bands were cut out with a sterile blade and placed in a clean Eppendorf tube. DNA fragments were extracted from the agarose gel by heating the gel to 70°C and using the NucleoSpin® Gel and PCR Clean-up Kit (Macherey-Nagel).

4.2.7 Restriction digestion

0.5 µg of a plasmid DNA was incubated with 0.5 µl restriction enzyme, 1 µl appropriate buffer and 1 µl BSA (concentration 10 mg/ml) in 10 µl reaction volume at the 37°C for 1 h. To linearize pQE30 plasmids, BamHI restriction enzyme and NEB3 buffer (New England BioLabs-NEB) were used. After incubation, enzymes were inactivated by incubation of samples for 20 min at 65°C. To determine the success of the reaction, both intact circular plasmid and the product of the restriction digestion were subjected to agarose gel electrophoresis. Linearized plasmid DNA was purified from the enzyme reaction as described above.

4.2.8 In Fusion cloning reaction

Once the linearized plasmid and DNA insert are purified, the In Fusion cloning reaction was performed as follows: 100 ng linearized plasmid and 100 ng insert (if the size is more than 0.5 kb) or 50 ng (if the size is less than 0.5 kb) were mixed with 2 µl of the 5 x In-Fusion HD Enzyme Premix (Clontech). If needed, deionized water was added to adjust the total reaction volume to 10 µl. The reaction was incubated for 15 min at 50°C and placed on ice afterwards. A small aliquot of the In-Fusion reaction was either used immediately to transform bacteria, or the In Fusion reaction was stored at -20°C until use.

4.2.9 Production of competent bacteria

E. coli bacteria were seeded on LB agar plates and grown overnight at 37°C. At the next day single colonies were inoculated in 50 ml of LB medium (containing antibiotics). Cells were grown at 37°C under constant agitation (~150 rpm) until the culture had reached an optical density (OD_{600}) of 0.35-0.45. Bacteria were placed on ice for 5 min and pelleted at 1,000 x g for 15 min at 4°C. After removal of the supernatant, the pellet was resuspended in 15 ml cold TBF1 buffer. After 30 min incubation on ice, the centrifugation was repeated. The bacterial pellet was resuspended in 4 ml cold TBF2 buffer and incubated for 15 min on ice. 50 µl aliquots of bacteria were frozen in liquid nitrogen and stored at –80°C.

4.2.10 Transformation of plasmid DNA into bacteria

Stellar competent cells were transformed with the In-Fusion reaction, NEB 5-alpha competent E. coli with the product of site-directed mutagenesis, while TOP10 and M15 E. coli were transformed with a purified plasmid following the same protocol. 3 µl of a plasmid/In-Fusion reaction was pipetted into an Eppendorf tube with 50 µl of bacteria and gently mixed. The tube was placed on ice for 30 min; then bacteria were heat-shocked for 45 s at 42°C and immediately after chilled down on ice for 2 min. SOC medium was added to the bacteria to adjust the total volume to 500 µl and bacteria were incubated for 1 h at 37°C (Thermomixer 5436; Eppendorf) with gentle shaking. Afterwards, 100 µl of the transformed bacteria were streaked on LB agar plates containing the appropriate antibiotic and grown overnight at 37°C. At the next day single colonies were isolated to inoculate 15 ml of LB medium and grown at 37°C under constant agitation (~150 rpm) until the cultures had reached an optical density of 0.4. 5 ml of the bacterial cultures were prepared for small scale plasmid isolation. The remaining 10 ml of the cultures were further grown in a larger volume of LB medium and prepared for large scale plasmid isolation.

4.2.11 Small scale plasmid isolation (Miniprep)

LB medium (5 ml, containing 100 µg/ml ampicillin or 25 µg/ml kanamycin) were inoculated with a single bacterial colony and incubated overnight at 37°C with constant agitation. Bacteria were pelleted at 11,000 x g for 30 s and lysed according to the NucleoSpin Plasmid kit (Macherey-Nagel) protocol. Plasmid DNA was liberated from bacteria by SDS/alkaline lysis and bound to the NucleoSpin columns. Pure plasmid DNA was eluted with alkaline elution buffer (5 mM Tris/HCl, pH 8.5).

4.2.12 Large scale plasmid isolation (Maxiprep)

10 ml of the overnight bacterial culture were transfer into a 1 l Erlenmeyer flask containing 300 ml of LB medium, 100 µg/ml ampicillin or 25 µg/ml kanamycin and cultured overnight at 37°C with constant agitation. To isolate large quantities of plasmid DNA the NucleoBond Xtra kit (Macherey-Nagel) was used. Cells were pelleted at 6,000 x g, for 15 min at 4°C and the cells were lysed as described in the manufacturer's protocol. The entire bacterial lysate was loaded onto the filter columns and cleared by gravity flow. Pure plasmid DNA was eluted from the columns with the provided buffer, precipitated with isopropanol, dissolved in nuclease-free water and stored at -20°C.

4.2.13 Sequencing of DNA

To prepare DNA samples for sequencing, 100 ng of sample DNA was diluted in 7 µl of ddH_2O and mixed with an appropriate primer (7 pM). Samples were analyzed using Step-by-Step protocols for DNA-sequencing with Sequenase-Version 2.0 (5th ed., USB, 1990) in the ZMNH sequence facility.

4.2.14 Site-directed mutagenesis

Mouse patched cDNA labeled with HA-tag cloned into the mammalian expression vector pRK-5 (a kind donation from Dr. Patrick Mehlen) served as template to generate pRK-5 vector carrying mouse patched with deleted first extracellular loop. The DNA sequence coding for the first extracellular loop of patched was deleted using the Q5 Site-Directed Mutagenesis technology *(*NEB). Primers were designed so that they flanked the sequence to be deleted – primers were in the opposite directions to each other and their 5' ends were adjacent to the

target sequence. Plasmids were then linearized and the target sequence was deleted performing the PCR reaction: Q5 Hot Start High-Fidelity 2X Master Mix, forward and reverse primers (10 μM) and 25 ng plasmid were mixed with nuclease-free water (adjust to reach a final volume of 25 μl). PCR conditions are given in a Table 4.2.

Table 4.2. PCR conditions

Cycle step	Temperature	Time	Number of cycles
Initial denaturation	98°C	30 s	1
Denaturation	98°C	10 s	
Annealing	50-72°C*	30 s	25
Extension	72°C	30 s/kb	
Final Extension	72°C	2 min	1
Cooling	4°C	Hold	

* Annealing temperature is a melting temperature (Tm) of a primer from a primer pair with a lower Tm.

Aliquots of the PCR products were subjected to agarose gel electrophoresis to analyze the size of linearized plasmid. PCR products that presents linearized plasmids were circularized using the enzyme mix (KLD mix-ligase, kinase, DpnI restriction enzymes). 1 μl of PCR product, 2 x KLD Reaction Buffer, 10 x KLD Enzyme Mix and nuclease-free water (adjust to reach a final volume of 10 μl) were gently mixed and incubated at room temperature for 5 min. 5 μl of ligase reaction was transformed into NEB 5-alpha competent *E. coli* using the protocol described above. Success of deletion was determined by DNA sequencing.

4.2.15 Expression and purification of recombinant proteins from *E. coli*

Expression of recombinant proteins in *E.coli* was performed by insertion of cDNA coding for the desired protein into the correct reading frame of an appropriate expression vector

(Sambrook et al., 1989). For this purpose, the cDNAs coding for the recombinant N-terminal vitronectin fragment or the recombinant N- and C-terminal PAI-2 fragments were cloned into the pQE30 plasmid using the In-Fusion cloning kit. Proteins were expressed as fusion proteins with 6 N-terminal Histidines. TheHis-tag sequence allows to purify proteins by Ni-NTA agarose affinity chromatography,

First, transformed *E. coli* M15 [pREP4] host cells were streaked out on LB plates supplemented with antibiotics (ampicillin and kanamycin). A 20 ml LB pre-culture with the appropriate antibiotic was inoculated with a single colony and incubated overnight at 37°C with constant agitation. Next day, the pre-culture was transferred to a 1 l Erlenmeyer flask containing 300 ml of LB medium and bacteria were grown at 37°C under constant agitation until the culture had reached an optical density of OD_{600} 0.6. Protein expression was induced by adding IPTG (1 mM) to the culture and further incubation for 4-6 h at 37°C. Bacteria were pelleted by centrifugation at 4,000 x g for 20 min and frozen on dry ice. Protein expression was monitored by removing small aliquots (1 ml) of the culture before starting the induction, and every hour after IPTG induction.

Afterwards, the bacterial pellets were thawed in cold water and lysed with lysis buffer (10 ml of buffer for 1 l of bacterial culture). Bacterial lysates were then sonicated 5 times for 20 s on ice using a sonicator (Branson Sonifier B 15, Emerson, Danbury, USA). To exclude bacterial debris, sonicated lysates were pelleted at 10,000 x g for 30 min. Pellets were discarded and bacterial proteins in the supernatant were incubated with Ni-NTA agarose beads (Qiagen) overnight at 4°C with the gentle agitation. Ni-NTA agarose beads with the bound protein were pelleted by centrifugation at 1,000 x g for 2 min. To reduce unspecific binding, beads were then washed for 30 min in washing buffers, starting with washing buffer 1 containing the lowest concentration of imidazole and finishing with washing buffer 4 containing the highest concentration of imidazole. Every washing step was followed centrifugation at 1,000 x g for 5 min. For elution of His-tagged proteins, elution buffer with 250 mM imidazole was used. His-tagged proteins were dialyzed and concentrated in PBS using appropriate Vivaspin 20 columns (GE Healthcare) for 30 min at 5,000 x g. Proteins were dissolved in PBS, subjected to SDS-PAGE and the gel was subsequently stained with Coomassie blue.

4.3 Real-time PCR

Primers for real-time PCR were selected from pre-designed primers in the mouse qPrimerDepot bank (https://primerdepot.nci.nih.gov/). Primer mix contained: 1 µl (10 µM) forward primer, 1 µl (10 µM) reverse primer, 1 µl 10x Reaction buffer, 1.4 µl $MgCl_2$ and 0.6 µl

nuclease free water, per one well. cDNA was diluted (1:10) in nuclease free water. SYBR Green (qPCR Core kit for SYBR Green I, Eurogentec) was diluted in 1 ml DMSO. Using the diluted SYBR Green, a master mix stock was created depending on the number of samples. Per one well, the master mix contained: 0.8 µl dNTPs, 1 µl 10x Reaction buffer, 0.6 µl SYBR Green, 0.1 µl Taq Polymerase (HotStart activatedTaq DNA polymerase, Eurogentec) and 7.5 µl of nuclease free water. 2x dilutions of cDNA were made, and 5 µl of cDNA samples were pipetted to each well. 5 µl of the primer mix and 10 µl of the master mix were then added. The plate was spun down and sealed, and real-time PCR was performed on the 7900HT Fast Real-Time PCR machine (Life Technologies).

For quantitative analysis of gene expression, four reference genes were used for normalization. Cycle threshold (Ct) values of the reference gene were subtracted from the Ct values of the target gene to obtain ΔCt values. ΔΔCt values were calculated by subtraction of ΔCt values of the target gene in the untreated group from the ΔCt value of the target gene in the treated group (Livak and Schmittgen, 2001). ΔΔCt values represent the fold change in expression of the target gene.

4.4 Histological methods and microscopy

4.4.1 Tissue preparation and sectioning

For tissue preparation and sectioning, 3-, 5-, 7-, 10- and 14-day-old CHL1 +/+ and CHL1 -/- mouse littermates were decapitated. Brains were quickly isolated and fixed in 4% paraformaldehyde solution overnight, then immersed and incubated in 15% sucrose solution (in 0.2 M cacodylate buffer) for cryoprotection and incubated in this solution for two days at 4°C. Afterwards, brains were frozen for 2 min in 2-methyl-butane precooled to -80°C and stored at -80°C for future use. Fixed VN -/- brains were received in15% sucrose solution.

Serial coronal sections of 25 µm thickness were cut in a cryostat (Leica CM3050, Leica Instruments) and collected on SuperFrost Plus glass slides (Carl Roth). The sections were then stored at −20°C.

4.4.2 Immunohistochemistry

For antigen retrieval, frozen fixed brain sections were incubated in sodium citrate solution (pH 9) for 30 min at 80°C. After cooling down, the sections were incubated in blocking solution containing normal donkey serum (1 h at room temperature) and primary antibodies diluted in

PBS-lambda-carrageenan solution (dilutions given in Table 3.2) for 2 days at 4°C in a humid chamber. After washing with PBS (3 x 5 min), sections were incubated with appropriate fluorescently labeled secondary antibodies (diluted 1:200 in PBS-lambda-carrageenan) in a humid chamber for 2 h at room temperature in the dark. Sections were washed in PBS (3 x 15 min), shortly dried and mounted with mounting solution containing the nuclear marker DAPI (Roti-Mount FluorCare DAPI, Carl Roth). For double or triple immune-labeling, sections were incubated with a mixture of primary antibodies and an appropriate mixture of pre-adsorbed secondary antibodies to eliminate cross-reactions with others species and with other immunoglobulin classes. As a negative control, sections were incubated only with PBS-lambda-carrageenan. Staining with CHL1 and vitronectin antibodies was controlled by staining CHL1 -/- and VN -/- brain sections, with the resulting lack of fluorescent signal.

4.4.3 Proximity ligation assay

The proximity ligation assay (PLA) technology allows detection and quantification of individual proteins, protein modifications and close protein interactions in tissues or cells. Species-specific secondary antibodies are labeled with a pair of oligonucleotide-PLA probes that generate a signal only when the two primary antibodies bound to their antigens in close proximity. The signal from each detected pair of PLA probes, visualized as an individual fluorescent spot, is amplified using the PCR strategy (Fredriksson et al., 2002).

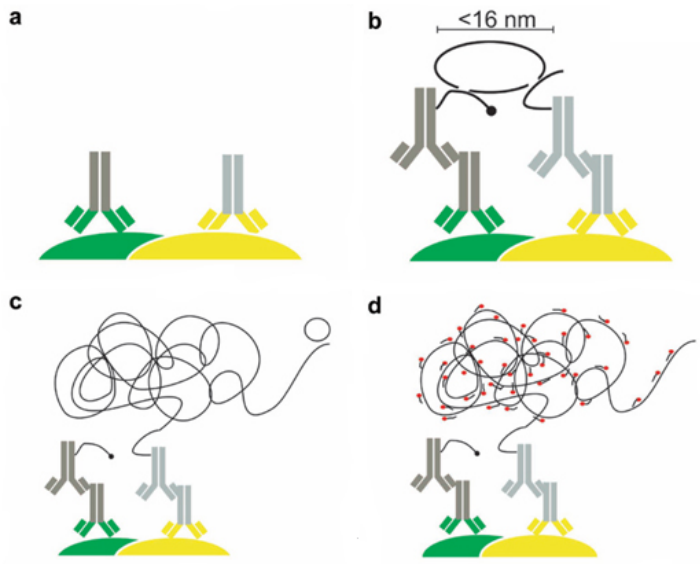

Figure 4.1. The principle of the proximity ligation assay. (a) Two antigens of interest (green and yellow) are detected by primary antibodies raised in different species (dark grey/green and light gray/yellow). (b) Each species-specific secondary antibody (dark and light gray) that recognizes one of

the primary antibody is labeled with oligonucleotides (black line). When the secondary antibodies are in close proximity (maximum 16 nm), the oligonucleotides hybridize to the homologues sequences of the two other circle-forming oligonucleotides (circular black line). (c) After enzymatic ligation, the two added oligonucleotides are amplified using a polymerase. One of the oligonucleotides acts as a primer for a rolling-circle amplification using the ligated circle as a template, generating a repeated sequence. (d) Fluorescently labeled oligonucleotide probes are added to highlight the product (red circles). The figure was adapted from Trifilieff et al. (2011).

Frozen brain section from mice of postnatal day 5, 7, 10 and 14 were labeled using Duolink *In situ*-Fluorescence kit (Sigma-Aldrich). After antigen retrieval, brain sections were incubated in the blocking solution in a humid chamber at 37°C for 30 min. Appropriate primary antibodies were diluted (dilutions given in the Table 3.2) in the antibody diluent solution and incubated with the sections in a humid chamber at 4°C for 2 days. Following washing (2 x 5 min, with washing buffer A), sections were incubated with two PLA probes – plus and minus PLA, each diluted 1:5 in the antibody diluent solution, in a humid chamber at 37°C for 1 h. Sections were then washed (2 x 5 min, with washing buffer A) and the ligation step was conducted at 37°C for 30 min using ligation solution diluted 1:5 and ligase diluted 1:40 in nuclease free water. After washing, the amplification mix containing amplification solution diluted 1:5 and polymerase diluted 1:80 in nuclease free water was added onto the sections and sections were incubated in a dark humid chamber at 37°C for 100 min. Sections were washed first with 1x washing buffer B (2 x 10 min) and then with 0.01x washing buffer B for 1 min, mounted with Duolink In Situ Mounting Medium with DAPI (Sigma-Aldrich) and stored at -20°C.

4.4.4 *In situ* cell death detection assay (TUNEL assay)

The characteristic event that occurs in the late stages of apoptosis is an extensive DNA degradation, when the chromosomal DNA is cleaved into oligonucleosomal fragments. TdT-mediated X-dUTP nick end labeling (TUNEL) assay is based on the ability of terminal dexoynucleotidyl transferase (TdT) to label blunt ends of double-stranded DNA breaks, independently of the template (Kyrylkova et al., 2012). Since the dUTP polymers have incorporated tetramethylrhodamine (TMR), a fluorescent label, this assay allows detection and quantification of TMR signal incorporated into DNA breaks by fluorescence microscopy (*In situ* Cell Death Detection Kit, TMR red, Roche). The assay was applied on histological sections from CHL1 +/+ and CHL1 -/- mice, postnatal day 10 and 14, to quantify and compare the number of apoptotic cells between genotypes.

Frozen brain sections were dried at room temperature for 15 min and washed with PBS (2 x 2 min). Immediately before incubating with the brain sections, the enzyme solution was mixed

with the label solution, applied onto sections (50 µl of TUNEL mixture per section) and left in a dark humid chamber to incubate for 1 h at 37°C. Sections were washed in PBS (3 x 15 min) and mounted with Roti-Mount FluorCare DAPI (Carl Roth). As a negative control instead of the TUNEL mixture, sections were incubated only with the label solution.

To label apoptotic cells with an appropriate tissue marker, TUNEL assay and immunohistochemistry were combined: after antigen retrieval, sections were incubated with TUNEL mixture, washed with PBS, incubated in blocking solution and then in a primary antibody solution (as described in the chapter 4.4.2). When combining TUNEL assay and immunohistochemistry, fluorescently labeled secondary antibodies had to have a different excitation and emission wavelength than TMR red.

4.4.5 Microscopy and image processing

Images were taken on the Olympus Fluoview FV1000 confocal laser-scanning microscope equipped with the Fluoview software package, in sequential mode with 60x objective. Images were processed for brightness and contrast using Adobe Photoshop CS5 software (Adobe Systems Inc.).

4.4.6 Co-localization analysis

To quantify the degree of co-localization between CHL1 and vitronectin, and CHL1 and PAI-2, the co-localization toolbox JACoP (Just Another Colocalization Plugin) included in the ImageJ software package was used (Bolte and Cordelieres, 2006). Images were reconstructed along the z-axis in three-dimensional images using the ImageJ software. The threshold for each image, from the red and green channel separately, was measured. The pixel gray values of each image from the red channel were plotted against the pixel gray values of each image from the green channel using the JACoP toolbox. For every dual-channel image a pixel distribution diagram was obtained. From the distribution diagrams, the Pearson's coefficient (PC) and the Mander's overlap coefficients (M1 and M2) were calculated. PC gives the information about the linear correlation between pixel intensity in the green and red images. M1 is the ratio of the summed intensities of pixels from a red image, for which the intensity in the green channel is in the range from zero to the maximal intensity, and M2 is defined conversely for a green image (Bolte and Cordelieres, 2006). The coefficient values are ranging between -1 and +1, where -1 is a total negative correlation, 0 is no correlation, and +1 is a total positive correlation.

4.4.7 Stereological analysis

Cell densities were estimated using the optical dissector method (Gundersen, 1986). Counting was performed on the Axio Imager.M1 microscope (Carl Zeiss) equipped with a motorized stage and Stereo Investigator 9 software-controlled computer system (MicroBrightField). Sections containing cerebellum were analyzed with a 10 x objective to delineate cerebellar layers by nuclear staining. Two fields of cerebellar cortex, one in the most caudal folium in the section and one in the third folium rostral to the first one, containing well defined morphological layers, were delineated using the Stereo Investigator software. These fields including the external granular layer, the internal granular layer, the molecular and the Purkinje cell layers were extended for 600 µm on both sides of the sagittal plane. Four sections (25 µm thickness; every 10th serial section) of the cerebellum were analyzed. Numerical densities were estimated by counting Ki67- (proliferating cells), NeuN- (neurons), Pax6- (glial cells), caspase-3- or TUNEL- (apoptotic cells) labeled cells within systematically randomly spaced optical dissectors. The parameters for this analysis were as follows: guard space depth 2 µm; base and height of the dissector 900 µm² and 10 µm, respectively; distance between the optical dissectors 90 µm; and objective 20 Plan-Neofluar 20/0.50.

4.5 Cell culture methods and assays

4.5.1 Primary culture of dissociated cerebellar neurons

Preparation of the dissociated cerebellar neurons was as described (Schnitzer and Schachner, 1981). Briefly, seven-day-old mice were decapitated and cerebella were isolated and transferred into a Petri dish with the ice-cold HBSS. Cerebella were cleaned from meninges using fine forceps under a dissection microscope. Clean cerebella were transferred into a new Petri dish with HBSS and each cerebellum was cut with a blade into three pieces. The following steps were performed under the sterile conditions in a laminar flow hood: Cerebella pieces were placed into a 15 ml Falcon tube and washed once with ice-cold HBSS (5 ml HBSS per 3 cerebella). Buffer was removed and pieces were incubated in trypsin/DNase solution at room temperature for 15 min (1 ml trypsin/DNase per 3 cerebella). Following three washing steps with HBSS, DNase solution was added (1 ml). Cerebella pieces were then passed through rounded fire polished Pasteur pipettes of different size, starting from the largest (10 times up and down with each pipette). Dissociated cells were suspended in HBSS and left on ice for 5 min. Cells were then centrifuged at 100 x g and 4°C for 15 min and the resulting cell pellet was resuspended in pre-warmed X-1 medium (5 ml X-1 per 3 cerebella). The X-1 medium was

either with or without fetal horse serum depending on the experiment. Cell concentrations were determined by mixing 10 µl of the cell suspension with 10 µl of a 0.4% Trypan blue solution and cells were counted in a hemocytometer.

Cells were seeded on poly-L-lysine (PLL) coated 6-, 12-, 24- or 96- well plastic cell culture plates (Greiner) or sterile plastic tissue culture coverslips (13 mm, Sarstedt). For coating of PLL, the surface was covered with sterile PLL (0.01 % PLL in autoclaved ddH_20) and incubated overnight at 4°C with or without gentle shaking. The next day, PLL was removed and the surface was first dried under the laminar flow hood and finally left under UV-light for 15 min. Before plating, cells were diluted in X-1 medium depending of the type of the experiment – for cell death and caspase assay 10^6 cells/ml; for Western blot, RhoA activation assay and RNA isolation 1.5 x 10^6 cells/ml; for neurite outgrowth 2.5 x 10^5 cells/ml. Cells were cultured at 37°C, 5% CO_2 and 90% relative humidity for different duration of time; the medium was changed every third day and different treatments were applied directly in the medium. Concentrations of the proteins and inhibitors are given in the Table 4.3.

Table 4.3. Concentrations of reagents applied in the cell culture medium

Protein/Inhibitor	Final concentration
CHL1-Fc	20 µg/ml
L1-Fc	20 µg/ml
SANT-1	20 nM
Tomatidine	20 nM
RhoA inhibitor (Y16)	10 µM
ROCK inhibitor (Y-27632)	10 µM

4.5.2 Neurite outgrowth assay

Dissociated cerebellar cells were seeded on the PLL-coated plastic coverslips as described previously (Makhina et al., 2009). Shortly before seeding of the cells, coverslips were rinsed

with the medium and placed in a 12-well plate. Different reagents/ compounds were applied directly in the culture medium (X-1 medium without serum) and plates were left in the incubator for 24 h (37°C, 5% CO_2 and 90% relative humidity). Cells were fixed by adding 100 µl 25% glutaraldehyde to 1 ml of medium for 1 h at room temperature. After washing with PBS, cells were stained with 1% toluidine blue and 1% methylene blue in 1% sodium-tetraborate buffer for 2 hours at room temperature. Cells were washed twice with PBS, placed onto filter paper and dried at room temperature. Coverslips were then mounted on the glass slide using Eukitt mounting solution (Fluka). Cells were imaged with an Axiovert microscope (Carl Zeiss) and their neurite length was measured using AxioVision 4.6 software (Carl Zeiss). For each experimental condition, at least 100 cells with neurites longer than the cell body diameter were measured.

4.5.3 Microexplant culture of cerebellar neurons

Migration of granule cells was measured in microexplant cultures from mouse cerebella as described previously (Fischer et al., 1986). Cerebella were isolated from 6– to 8-day-old old mice, cleaned from meninges, cut into three pieces and transferred into ice-cold HBSS. Pieces were then washed in HBSS three times and pressed through a metal net with a pore width of 300 µm – resulting in cerebellar microexplants. Microexplants were washed three times in HBSS. They were re-suspended in X-1 medium containing 20% FBS (1 ml of medium per cerebellum) and seeded on PLL-coated plastic coverslips (80 µl explant solution per 13 mm coverslip). Shortly before seeding explants, coverslips were rinsed with the medium and placed onto sterilized Parafilm foil in a culture Petri-dish (145 x 20 mm, Greiner). Microexplants were cultured in the incubator for 16 h (37°C, 5% CO_2 and 90% relative humidity) to adhere. Afterwards, coverslips with explants were gently transferred into 12-well plates; 1 ml X-1 medium without serum was added slowly in each well and different treatments were applied directly in the medium. Microexplants were cultured in the incubator for additional 24 h. Explants were fixed in 2.5% glutaraldehyde for 1 h at room temperature. Following a washing steps with PBS, cells were stained with 1% toluidine blue and 1% methylene blue in 1% sodium-tetraborate buffer for 2 h at room temperature. Cells were washed twice with PBS, placed onto filter paper and dried at room temperature. Coverslips were then mounted on glass slides using Eukitt (Fluka). Microexplants were imaged with an Axiovert microscope (Carl Zeiss). Cell migration was quantified by measuring the number of cell bodies in defined distance intervals of 10 explants per condition using the Multi-point Tool of the ImageJ software.

4.5.4 Maintenance and long-term storage of HEK cells

HEK293 cells were cultured in the incubator at 37˚C, 5% CO_2 and 90% relative humidity. DMEM culture medium was changed every second day and the cells were passaged when they reach approximately 70% of confluence. For passaging, cells were washed with pre-warmed HBSS and then incubated with Trypsin-EDTA solution in the incubator until they detached from the surfaces. Trypsin activity was then stopped by adding serum containing culture medium, cells were then centrifuged (1,000x g, 5 min, at room temperature), re-suspended in culture medium and split in a 1:5 ratio.

For long-term storage, cells were grown to 70% confluence, detached by addition of Trypsin-EDTA solution and re-suspended in DMEM containing freezing medium, in 1 ml aliquots containing 10^7 cells. Tubes with cells were then placed in containers with isopropanol and frozen in a -80˚C freezer. After couple of days, cells were transferred to a liquid nitrogen tank. If necessary, frozen cells were thawed again and quickly re-suspended in pre-warmed DMEM medium, centrifuged as described above and cultivated in DMEM culture medium.

4.5.5 Transient transfection of HEK cells

For transient transfection of HEK cells with the pRK-5 plasmid carrying the mouse patched sequence, Lipofectamine LTX & Plus Reagent (Invitrogen) was used. Two days before transfection, cells were passaged and seeded in 6- or 24-well plates. Lipofectamine LTX & Plus reagent and plasmid DNA were diluted in DMEM medium without serum, according to the manufacturer´s manual. After 30 min, the solution was applied directly in the cell medium and cells were maintained in the incubator. After 5-6 h, medium was exchanged, different treatments were added and cells were cultured for further 24 h.

4.5.6 Cell death assay

Cultures of dissociated cerebellar neurons were maintained on 24-well plates in X-1 medium with 7.5% horse serum for 5 days, then medium was exchanged to serum free X-1 medium and different reagents were applied directly to the cells. After 48 h, cells were incubated with 1 µl of 1 µg/ml calcein (Molecular Probes) and 1 µl of 1 µg/ml propidum-iodide (Sigma-Aldrich) for 30 min at 37°C; cells were then immediately imaged with an Axiovert microscope (Carl Zeiss). Pictures of five randomly chosen areas per well were taken with the AxioVision 4.6 software (Carl Zeiss). Cell viability was determined by counting calcein-positive (viable) and propidium-iodide-positive (dead) cells using the Analyze Particle tool of the ImageJ software.

Number of dead cells was calculated as a percentage of the total number of cells (dead and viable) per well. For each treatment four wells were evaluated.

The same procedure was applied on the transfected HEK cells, 24 h after their transfection.

4.6 Organotypic slice culture

4.6.1 Isolation and maintenance of cerebellar organotypic slices

To generate cerebellar organotypic slice cultures 7-day-old CHL1-/- mice were used. The preparation protocol was modified from Stoppini et al. (1991). All steps were conducted under semi-sterile conditions in a horizontal laminar flow.

Mice were decapitated and the brains were isolated and placed in a Petri-dish with the ice-cold preparation medium under a dissection microscope. The cerebellum was carefully separated from the rest of the brain using a sterile blade. The cortex was fixed with forceps and the medulla oblongata was separated from the rest of the brain, then the cerebellum and the pons was separated from the rest of the brain, and finally the cerebellum was separated from the pons. To preserve original layer organization, the cerebellum was not cleaned from meninges but immediately transferred to a sterile stage placed on a tissue chopper (McIlwain Tissue chopper, Ted Pella inc., Redding, USA). The cerebellum was sliced in 300 µm thick sections, and slices were carefully collected using two spatulas and transferred to a new Petri-dish (containing ice-cold preparation medium). Since the slices were sticking to each other, they were placed on one spatula, one drop of medium was added on top, and the other spatula was gently sliding over the liquid surface using only surface tension to separate the slices. The slices were one by one placed on a Millicell cell culture insert (Millipore) using spatulas (maximum four slices per one insert). Inserts were placed in 6-well plates with pre-warmed incubation medium (1.2 ml of medium per well), so that they floated on the surface of the medium.

The slices were cultured in the cell culture incubator at 37°C, 5% CO_2 and 90 % relative humidity for 7 days. Incubation medium was changed every third day. On the 5th day the medium was exchanged with serum-free medium, different reagents were added directly in the medium, and the inserts with cerebellum slices were incubated for additional 48 h. Concentrations of the reagents are given in Table 4.4.

Table 4.4. Concentrations of reagents applied in the culture medium

Protein/Inhibitor	Final concentration
CHL1-Fc	120 µg/ml
L1-Fc	120 µg/ml
SANT-1	120 nM
Tomatidine	120 nM
RhoA inhibitor (Y16)	60 µM
ROCK inhibitor (Y-27632)	60 µM

4.6.2 Immunohistochemistry, TUNEL assay and stereological analysis

After culturing organotypic cerebellar slices for seven days, they were stained using a modified protocol (Gogolla et al. 2006).

Slices were washed once with PBS and 4% PFA in PBS was added (1 ml above and 1 ml beneath the cell culture insert, as for all following steps) to fix the slices for 1 h at room temperature. Following washing steps with PBS, slices were incubated in cold 20% methanol in PBS for 5 min, and washed again in PBS. Permeabilization was conducted with 0.5% Triton X-100 in PBS at 4°C for 2 days. Sections were blocked with 20% BSA in PBS overnight at 4°C. To reduce the volume of antibody solution, the slices were cut off the inserts (1-2 mm of insert was left around the slice) and transferred with forceps to a 48-well plate with the top side of the insert facing up. Slices were either incubated in antibody solution or first TUNEL-labeled.

TUNEL assay was conducted as described in the Chapter 4.4.4. Each slice was incubated with 50 µl of the TUNEL mix in the dark at 37°C for 1 h and then washed with PBS (3 x 10 min). Incubation with a primary antibody solution was immediately following (incubation was conducted in the dark).

An appropriate primary antibody, or a mixture of two antibodies, was diluted in 5% BSA in PBS (dilutions given in a Table 3.2) and incubated with the slices for 2 days at 4°C. Following washing (3 x 10 min with PBS), slices were incubated in the secondary antibody or a mixture of two antibodies (diluted 1:200 in 5% BSA in PBS) in the dark for 3 h at room temperature.

After washing (3 x 10 min with PBS), slices were transferred on glass slides with the top side of the insert facing up and mounted with a drop of DuoLink In Situ Mounting Medium with DAPI (Sigma-Aldrich).

Cell density of caspase-3 and TUNEL labeled cells was compared between the slices treated differently using the optical dissector method described in Chapter 4.4.7. Counting was performed on the Axio Imager.M1 microscope (Carl Zeiss) equipped with a motorized stage and Stereo Investigator 9 software-controlled computer system (MicroBrightField).

4.6.3 Cell death assay

To estimate the effect of different treatments on cell survival after seven days in the culture, organotypic cerebellar slices were stained with calcein and propidium iodide. Slices were incubated with 6 µl of 1 µg/ml calcein (Molecular Probes) and 6 µl of 1 µg/ml propidum iodide (Sigma-Aldrich) for 30 min at 37°C, as described in the Chapter 4.5.6. Immediately afterwards, slices were imaged with the BZ-9000 Keyence laser microscope. Cell viability was determined by counting calcein-positive (viable) and propidium iodide-positive (dead) cells, using the Hybrid Cell Count software (Keyence). The number of dead cells was calculated as the percentage of the total number of cells (dead and viable) per well. For each treatment five images of each slice were evaluated.

4.7 Statistical analysis

All numerical data are presented as group mean values with standard error of the mean (SEM) or standard deviations (SD). Statistical tests used for comparisons are indicated in the text and figure legends. The threshold value for acceptance of differences was 5%. Analyses were performed using the IBM SPSS Statistics 23 software package.

5 RESULTS

5.1 Interaction of CHL1 with vitronectin and plasminogen activator inhibitor-2 regulates cerebellar development during the first postnatal week

Based on previous data showing an increased number of migrating granular cells in the molecular layer of the CHL1-deficient cerebellar cortex at the end of the first postnatal week and the loss of granular and Purkinje cells in the adult CHL1-deficient mice relative to wild-type control (Jakovcevski et al., 2009), we were searching for the cellular mechanisms and potential interaction partners of CHL1 that can explain these phenomena. In this part of the results, I am presenting already published data obtained by my colleagues and myself (Katic et al., 2014).

5.1.1 CHL1 binds directly to vitronectin via its extracellular domain

To identify novel interaction partners of CHL1, we used a biochemical cross-linking method. The extracellular part of mouse CHL1 fused to the Fc part of human IgG (CHL1-Fc) was used as “bait” in this experiment, while the extracellular domain of the amyloid precursor protein fused to human Fc (APP-Fc) was used as control. Trifunctional biotin-carrying crosslinker sulfo-SBED was coupled to the Fc proteins. The crosslinker conjugates were immobilized on protein A-coupled beads, incubated with a synaptosomal fraction and exposed to UV light leading to covalent attachment to bound “prey” proteins. Elution under reducing conditions led to release of the bound prey proteins from the bait and transfer of the biotin tag from the conjugated crosslinker to the prey proteins. Eluted proteins were separated by subjected to SDS-PAGE and Western blot analysis using peroxidase-conjugated streptavidin or silver staining (Katic et al., 2014).

Six major biotinylated proteins with molecular masses of ~40, ~50, ~60, ~70, ~165 and ~200 kDa were detected in the eluates from the CHL1-Fc beads, while only three major biotinylated proteins of ~40, ~110 and ~190 kDa were detected in the eluates from APP-Fc beads (Fig. 5.1 A). The ~165 and ~200 kDa bands in the CHL1-Fc eluate and the ~190 and ~110 kDa bands in the APP-Fc eluate were detected by HRP anti-human Fc antibody (Fig. 5.1 A), indicating that these Fc labeled proteins derived from the bait proteins. Upon silver staining, the protein bands with molecular masses of ~40, ~50, ~60, ~70 kDa were observed in the eluate from CHL1-Fc beads (Fig. 5.1 A), while only the bands of ~40 and ~50 kDa were observed in the eluate from APP-Fc beads. Thus, the ~60 and ~70 kDa proteins are exclusively CHL1-binding proteins. The silver stained ~60 and ~70 kDa protein bands were subjected to mass spectrometry and two of the detected peptides from the ~70 kDa band could be assigned to vitronectin (Preissner and Reuning, 2011), while the ~60 kDa band could not be assigned to a

known protein. The MS/MS spectrum of a 1645.8 and 1384.86 Da precursor mass (detected as doubly charged ion at m/z=823.4 and 692.93) matched the tryptic peptide DVWGIEGPIDAAFTR (1644.79 Da) and INCQGKTYLFK (1385.72 Da) of mouse vitronectin. Biochemical cross-linking experiment and mass spectrometry were performed by Nicole Karl and Friedrich Buck, respectively.

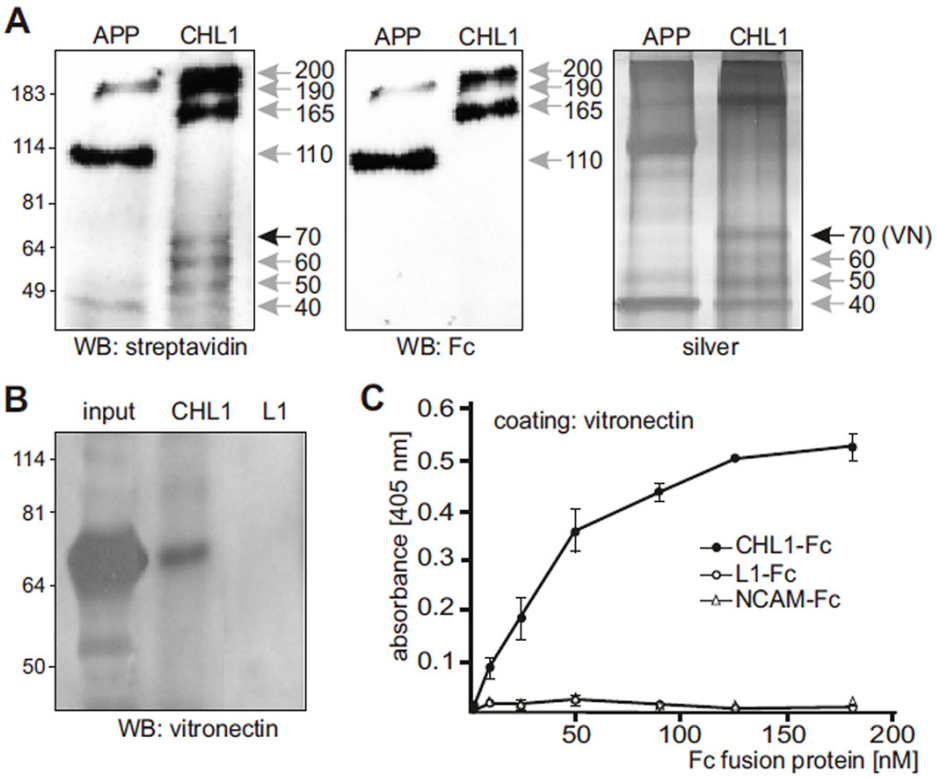

Figure 5.1. CHL1 interacts with vitronectin via its extracellular domain. ***A,*** CHL1-Fc and APP-Fc proteins were conjugated to the biotin labeled cross-linker sulfo-SBED and the resulting conjugates were bound to Protein-A beads and incubated with a synaptosomal fraction. After exposure to UV light bound prey proteins were eluted under reducing conditions leading to detachment of the prey proteins and transfer of the biotin to the prey proteins. Biotin-labelled proteins were isolated and subjected to Western blot (WB) analysis and silver staining. Biotinylated proteins were detected using HRP-conjugated streptavidin or anti-human Fc antibody. Arrows indicate distinct protein bands. The 70 kDa protein band was identified as vitronectin (VN) and marked with a black arrow. Note that CHL1-Fc but not APP-Fc bait binds vitronectin. ***B,*** CHL1-Fc and L1-Fc proteins were incubated with brain homogenate and pulled down with protein A beads. Bound proteins were subjected to Western blot (WB) analysis using vitronectin antibody. Only CHL1-Fc protein binds vitronectin. ***C,*** In ELISA experiments, surface coated with vitronectin protein was incubated with different concentrations of CHL1-Fc, L1-Fc and NCAM-Fc. Binding was determined using anti-human Fc antibody. Three independent experiments were performed in triplicates and mean values ± SD for the absorbance at 405 nm is shown.

Interaction of CHL1 with vitronectin was further confirmed in pull-down experiments performed by Nicole Karl. CHL1-Fc was immobilized on protein A beads and used to pull-down CHL1-binding proteins from mouse brain homogenate. The extracellular part of L1 protein fused to human Fc was used as a control. Bound proteins were eluted and subjected to Western blot analysis using the vitronectin antibody. Vitronectin was detected only in the CHL1-Fc and not in the L1-Fc eluate (Fig. 5.1 B), confirming that vitronectin binds to CHL1.

Direct binding of vitronectin to the extracellular domain of CHL1 was analyzed further by ELISA using immobilized vitronectin and increasing concentrations of CHL1-Fc, L1-Fc or NCAM-Fc. L1 and NCAM were chosen as controls because they also belong to the Ig-superfamily of cell adhesion molecules and are closely related to CHL1. CHL1-Fc binds to vitronectin in a concentration-dependent manner, whereas no binding of L1-Fc or NCAM-Fc to vitronectin was detected (Fig. 5.1 C).

5.1.2 CHL1 binds to vitronectin and triggers neurite outgrowth in primary cerebellar neurons

Previous data show that homophilic CHL1 *trans*-interactions inhibit neurite outgrowth, while heterophilic CHL1 *trans*-interactions promote neurite outgrowth (Jakovcevski et al., 2007). Since we identified vitronectin as one of the heterophilic CHL1 binding partners, the next step was to investigate whether the CHL1-vitronectin interaction contributes to the promotion of neurite outgrowth. Dissociated cerebellar neurons from seven-day-old wild-type and CHL1-deficient mice were cultured on PLL and CHL1-Fc substrate in the presence or absence of vitronectin or vitronectin antibody. Cerebellar neurons from wild-type and CHL1-deficient mice had longer neurites in the presence of vitronectin than on PLL and neurite outgrowth of wild-type and CHL1-deficient neurons was similar in the presence of vitronectin (Fig. 5.2. A; performed by Nicole Karl). This result suggests that exogenous vitronectin-induced neurite outgrowth is not CHL1-dependent. To test whether vitronectin can affect CHL1-induced neurite outgrowth, we maintained wild-type and CHL1-deficient cerebellar neurons on CHL1-Fc in the absence or presence of exogenous vitronectin. Neurons from CHL1-deficient and from wild-type mice had longer neurites on CHL1-Fc than on PLL, but CHL1-deficient neurons were significantly longer on CHL1-Fc substrate than wild-type neurons (Fig. 5.2 B). However, exogenous vitronectin did not alter the CHL1-enhanced neurite outgrowth from wild-type and CHL1-deficient cerebellar neurons (Fig. 5.2 B).

Next, we tested whether CHL1-enhanced neurite outgrowth is affected when the function of endogenous vitronectin is blocked by a vitronectin antibody. CHL1-induced neurite outgrowth was reduced to control values in the presence of the vitronectin antibody, but was not altered

by a non-immune control antibody (Fig. 5.2 C). This result indicates that CHL1-enhanced neurite outgrowth depends on endogenous vitronectin.

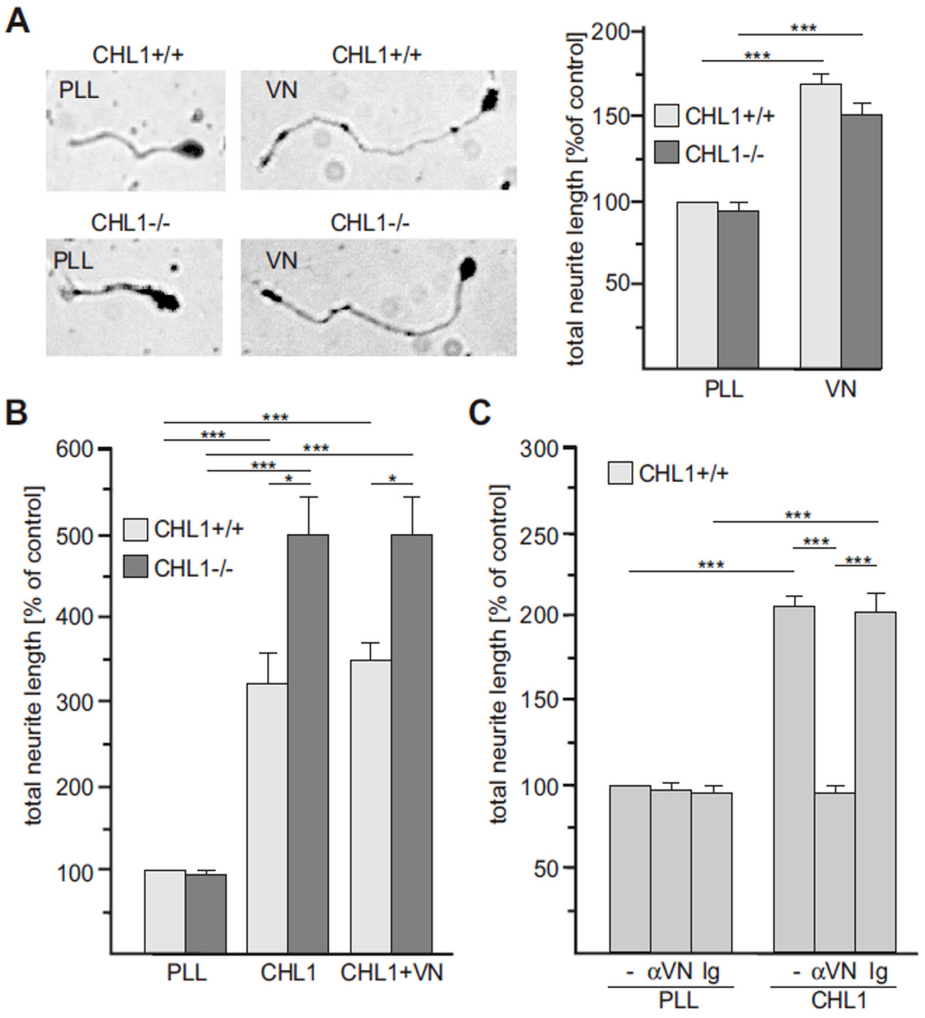

Figure 5.2. CHL1 interacts with vitronectin and induces neurite outgrowth. ***A-C,*** Dissociated cerebellar neurons from seven-day-old wild-type (CHL1 +/+) and CHL1-dficient (CHL1 -/-) mice are cultured on PLL or CHL-Fc (***B-C***) in the presence or absence of vitronectin (VN, ***A, B***) or in the presence or absence of vitronectin antibody or non-immune control antibody (αVN, -, Ig, ***C***). Images of representative neurons are shown (***A***). Total length of neurites per neuron was measured from three independent experiments, analyzing at least 100 neurons per each group and experiment (***A-C***). Mean values ± SEM are indicated and the groups were analyzed by one-way ANOVA followed by Tukey's multiple-comparison test. Significant differences between groups (*p< 0.05; ***p <0.005) are indicated.

5.1.3 CHL1 binds directly to PAI-2 via its extracellular domain

In unrelated studies performed by different members of the research group of Prof. Schachner, a phage display peptide library and CHL1-Fc were used to identify CHL1 binding partners. Briefly, phages expressing approx. 10^9 random 12-mer peptides were exposed to immobilized

CHL1-Fc. Unbound phage were washed away and specifically-bound phage were eluted, and subjected to DNA sequencing to determine which peptides were expressed by the eluted phages. The majority of eluted phages had a sequence similar to a sequence stretch within PAI-2 (Fig. 5.3 A).

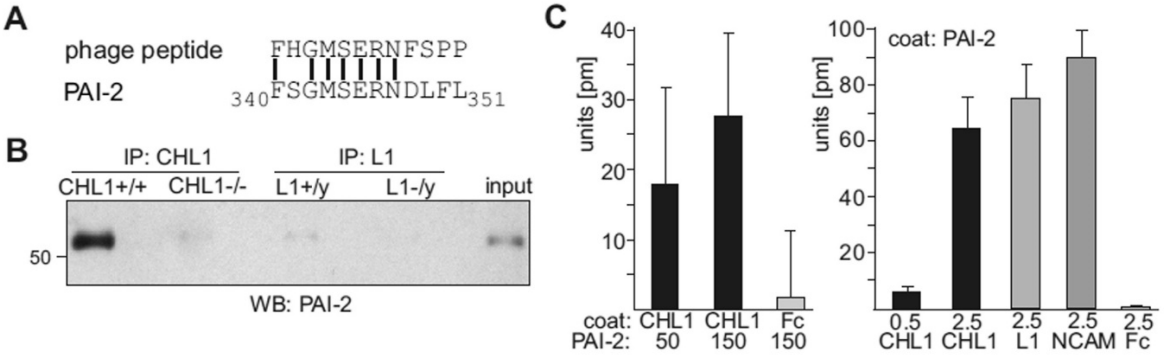

Figure 5.3. CHL1 interacts with PAI-2 via its extracellular domain. ***A,*** Sequence similarities between peptides found in eluted CHL1-Fc-binding phages and a peptide stretch of PAI-2 protein are presented. Bars indicate identical amino acids. ***B,*** Brain homogenates from CHL1-deficient (CHL1-/-), L1 deficient (L1-/y) and their wild-type littermate mice (CHL1+/+, L1+/y) were subjected to immunoprecipitation with CHL1 or L1 antibodies and protein A beads followed by Western blot analysis (WB) with PAI-2 antibody. PAI-2 protein bands were detected in the brain homogenate from wild-type mice and in the CHL1, but not L1 immunoprecipitates. ***C,*** For label-free binding assay, immobilized CHL1-Fc and Fc were incubated with 50 nM and 150 nM soluble recombinant PAI-2 protein (left), and immobilized PAI-2 was incubated with 0.5 and 2.5 nM CHL1-Fc, L1-Fc, NCAM-Fc and Fc (right). Mean values ± SD of reflected wavelength shifts (pm) from three independent experiments performed in triplicate are shown.

To verify the interaction between CHL1 and PAI-2 co-immunoprecipitation experiments were performed by Nicole Karl. Brain homogenates from wild-type, CHL1-deficient and L1-deficient mice were incubated with CHL1 and L1 antibodies and subsequently with protein A/G beads. When CHL1 antibody was used for immunoprecipitation, Western blot analysis with a PAI-2 antibody detected PAI-2 in CHL1 immunoprecipitates from the brain homogenate of wild-type, but not from CHL1-deficient mice (Fig. 5.3 B). Minor amounts of PAI-2 were observed in the immunoprecipitates from wild-type brains when L1 antibody was used (Fig. 5.3 B). These findings suggest that CHL1 and PAI-2 associate with each other. To determine if CHL1 and PAI-2 directly bind to each other, a label-free binding assay was performed using recombinant PAI-2, CHL1-Fc, L1-Fc, NCAM-Fc and Fc. Recombinant PAI-2 protein bound to immobilized CHL1-Fc in a concentration-dependent manner, indicating a direct interaction between PAI-2 and CHL1. (Fig. 5.3 C, left). Similarly, CHL1-Fc, but not Fc, bound to immobilized PAI-2 in a concentration-dependent manner (Fig. 5.3 C, right). L1-Fc as well as NCAM-Fc showed also

binding to immobilized PAI-2 (Fig. 5.3 C, right), suggesting that PAI-2 not only binds to CHL1, but also to other cell adhesion molecules of the immunoglobulin superfamily.

5.1.4 The extracellular part of CHL1 binds directly to the N-terminus of vitronectin and to the N- and C-terminus of PAI-2

To narrow down the region in vitronectin and PAI-2 that mediate the interaction with CHL1, I produced a recombinant N-terminal vitronectin fragment and recombinant N- and C-terminal PAI-2 fragments.

In the label-fee binding assay, immobilized recombinant N- and C-terminal PAI-2 fragments and the N-terminal vitronectin fragment were incubated with soluble CHL1-Fc, L1-Fc and vitronectin. CHL1-Fc showed a pronounced binding to all fragments, whereas vitronectin showed no binding to any of the PAI-2 fragments (Fig. 5.4). L1-Fc showed binding to the C-terminal PAI-2 fragment, but low binding to the N-terminal PAI-2 and vitronectin fragments (Fig. 5.4). Notably, the N-terminal parts of vitronectin and PAI-2 mediate the specific interaction with CHL1. The C-terminal part of PAI-2 mediates not only the interaction of PAI-2 with CHL1-Fc, but also with L1-Fc, which was seen before (Chapter 5.1.3).

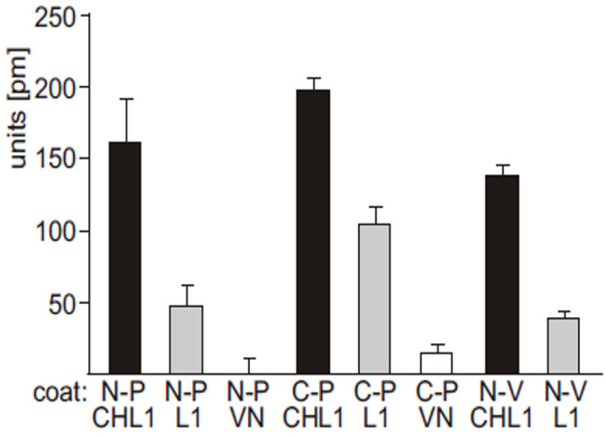

Figure 5.4. The extracellular domain of CHL1 interacts with the N- and C-terminus of PAI-2 and with the N-terminus of vitronectin. Immobilized recombinant N-terminal PAI-2 (N-P), C-terminal PAI-2 (C-P), and N-terminal vitronectin (N-V) fragments were incubated with 125 nM soluble CHL1-Fc, L1-Fc and vitronectin and subjected to label-free binding assay. Mean values ± SD of reflected wavelength shifts (pm) from three independent experiments performed in triplicate are shown.

To confirm the results obtained using the label-free binding assay, ELISA was performed. In ELISA, immobilized recombinant N- and C-terminal PAI-2 fragments and the N-terminal

vitronectin fragment were incubated with soluble CHL1-Fc, L1-Fc and Fc. CHL1-Fc showed high binding to recombinant N- and C-terminal PAI-2 fragments as well as the N-terminal vitronectin fragment, whereas Fc showed no binding to any of the PAI-2 fragments or the N-terminal vitronectin fragment (Fig. 5.5). A significant binding of L1-Fc to the C-terminal PAI-2 fragment was observed, while it showed low binding to the N-terminal PAI-2 and vitronectin fragments (Fig. 5.5).

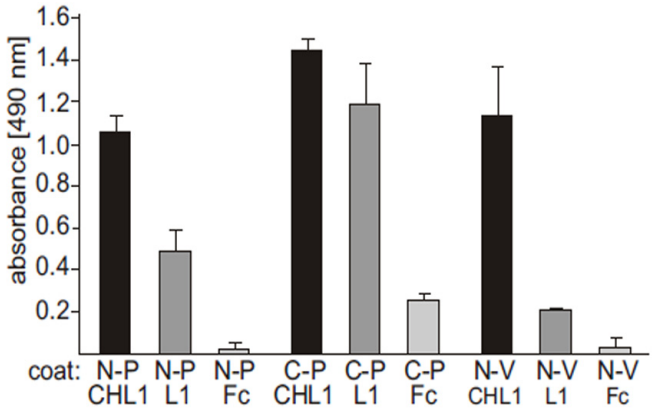

Figure 5.5. The extracellular domain of CHL1 interacts with the N- and C-terminus of PAI-2 and with the N-terminus of vitronectin. Immobilized recombinant N-terminal PAI-2 (N-P), C-terminal PAI-2 (C-P), and N-terminal vitronectin (N-V) fragments were incubated with 5 nM soluble CHL1-Fc, L1-Fc and Fc. Binding was determined by ELISA using anti-human Fc antibody. Three independent experiments were performed in triplicates and mean values ± SD are shown for the absorbance at 490 nm.

ELISA and label-free binding assay results show that the CHL1 binds directly to the N-terminus of vitronectin and to the N- and C-terminus of PAI-2 via its extracellular part.

5.1.5 CHL1 binds to vitronectin and PAI-2 and triggers neuronal migration in explant cultures of cerebellar neurons

The increased number of migrating granular cells in the molecular layer of the cerebellar cortex at the end of the first postnatal week (Jakovcevski et al., 2009) can be the consequence of an impaired inward granular cell migration. Thus, we investigated whether CHL1 influence granular cell migration *in vitro*.

Explant cultures of cerebellar neurons from wild-type or CHL1-deficient mice were prepared by Nicole Karl, Gabriele Loers and Ralf Kleene. Explants were cultured on PLL and CHL1-Fc.

Only a few cell bodies are migrating from explants seeded on PLL substrate (Fig. 5.6 A), while a large number of migrating cells is found when explants were maintained on CHL1-Fc substrate (Fig. 5.6 B). Cell bodies migrating from the explant core were counted and a significant difference between cells migrating on the PLL and CHL1-Fc substrates in both genotypes was observed (Fig. 5.6 C). On both substrates, the total number of migrating CHL1-deficient cells was lower than those of wild-type cells (Fig. 5.6 C). This result suggests that homophilic and heterophilic CHL1 interactions trigger granular cell migration.

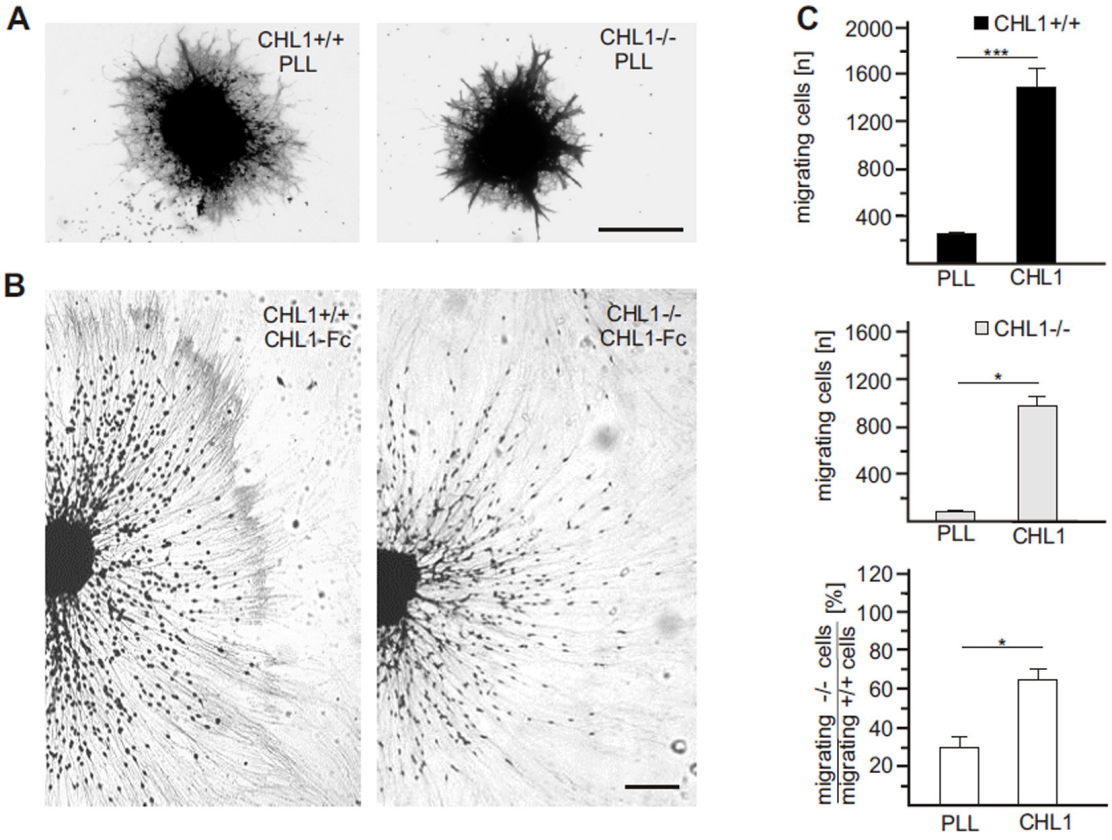

Figure 5.6. CHL1 stimulates granule cell migration. Cerebellar explants from six-day-old wild-type (CHL1+/+) and CHL1-deficient (CHL1-/-) mice were cultured on PLL or CHL1-Fc substrate. ***A–B***, Representative images of explants are shown. ***C,*** The total number of cell bodies migrating out of the explants, and the number of migrating CHL1-deficient cells relative to the number of migrating wild-type cells are shown. Mean values ± SEM from three independent experiments counting all migrating cells from 10 explants per group in each experiment are shown. The groups were analyzed by two-tailed Student's *t* test, and significant differences between groups (**p*<0.05; ****p*< 0.005) are indicated. Scale bars, 100 µm.

Moreover, CHL1-triggered granular cell migration could depend on the interaction of CHL1 with vitronectin and PAI-2. To exclude homophilic CHL1 interactions we used explants from CHL1-deficient mice. Since the interaction of vitronectin with the urokinase type plasminogen

activator (uPA) and the urokinase type plasminogen activator receptor (uPAR) regulates cell migration, and since PAI-2 and its homolog PAI-1 inhibits uPA function (Lobov and Ranson, 2011), we tested whether PAI-1, PAI-2, uPA and uPAR are involved in CHL1-induced granule cell migration. Explants were maintained on PLL or CHL1-Fc substrates in the absence or presence of antibodies against vitronectin, PAI-1, PAI-2, uPA and uPAR well as in the presence of PAI-2 peptide and the scrambled version of the PAI-2 peptide. CHL1-Fc-triggered granular cell migration was reduced by antibodies against vitronectin, PAI-2, uPA and uPAR, but not by an antibody against PAI-1 (Fig. 5.7). Also, a peptide containing the putative CHL1-binding site of PAI-2 (comprising amino acids 335-349 of PAI-2) inhibited CHL1-induced granule cell migration, while the scrambled version of this peptide (containing the same amino acids in a random order) had no effect (Fig. 5.7). These results indicate that CHL1-triggered migration of granule cells depends on the interaction of CHL1 with vitronectin, PAI-2, uPA, uPAR.

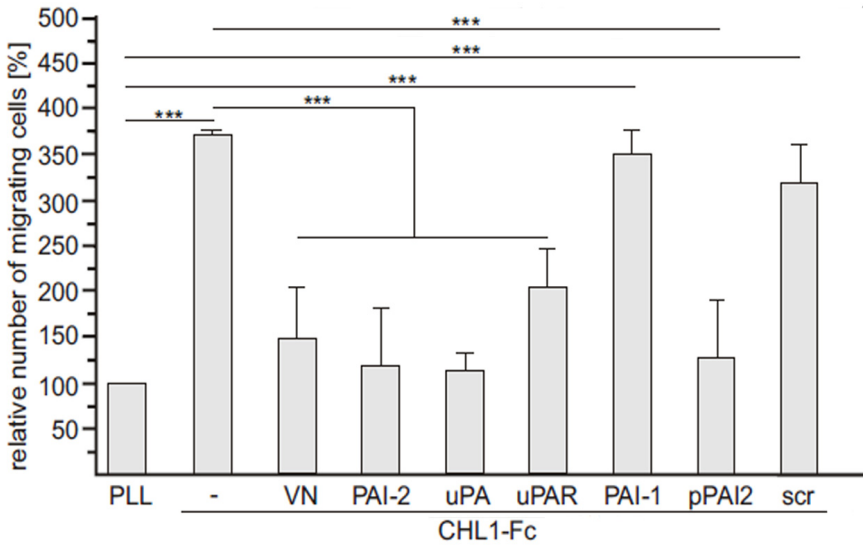

Figure 5.7. CHL1-induced granule cell migration depends on vitronectin, PAI-2, uPA, and uPAR. Cerebellar explants from six-day-old CHL1-deficient mice were maintained on PLL or CHL1-Fc, in the absence (-) or presence of antibodies against vitronectin (VN), PAI-1, PAI-2, uPA, and uPAR, and the presence of the PAI-2 peptide (pPAI2) or the scrambled version of the PAI-2 peptide (scr). The relative numbers of migrating cells are shown. Mean values ± SEM from three independent experiments counting all migrating cells from 10 explants per group in each experiment are shown. The groups were analyzed by two-tailed Student's *t* test, and significant differences between groups (***$p < 0.005$) are indicated.

Since CHL1-triggered migration is inhibited by vitronectin and PAI-2 antibodies reacting with N-terminal epitopes and by the PAI-2-derived peptide comprising a C-terminal sequence stretch, I tested whether a recombinant N-terminal vitronectin fragment or recombinant N- and/or C-terminal PAI-2 fragments affect CHL1-dependent migration. In the absence of CHL1-

Fc, the N-terminal vitronectin fragment enhanced migration of neurons from wild-type, but not from CHL1-deficient explants (Fig. 5.8). In the presence of CHL1-Fc, the N-terminal vitronectin fragment enhanced migration of CHL1-deficient neurons compared to the wild-type neurons but did not affect migration compared to the untreated control. Wild-type neurons treated both with CHL1-Fc and N-terminal vitronectin migrate less compared to wild-type neurons treated only with CHL1-Fc (Fig. 5.8). This suggests that the N-terminal vitronectin fragment enhances migration in the presence of either endogenous or exogenous CHL1 alone, but not when both of them are present at the same time. In the absence of CHL1-Fc, the N-terminal PAI-2 fragment did not stimulate migration, while the C-terminal PAI-2 fragment triggered migration of neurons from both wild-type and CHL1-deficient explants compared to the untreated control (Fig. 5.8), suggesting that the C-terminal PAI-2 fragment enhances migration independently of CHL1. In the presence of CHL1-Fc, CHL1-deficient neurons treated both with N- and C-terminal PAI-2 fragment migrate less from the explant core compared to the untreated control (Fig. 5.8). This suggests that N- and C-terminal PAI-2 fragments could interfere with binding of CHL1-Fc to endogenous PAI-2.

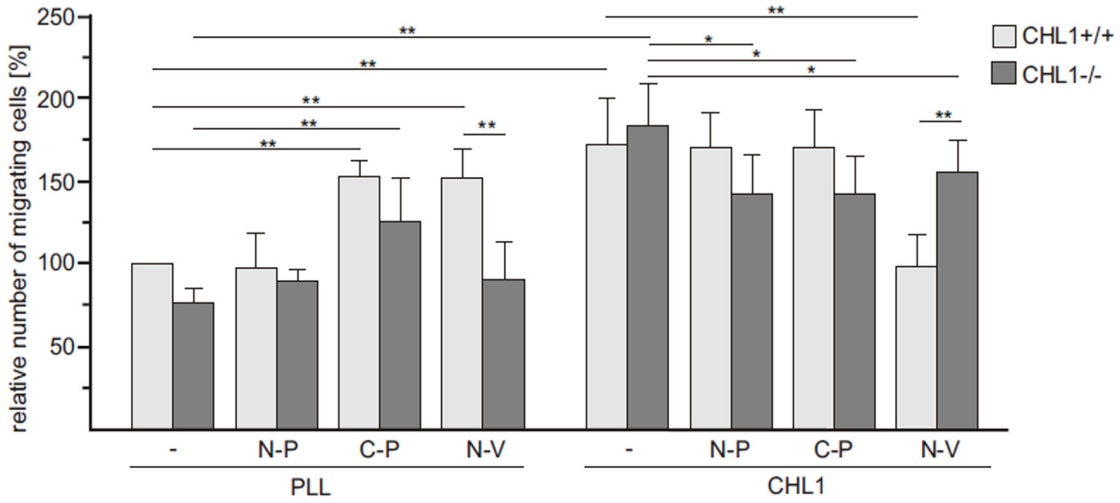

Figure 5.8. N-terminal vitronectin and N- and C-terminal PAI-2 domains are involved in CHL1-dependent granule cell migration. Cerebellar explants from six-day-old wild-type (CHL1+/+) and CHL1-deficient (CHL1-/-) mice were maintained on PLL or CHL1-Fc substrates in the absence (-) or presence of N-terminal PAI-2 (N-P), C-terminal PAI-2 (C-P), and N-terminal vitronectin (N-V) fragments. Numbers of migrating cells from each group relative to the number of cells migrating from wild-type non-treated explants on PLL are shown. Mean values ± SEM from three independent experiments counting all migrating cells from 10 explants per group in each experiment are shown. The groups were analyzed by two-tailed Student's *t* test, and significant differences between groups (*p< 0.05; **p <0.01) are indicated.

5.1.6 CHL1 co-localizes with vitronectin and PAI-2 during the development of the cerebellar cortex

So far, we identified novel binding partners of CHL1 and confirmed the direct interaction of CHL1 with vitronectin and PAI-2 *in vitro*. We also showed the functional implication of these interactions in cerebellar neurons from six and seven-day-old mice in *in vitro* systems. To confirm an interaction of CHL1 with vitronectin and PAI-2 *in vivo*, I stained cerebella of five and seven-day-old wild-type mice with CHL1, vitronectin and PAI-2 antibodies (Fig. 5.9 A, B, D, E; Fig. 5.10 A, B, D, E). Interestingly, co-localization of CHL1 with vitronectin and PAI-2 occurs only in 7-day-old cerebellum (Fig. 5.9 C; Fig. 5.10 C) but not in 5-day-old cerebellum (Fig. 5.9 F; Fig. 5.10 F). CHL1 and vitronectin co-localized along radial fibers of Bergmann glial cells (Fig. 5.9 C); CHL1 and vitronectin and CHL1 and PAI-2 co-localized at cells located within the inner part of the external granular layer, within the molecular layer and within in the internal granular layer near the Purkinje cell layer (Fig. 5.9 C, Fig. 5.10 C). Since in those regions granule cell migration occurs by the end of the first postnatal week, this result suggests that CHL1 interacts with vitronectin and PAI-2 in the region of granule cell migration. Even though expressed in the five-day-old cerebellum, CHL1 and vitronectin or CHL1 and PAI-2 do not co-localize (Fig. 5.9 F; Fig. 5.10 F).

Quantification of the co-immunostainings of CHL1 with vitronectin or PAI-2 showed that a pronounced fraction of the CHL1 signals overlapped with the vitronectin and PAI-2 signals in cerebella of seven-day-old mice, while only a small fraction of the CHL1 signals overlapped with the vitronectin and PAI-2 signals in cerebella of five-day-old mice (Fig. 5.9 G; Fig. 5.10 G). Quantification analysis confirms previous conclusion: CHL1 co-localizes with vitronectin and PAI-2 in the cerebellum of seven-day-old mice, but does not co-localize with these proteins in the cerebellum of five-day-old mice.

To supplement immunohistochemical analysis, I performed proximity ligation assays. This strategy is based on amplifying fluorescent signals from a pair of oligonucleotide-labeled secondary antibodies, when two primary antibodies are bound to their antigens in close proximity. Red fluorescent signals were found in cerebella of seven-day-old mice, at cells located within the inner region of the external granular layer, within the molecular layer and within in the internal granular layer (Fig.5.9 H; Fig. 5.10 H), indicating that CHL1 interacts with vitronectin and PAI-2 at this developmental stage. No or only a few small fluorescent spots were found in cerebella of five-day-old mice (Fig. 5.9 I; Fig. 5.10 I), indicating that CHL1 does not interact with vitronectin or PAI-2 at this earlier developmental stage.

CHL1 interacts with vitronectin and PAI-2 on migrating granule cells at postnatal day seven, when the inward granule cell migration from the external to the internal granular layer is

prominent. This finding supports previous *in vitro* results demonstrating that the interaction of CHL1 with vitronectin and PAI-2 influences cerebellar neuron migration.

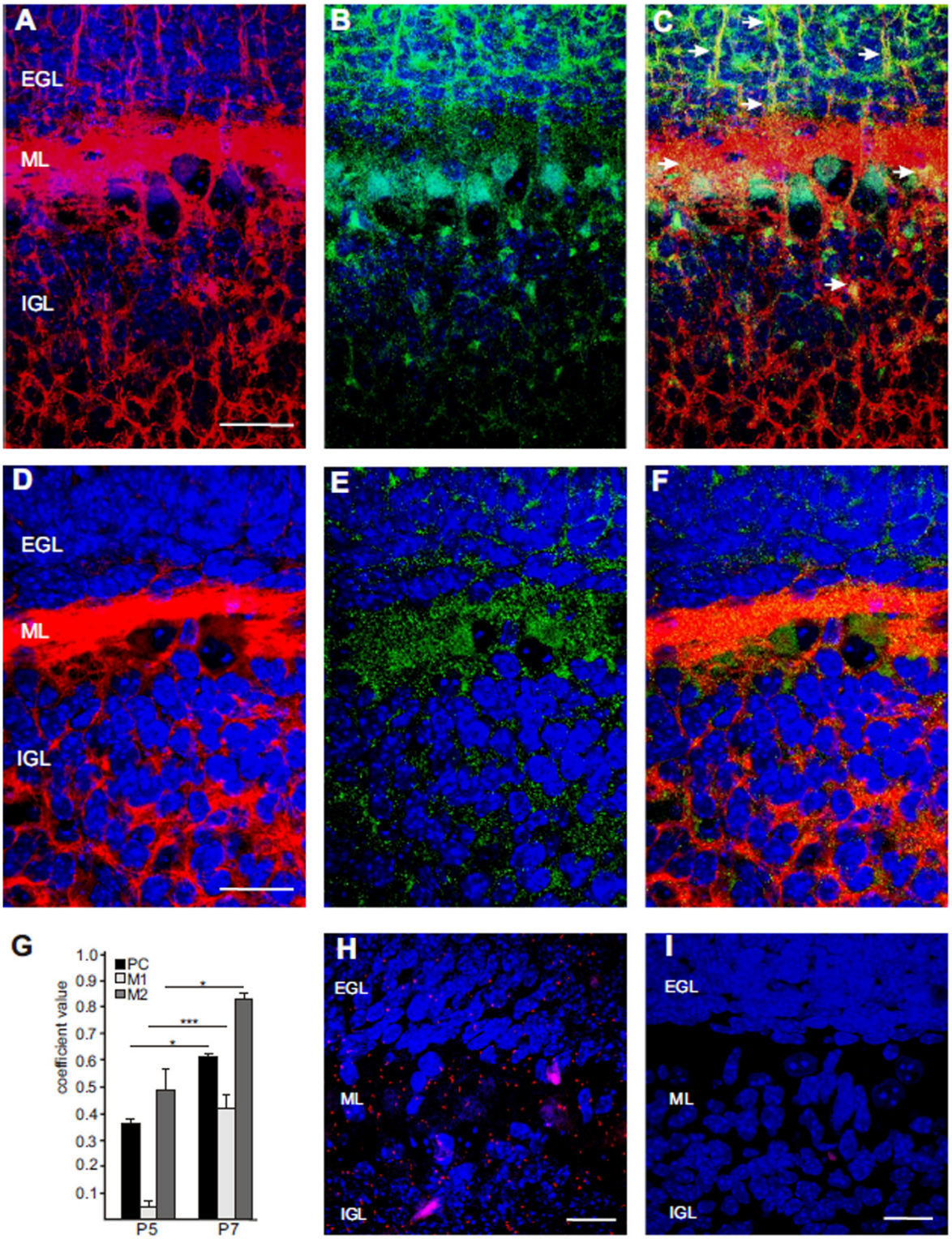

Figure 5.9. CHL1 and vitronectin co-localize in the cerebellum of seven-day-old mice, but not five-day-old mice. ***A***, ***B***, ***D***, ***E***, Representative images of immune-fluorescence staining for DAPI (blue)

and CHL1 (red; *A*, *D*), and DAPI and vitronectin (green; *B*, *E*) are shown. ***C*, *F*,** Superimposition indicates co-localizations as yellow along radial fibers of Bergmann glial cells (arrow heads), and at cells located within the molecular layer and the external and internal granular layers (arrows). Scale bars, 15 µm. ***G*,** Pearson's coefficient PC and the Mander's overlap coefficients M1 and M2 were calculated as parameters for the degree of co-localization between CHL1 and vitronectin. Coefficient values ± SEM for cerebellum from postnatal day 5 (P5) and 7 (P7) in wild-type mice (n = 6) are shown. The groups were analyzed by two-tailed Student's t test, and significant differences between groups (* $p < 0.05$; *** $p < 0.005$) are indicated. ***H*, *I*,** Representative image from the proximity ligation assay are shown. Red spots indicate a close interaction of CHL1 with vitronectin. Scale bars, 60 µm. ***A-C*, *H*,** seven-day-old cerebellum. ***D–F*, *I*,** five-day-old cerebellum. EGL - external granular layer; ML - molecular layer; PCL - Purkinje cell layer; IGL - internal granular layer.

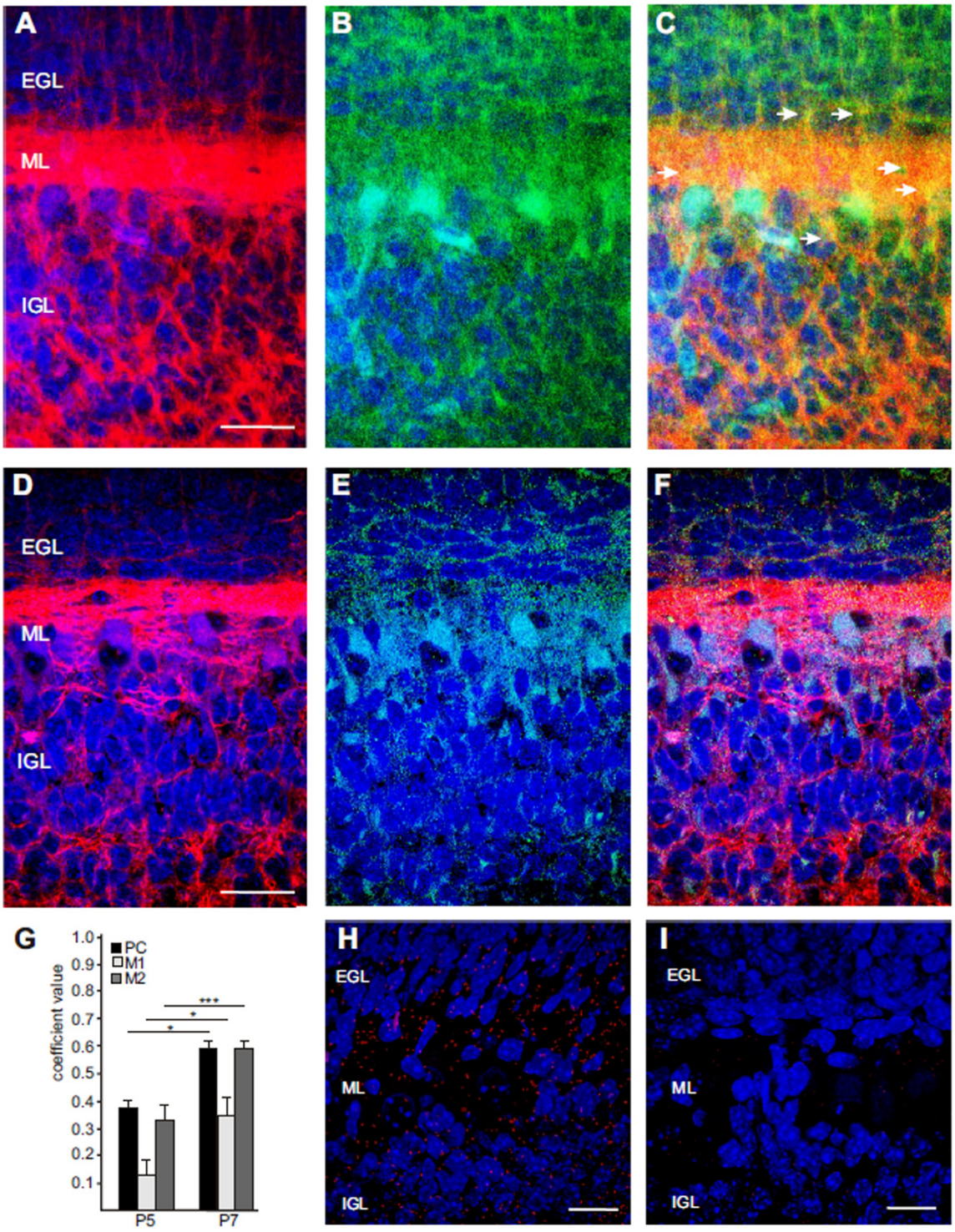

Figure 5.10. CHL1 and PAI-2 co-localize in the cerebellum of seven-day-old mice, but not five-day-old mice. *A*, *B*, *D*, *E*, Representative images of immune-fluorescence staining for DAPI (blue) and CHL1 (red; *A*, *D*), and DAPI and PAI-2 (green; *B*, *E*) are shown. ***C*, *F*,** Superimposition indicates co-localizations as yellow at cells located within the molecular layer and the external and internal granular layers (arrows). Scale bars, 15 µm. ***G*,** Pearson's coefficient PC and the Mander's overlap coefficients M1 and M2 were calculated as parameters for the degree of co-localization between CHL1 and PAI-2. Coefficient values ± SEM for cerebellum from postnatal day 5 (P5) and 7 (P7) in wild-type mice (n = 6) are shown. The groups were analyzed by two-tailed Student's t test, and significant differences between groups (* $p < 0.05$; ***$p < 0.005$) are indicated. ***H*, *I*,** Representative image from the proximity ligation assay are shown. Red spots indicate a close interaction of CHL1 with PAI-2. Scale bars, 60 µm. ***A-C*,**

***H*,** seven-day-old cerebellum. ***D–F*, *I*,** five-day-old cerebellum. EGL - external granular layer; ML - molecular layer; PCL - Purkinje cell layer; IGL - internal granular layer.

5.1.7 CHL1 and vitronectin prevent proliferation and differentiation but enhance inward radial migration of granule cells at the end of the first postnatal week

Previous studies showed that seven-day-old CHL1-deficient mice have more NeuN- positive cells in the molecular layer relative to their wild-type littermates, during the phase of the active inward migration. Moreover, there is no difference in the number of actively proliferating Ki67-positive cells in the seven-day-old external granular layer, the region where granular cells are migration from (Jakovcevski et al., 2009). Having in mind that granule cell precursors from the external granular layer proliferate before they start the active inward migration (Soltelo, 2004.), it was crucial to investigate their proliferation in the earlier stages before the migration occurs. Thus, I immunostained brain sections from three- and five-day-old CHL1-deficient mice and their wild-type littermates with Ki67 antibody, a marker of proliferation, and estimated the density of Ki67-positive cells using stereological analysis. Since vitronectin regulates CHL1-triggered neurite outgrowth and migration, I also stained brain sections from five-day-old vitronectin-deficient mice with Ki67 antibody.

In the external granular layer of three-day-old mice, proliferation is not altered in the absence of CHL1 (n=6: 545.08 ± 24.74 versus 563.99 ± 48.61 × 10^3 cells/mm^{-3}, $p<0.75$). However, the number of Ki67-positive cells was higher in the external granular layer of five-day-old CHL1-deficient and vitronectin-deficient mice relative to the number of Ki67-positive cells in the external granular layer of wild-type mice (Fig. 5.11), indicating that CHL1 and vitronectin inhibit proliferation of granular cell precursors from the external granular layer at this specific time point of development.

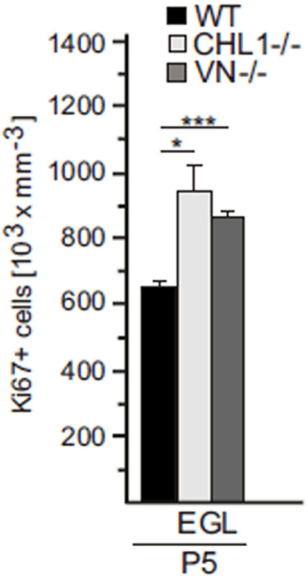

Figure 5.11. CHL1 and vitronectin prevent granular cell proliferation in five-day-old cerebellum *in vivo*. Tissue sections of cerebella from postnatal day 5 (P5) wild-type (WT) and CHL1-deficient (CHL1-/-) or vitronectin-deficient (VN-/-) mice were immune-stained for Ki67, a marker of proliferation. The density of Ki67-immunopositive cells was determined using stereological analysis. Mean values ± SEM of Ki67-positive cells per area in the external granular layer (EGL) of cerebella from five-day-old wild-type mice (n= 8), CHL1-deficient mice (n= 8), and vitronectin-deficient mice (n= 5) are shown. More Ki67-positive cells were observed in the external granular layer of CHL1- and vitronectin-deficient mice relative to wild-type control. The groups were analyzed by two-tailed Student's t test, and significant differences between groups (*p< 0.05; ***p <0.005) are indicated.

Next, I determined the number of differentiated neurons in the five- and seven-day-old cerebella. Brain sections from vitronectin-deficient mice, CHL1-deficient mice and their wild-type littermates were stained with NeuN antibody, which specifically stains differentiated neurons *in vivo*, and the density of NeuN-positive cells was analyzed using stereological analysis. I counted densities of differentiated (NeuN-positive) cells in the molecular and internal granular layer. Since the external granule layer is the pull of granule cell precursors, there were no differentiated (NeuN-positive) cells in this layer.

An increased number of NeuN-positive cells was observed in the molecular layer of five- and seven-day-old CHL1-deficient and vitronectin-deficient cerebella (Fig. 5.12), while only the CHL1-deficient cerebellum contained more differentiated cells in the internal granular layer (Fig. 5.12). Thus, it is likely that CHL1 and vitronectin delay differentiation of granular cell precursors that should start their inward radial migration from the external granular layer to form the internal granular layer.

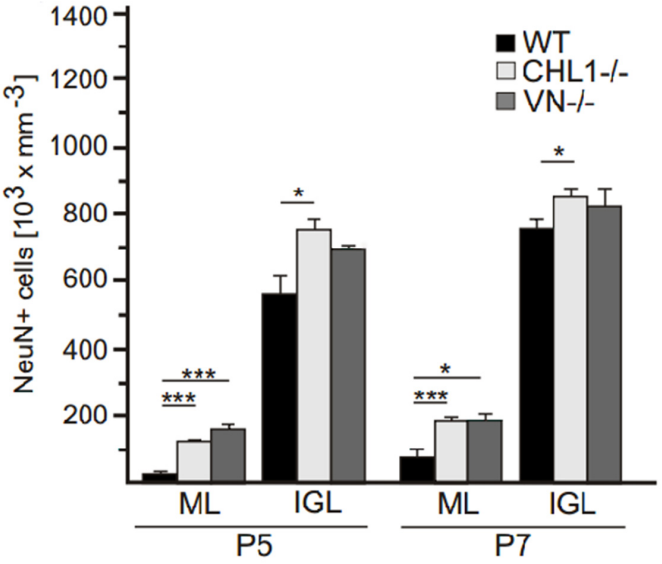

Figure 5.12. CHL1 and vitronectin prevent granular cell differentiation in five- and seven-day-old cerebellum *in vivo*. Tissue sections of cerebella from postnatal day 5 and 7 (P5; P7) wild-type (WT) and CHL1-deficient (CHL1-/-) or vitronectin-deficient (VN-/-) mice were immune-stained for NeuN, a marker of differentiated neurons. The density of NeuN-immunopositive cells was determined using stereological analysis. Mean values ± SEM of NeuN-positive cells per area in the molecular and internal granular layer (ML; IGL) of cerebella from five and seven-day-old wild-type mice (*n*= 6), CHL1-deficient mice (*n*= 6), and vitronectin-deficient mice (*n* =5) are shown. More NeuN-positive cells were observed in the molecular layer of CHL1- and vitronectin-deficient mice, while in the internal granular layer more NeuN-positive cells were observed only in CHL1-deficient mice relative to wild-type control. The groups were analyzed by two-tailed Student's *t* test, and significant differences between groups (*$p < 0.05$; ***$p < 0.005$) are indicated.

Since the higher number of differentiated granule cells observed in the CHL1- and vitronectin-deficient cerebellum could be the consequence of a higher number of granule cell precursors that terminate differentiation, it was important to count the total number of granule cells and their precursors. For that purpose, an appropriate cell marker that can label all granular cells and their precursors was used (Swanson et al., 2005). Brain sections from five- and seven-day-old vitronectin-deficient mice, CHL1-deficient mice and their wild-type littermates were stained with Pax6 antibody. The number of Pax-6-positive cells was analyzed in the external granular, molecular and internal granular layer using stereological analysis.

No significant differences between genotypes were found for numbers of Pax6-positive cells in the molecular and internal granular layers of cerebella from five- and seven-day-old mice (Fig. 5.13). Only in the external granular layer of five-day-old vitronectin-deficient mice the number of Pax6-positive cells was slightly higher compared to the number in wild-type mice (Fig. 5.13), which could be due to their enhanced proliferation.

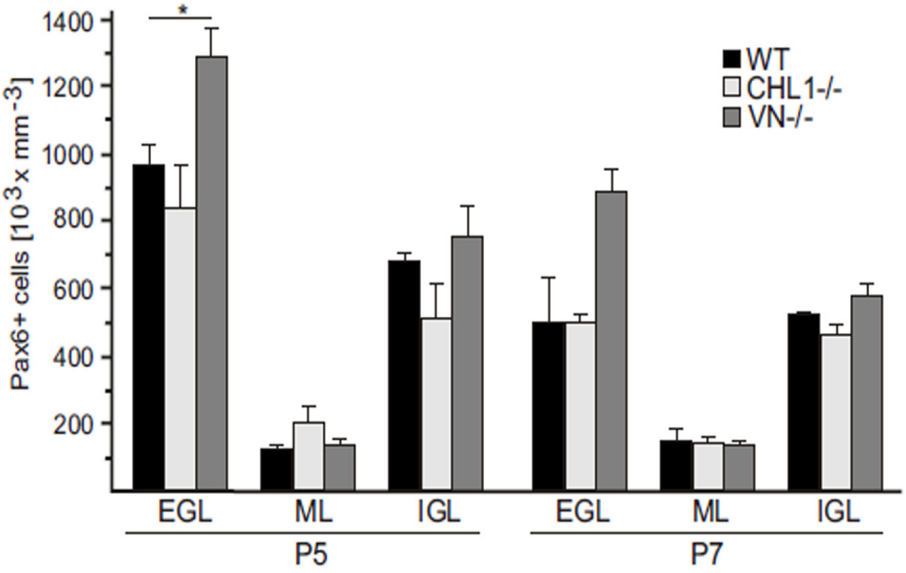

Figure 5.13. CHL1 does not influence and vitronectin slightly affects the number of granular cells in five- and seven-day-old cerebellum *in vivo*. Tissue sections of cerebella from postnatal day 5 and 7 (P5; P7) wild-type (WT) and CHL1-deficient (CHL1-/-) or vitronectin-deficient (VN-/-) mice were immune-stained for Pax6, an embryonic and early postnatal marker of granular cells. The density of Pax6-immunopositive cells was determined using stereological analysis. Mean values ± SEM of Pax6-positive cells per area in the external granular layer, molecular layer and internal granular layer (EGL; ML; IGL) of cerebella from five and seven-day-old wild-type mice (n= 6), CHL1-deficient mice (n= 6), and vitronectin-deficient mice (n= 5) are shown. No difference in number of Pax6-positive cells was detectable between CHL1-deficient and wild-type mice in all three layers, while a slight difference in Pax6 cell numbers in the P5 external granular layer in vitronectin-deficient mice relative to wild-type mice was observed. The groups were analyzed by two-tailed Student's t test, and significant differences between groups (*p< 0.05) are indicated.

However, the number of NeuN/Pax6-double positive granular cells in the internal granular layer changes from postnatal day 5 to 7. An increased number of NeuN/Pax6-double positive cells was found in the internal granular layer of five day old CHL1-deficient cerebellum, while a decreased number of NeuN/Pax6-double positive cells was found in the internal granular layer of seven-day-old CHL1-deficient and vitronectin-deficient cerebella relative to the number observed in wild-type cerebella (Fig. 5.14). These changes in numbers of differentiated granule cells in CHL1-deficient and vitronectin-deficient mice suggest that differentiation of granule cells at this developmental stage is regulated by CHL1 and vitronectin.

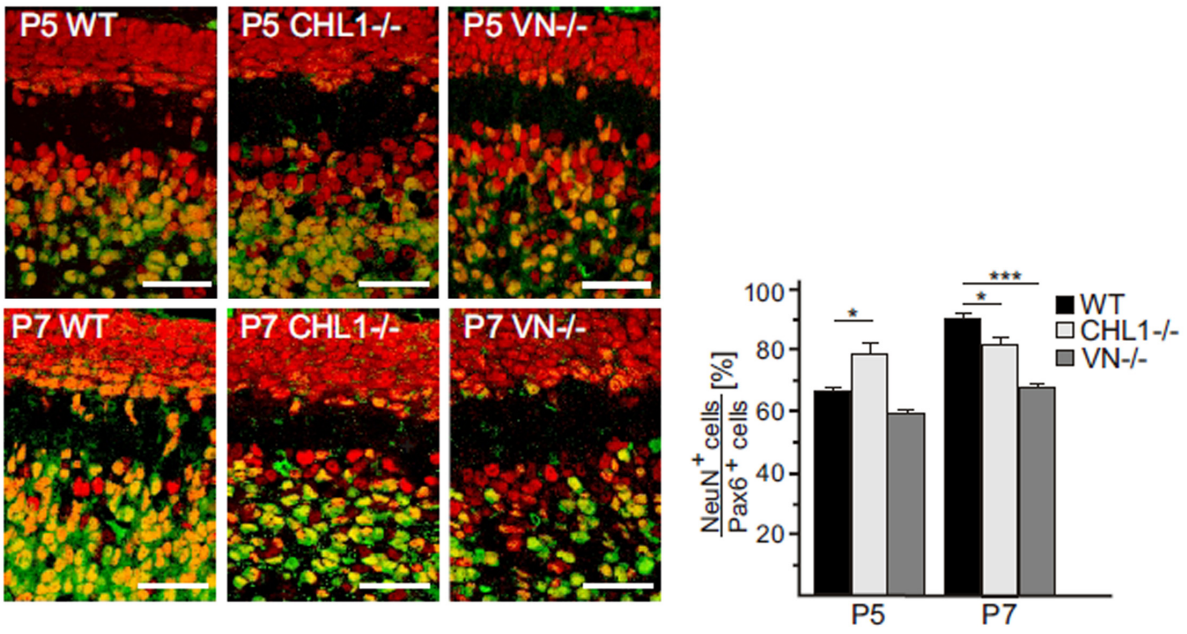

Figure 5.14. CHL1 and vitronectin regulate differentiation of granule cells in five and seven-day-old cerebellum *in vivo*. Tissue sections of cerebella from postnatal day 5 and 7 (P5; P7) wild-type (WT) and CHL1-deficient (CHL1-/-) or vitronectin-deficient (VN-/-) mice were immune-stained for Pax6 (red), embryonic and early postnatal marker of granular cells, and NeuN (green), marker of differentiated neurons. Representative immune-fluorescence images and mean values ± SEM of relative numbers of NeuN/Pax6 double-positive cells (yellow and orange) in the internal granular layer of cerebella from five and seven day old wild-type mice (n= 6), CHL1-deficient mice (n= 6), and vitronectin-deficient mice (n= 5) are shown. The groups were analyzed by two-tailed Student's t test, and significant differences between groups (*p <0.05; ***p <0.005) are indicated. Scale bars, 20 µm.

Our *in vitro* studies suggest that the interaction of CHL1 and vitronectin regulates granular cell migration. The higher number of granular NeuN-positive cells in the molecular layer of CHL1- and vitronectin-deficient mice could be a consequence of retarded migration and consequential cellular accumulation within the molecular layer. Thus, I tested whether CHL1 and vitronectin alter migration of granule cells in the cerebellum *in vivo* by staining of brain sections with antibodies against Pax6 and doublecortin (DCX), a marker for migrating neurons. The number of Pax6/DCX double-positive cells can be used as a measure to assess how many granular cells are migrating from the external granular layer.

The numbers of Pax6/DCX double-positive cells in the external granular layers of cerebella from five day old wild-type, CHL1- and vitronectin-deficient mice were similar, while a reduced number was found in the external granular layers of cerebella of seven-day-old CHL1- and vitronectin-deficient mice relative to the number observed in cerebellar of wild-type mice (Fig. 5.15). This result indicates that the migration of cerebellar granule cells does not depend on CHL1 and vitronectin at early stages, but depends on CHL1 and vitronectin at later developmental stages. The similar histological phenotypes detected in CHL1- and vitronectin-

deficient cerebellum suggest that migration and differentiation in the mouse cerebella depend on CHL1 and vitronectin. The interaction between CHL1 and vitronectin regulates migration of granule cells *in vivo*.

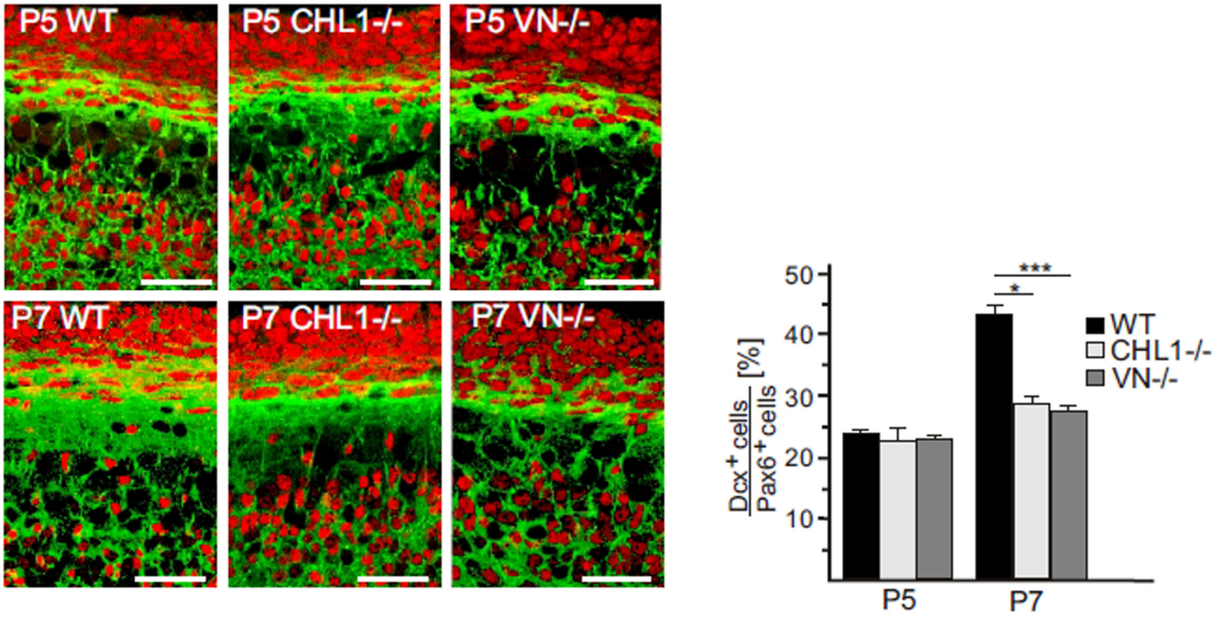

Figure 5.15. CHL1 and vitronectin regulate migration of granule cells in seven-day-old cerebellum *in vivo*. Tissue sections of cerebella from postnatal day 5 and 7 (P5; P7) wild-type (WT) and CHL1-deficient (CHL1 -/-) or vitronectin-deficient (VN- /-) mice were immune-stained for Pax6 (red), embryonic and early postnatal marker of granular cells, and doublecortin (DCX; green), marker of migrating neurons. Representative immune-fluorescence images and mean values ± SEM of relative numbers of DCX/Pax6 double-positive cells in the inner part of the external granular layer of cerebella from five and seven day old wild-type mice (*n*= 6), CHL1-deficient mice (*n*= 6), and vitronectin-deficient mice (*n*= 5) are shown. The groups were analyzed by two-tailed Student's *t* test, and significant differences between groups (**p* <0.05; ****p* <0.001) are indicated. Scale bars, 20 µm.

Results in the Chapter 5.1 show that CHL1 binds to vitronectin and plasminogen activator inhibitor-2 (PAI-2), both present in the extracellular matrix, and regulates granule cell development during a very narrow time window. After they exit mitosis, granule cell precursors start to differentiate by changing their cell morphology and elongating their leading process towards the internal granule layer, prior to their inward radial migration. CHL1 seems to regulate these events by interaction with vitronectin and PAI-2.

5.2 The interaction of CHL1 with patched-1 triggers cerebellar neuron migration and neurite outgrowth during the end of the first postnatal week and inhibits apoptosis of granule cells during the second postnatal week of cerebellar development

CHL1 inhibits granule cell proliferation and differentiation during the first week of murine brain development and enhances granule cell migration and neurite formation during the end of the first week of cerebellar development. However, those findings cannot explain the loss in granule cell number found in the adult cerebellum of CHL1-deficiend mice. Thus, it was important to understand when this loss of granule cells occurs and how CHL1 regulates the number of granule cells. Since CHL1 has a pro-survival effect, it presumably could regulate the cell number by regulating apoptosis. Therefore, I searched for other interaction partners of CHL1 that could affect apoptosis.

5.2.1 CHL1 binds directly to patched via its extracellular domain

Searching for other binding partners of CHL1, a phage display peptide library and CHL1-Fc were used, as described in the Chapter 5.1.3. The majority of eluted phages on the surface with immobilized CHL1-Fc had a sequence similar to a sequence stretch within patched (Fig. 5.16).

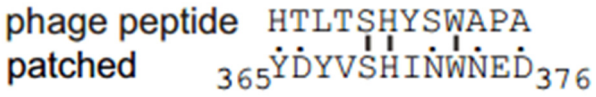

Figure 5.16. The extracellular domain of CHL1 binds a peptide with sequence similarity to patched. Sequence similarities between a peptide expressed by CHL1-Fc-binding phages and a patched sequence located in the first extracellular loop are presented. Bars are indicating identical amino acids (|), spots weakly conserved (.) amino acids, and numbers indicate amino acid positions.

To further verify a CHL1-patched interaction, I performed a co-immunoprecipitation experiment. Cerebellar homogenates from ten-day-old wild-type and CHL1-deficient mice were used for immunoprecipitation with an antibody that recognizes the first extracellular loop of patched. Immunoprecipitates were subjected to Western blot analysis using an antibody against the extracellular CHL1 domain. A strong CHL1 protein band ~200 kDa was detected

only in the patched precipitate from wild-type cerebellum, whereas no band was detected in the precipitate from CHL1-deficient cerebellum (Fig. 5.17). The same size of the CHL1 band was detected in the input control from wild-type cerebellum. This result suggests a direct or indirect interaction between CHL1 and patched.

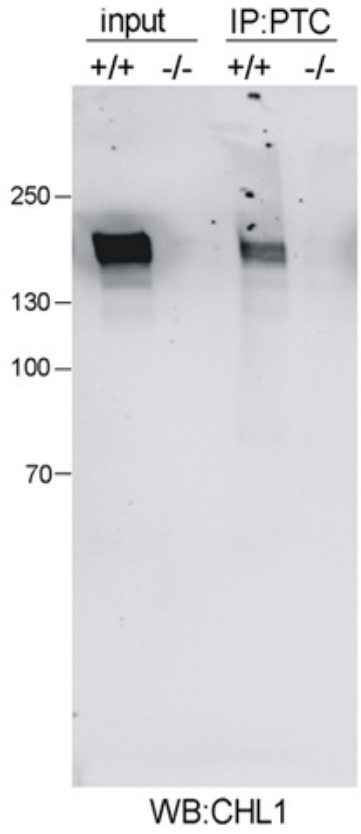

Figure 5. 17. CHL1 co-precipitates with patched. Cerebella homogenates from CHL1-deficient (CHL1-/-) mice and their wild-type littermates were subjected to immunoprecipitation (IP) with patched (PTC) antibody against the first extracellular loop followed by Western blot analysis (WB) with the antibody that recognizes the extracellular domain of CHL1. A CHL1 protein band of ~200 kDa was detected only in the patched immunoprecipitate from the cerebellum homogenate of wild-type mice.

Since patched binds to smoothened and forms a complex with smoothened, I wanted to analyze by immunoprecipitation if CHL1 also associates with smoothened. Cerebellar homogenates from ten-day-old wild-type and CHL1-deficient mice were subjected to immunoprecipitation with smoothened antibody and Western blot analysis with CHL1 antibody. A very weak CHL1 protein band of ~200 kDa was found in the immunoprecipitate from wild-type cerebellum but not in the immunoprecipitate from CHL1-deficient cerebellum (Fig. 5.18). The same size of the CHL1 band was detected in the input control from wild-type cerebellum. The detection of the weak CHL1 band in the smoothened precipitate does not allow a

conclusion about a direct or indirect interaction between smoothened and CHL1. CHL1 might directly interact with smoothened or associate with smoothened via patched within the patched-smoothened complex.

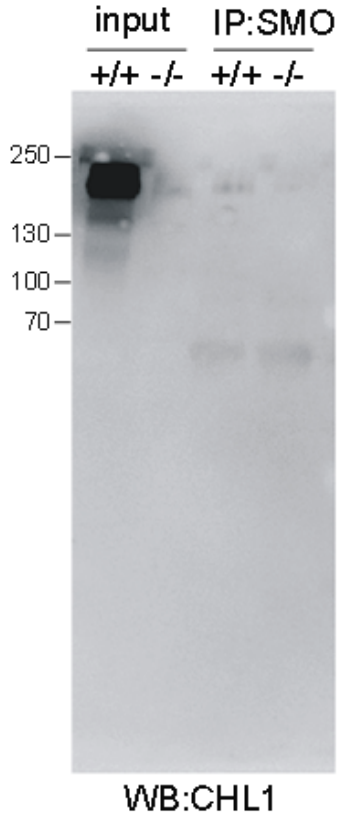

Figure 5.18. CHL1 co-precipitates with smoothened. Cerebella homogenates from CHL1-deficient (CHL1-/-) mice and their wild-type littermates were subjected to immunoprecipitation (IP) with smoothened (SMO) antibody followed by Western blot analysis (WB) with the antibody that recognizes the extracellular domain of CHL1. A week CHL1 protein band of ~200 kDa was detected only in the smoothened immunoprecipitate from the cerebellum homogenate of wild-type mice.

To demonstrate a direct interaction between CHL1 and patched I performed ELISA (Fig. 5.19) and label-free binding assay (Fig. 5.20) using an immobilized recombinant patched protein fragment comprising the amino acids from 213-422 and containing part of the first extracellular loop (amino acids 108-422) as well as the putative CHL1-binding site (amino acids 365-376) identified by phage display. A concentration-dependent binding of CHL1-Fc, but not of NCAM-Fc or Fc, to the patched fragment suggests that the extracellular domain of CHL1 binds directly to the first extracellular loop of patched protein (Figure 5.19).

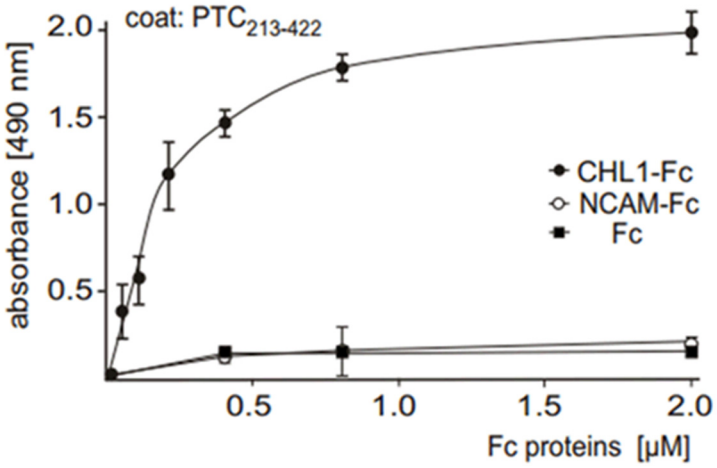

Figure 5.19. The extracellular domain of CHL1 binds directly to a patched fragment containing the first extracellular loop. Immobilized recombinant patched (PTC) fragment comprising amino acids 213-422 was incubated with increasing concentrations of soluble CHL1-Fc, NCAM-Fc or Fc. Binding was determined by ELISA using HRP-conjugated anti-human Fc antibody. Three independent experiments were performed in triplicates and mean values ± SD for absorbance at 490 nm is shown.

In a label-free binding assay, immobilized CHL1-Fc, NCAM-Fc or Fc fragments were incubated with increasing concentration of patched recombinant fragment. The patched fragment containing the first extracellular loop bound to CHL1-Fc, whereas only a negligible binding of patched to NCAM-Fc, which was used as control, was observed (Fig. 5.20).

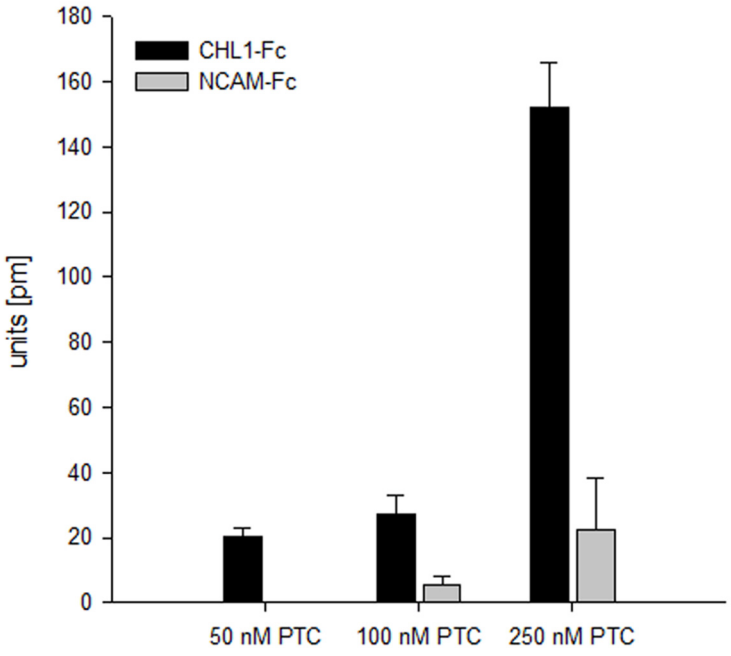

Figure 5.20. The extracellular domain of CHL1 binds directly to a patched fragment containing the sequence from the first extracellular loop. Immobilized CHL1-Fc, NCAM-Fc and Fc were incubated with recombinant patched (PTC) fragment (50 nM, 100 nM, 250 nM) in a label-free binding assay. Mean values ± SD of reflected wavelength shifts (pm) from three independent experiments performed in triplicate are shown. Values for binding of CHL1-Fc or NCAM-Fc to patched fragment were subtracted of Fc binding.

As CHL1 seems to be a novel ligand for patched, the receptor for hedgehog proteins, the question arose whether CHL1 shares sequence similarities with the already known patched ligands, such as sonic, desert and indian hedgehog. Alignments showed that amino acids 851-874 in the third FNIII domain (comprising amino acids 809 to 915), amino acids 1007-1027 in the fourth FNIII domain (comprising amino acids 916 to 1029) and amino acids 1050-1070 in the partial FNIII domain (comprising amino acids 1030 to1081) of murine CHL1 show sequence similarity to amino acids in the N-terminal domain of murine sonic hedgehog (amino acids 26-50, 51-72 and 77-98, respectively). Other members of the hedgehog family did not show sequences similarity to CHL1. Moreover, CHL1 and sonic hedgehog from several vertebrate species share three common motifs: TLGXXXK/RXXXKIT, DXIFXDXXXT and RXHPKXXXXL, suggesting that they are highly conserved among vertebrates (Fig. 5.21).

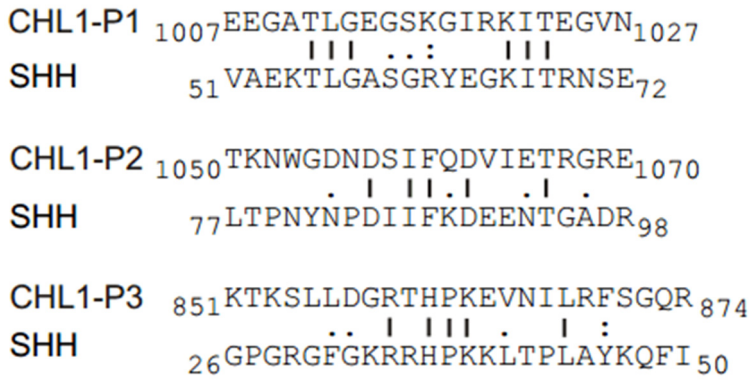

Figure 5.21. Sequence similarities between CHL1 and sonic hedgehog. CHL1-derived peptides (CHL1-P1, -P2 and -P3) show sequence similarities with sonic hedgehog (SHH). Bars are indicating identical amino acids (|), colon highly conserved (:), spots weakly conserved (.) amino acids, and numbers indicate amino acid positions.

Next, I tested by ELISA whether CHL1-derived peptides containing these motifs compete with CHL1-Fc in binding to patched. Immobilized recombinant patched protein fragment was incubated with CHL1-Fc in the absence and presence of CHL1-derived peptides. The peptides containing the TLGXXXK/RXXXKIT motif and the DXIFXDXXXT motif, but not the peptide with

the RXHPKXXXXL motif interfered with the binding of CHL1-Fc to the patched fragment (Fig. 5.22), suggesting that CHL1 might interact with patched via TLGXXXK/RXXXKIT and/or DXIFXDXXXT motif.

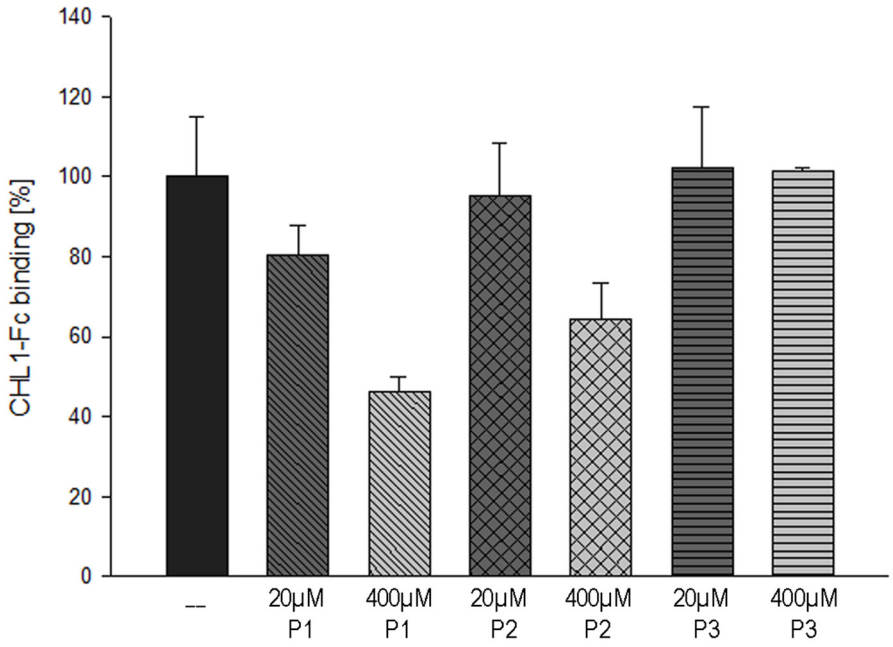

Figure 5.22. CHL1-derived peptides compete with the extracellular domain of CHL1 for binding to patched. Immobilized recombinant patched (PTC) fragment comprising amino acids 213-422 was incubated with 400 nM CHL1-Fc in the absence (-) or presence of different concentrations (20 µM, 400 µM) of the CHL1-derived peptides CHL1-P1, -P2 or -P3. Binding was determined using HRP-conjugated anti-human Fc antibody. Mean values ± standard deviation from three independent experiments performed in triplicates are shown for the binding of CHL1-Fc to the patched fragment in the presence of peptides relative to the binding in their absence.

5.2.2 CHL1 binds to patched and triggers neurite outgrowth and cerebellar migration *in vitro* in a smoothened dependent manner

The interaction between CHL1 and vitronectin triggers neurite outgrowth and granule cell migration, while the interaction between CHL1 and PAI-2 triggers granule cell migration, as shown in Chapter 5.1. In addition, it was reported that sonic hedgehog is a morphogen that controls cell motility and axonal guidance via patched-smoothened signaling (Charron and Tessier-Lavigne, 2005). Since CHL1 binds directly to patched and patched interacts with smoothened, we searched for the functional consequences of these interactions and investigated whether CHL1 binding to patched also influences neurite outgrowth and cell migration.

Dissociated cerebellar neurons from seven-day-old CHL1-deficient mice were maintained on PLL in the presence or absence of CHL1-Fc or L1-Fc, as control, and the active smoothened antagonist SANT-1 (Chen et al., 2002). Tomatidine, an inactive smoothened antagonist was used as a negative control (Rominger et al., 2009). The neurite outgrowth experiments were performed by Nicole Karl. CHL1-Fc enhanced neurite outgrowth around three-fold compared to the untreated PLL control (Fig. 5.23 A). In the presence of the active smoothened antagonist SANT-1 CHL1-induced neurite outgrowth was inhibited, whereas the inactive smoothened antagonist tomatidine did not have any effect. Moreover, L1-Fc enhanced neurite outgrowth around two-fold compared to the untreated PLL control, but this induction was not affected by addition of the smoothened antagonist SANT-1 (Fig. 5.23 A). Thus it can be concluded that the extracellular part of CHL1 interacts with smoothened and triggers the smoothened pathway to enhance neurite outgrowth.

Based on the previous finding that CHL1 also interacts with patched, we suspected that CHL1 triggers smoothened signaling via binding to the patched receptor. Thus, patched antibody against an epitope in the first extracellular loop (108-422 aa) or a peptide stretch comprising the CHL1 binding site in the first extracellular loop of patched were applied together with CHL1-Fc to cerebellar neuron cultures. A scrambled version of the patched peptide and smoothened antibody were used as negative control. Patched peptide and patched antibody reduced CHL1-triggered neurite outgrowth, whereas a scrambled version of the patched peptide or a smoothened antibody had no effect (Fig. 5.23 B). These results suggest that the extracellular part of CHL1 binds to patched, leading to recruitment of smoothened and triggering of the smoothened pathway to enhance neurite outgrowth.

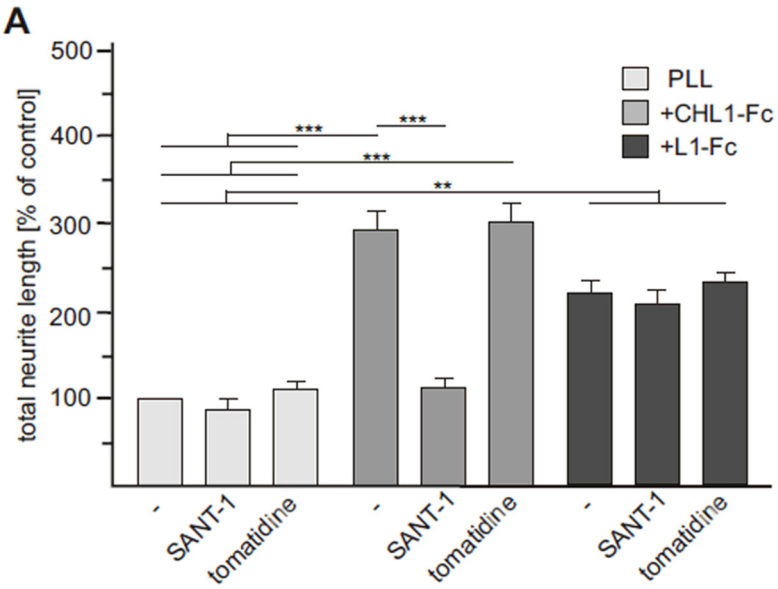

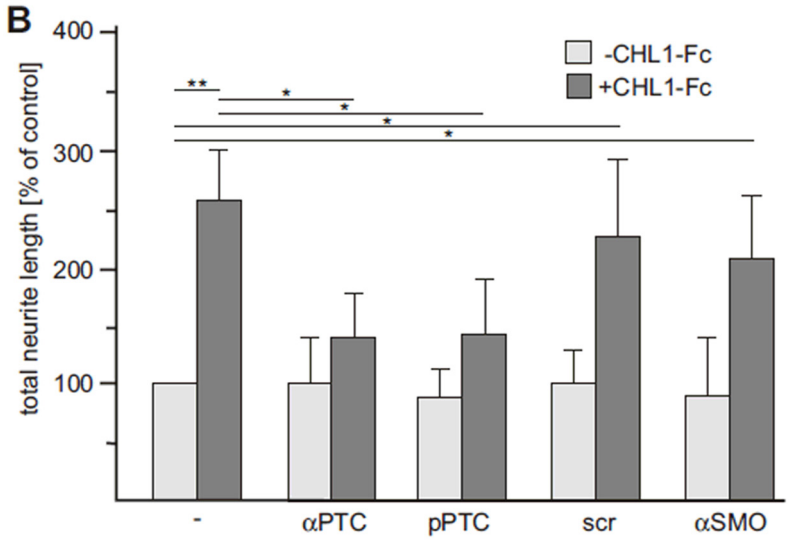

Figure 5.23. CHL1 enhances neurite outgrowth in a patched- and smoothened-dependent manner. ***A, B*** Dissociated cerebellar neurons from CHL1-deficient mice were cultured on a substrate without (PLL) or with CHL1-Fc or L1-Fc in the absence (-) or presence of the active smoothened (SMO) antagonist SANT-1 or the inactive antagonist tomatidine (*A*), or in the absence (-) or presence of the patched-derived synthetic peptide (pPTC), the scrambled version of pPTC (scr), or antibodies against patched (αPTC), or smoothened (αSMO) (*B*). Total neurite lengths of at least 100 neurons per condition were measured. Mean values ± SEM from three independent experiments are shown for the total lengths of neurites per neuron relative to the values in the untreated group (-). Group values were analyzed by one-way ANOVA with Tukey's multiple comparison test and differences between groups are indicated (* p< 0.05; ** p< 0.01; *** p< 0.005).

Next, we tested whether the CHL1 interaction with patched and smoothened is also involved in the CHL1-induced migration of cerebellar granule neurons. Cerebellar explant cultures from CHL1-deficient mice were maintained on PLL in the presence or absence of CHL1-Fc, and patched and smoothened antibodies, patched derived peptide and its scrambled version and the active smoothened antagonist SANT-1. Cell bodies migrating from the explant core were counted by Gabriele Loers, Ralf Kleene and myself.

The CHL1-enhanced cell migration was reduced in the presence of the patched peptide, the patched antibody and the SANT-1 antagonist, whereas the scrambled patched peptide and the smoothened antibody had no effect (Fig. 5.24). CHL1-Fc is not able to conduct the signaling responsible for induction of neurite outgrowth and cell migration when the binding site in the first extracellular loop of patched is masked. This result suggests that the extracellular part of CHL1 binds to patched and triggers a smoothened-dependent pathway which in turn contributes to enhancement of cell migration.

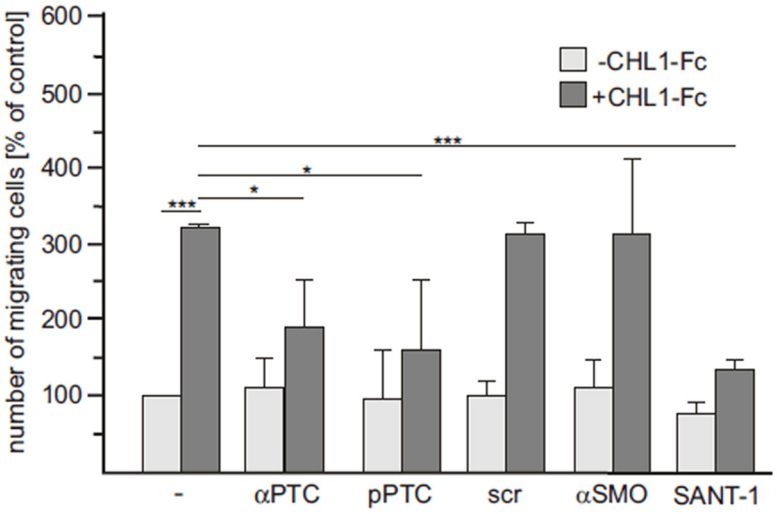

Figure 5.24. CHL1 enhances cerebellar cell migration in a patched- and smoothened-dependent manner. Explants from cerebella of CHL1-deficient mice were incubated without or with CHL1-Fc in the absence (-) or presence of the patched-derived synthetic peptide (pPTC), a scrambled version of pPTC (scr), or antibodies against patched (αPTC), or smoothened (αSMO). The number of migrating cells bodies from at least five explants per condition was measured. Mean values ± SEM from three independent experiments are shown for the total numbers of cell bodies migrating out of the explants relative to the values in the untreated group (-). Group values were analyzed by one-way ANOVA with Tukey's multiple comparison test and differences between groups are indicated (* $p < 0.05$; *** $p < 0.005$).

5.2.3 CHL1 binds to the first extracellular loop of patched and prevents patched-induced cell death in a smoothened dependent manner

Previous data indicate that CHL1 induces cell survival in dissociated cerebellar neuron cultures (Chen et al., 1999; Jakovcevski et al., 2009). Here, I showed that CHL1 binds directly to the first extracellular loop of patched (Chapter 5.2.1). Furthermore, patched is known as a pro-apoptotic ''dependence receptor": in the absence of its ligand of the hedgehog family, patched induces apoptosis (Robbins et al., 2012). This patched property raised the question whether CHL1 is a patched ligand that also inhibits apoptosis induced by patched. Since apoptosis in patched-overexpressing HEK 293T cells is blocked by application of sonic hedgehog (Thibert et al., 2003), I investigated whether CHL1-Fc application could have a similar effect. I transfected HEK 293 cells with the mammalian expression plasmid pRK-5 carrying the whole patched sequence. After transfection, I applied CHL1-Fc, the smoothened inhibitor SANT-1, L1-Fc and tomatidine as a negative control, and counted dead and live cells. CHL1-Fc inhibits cell death induced by overexpression of patched, whereas L1-Fc did not affect cell death by overexpression of patched (Fig. 5.25). Moreover, CHL1-induced cell survival is blocked by

SANT-1 inhibitor but not by tomatidine suggesting that CHL1 binds to patched and inhibits apoptosis via smoothened signaling pathway.

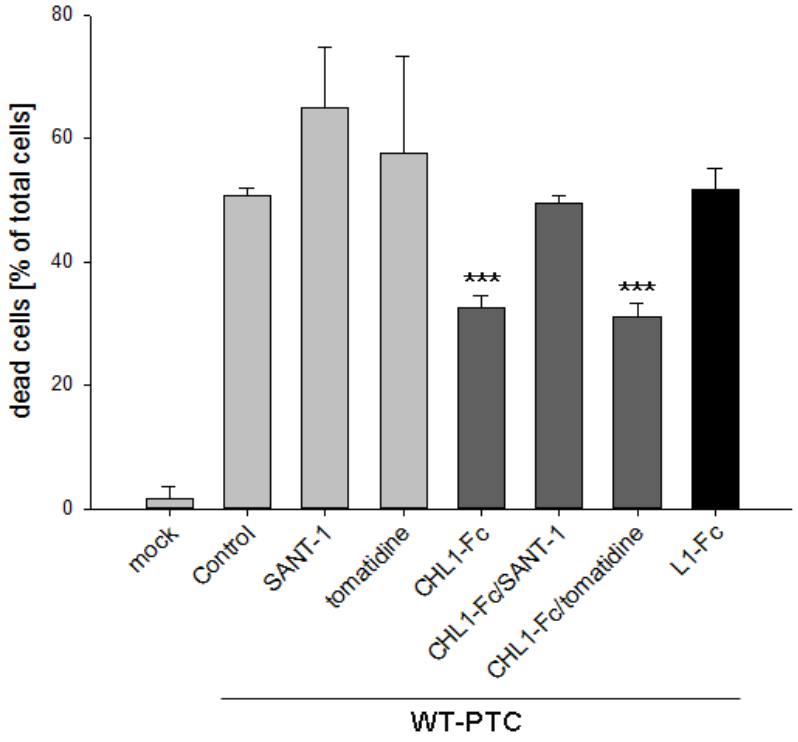

Figure 5.25. CHL1-Fc inhibits patched-induced cell death in transfected HEK293 cells via smoothened-dependent pathway. HEK293 cells were mock-transfected or transfected with a pRK5 mammalian expression vector carrying the sequence for whole mouse patched (WT-PTC). After transfection, cells were incubated in the absence (control) or presence of CHL1-Fc, L1-Fc, SANT-1 or tomatidine. The numbers of dead and live cells in twelve areas per microscopic field from two cell culture wells per treatment and experiment were counted. Mean values ± SEM from three independent experiments are shown for the number of dead cells relative to total number of dead and live cells. Group values were analyzed by one-way ANOVA with Tukey's multiple comparison test and differences between groups are indicated (*** $p < 0.005$).

Since CHL1-Fc binds directly to the first extracellular loop of patched, I tested whether CHL1 affects cell survival in the absence of this patched domain. It is worth noting that patched induces apoptosis via its intracellular C-terminus (Thibert et al., 2003). Thus, I deleted the whole extracellular loop in the patched-carrying vector and transfected HEK293 cells with the vectors expressing full-length or truncated patched. Deletion of the first extracellular loop did not affect the ability of patched to induce apoptosis. Moreover, CHL1-Fc inhibited apoptosis only when full length patched was present. This result indicates that CHL1 binds to the first extracellular loop of patched and thereby inhibits apoptosis.

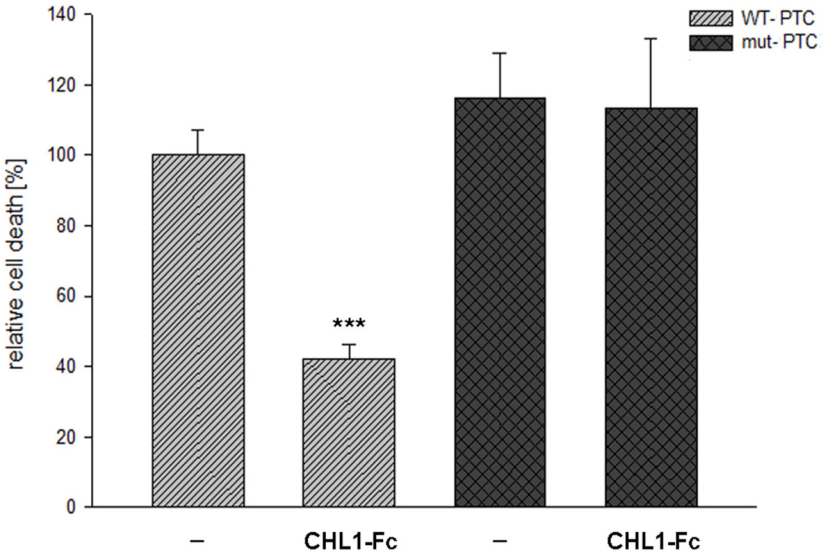

Figure 5.26. CHL1-Fc binds to the first extracellular loop of patched and inhibits patched-induced cell death in HEK293 cells. HEK293 cells were transfected with a pRK5 mammalian expression vector carrying the sequence for whole mouse patched (WT-PTC) or with the mutated WT-PTC vector with deletion of the first extracellular loop (mut-PTC). After transfection, cells were incubated in the absence (-) or presence of CHL1-Fc. The numbers of dead and live cells in twelve areas per microscopic field from two cell culture wells per treatment and experiment were counted. Mean values ± SEM from three independent experiments are shown for the number of dead cells relative to the values from untreated (-) group where cells were transfected with WT-PTC. Group values were analyzed by Mann-Whitney U test and differences between groups are indicated (*** $p < 0.005$).

During development of the cerebellum apoptosis occurs in two phases. The first wave occurs during the first postnatal week within the external granular layer, when the granule cells precursors that could not manage to exit mitosis are eliminated. The second wave starts within the internal granular layer at the end of the second postnatal week to eliminate the post-migratory granular cells that did not establish proper synapses with Purkinje cells (Lossi et al., 2002; Sotelo 2004). CHL1-deficient cerebellar neurons showed increased cell death during the second postnatal week relative to wild-type neurons upon serum-deprivation, which may cause the granular cell loss in the adult internal granular layer of CHL1-deficient mice compared to wild-type mice (Jakovcevski et al., 2009). Since 95% of all cells in a dissociated cerebellar cell culture represent granular cells this cell system was used to study granular cell death *in vitro*. Cerebellar neurons from seven-day-old CHL1-deficient cerebella were maintained in medium containing horse serum for five days followed by incubation in serum-free medium for two days to induce apoptosis.

Less cells died in the presence of soluble CHL1-Fc when compared to control conditions (Fig. 5.27), suggesting that CHL1-Fc induces granular cell survival. L1-Fc did not show any

significant effect on granular cell survival under this condition (Fig. 5.27). However, CHL1-induced granular cell survival was impaired when CHL1-Fc was applied together with the smoothened inhibitor SANT-1, but was not affected in the presence of CHL1-Fc and tomatidine (Fig. 5.27). This result suggests that CHL1-triggered survival of granular cells at the end of the second postnatal week *in vitro* is smoothened-dependent.

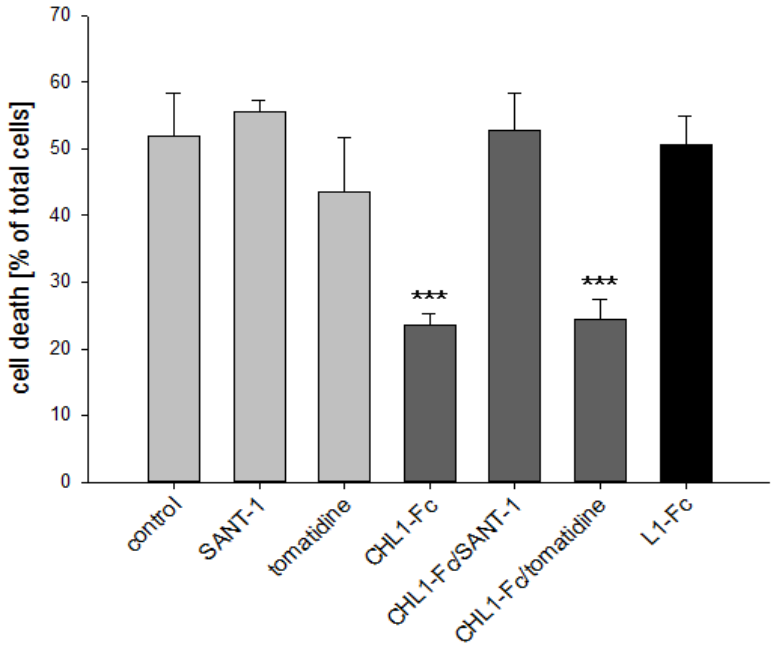

Figure 5.27. CHL1-Fc inhibits cell death in cultures of dissociated cerebellar neurons via a smoothened-dependent pathway. Dissociated cerebellar neurons from seven-day-old CHL1-deficient mice were cultured for five days in a medium containing serum and then exposed to serum-deprivation for 48 h in the absence (control) or presence of CHL1-Fc, L1-Fc, SANT-1 or tomatidine. The numbers of dead and live cells in twelve areas per microscopic field from three cell culture wells per treatment and experiment were counted. Mean values ± SEM from six independent experiments are shown for numbers of dead cells relative to total number of dead and live. Group values were analyzed by one-way ANOVA with Tukey's multiple comparison test and differences between groups are indicated (*** $p < 0.005$).

Since the CHL1-derived peptides which contain putative patched-binding motifs interfere with CHL1 binding to patched (Fig. 5.28), I investigated if these peptides influence CHL1-mediated cell survival in the cell death assay. Only the peptide containing the TLGXXXK/RXXXKIT/S motif (P1) reduced granular cell death when applied to the culture (Fig. 5.28). Moreover, this peptide seemed to interfere with the CHL1-triggered cell survival when applied in the culture together with CHL1-Fc (Fig. 5.28). In contrast, peptides containing the other two potential patched binding motifs within the CHL1 sequences (amino acids 851-874 (P2) and 1050-1070 (P3)) did not alter CHL1-induced cell survival. This result suggests that CHL1 binds to patched

via its TLGXXXK/RXXXKIT/S sequence (amino acids 1007-1027) and thereby triggers granular cell survival. Although the CHL1 peptide containing the DXIFXDXXXT (P2) motif might also mediate binding of CHL1 to patched (Fig. 5.22), results here show that binding of CHL1 to patched via this motif is not important for CHL1-mediated cell survival.

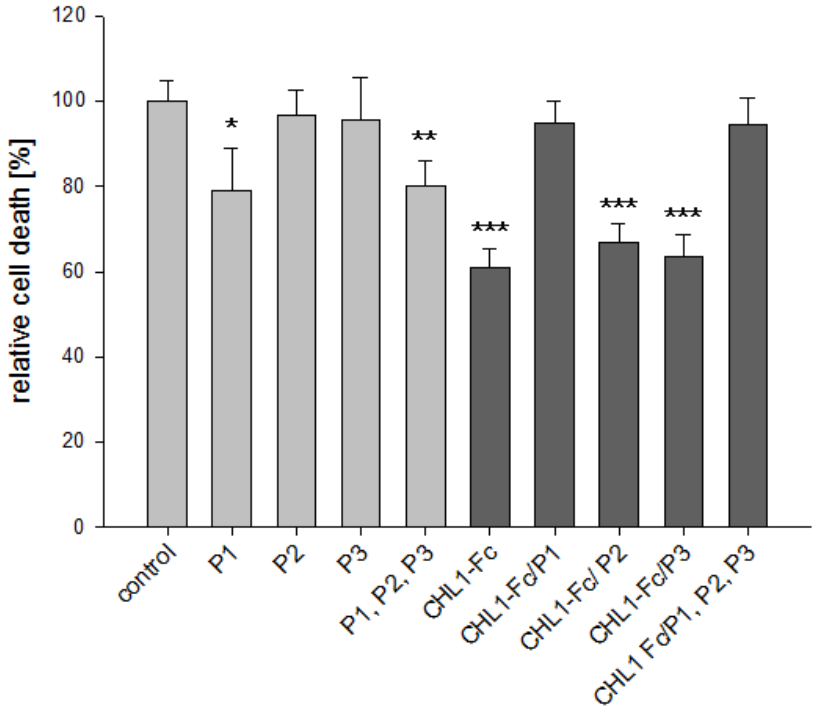

Figure 5.28. CHL1-Fc-induced cell survival is impaired in the presence of a CHL1-derived peptide containing the patched binding motif TLGXXXK/RXXXKIT/S. Cultures of dissociated cerebellar neurons from seven-day-old CHL1-deficient mice were cultured for five days in a medium containing serum and then exposed to serum-deprivation for 48h in the absence (control) or presence of CHL1-Fc or CHL1-derived peptides (P1, P2, P3). The numbers of dead and live cells in twelve areas per microscopic field from three cell culture wells per treatment and experiment were counted. Mean values ± SEM from three independent experiments are shown for cell death in each group relative to the untreated group (control). Group values were analyzed by one-way ANOVA with Tukey's multiple comparison test and differences between groups are indicated (* p< 0.05; ** p< 0.01; *** p< 0.005).

The disadvantage of the dissociated neuron cultures is that they cannot provide information about the cellular/layer organization. Due to the preparation procedures, the well defined layer organization of the cerebellar cortex is disrupted. Moreover, the majority of cells in the dissociated culture are granule neurons, isolated from synaptic contacts they had established with Purkinje cells. To study cell survival under more natural conditions in cells still maintaining their synaptic contacts organotypic cell cultures can be used. The organotypic cerebellar culture technique is preserving the original cerebellar structure and allows the study of other

cell types apart from granule neurons, such as Purkinje cells (Hurtado de Mendoza et al., 2011). Organotypic cell cultures are used here to characterize specific cell types in the cerebellum and to analyze CHL1-dependent and patched-mediated apoptotic processes in more detail.

Organotypic cerebellar slices were isolated from seven-day-old CHL1-deficient mice, maintained for five days in the culture, exposed to serum deprivation for 48 h and treated with CHL1-Fc, SANT-1, tomatidine and L1-Fc. To estimate the ratio of cell death after the treatments, slices were stained with the markers for dead and live cells - propidium iodide (PI) and calcein, respectively. Lower number of PI-positive cells is observed in slices treated with CHL1-Fc compared to the untreated slices, slices treated with SANT-1 alone or SANT-1 and CHL1-Fc together (Fig. 5.29 A). The cell death ratio, calculated as a percentage of PI-positive cells relative to the total cell number, is lower in the slices treated with CHL1-Fc compared to the untreated slices (Fig. 5.29 B). The treatment with tomatidine and CHL1-Fc together reduced the cell death, whereas the treatment with SANT-1, L1-Fc or SANT-1 and CHL1-Fc together did not change cell death compared to untreated control (Fig. 5.29 B). This result suggests that CHL1 triggers cell survival in organotypic cerebellar slices at the end of the second postnatal week *in vitro* in a smoothened-dependent manner.

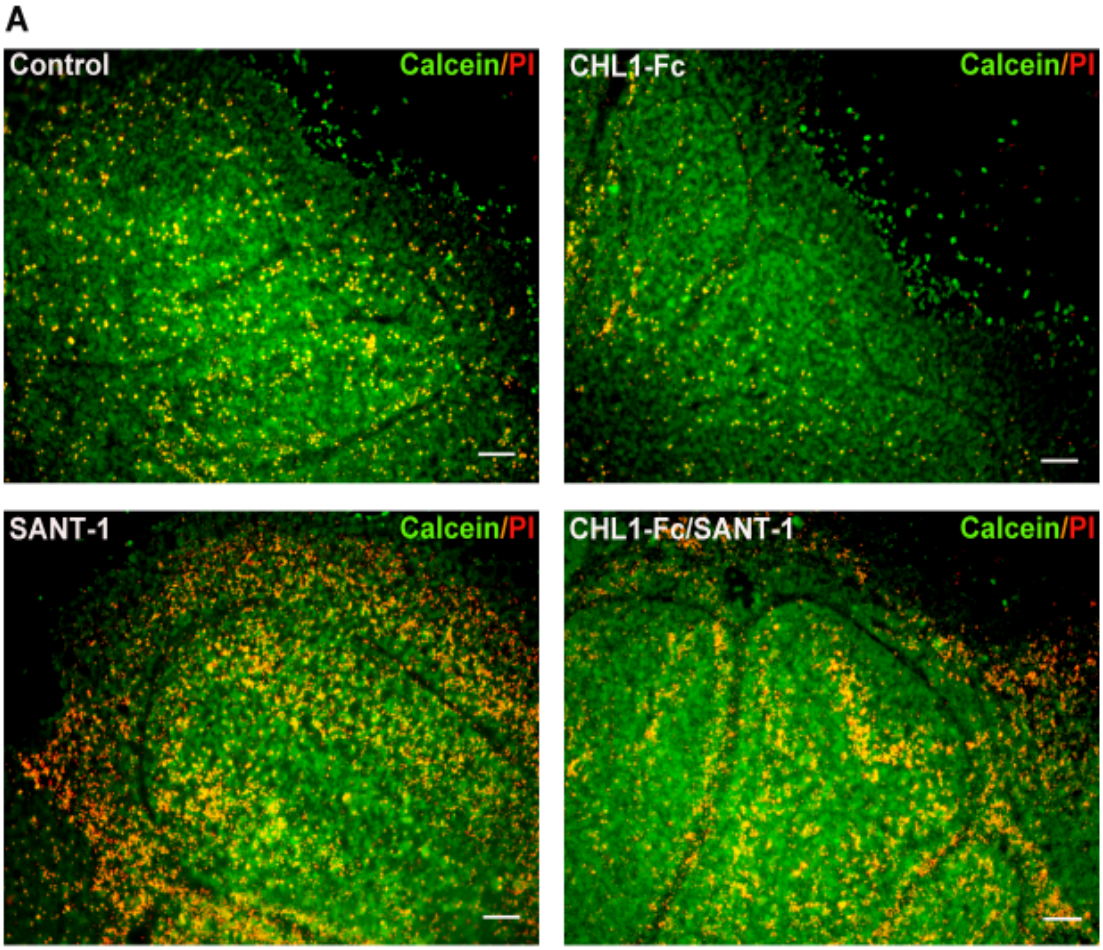
A
Control
Calcein/PI
CHL1-Fc
Calcein/PI
SANT-1
Calcein/PI
CHL1-Fc/SANT-1
Calcein/PI

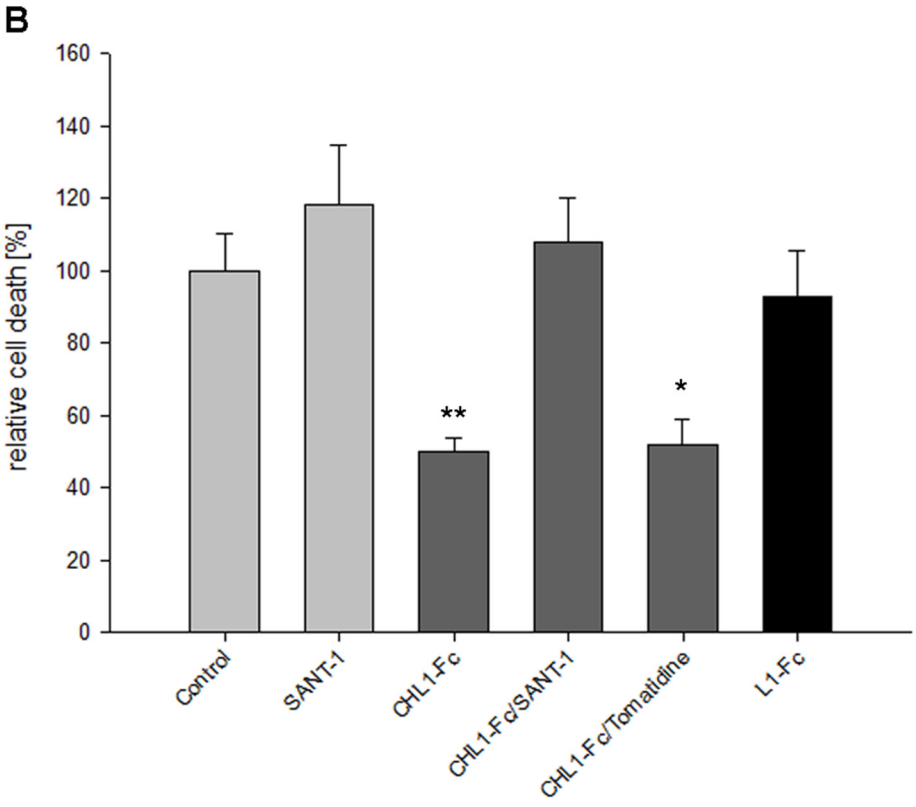
B
relative cell death [%]
160
140
120
100
80
60
40
20
0
**
*
Control
SANT-1
CHL1-Fc
CHL1-Fc/SANT-1
CHL1-Fc/Tomatidine
L1-Fc

Figure 5.29. CHL1-Fc inhibits cell death in organotypic slices via a smoothened-dependent pathway. Organotypic slices of cerebella from seven-day-old CHL1-deficient mice were cultured for five days in medium containing serum and then exposed to serum-deprivation for 48 h in the absence (control) or presence of CHL1-Fc, L1-Fc, SANT-1 or tomatidine. The numbers of dead propidium iodide-positive (PI) and live calcein-positive cells from five images per slice and two slices per condition were counted. ***A,*** Representative images are shown with the scale bar 100 µm. ***B,*** Mean values ± SEM from four independent experiments are shown for cell death in each group relative to the untreated group (control). Group values were analyzed by one-way ANOVA with Tukey's multiple comparison test and differences between groups are indicated (*p< 0.05; ** p< 0.01).

5.2.4 CHL1 binds to patched and inhibits caspase-3 activity in a smoothened dependent and caspase-9 activity in a smoothened independent manner

Activation of caspase-3 is one of the characteristics of early apoptosis process. Caspase-3 was shown to cleave the C-terminus of patched in the absence of patched ligands, leading to patched-induced cell death (Thibert et al., 2003). Since patched is able to induce cell death in the absence of CHL1, I investigated whether activation of caspase-3 in the early apoptotic process can be influenced by CHL1. HEK 293 cells were transfected with the mammalian expression plasmid pRK-5 carrying the whole patched sequence. After transfection, cells were treated with CHL1-Fc, SANT-1 inhibitor, L1-Fc and tomatidine. I detected ceaspase-3 activation by adding a caspase-3 substrate labeled with a chromophore to the culture and measuring the absorbance of the chromophore that is released after cleavage. A decrease in caspase-3 activity was seen after treatment with CHL1-Fc but not with L1-Fc (Fig. 5.30). However, after application of CHL1-Fc together with SANT-1, caspase-3 activity increased to the level measured in the control. Tomatidine did not change the reduction of caspase-3 activity after CHL1-Fc treatment (Fig. 5.30). This result shows that CHL1 binds to patched and inhibits caspase-3 activation in a smoothened-dependent manner.

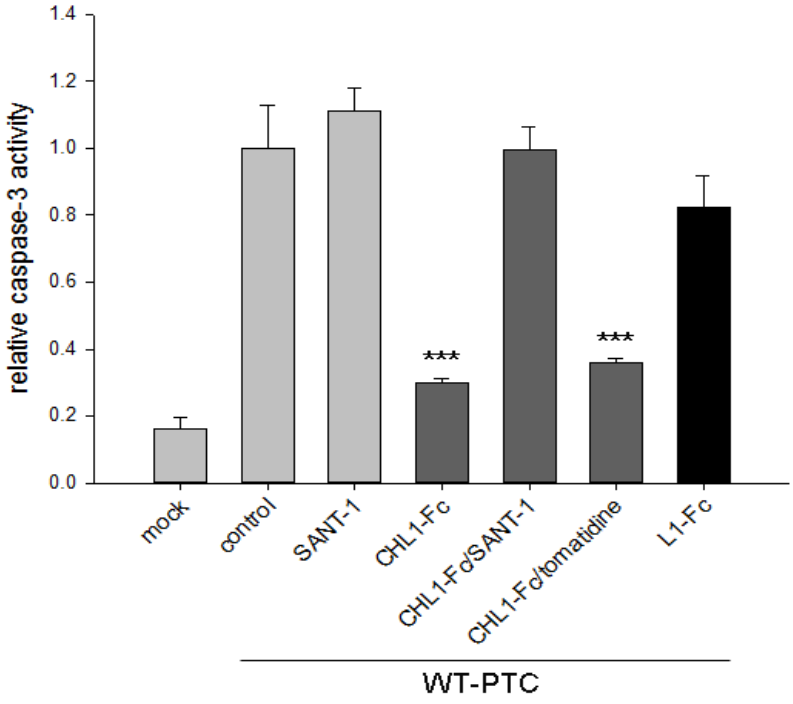

Figure 5.30. CHL1-Fc inhibits patched-induced caspase-3 activity in transfected HEK293 cells via a smoothened-dependent pathway. HEK293 cells were mock-transfected or transfected with a pRK5 mammalian expression vector carrying the sequence for whole mouse patched (WT-PTC). After transfection, cells were incubated in the absence (control) or presence of CHL1-Fc, L1-Fc, SANT-1 or tomatidine. The absorbance of caspase-3 cleaved substrate from two cell culture wells per treatment and experiment was measured. Mean values ± SEM from three independent experiments are shown for measured caspase-3 activity from each group relative to the untreated (control) group. Group values were analyzed by one-way ANOVA with Tukey's multiple comparison test and differences between groups are indicated (*** $p < 0.005$).

A similar pattern of caspase-3 activation was detected in cultures of dissociated cerebellar neurons exposed to serum deprivation: CHL1-deficient cells treated with CHL1-Fc displayed 50% lower caspase-3 activation relative to the untreated control, while SANT-1, but not tomatidine blocked CHL1-Fc-induced inhibition of caspase-3 activation (Fig. 5.31). Treatment with L1-Fc did not change the level of active caspase-3 compared to the untreated control. These results suggest that CHL1 inhibits caspase-3 activation in serum-deprived cerebellar neurons in a smoothened dependent manner.

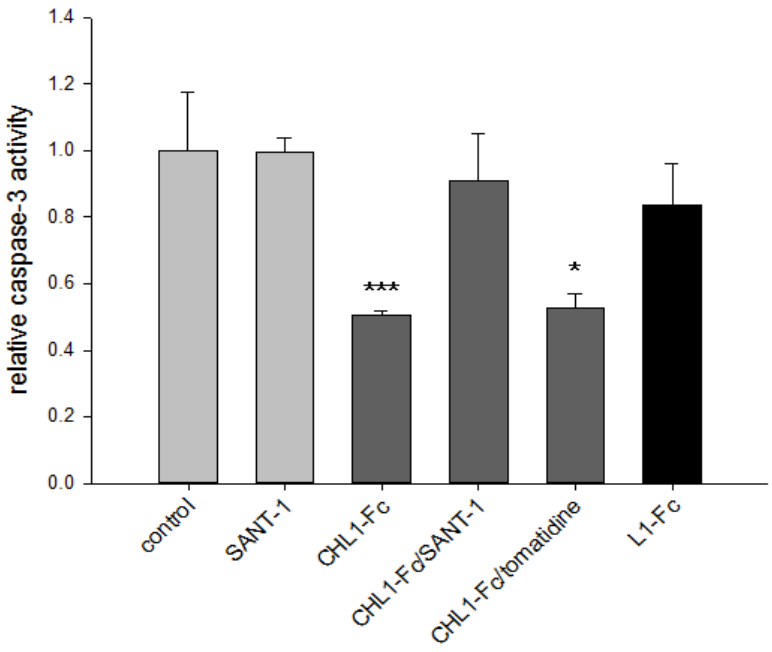

Figure 5.31. CHL1-Fc inhibits caspase-3 activation in cultured dissociated cerebellar neurons via a smoothened-dependent pathway. Dissociated cerebellar neurons from seven-day-old CHL1-deficient mice were cultured for six days in serum containing medium and then exposed to serum-deprivation for 24 h in the absence (control) or presence of CHL1-Fc, L1-Fc, SANT-1 or tomatidine. The absorbance of caspase-3 cleaved substrate from two cell culture wells per treatment and experiment was measured. Mean values ± SEM from three independent experiments are shown for measured caspase-3 activity from each group relative to the untreated (control) group. Group values were analyzed by one-way ANOVA with Tukey's multiple comparison test and differences between groups are indicated (*p< 0.05; *** p< 0.005).

In the absence of its ligand, patched induces activation of caspase-9 which in turn cleaves and activates caspase-3 (Mille et al., 2009; Fombonne et al., 2012). In CHL1-deficient cerebellar neurons caspase-3 is activated by serum deprivation, which can be abolished with CHL1-Fc treatment. Thus, I tested whether caspase-9 activation changes after CHL1-Fc treatment. CHL1-deficient cells treated with CHL1-Fc display 25% lower caspase-9 activation relative to the untreated control (Fig. 5.32). L1-Fc treatment did not show a significant effect. SANT-1 did not change CHL1-dependent reduction of caspase-9 activity. This result suggests that CHL1 inhibits caspase-9 activity via smoothened independent pathways.

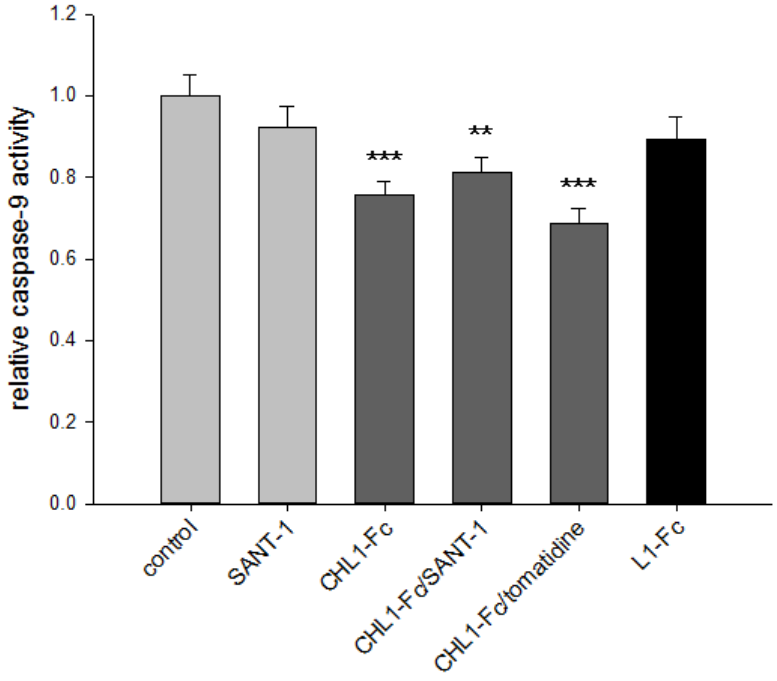

Figure 5.32. CHL1-Fc inhibits caspase-9 activity in cultured dissociated cerebellar neurons via a smoothened-independent pathway. Dissociated cerebellar neurons from seven-day-old CHL1-deficient mice were cultured for six days in serum containing medium and then exposed to serum-deprivation for 24 h in the absence (control) or presence of CHL1-Fc, L1-Fc, SANT-1 or tomatidine. The luminescence of caspase-9 cleaved substrate from two cell culture wells per treatment and experiment was measured. Mean values ± SEM from three independent experiments are shown for measured caspase-9 activity from each group relative to the untreated (control) group. Group values were analyzed by one-way ANOVA with Tukey's multiple comparison test and differences between groups are indicated (**p< 0.01; *** p< 0.005).

5.2.5 CHL1-Fc inhibits apoptosis of cerebellar granule and Purkinje cells in cerebellar organotypic slices via smoothened signaling pathways

CHL1-Fc inhibits cell death in two weeks old CHL1-deficient organotypic cerebellar slices. However, the cell death assay could not provide information in which cell type apoptosis is induced. Thus, I stained organotypic slices with antibodies against markers of granular and Purkinje cells (NeuN and calbinding, respectively). In parallel, slices were stained with two different markers of apoptosis: caspase-3- marker for early apoptotic events and TUNEL-marker for later apoptotic events during which DNA fragmentation occurs. Thus, I could determine which cell type undergoes apoptosis and in which stage of apoptosis the cells are. To induce apoptosis, I exposed CHL1-deficient organotypic slices to serum deprivation for 48 h in the absence or presence of CHL-Fc, L1-Fc, SANT-1 and tomatidine. Afterwards, I quantified the number of dead granule cells by counting the number of NeuN/caspase-3- or NeuN/TUNEL-double positive cells, using Stereo Investigator. To estimate Purkinje cell death, I counted the number of calbindin/caspase-3- or calbindin/TUNEL-double positive cells. A

lower number of TUNEL positive granular cells was observed in the group treated with CHL1-Fc relative to the control group, and the groups treated with CHL1-Fc and SANT-1 or L1-Fc (Fig. 5.33). The group treated with CHL1-Fc shows also a lower number of TUNEL positive Purkinje cells compared to the groups treated with CHL1-Fc and SANT-1 or L1-Fc (Fig. 5.33). Generally, there are just a few granular and Purkinje cells that are TUNEL positive in the group treated with CHL1-Fc (Fig. 5.33).

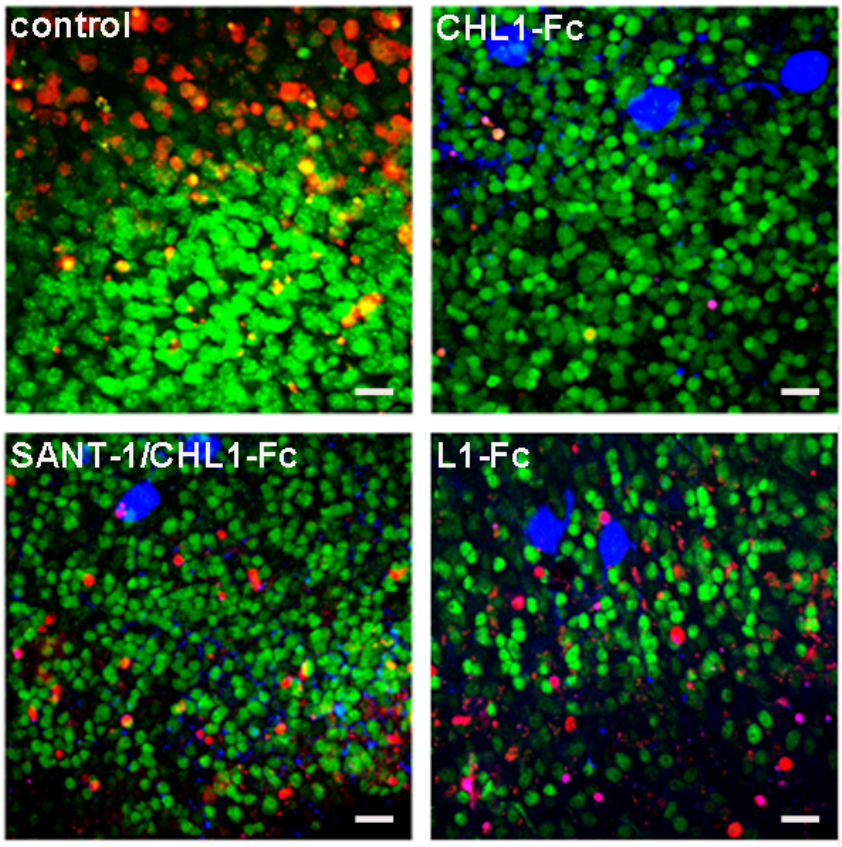

Figure 5.33. CHL1-Fc inhibits apoptosis of cerebellar granule and Purkinje cells in a smoothened-dependent manner. Organotypic slices from cerebella of CHL1-deficient mice were cultured for five days in serum containing medium and then exposed to serum-deprivation for 48 h in the absence (control) or presence of CHL1-Fc, CHL1-Fc and SANT-1 together, and L1-Fc. Slices were labeled with TUNEL (red) or stained against NeuN (green) or calbindin (blue) antibody. Representative images are shown. Scale bar, 20 µm.

After quantification, I noticed a significantly lower density of apoptotic granule cells, both TUNEL and caspase-3 labeled, in the CHL1-Fc treated group relative to the control group (Fig. 5.34 A, B). Groups treated with L1-Fc, SANT-1 alone and SANT-1 and CHL1-Fc together have the same density of apoptotic granule cells relative to the control group (Fig. 5.34 A, B). The density of apoptotic Purkinje cells was much lower than the density of apoptotic granule cells

(Fig. 5.34 C, D). However, apoptotic Purkinje cell density was significantly lower in the group treated with CHL1-Fc relative to the control group: less caspase-3- and TUNEL-labeled Purkinje neurons were observed after CHL1-Fc treatment (Fig. 5.34 C, D). The density of the apoptotic Purkinje cells was similar after treatment with L1-Fc, SANT-1 alone and SANT-1 and CHL1-Fc together (Fig. 5.34 C, D). These results indicate that CHL1-Fc prevents apoptosis of both granule and Purkinje cells in a smoothened-dependent manner in two weeks old organotypic cerebellar slices.

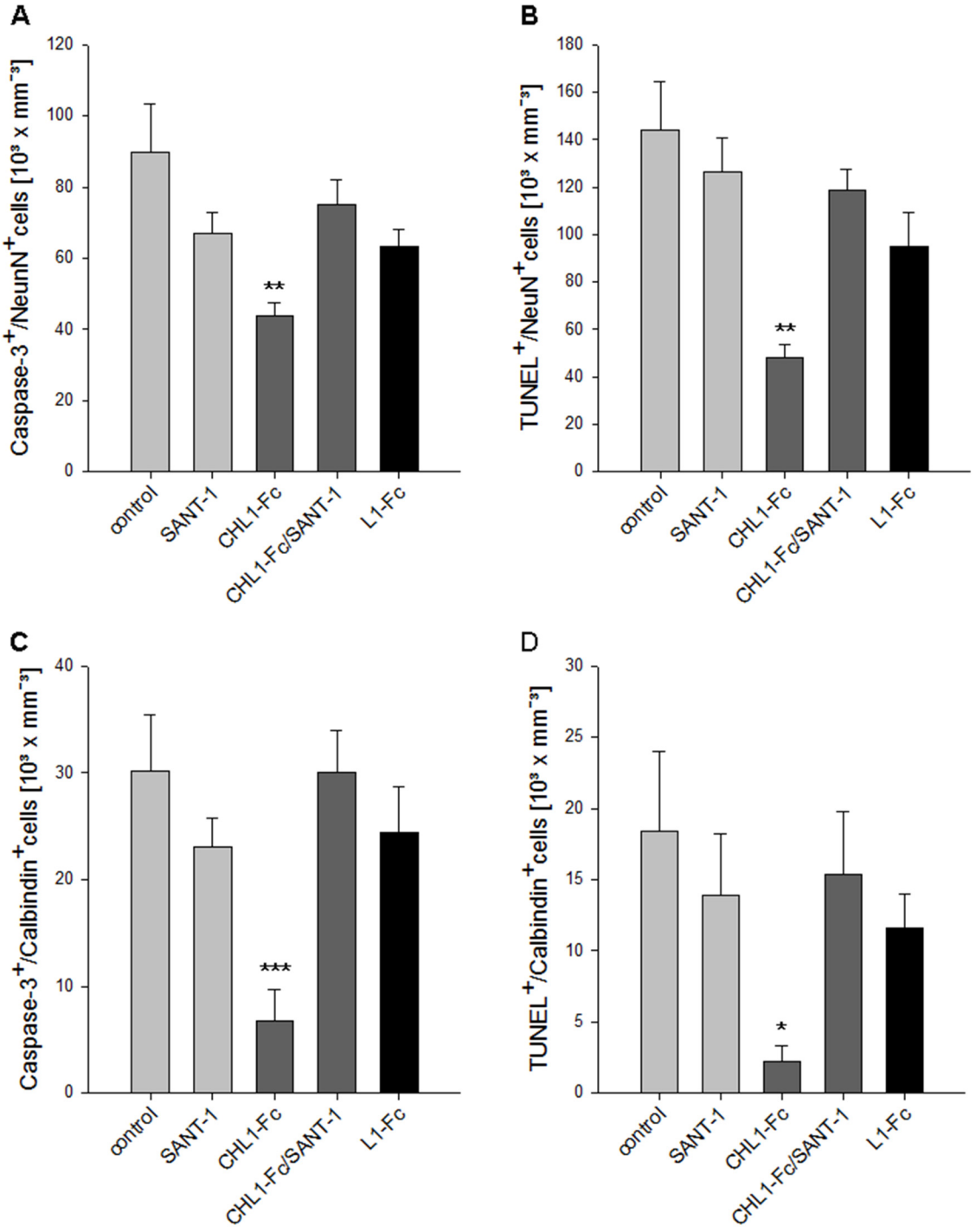

Figure 5.34. CHL1-Fc inhibits apoptosis of cerebellar granule and Purkinje cells in a smoothened-dependent manner. Organotypic slices from cerebella of CHL1-deficient mice were cultured for five days in serum containing medium and then exposed to serum-deprivation for 48 h in the absence (control) or presence of CHL1-Fc, L1-Fc, or SANT-1. Mean values ± SEM from eight independent experiments including two images per slice and two slices per condition and experiment are shown for the number of cells positive for active caspase-3 and NeuN (***A***), TUNEL and NeuN (***B***), active caspase-3 and calbindin (***C***), or TUNEL and calbindin (***D***) staining. Group values were analyzed by one-way ANOVA with Tukey's multiple comparison test and differences between groups are indicated (* p< 0.05, ** p< 0.01; *** p< 0.005).

5.2.6 CHL1 triggers cellular responses via "non-canonical" Gli-independent signaling pathways

After sonic hedgehog binds to patched, smoothened is released from inhibition by patched and triggers a signal transduction cascade that results in expression of transcription factors, such as GLI1, GLI2 and GLI3. This signaling cascade is known as the "canonical pathway" (Goodrich et al., 1997; Robbins et al., 2012). Since CHL1 binds to patched and activates smoothened, I investigated whether the expression levels of the GLI transcription factors were altered after treatment of cells with CHL1. Since the patched gene is a direct transcriptional target of GLI3 and since the patched ligand sonic hedgehog induces expression of patched (Goodrich et al., 1996), I examined whether patched mRNA levels were increase after CHL1-Fc stimulation. To this aim, I stimulated CHL1-deficient and wild-type cerebellar neurons with CHL1-Fc or L1-Fc and measured patched, GLI1, and GLI3 mRNA levels by quantitative real-time PCR. Surprisingly, the CHL1-Fc treatment did not change the mRNA level of the target genes in CHL1-deficient and wild-type neurons (Fig. 5.35). The mRNA levels of target genes were also not changed after L1-Fc treatment relative to the mRNA levels of untreated control (Fig. 5.35). This result suggests that CHL1 does not trigger the "canonical pathway".

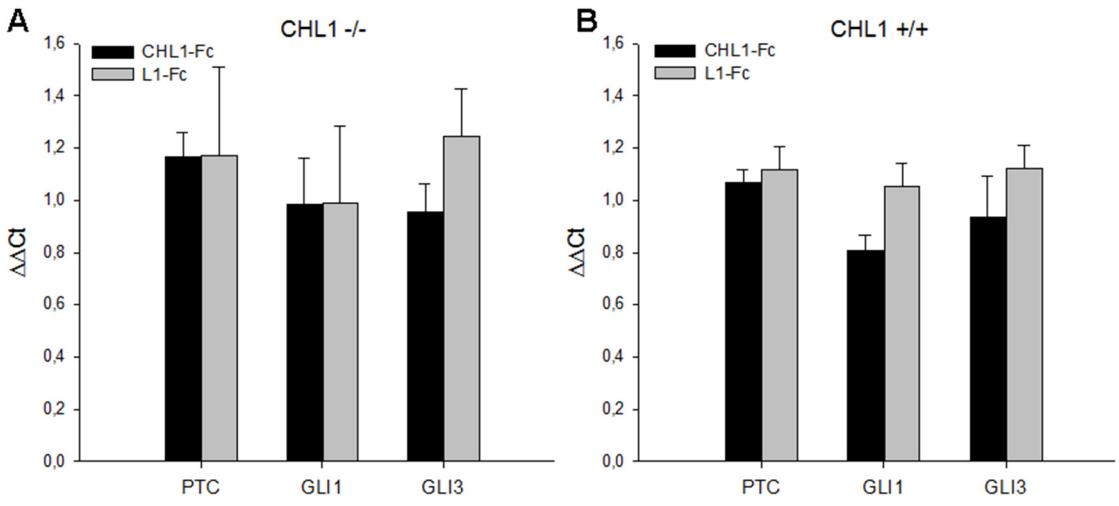

Figure 5.35. CHL1-stimulation does not induce gene expression of GLI transcription factors. Cultures of dissociated cerebellar neurons from cerebella of seven-day-old CHL1-deficient (CHL1-/-, ***A***) or wild-type (CHL1+/+, ***B***) mice were incubated in the absence or presence of CHL1-Fc or L1-Fc. Neurons were then subjected to real-time PCR using patched (PTC)-, GLI-1-, or GLI-3-specific primers. Mean values ± SEM from seven independent experiments are shown for patched, GLI-1 and GLI-3 RNA levels relative to the RNA levels of reference genes in neurons treated with CHL1-Fc or L1-Fc relative to levels in non-treated neurons (ΔΔCt). Group values were analyzed by one-way ANOVA with Tukey's multiple comparison test, no statistically significant differences between groups were noticed.

Besides the "canonical" signaling, patched also mediates hedgehog-induced "non-canonical" GLI-independent signaling (Brennan et al., 2012; Robbins et al., 2012). The "non-canonical" signaling involves rapid cellular responses that do not include gene transcription. This pathway also depends on smoothened activation. Smoothened stimulates small guanosine triphosphatases (GTPase), namely RhoA and Rac1, which trigger rearrangement of the actin cytoskeleton and thereby promote migration and axonal guidance (Yam et al., 2009; Polizio et al., 2011b). Besides its function in remodeling of the cytoskeleton, RhoA is also involved in regulation of the cell cycle and apoptosis (Jaffe and Hall, 2005; Li et al., 2013). Since CHL1 promotes smoothened-dependent cerebellar neuron migration and neurite outgrowth, but does not change GLI expression, I hypothesize that CHL1 could be involved in the "non-canonical" patched signaling pathway and might activate RhoA.

To determine whether CHL1 regulates RhoA, I measured RhoA activation in wild-type and CHL1-deficient cerebellar neurons after treatment with CHL1-Fc and SANT-1. The level of activated RhoA in CHL1-deficient neurons increased after CHL1-Fc treatment and declined to the control level in the concomitant presence of SANT-1 and CHL1-Fc (Fig. 5.36). In wild-type neurons, the level of activated RhoA was high in the untreated control and decreased after CHL1-Fc or SANT-1/CHL1-Fc application (Fig. 5.36). This result indicates that CHL1 activates RhoA via a smoothened-dependent pathway.

Quantification of the protein levels of activated RhoA measured by Western blot analysis showed the same pattern of RhoA activation. In CHL1-deficient neurons, CHL1-Fc treatment increased the level of activated RhoA for around 50% relative to the untreated control, whereas after CHL1-Fc and SANT-1 treatment the level of activated RhoA declined to control level (Fig. 5.37). In wild-type mice, CHL1-Fc application did not significantly decrease the level of activated RhoA, whereas CHL1-Fc and SANT-1 application significantly decreased the level of activated RhoA compared to the untreated control (Fig. 5.37).

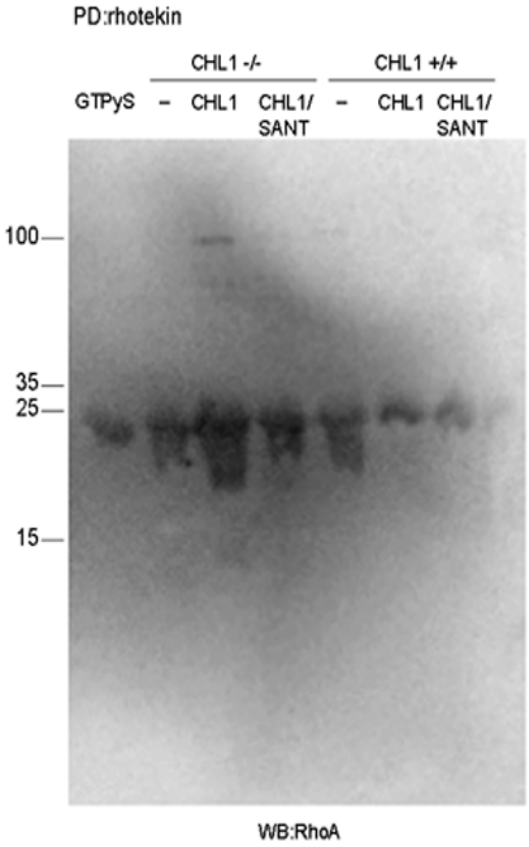

Figure 5.36. CHL1 triggers RhoA activation in a smoothened-dependent manner. Cultures of dissociated cerebellar neurons from cerebella of seven-day-old CHL1-deficient (CHL1-/-) or wild-type (CHL1+/+) mice were incubated in the absence (-) or presence of CHL1-Fc or SANT-1. Cell lysates were subjected to pull-down with rhotekin beads which bind preferentially to RhoA-GTP complex, to determine the level of activated RhoA. Cell lysates incubated with GTPγS served as positive control. Samples were subjected to Western blot analysis using anti-RhoA antibody and HRP-conjugated secondary antibody. RhoA protein bands of ~20 kDa were detected in all cell lysates.

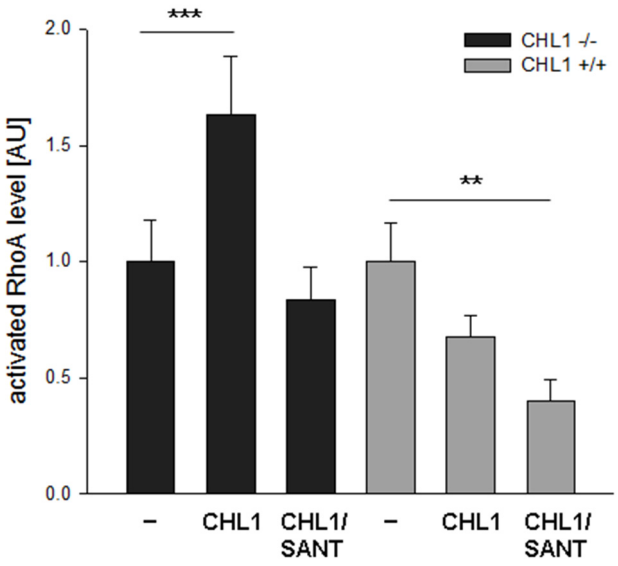

Figure 5.37. CHL1 triggers RhoA activation in a smoothened-dependent manner. Cultures of dissociated cerebellar neurons from cerebella of seven-day-old CHL1-deficient (CHL1-/-) or wild-type (CHL1+/+) mice were incubated in the absence (-) or presence of CHL1-Fc or SANT-1. Neurons were then subjected to a pull-down assay and Western blot analysis to determine activated RhoA and to quantify levels of activated RhoA. Mean values ± SEM from three independent experiments are shown for activated RhoA levels relative to values in the untreated group. Group values were analyzed by one-way ANOVA with Tukey's multiple comparison test and differences between groups are indicated (*** $p < 0.005$).

5.2.7 CHL1 triggers neurite outgrowth and cerebellar migration in a RhoA-dependent manner

I showed that CHL1 enhances cerebellar neuron migration and neurite outgrowth via a smoothened dependent pathway. Moreover, CHL1 activates RhoA GTPase which was identified as an important player of the "non-canonical" patched pathway. Granule cell migration is known to be initiated by Rho-dependent pathways (Chédotal, 2010). Thus, I determined whether CHL1 triggers "non-canonical" RhoA-dependent patched pathways which consequentially lead to enhanced cell migration and neurite outgrowth.

To investigate whether CHL1-induced cell migration depends on RhoA activation, I applied a selective RhoA inhibitor (Shanga et al., 2013) to CHL-deficient cerebellar explants. RhoA activates its direct downstream interaction partner RhoA associated kinase (ROCK) which further regulates migration and apoptosis of myeloid leukemia, fibroblast and mouse embryonal carcinoma P19 cells (Tsai and Wei, 2010; Street and Bryan, 2011). Thus, I also applied a selective ROCK inhibitor to the explants cultures (Liao et al., 2007). Cerebellar neurons migrated from the explant core extensively after application of CHL1-Fc to the cultures. CHL1-enhanced migration was inhibited by application of RhoA and ROCK inhibitor (Fig. 5.38). Inhibitors alone did not have any effect on cell migration on PLL substrate. Thus, CHL1-triggered migration depends on both RhoA and ROCK.

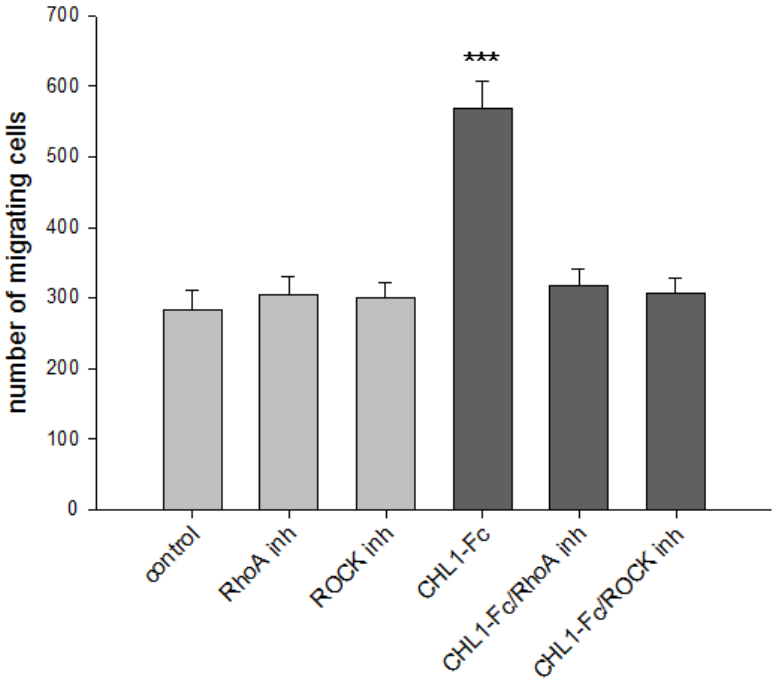

Figure 5.38. CHL1-Fc promotes neuronal cell migration via RhoA- and ROCK-dependent pathways. Cerebellar explants from six-day-old CHL1-deficient mice were cultured in the absence (control) or presence of CHL1-Fc and RhoA inhibitor (RhoA inh) or ROCK inhibitor (ROCK inh). The number of migrating cells from at least five explants per condition was determined. Mean values ± SEM from three independent experiments are shown for the total numbers of cell bodies migrating out of the explants. Group values were analyzed by one-way ANOVA with Tukey's multiple comparison test and differences between groups are indicated (*** $p < 0.005$).

To analyze whether CHL1-induced neurite outgrowth depends on RhoA activation, I applied RhoA and ROCK inhibitors to dissociated cerebellar neurons isolated from CHL-deficient mice. Cerebellar neurites grew longer when CHL1-Fc was applied to the culture. CHL1-enhanced neurite outgrowth was inhibited when RhoA or ROCK inhibitor was applied together with CHL1-Fc to dissociated cerebellar cells, while inhibitors alone did not have any effect (Fig. 5.39), indicating that CHL1-triggered neurite outgrowth depends on RhoA and ROCK.

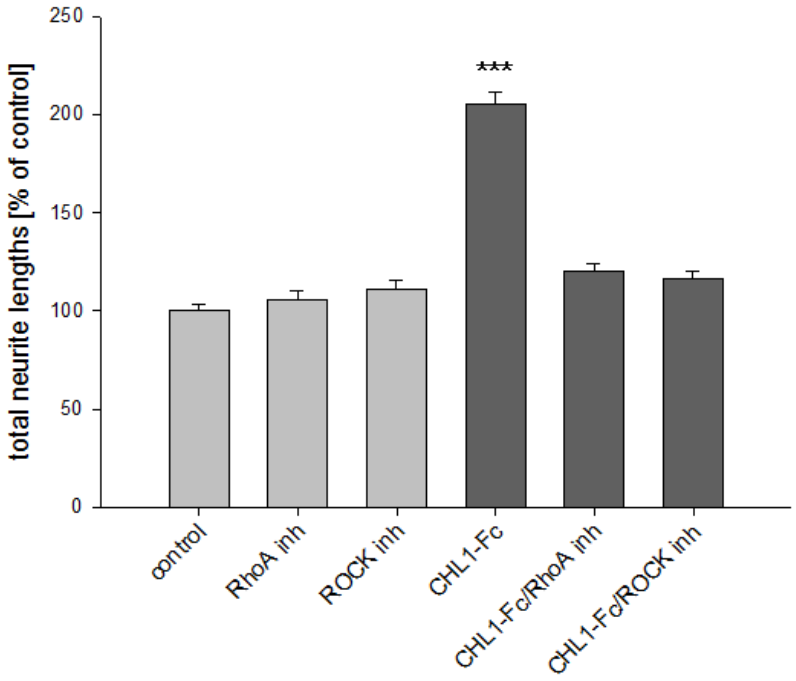

Figure 5.39. CHL1-Fc promotes neurite outgrowth via RhoA- and ROCK-dependent pathways. Cultures of dissociated cerebellar neurons from seven-day-old CHL1-deficient mice were incubated in the absence (control) or presence of CHL1-Fc and RhoA inhibitor (RhoA inh) or ROCK inhibitor (ROCK inh). Total neurite lengths of at least 100 neurons per condition were determined. Mean values ± SEM from three independent experiments are shown for the total lengths of neurites per neuron relative to the values in control group. Group values were analyzed by Mann-Whitney U test and differences between groups are indicated (*** $p < 0.005$).

5.2.8 CHL1-Fc inhibits apoptosis of cerebellar neurons in a RhoA-dependent manner

To examine whether CHL1 prevents cell death by serum deprivation via RhoA and ROCK activation, I measured cell death in the absence or presence of RhoA and ROCK inhibitors. Cell death assay was performed on cultures of dissociated neurons and organotypic slices isolated from CHL1-deficient cerebellum. Cells treated with CHL1-Fc survived more compared to the untreated control both in dissociated culture and organotypic slices (Fig. 5.40 and Fig. 5.41). In the absence of CHL1, no effect was observed for either inhibitor, but both inhibitors blocked the pro-survival effect of CHL1-Fc (Fig. 5.40 and Fig. 5.41). These results suggest that CHL1 inhibits apoptosis in a RhoA/ROCK-dependent manner.

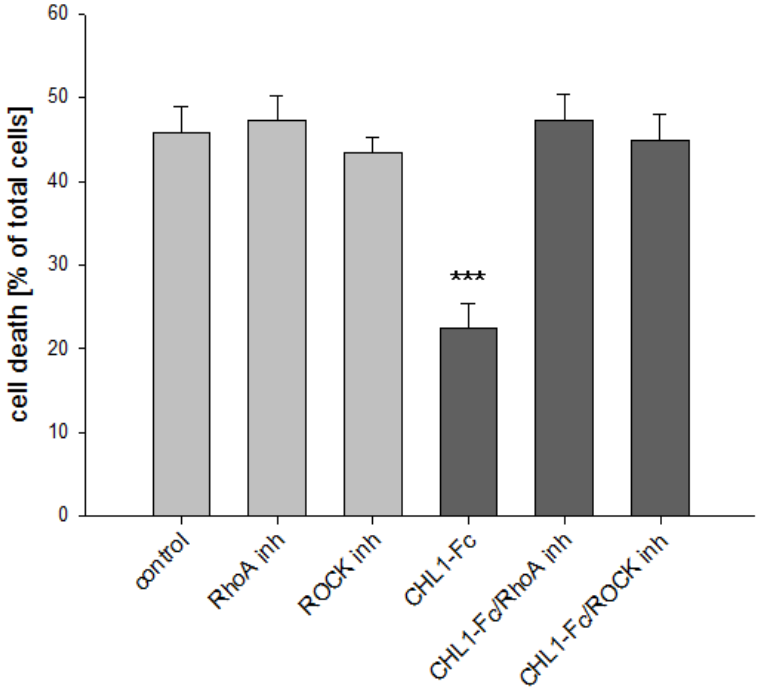

Figure 5.40. CHL1-Fc inhibits death of dissociated cerebellar neurons via RhoA- and ROCK-dependent pathways. Cultures of dissociated neurons from cerebella of seven-day-old CHL1-deficient mice were cultured for five days in medium containing serum and then exposed to serum-deprivation for 48 h in the absence (control) or presence of CHL1-Fc and RhoA (RhoA inh) or ROCK inhibitors (ROCK inh). Mean values ± SEM from six independent experiments are shown for the numbers of dead cells relative to number of dead and live cells. Twelve areas per microscopic field from three cell culture wells per treatment and experiment were counted. Group values were analyzed by one-way ANOVA with Tukey's multiple comparison test and differences between groups are indicated (*** $p < 0.005$).

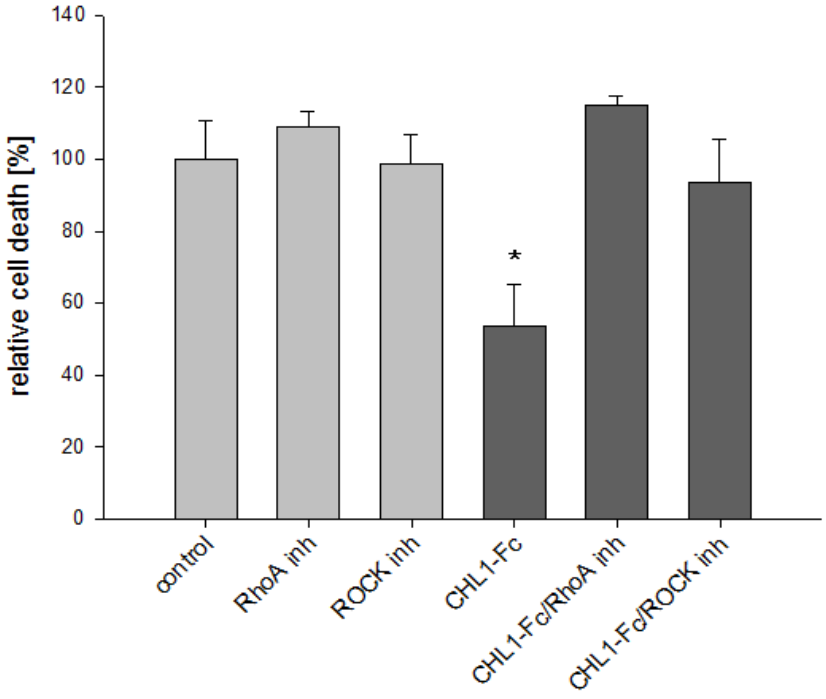

Figure 5.41. CHL1-Fc inhibits cell death in organotypic cerebellar slices via RhoA- and ROCK-dependent pathways. Organotypic slice cultures from cerebella of seven-day-old CHL1-deficient mice were cultured for five days in medium containing serum then exposed to serum-deprivation for 48 h in the absence (control) or presence of CHL1-Fc and RhoA (RhoA inh) or ROCK inhibitors (ROCK inh). Mean values ± SEM from four independent experiments are shown for cell death relative to the values in control group. Five images per slice from two slices per condition were counted. Group values were analyzed by one-way ANOVA with Tukey's multiple comparison test and differences between groups are indicated (* $p < 0.05$).

Since CHL1-Fc prevents apoptosis of both granule and Purkinje cells in a smoothened-dependent manner, I examined the role of RhoA and ROCK in this pathway. Organotypic slices were isolated from seven-day-old CHL1-deficient cerebellum, maintained in culture for five days, exposed to serum deprivation for 48 h and treated with CHL1-Fc, and with and without RhoA or ROCK inhibitor. Slices with were stained with antibodies against markers of granular and Purkinje cells (NeuN and calbinding, respectively) and markers of apoptosis (caspase-3 and TUNEL). I quantified the number of dead granule cells by counting the number of NeuN/caspase-3- or NeuN/TUNEL-double positive cells. To estimate Purkinje cell death, the number of calbindin/caspase-3- or calbindin/TUNEL-double positive cells was counted in a similar manner.

Higher numbers of granular cells that were TUNEL-positive were observed in control slices compared with slices treated with CHL1-Fc (Fig. 5.42). In slices treated with CHL1-Fc and RhoA inhibitor as well as in the slices treated with CHL1-Fc and ROCK inhibitor, a lot more TUNEL-positive granular and Purkinje cells were observed when compared to the group treated with CHL1-Fc (Fig. 5.42).

Quantification of TUNEL-positive cells and of cells positively stained for active caspase-3 showed that both inhibitors blocked CHL1-induced granule and Purkinje cell survival. Much more NeuN/caspase-3 and NeuN/TUNEL-double positive neurons were detectable in slices treated with CHL1-Fc and RhoA or ROCK inhibitor compared to slices treated with CHL1-Fc alone (Fig. 5.43). The same trend was seen in Purkinje cells – there are more apoptotic neurons in the group treated with CHL1-Fc and RhoA or ROCK inhibitor compared to the group treated with CHL1-Fc alone (Fig. 5.43). There was no significant difference in apoptosis between groups treated only with RhoA or ROCK inhibitor relative to the control group (Fig. 5.43). These results show that cell survival mediated by CHL1 requires RhoA and ROCK activation and suggest that binding of CHL1 to patched triggers "non-canonical" RhoA-dependent signal cascades which inhibits apoptosis of granule and Purkinje cells.

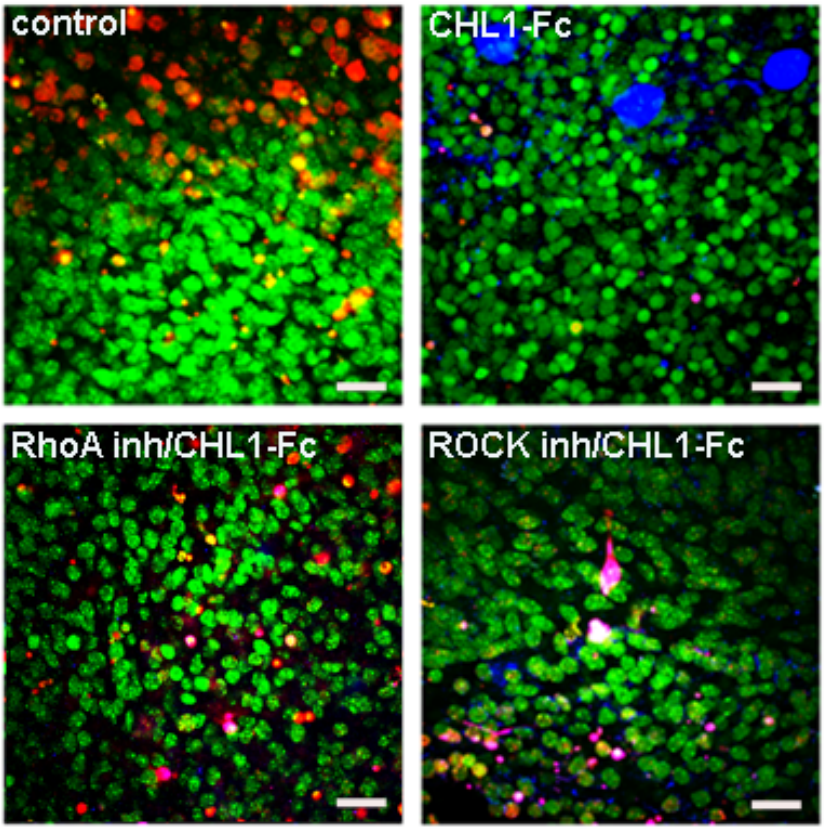

Figure 5.42. CHL1-Fc inhibits apoptosis of cerebellar granule and Purkinje cells via RhoA- and ROCK-dependent pathways. Organotypic slice cultures from cerebellum of CHL1-deficient mice were cultured for five days in medium containing serum and then exposed to serum-deprivation for 48 h in the absence (control) or presence of CHL1-Fc alone or CHL1 and RhoA or ROCK inhibitors. Slices were TUNEL labeled (red) and stained against NeuN (green) or calbindin (blue) antibody. Representative images are shown. Scale bar, 20 µm.

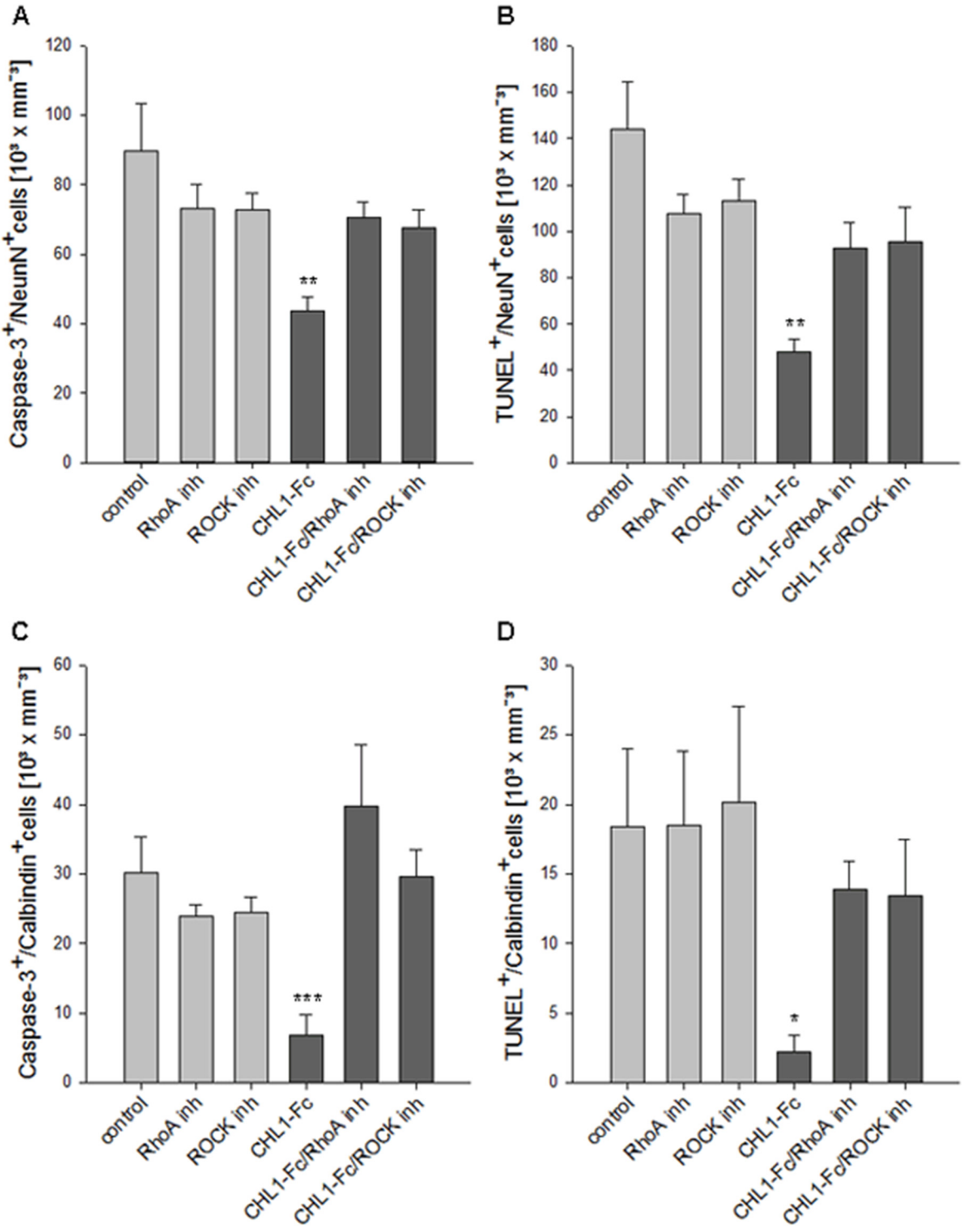

Figure 5.43. CHL1-Fc inhibits apoptosis of cerebellar granule and Purkinje cells via RhoA- and ROCK-dependent pathways. Organotypic slice cultures from cerebellum of CHL1-deficient mice were cultured for five days in medium containing serum and then exposed to serum-deprivation for 48 h in the absence (control) or presence of CHL1-Fc, RhoA or ROCK inhibitors. Mean values ± SEM from eight independent experiments including two images per slice and two slices per condition and experiment are shown for the number of cells positive for active caspase-3 and NeuN (***A***), TUNEL and NeuN (***B***), active caspase-3 and calbindin (***C***), or TUNEL and calbindin (***D***) staining. Group values were

analyzed by one-way ANOVA with Tukey's multiple comparison test and differences between groups are indicated (* p< 0.05, ** p< 0.01; *** p< 0.005).

5.2.9 CHL1 co-localizes with patched and smoothened within the cerebellar cortex at the first and second postnatal week

I showed that CHL1 directly binds to patched and associates with smoothened in the early postnatal cerebellum. Since all previous experiments were performed in *in vitro* systems such as cell cultures and organotypic slices, I looked for a confirmation of CHL1-patched or CHL1-smoothened interactions *in vivo*.

Tissue slices from seven-day-old wild-type cerebellum were immuno-stained with CHL1, patched or smoothened antibodies. A strong co-localization of CHL1 with patched and a less pronounced co-localization of CHL1 with smoothened were observed on parallel fibers in the molecular layer and on cells within the internal granular layer (Fig. 5.44). CHL1 co-localized with smoothened within the inner part of the external granular layer (Fig. 5.44 B).

To verify co-localization of CHL1 with patched or smoothened, I used a more sensitive method – proximity ligation assay. For patched and CHL1 many fluorescent spots were found in the molecular and internal granular layers of cerebella from 7-, 10- and 14-day-old wild-type mice and in the inner part of the external granule layer of cerebella from 7- and 10-day-old wild-type mice (Fig. 5.45 A-C). No fluorescent signals were detectable in sections of 7-day-old CHL1-deficient mice (Fig. 5.45 D). For smoothened and CHL1, fewer fluorescent spots were observed in the molecular and internal granular layers of cerebella from 7-, 10- and 14-day-old wild-type mice and in the external granule layer of cerebella from 7- and 10-day-old wild-type mice (Fig. 5.45 E-G). No fluorescent signals were observed in sections from 7-day-old CHL1-deficient mice (Fig. 5.45 H).

These results indicate close interactions of CHL1 with patched along the parallel fibers and cells within the internal granular layer, from the end of the first until the end of the second postnatal week of cerebellar development. However, the CHL1 and smoothened interaction is less prominent but also observed at the same stages of cerebellar development.

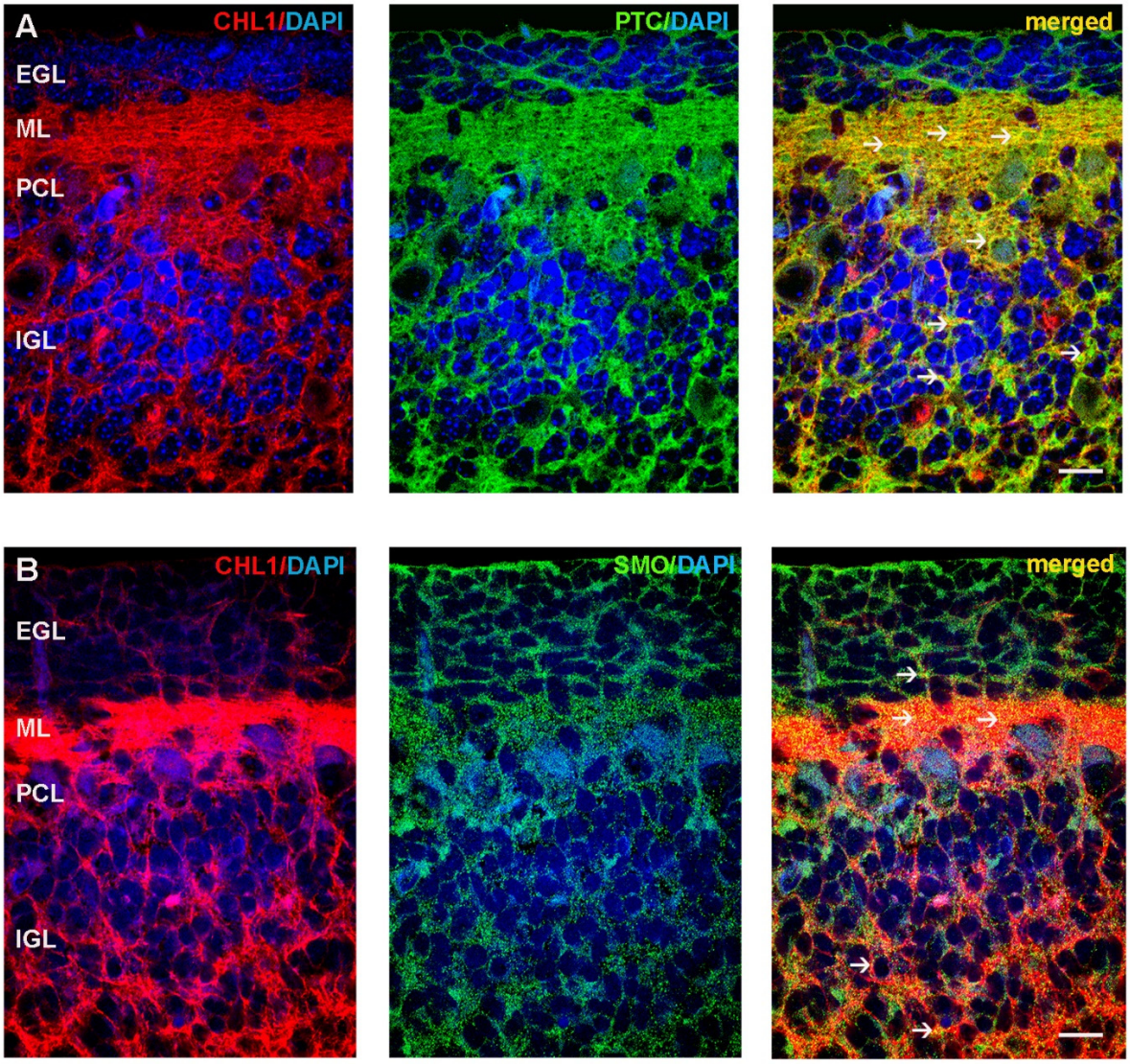

Figure 5.44. CHL1 co-localizes with patched and smoothened in the cerebellum of seven-day-old mice. ***A***, ***B***, Representative images of immunofluorescence staining for DAPI (blue) and CHL1 (red; ***A***, ***B***), and DAPI and patched (green; ***A***) or DAPI and smoothened (green; ***B***) are shown. Superimposition indicates co-localizations as yellow at cells located within the molecular layer and the internal granular layers (arrows). Scale bars, 15 µm. EGL - External granular layer; ML - molecular layer; PCL - Purkinje cell layer; IGL - internal granular layer.

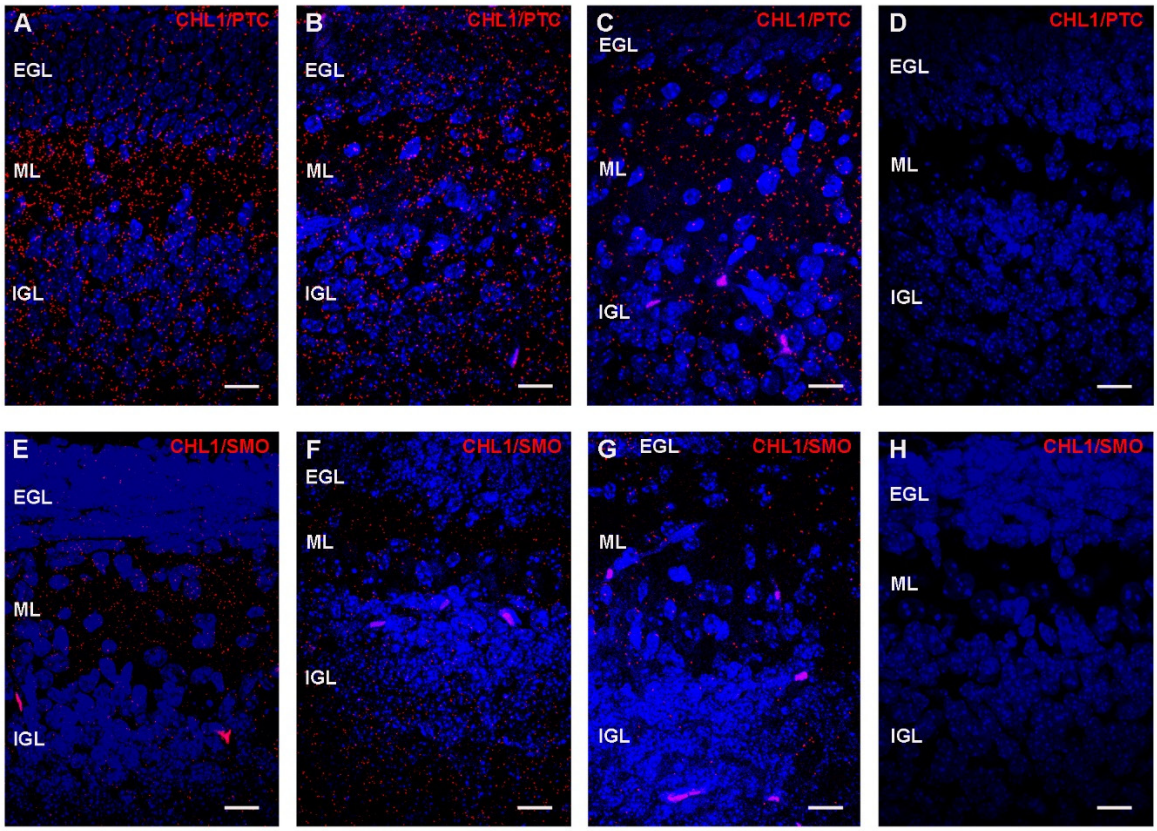

Figure 5.45. CHL1 co-localizes with patched and smoothened in the early postnatal cerebellum. Co-localization of CHL1 with patched (PTC) (***A-D***) and smoothened (SMO) (***E-H***) at different postnatal stages of cerebellar development is shown. ***A-H***, Representative images from proximity ligation assay of histological sections from 7- (***A, D, E, H***), 10- (***B, F***) and 14-day old (***C, G***) wild-type (***A-C, E-G***) and CHL1-deficient (***D, H***) mice are shown. Red spots indicate close interaction of CHL1 with patched (***A-C***) or smoothened (***E-G***) in wild-type mice. Nuclei are stained with DAPI (blue). EGL - external granular layer; ML - molecular layer; IGL - internal granular layer. Scale bars: 15 µm.

5.2.10 CHL1 inhibits apoptosis of cerebellar granule cells at the second postnatal week *in vivo*

The results of my *in vitro* experiments indicated that CHL1 binding to patched enhances survival of cerebellar neurons by inhibiting patched-mediated apoptosis. Thus, CHL1-deficiency consequentially leads to increased apoptosis of cerebellar neurons. Previous data indeed showed a loss of granule and Purkinje cells in two months old CHL1-deficient cerebellum (Jakovcevski et al., 2009). This cell loss could be the consequence of an earlier apoptotic event which occurrs during the postnatal development of the cerebellum. However, authors did not observe an increased apoptosis in one-week-old CHL1-deficient cerebellum. Since my *in vitro* data suggest that the apoptosis of cerebellar neurons occurs during the second postnatal week, I labeled CHL1-deficient and wild-type brains with markers of apoptosis and quantified labeled cells. Based on the results obtained from the organotypic

slices where CHL1-Fc promotes survival of Purkinje and granule cells at the end of the second postnatal week, I stained 10- and 14-day-old cerebellum against markers for both Purkinje and granule cell neurons simultaneously with the caspase-3 and TUNEL staining.

The density of caspase-3/NeuN-positive neurons in the external granular layer of 10-day-old CHL1-deficient cerebellum were similar to the density in the wild-type cerebellum (Fig. 5.46 A). No caspase-3/NeuN-double positive neurons were detectable in the external granular layer of 14-day-old cerebellum (Fig. 5.46 A). The density of caspase-3/NeuN-positive neurons in the internal granular layer of both 10- and 14-day-old CHL1-deficient cerebellum were significantly higher compared to the density in wild-type cerebellum (Fig. 5.46 A).

There was no difference in the density of caspase-3/calbindin-positive cells in 10- and 14-day-old CHL1-deficient and wild-type cerebellum (Fig. 5.46 B). Generally, the density of caspase-3/calbindin were much lower than the density of caspase-3/NeuN-positive neurons (Fig. 5.46 A, B).

The density of TUNEL/NeuN-positive neurons were similar in the external granular layers of 10- and 14-day-old CHL1-deficient and wild-type cerebellum, whereas the density were increased in the internal granular layer of 10- and 14-day-old CHL1-defcient cerebellum compared to wild-type cerebellum (Fig. 5.46 C). No TUNEL/calbindin-positive neurons were detectable neither in the Purkinje cell layer of 10- nor of 14-day-old CHL1-deficient nor wild-type cerebellum.

These results suggest that apoptosis of granule cells in the external granular layer is a CHL1-independent process, whereas apoptosis of granule cells from the internal granular layer of 10- and 14-day-old cerebellum depends on CHL1. Besides, apoptosis of the very few Purkinje cells seems not to be dependent on the presence of CHL1 during the second postnatal week.

In this chapter, I presented results showing that CHL1- triggered neuronal survival is conducted via the patched and smoothened signaling pathway. Moreover, granular cell loss observed in the adult CHL1-deficient mice occurs during the second week of cerebellar development.

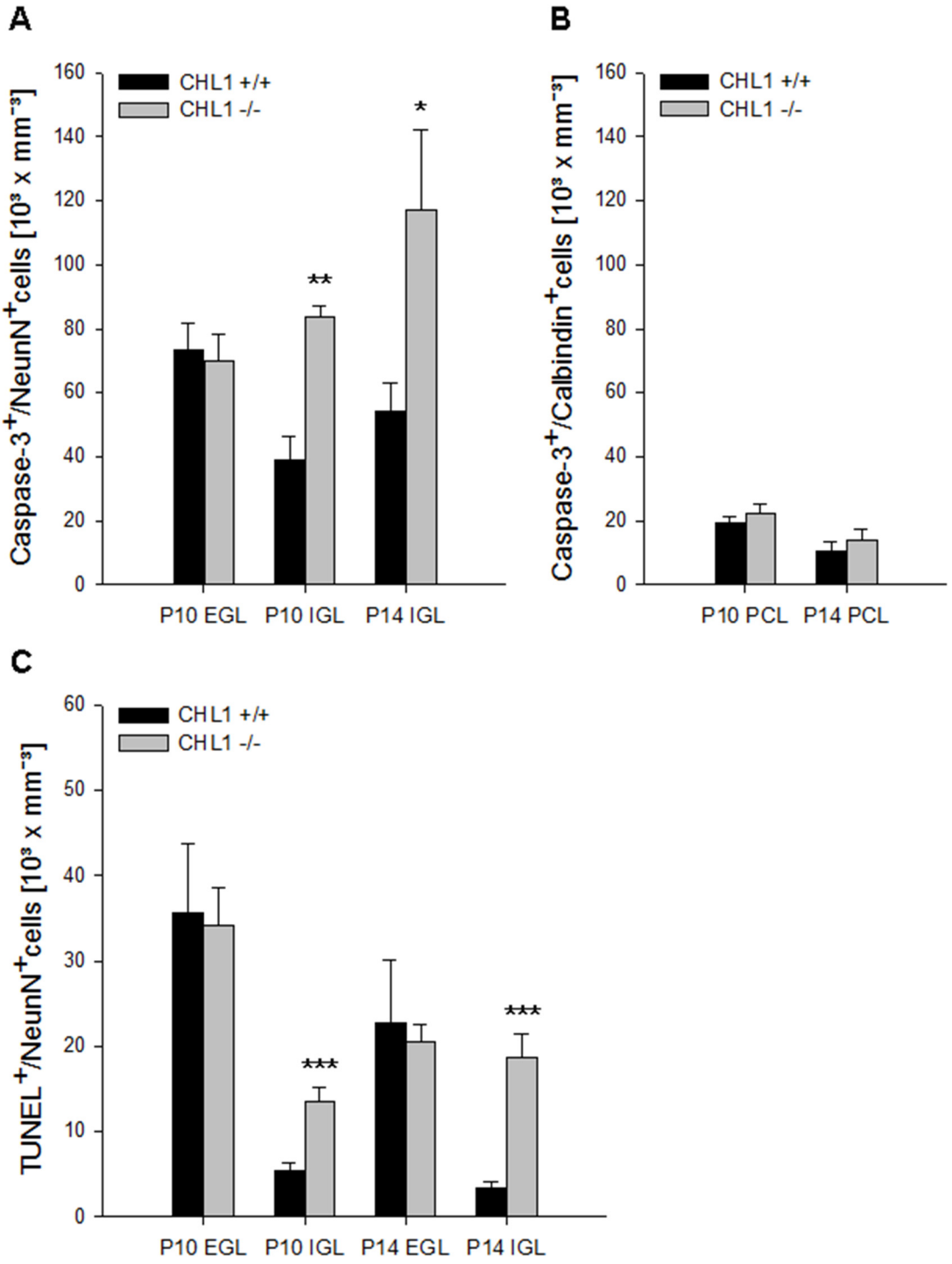

Figure 5.46. CHL1 regulates apoptosis of granule cells at the second postnatal week of cerebellar development *in vivo*. *A*-*C*, Sections of cerebella from 10- or 14-day old (P10, P14) wild-type (CHL1+/+) and CHL1-deficient (CHL1-/-) mice were stained for active caspase-3 and NeuN (***A***), active caspase-3 and calbindin (***B***) or for TUNEL and NeuN (***C***). Mean values ± SEM are shown for the number of active caspase-3- and NeuN-positive cells (***A***), active caspase-3- and calbindin-positive cells (***B***) or TUNEL- and NeuN-positive cells (***C***) per area in the external granular layer (EGL), internal granular layer (IGL) or Purkinje cell layer (PCL). N=6, per each group. Group values were analyzed by two-tailed Student's *t* test and differences between groups (* $p< 0.05$, ** $p< 0.01$; *** $p< 0.005$) are indicated.

6 DISCUSSION

In the present thesis I could show for the first time that CHL1 directly binds to vitronectin and PAI-2 to enhance granule cell migration *in vitro*. Additionally, CHL1 binds vitronectin and triggers neurite outgrowth of granule cells *in vitro*. CHL1-vitronectin and CHL1-PAI-2 interactions are also important *in vivo* in the developing cerebellar cortex. CHL1 and vitronectin prevent proliferation and differentiation of granule cells in five-day-old cerebellum but enhance their migration in seven-day-old cerebellum *in vivo*. Furthermore, the results of my thesis demonstrate that CHL1 is a novel ligand of patched, which is the receptor of the morphogen sonic hedgehog. CHL1 directly binds to the first extracellular loop of patched and prevents patched-induced cell death in a smoothened dependent manner. CHL1 prevents apoptosis of granule and Purkinje cells in two weeks old organotypic cerebellar culture and the anti-apoptotic role of CHL1 depends on smoothened, RhoA and ROCK activation. CHL1 prevents apoptosis of granule cells in the internal granule layer of two weeks old cerebellum *in vivo*. Additionally, CHL1-triggered granule cell migration and neurite outgrowth *in vitro* also depends on smoothened, RhoA and ROCK activation.

6.1 CHL1 binds directly to vitronectin, plasminogen activator inhibitor 2 and patched via its extracellular domain

Our studies identified vitronectin as a novel interaction partner of CHL1 using CHL1-Fc as bait in a biochemical cross-linking approach. Here, in pull-down experiments vitronectin was precipitated with CHL1-Fc and in ELISA experiments vitronectin was shown to bind to immobilized CHL1-Fc. Since CHL1-Fc contains only the extracellular part of the CHL1 molecule, it is indicative that CHL1 binds the secreted extracellular matrix protein vitronectin (Dahm and Bowers, 1998) via its extracellular domain.

A phage-display experiment revealed that PAI-2 and patched might also be potential interaction partners of CHL1. Binding of CHL1 to PAI-2 was further confirmed by immunoprecipitation and ligand-free binding assay. In both phage-display and ligand-free binding assay, CHL1-Fc was used to show the direct interaction with PAI-2, which leads to conclusion that PAI-2 also interacts with the extracellular part of CHL1. Since PAI-2 is present in both intracellular and extracellular forms in the tissue (von Heijne et al., 1991), our results indicate that only the extracellular form of PAI-2 can bind the extracellular part of CHL1. Results presented here also show that recombinant N-terminal fragments of PAI-2 and vitronectin bind specifically to CHL1-Fc in ELISA and label-free binding assays, whereas the C-terminal fragment of PAI-2 interacts both with CHL1-Fc and L1-Fc. These results suggest that CHL1 binds vitronectin and PAI-2 via their N-terminal fragments.

In the phage display experiments with CHL1-Fc as bait a CHL1-binding peptide was identified that showed sequence similarities with the amino acids 365-376 within the first extracellular loop of patched. Here, I verified that patched indeed interact with CHL1 by immunoprecipitation. Additionally, in ELISA and in a label-free binding assay, I used CHL1-Fc and the recombinant patched protein comprising amino acids 213-422 and containing the first extracellular loop of patched (amino acids 108-422), and could demonstrate that the extracellular part of CHL1 directly binds to sequences within the first extracellular loop of patched. Furthermore, sequence screening shows that amino acids 1007-1027 of murine CHL1 show a similarity to amino acids 51-72 of murine sonic hedgehog, positioned in the N-terminus of sonic hedgehog which binds to patched. The murine CHL1 sequence stretch 1007-1027 and the sonic hedgehog sequence stretch 51-72 share the common motif TLGXXXK/RXXXKIT/S, suggesting that this motif mediates the binding of CHL1 and sonic hedgehog homologs to their receptor patched. This common motif is not present in other patched ligands, neither in indian nor in desert hedgehog, suggesting that this motif is important for binding of sonic hedgehog and CHL1 to patched. By ELISA I could show that murine CHL1 binds to a sequence stretch in the first extracellular loop of patched not only via amino acids 1007-1027 but also via amino acids 1050-1070 in its membrane-proximal FNIII domain.

6.2 Heterophilic interactions of CHL1 with its novel binding partners enhance granule cell migration and neurite outgrowth during the first postnatal week of cerebellar development

From literature data it can be concluded that the expression of CHL1 both during cerebellar development and in the adult is of high importance for normal tissue organization and establishment of proper connections between cells (Holm et al., 1996; Ango et al., 2006; Nikonenko et al., 2006). It is known that CHL1 promotes integrin-dependent migration of cerebellar neurons (Buhusi et al., 2003) and that CHL1-ablation causes retarded inward radial migration of granule cell precursors along the Bergman glia fibers (Jakovcevski et al., 2009). However, CHL1 binding partners and mechanisms via which CHL1 regulates development and migration of granule neurons remain unknown. We identified novel binding partners of CHL1, vitonectin, PAI-2 and patched, which are known to be expressed in the developing cerebellum where they regulate granule cell differentiation and migration (Jensen, 1997; Murase and Hayashi, 1998; Traiffort et al., 1998; Traiffort et al., 1999; Pons et al., 2001; Lewis et al., 2004; Varjosalo and Taipale, 2008; Zheng et al., 2010; Petralia et al., 2012). The results of this thesis demonstrate that heterophilic interactions of CHL1 with vitonectin, PAI-2 and patched enhance

granule cell migration and neurite outgrowth in cultured dissociated cerebellar neurons from the seven-day-old cerebellum.

Granule cell migration and neurite outgrowth was enhanced when CHL1-Fc was applied in the dissociated culture of neurons from one week old CHL1-deficient cerebellum. The pro-migratory effect of CHL1-Fc, however, was reduced by application of antibodies against vitronectin, PAI-2 and patched, and with addition of the PAI-2 and patched-derived synthetic peptides. Similarly, CHL1-triggered neurite outgrowth was also reduced when antibodies against vitronectin and patched were applied. Our results suggest that CHL1 can trigger migration and neurite outgrowth of cerebellar neurons only if it binds to vitronectin, PAI-2 or patched. Furthermore, to understand molecular mechanism via which CHL1 regulates migration and neurite outgrowth, we tested if other vitronectin, PAI-2 or patched interaction partners are involved in those processes.

Other authors suggested that vitronectin and PAI-2 interact with uPA and uPAR (Lobov and Ranson, 2011), and that PAI-2 influences cell migration by inhibiting uPA in the presence of vitronectin. Here, we tested whether CHL1-triggered cell migration of dissociated cerebellar neurons is altered after application of uPA and uPAR antibodies. Indeed, both antibodies against uPA and uPAR reduced CHL1-triggered granule cell migration, leading to the conclusion that granule cell migration depends on the complex interactions between CHL1 and vitronectin, CHL1 and PAI-2, vitronectin and uPAR, uPA and uPAR and PAI-2 and uPA. Even though it was suggested that PAI-2 binds directly to vitronectin (Lobov et al., 2004), we did not detect this binding neither with ELISA nor with label-free bind assay when using recombinant N-terminal fragments of vitronectin and N- and C-terminal fragments of PAI-2. It is likely that vitronectin and PAI-2 interact either indirectly via binding to CHL1, or that the binding of CHL1 to PAI-2 shifts the PAI-2 protein into a conformation that allows binding of PAI-2 to vitronectin. Another possibility is that vitronectin binds CHL1 via its N-terminus and PAI-2 via its C-terminus.

There are indications that uPAR and CHL1 induce similar disorders both in mice and in human. uPAR- and CHL1-deficient mice display a reduced number of GABAergic interneurons and an atypical social behavior (Montag-Sallaz et al., 2002; Powell et al., 2003; Pratte et al., 2003; Irintchev et al., 2004; Levitt, 2005; Morellini et al., 2007; Kolata et al., 2008; Nagai et al., 2008; Pratte and Jamon, 2009; Archinti et al., 2011; Kleene et al., 2015; Schmalbach et al., 2015;). In humans uPAR is linked to epilepsy and autism spectrum/cognitive disorders like CHL1 (Campbell et al., 2008; Lahtinen et al., 2009; Eagleson et al., 2010; Liu et al., 2010; Bruneau and Szepetowski, 2011), suggesting an involvement of PAI-2, uPA, and uPAR in synaptic plasticity under physiological conditions and in neuropathological disorders. Since CHL1 is also involved in regulation of synaptic plasticity and behavior (Angeloni et al., 1999; Sakurai et

al., 2002; Frints et al., 2003; Chen et al., 2005; Chu and Liu, 2010; Tam et al., 2010; Cuoco et al., 2011; Morag et al., 2011; Salyakina et al., 2011; Shoukier et al., 2013), CHL1´s role in synaptic plasticity might be triggered by CHL1-mediated regulation of the PAI-2/uPA/uPAR signaling pathway via its interaction with a major player of this pathway, namely PAI-2. However, the involvement of CHL1 interactions in the PAI-2/uPA/uPAR signaling pathway in synaptic plasticity and behavior needs to be further studied.

Since we showed that interaction of CHL1 with patched induced granule cell migration and neurite outgrowth, it was important to show whether downstream members of the signaling cascade triggered by patched are involved in those processes. Interaction of patched and its direct binding partner smoothened has been shown to control cell motility and axonal guidance (Charron and Tessier-Lavigne, 2005). Once activated, smoothened triggers the small GTPase RhoA that is involved in cytoskeleton regulation and cell motility and triggers granule cell migration (Chédotal, 2010; Robbins et al., 2012). Here we show that the stimulation of granule cell migration and neurite outgrowth by CHL1-Fc are also inhibited after application of the smoothened antagonist SANT-1, an inhibitor of RhoA and an inhibitor of RhoA associated kinase ROCK. Granule cell migration and neurite outgrowth are regulated by CHL1 binding to patched, which further activates smoothened, RhoA and ROCK.

Taken together, our results indicate that CHL1 triggers different signaling pathways by different heterophilic *trans*-interactions to regulate neuritogenesis and migration of cerebellar neurons *in vitro*. Next, it was necessary to investigate the presence of CHL1 heterophilic interactions *in vivo,* during the developmental period when granule cells change their morphology and start their active migration. Granule cells from the inner EGL stack their axons (parallel fibers) in the molecular layer and start radial migration at the end of the first postnatal week using Bergman glia fibers as a scaffold (Espinosa and Luo, 2008). CHL1 proved to be strongly expressed in the parallel and Bergmann glia fibers at the end of the first postnatal week (Ango et al., 2008). Besides, CHL1-deficiency causes impaired radial migration of granule cells and their accumulation in the molecular layer in seven-day-old cerebellum (Jakovcevski et al., 2009), suggesting that the expression of CHL1 is necessary for the normal granule cell migration in the first postnatal week.

To verify an interaction between CHL1 and its heterophilic partners *in vivo*, I stained histological sections from five- and seven-day-old cerebellum with CHL1, vitronectin and PAI-2 antibodies. CHL1 co-localizes with vitronectin and PAI-2 along radial fibers of Bergmann glial cells, at cells located within the inner part of the external granular layer, within the molecular layer along the parallel fibers and within in the internal granular layer near the Purkinje cell layer. This co-localization was observed in seven- but not in five-day-old cerebellum. Taken together, CHL1 likely regulates the organization of the molecular layer and radial migration of

granule cells in seven-day-old cerebellum. Cells from seven-day-old CHL1-deficient and wild-type mice showed enhanced migration and neuritogenesis after treatment with CHL1-Fc, indicating that heterophilic *trans*-interactions regulate migration and neuritogenesis at later stages when granule cell bodies initiate migration along radial Bergmann glial processes. Moreover, axons of granule cells form synaptic contacts with basket and stellate cells (Lemkey-Johnston and Larramendi, 1968), and CHL1 ablation causes aberrant branching and orientation of axons of stellate cells, but not of basket cells (Ango et al., 2008). Interactions of CHL1 expressed on Bergmann glial processes with its binding partners expressed on leading processes and on granule cell bodies may stimulate radial migration of granule cells to the internal granular layer. The receptors for CHL1 on the migrating granule cells might be vitronectin and/or PAI-2. Post-mitotic granule cells extend their axons prior to their radial migration, and this extension can rely on the heterophilic *trans*-interaction of CHL1 on Bergmann glia with its binding partner vitronectin expressed on parallel fibers.

In the histological sections from seven-day-old cerebellum stained with CHL1, patched and smoothened antibodies, I showed that CHL1 co-localizes with patched along the parallel fibers, in the internal granule layer and less in within the external granule layer. CHL1 proved to co-localize with smoothened within the same regions. However, CHL1-smoothened co-localization signals obtained both from immunohistochemistry and proximity ligation assay are less prominent than CHL1-patched co-localization signals. These results indicate that CHL1 binds to patched on the surface of granule cell bodies and their axons during the period of active granule cell migration. Furthermore, CHL1-smoothened co-localization data, accompanied with immunoprecipitation results (Fig. 5.18), show a week interaction between smoothened and CHL1 suggesting that CHL1 probably associates with smoothened indirectly, most likely via binding to patched within the patched-smoothened complex.

6.3 CHL1 and vitronectin regulate the development of granule cells *in vivo* during the first postnatal week of cerebellar development

In the previous chapter I provide evidence that CHL1 interacts with vitronectin in the seven-day-old cerebellar cortex *in vivo* and discussed how this interaction regulates granule cell migration and neuritogenesis *in vitro.* Here, I present and discuss the evidence that CHL1 and vitronectin play an important role in granule cell development and migration *in vivo* by staining histological sections from wild-type, CHL1- and vitronectin-deficient cerebellum of different age with markers for proliferation, differentiation and migration.

CHL1 and vitronectin ablation influences proliferation, differentiation and migration of granule cells during the first postnatal week of cerebellar development *in vivo*. The number of

proliferating Ki67-positive granule cell precursors from the external granule layer in three-day-old CHL1-deficient mice was similar to the number in wild-type mice, while in five-day-old CHL1-deficient mice this number was higher. Of note, the number of proliferating Ki67-positive granule cells in seven-day-old cerebellum did not differ between genotypes (Jakovcevski et al., 2009). However, the total number of Pax6-positive granule cells was similar both in five- and seven-day-old wild-type and CHL1-deficient mice. A higher proliferation rate of granule cells in five-day-old CHL1-deficient cerebellum indicates that CHL1 ablation and lack of its heterophilic interactions enhance proliferation of granule cell precursors. Interestingly, a higher number of proliferating granule cells precursors is also observed in five-day-old vitronectin-deficient cerebellum. Vitronectin has been shown to block sonic hedgehog-induced proliferation and to trigger differentiation of granule precursor cells (Pons et al., 2001), which points to a higher proliferation of granule cells that after vitronectin-ablation. Vitronectin- and CHL1-ablation induces higher rates of granule cell proliferation, possibly at the expense of proper granule cell differentiation. However, there is no evidence that vitronectin and CHL1 act synergistically to inhibit proliferation.

The numbers of differentiated NeuN-positive granule cells in the molecular layer were increased in five- and seven-day-old CHL1-deficient mice, while the total number of Pax-6-positive granule cells in five- and seven-day-old CHL1-deficient mice does not differ from that in wild-type mice. The lack of heterophilic CHL1 *trans*-interactions impairs neuronal migration and results in an accumulation of granule cells in the molecular layer. The numbers of NeuN-positive granule cell neurons in the internal granular layer are also increased in five- and seven-day-old CHL1-deficient mice, while the numbers of NeuN/Pax6 double-positive granule neurons in the internal granular layer are increased in five-day-old CHL1-deficient cerebella, but decreased in seven-day-old CHL1-deficient cerebella compared to wild-type cerebella. This result indicates that CHL1-deficiency causes premature differentiation of granule cell precursors and that this premature differentiation leads to increased numbers of NeuN-positive differentiated granule cells in the internal granule layer of five- and seven-day-old CHL1-deficient mice. Since Pax6 levels in granule neurons in the internal granule layer decline after radial migration (Yamasaki et al., 2001), post-migratory granule cells in the CHL1-deficient cerebella are likely Pax6 negative in seven-day-old mice. The reduction in the numbers of Pax6/NeuN double-positive cells in the internal granular layer of seven-day-old CHL1-deficient mice can be explained by premature differentiation of granule cells that stop expression of Pax6 and continue to express only NeuN. Moreover, retardation of neuronal differentiation via homophilic CHL1-CHL1 interactions (Jakovcevski et al., 2007; Huang et al., 2011) could prevent premature neuronal differentiation. The prematurely differentiated granule cells in the IGL of CHL1-deficient mice could be eliminated in later phases of cerebellar development leading to the loss of granule cells reported in the adult CHL-deficient cerebellum (Jakovcevski

et al., 2009). A similar histological phenotype is seen in vitronectin-deficient mice, suggesting that both CHL1 and vitronectin are necessary for proper granule cell differentiation.

The number of migrating doublecortin/Pax-6 double positive granule cells from the inner part of the external granule layer is lower in CHL1- and vitronectin-deficient cerebella, in seven-day-old but not in five-day-old mice. Since *in vitro* results from experiments using dissociated cerebellar neurons suggest an involvement of the CHL1-vitronectin interaction in granule cell migration in the seven-day-old cerebellum, it can be expected that CHL1 and vitronectin ablation impairs granule cell migration also *in vivo*. Since CHL1 and vitronectin co-localize in seven- but not in five-day-old cerebellum and since the number of migrating granule cells in CHL1- and vitronectin-deficient mice is lower only in seven-day-old cerebellum and is unaltered in five-day-old cerebellum, it is likely that the CHL1-vitronectin interaction triggers granule cell migration only during the 7th postnatal day.

Taken together the results from the histological analysis and the *in vitro* data from dissociated cerebellar cultures, they indicate that the CHL1-vitronectin interaction enhances neurite outgrowth and triggers radial migration of granule cells in seven-day-old cerebellum. CHL1 and vitronectin inhibit proliferation of granule cell precursors and inhibit premature granule cell differentiation in five-day-old cerebellum, either via independent mechanisms or via interacting indirectly with each other.

6.4 Interaction of CHL1 with patched inhibits apoptosis of granule cells during the second postnatal week of cerebellar development

Here I could show that CHL1 is involved in cellular processes during granule cell development, such as proliferation, differentiation, neurite outgrowth and migration. During the last developmental phase of the cerebellum, programmed cell death of distinct neurons is necessary to ensure proper neuron numbers and connections in the adult. Apoptosis of granule cells occurs during the later stages of postnatal cerebellar development (second postnatal week) and regulates their final number (Wood et al., 1993; Altman and Bayer, 1997; Lossi et al., 1998; Jankowski et al., 2009; Cheng et al., 2011). Loss of granule and Purkinje cells in the adult CHL1-defficient cerebellum was observed, which is not the consequence of a lower proliferation rate of cerebellar neurons during development (Jakovcevski et al., 2009). Results in this thesis show that granule cells from CHL1-deficient cerebellum display a higher rate of proliferation during the first postnatal week. Thus, we hypothesized that ablation of the CHL1 molecule and its heterophilic interactions induce a higher rate of apoptosis during the development of granule cells, which then leads to a loss of the granule cells in the adult cerebellum. Moreover, the novel CHL1 interaction partner patched was shown to trigger

caspase-3 activation and apoptosis in the absence of its ligand sonic hedgehog (Thibert et al., 2003). Since CHL1 displays pro-survival effects (Chen et al., 1999), it was important to understand whether the interaction of CHL1 with patched can inhibit patched-induced apoptosis.

Thus, I transfected HEK cells with a vector carrying full length patched to induce apoptosis and treated them with CHL1-Fc to investigate whether apoptosis is altered after application of CHL1-Fc. HEK cells overexpressing full length mouse patched display a high rate of cell death and high caspase-3 activity, which are reduced after application of CHL1-Fc. CHL1 binds to the first extracellular loop of patched to conduct its pro-survival effect. The rate of cell death in HEK cells transfected with a vector carrying patched without the fist extracellular loop is also enhanced but not altered after CHL1-Fc application. Thus, to inhibit patched-induced apoptosis CHL1-Fc depends on the presence of the first extracellular loop of patched. I propose that CHL1-Fc binds directly to the extracellular loop of patched and thereby inhibits patched-induced apoptosis. In this context it is noteworthy to mention that caspase-3 activity and apoptosis are triggered by the intracellular C-terminus of patched and do not depend on the presence of the first extracellular loop of patched (Thibert et al., 2003), while the inhibition of patched pro-apoptotic activity depends on the binding of the sonic hedgehog ligand to the first extracellular loop of patched (Briscoe et al., 2001). From the results present here it can be suggested that CHL1 is a novel ligand that binds to the first extracellular loop of patched and thereby inhibits caspase-3 activity and apoptosis. The CHL1-induced pro-survival effect is blocked with the smoothened antagonist SANT-1, indicating that CHL1 inhibits patched-induced apoptosis in a smoothened dependent manner.

Since the main interest of this study is to unravel the role of CHL1 in apoptosis of cerebellar neurons, I induced apoptosis in CHL1-deficient cerebellar neurons by serum withdrawal and treated cells with and without CHL1-Fc. Caspase-3 activity and apoptosis of granule cells were reduced after CHL1-Fc treatment. The CHL1-prosurvival effect was however blocked after application of the smoothened antagonist SANT-1, suggesting that CHL1 inhibits granule cells death in a smoothened dependent manner. Moreover, when a CHL1-derived peptide comprising amino acids 1007-1027 and mediating the binding of CHL1 to patched, was applied in the cerebellar culture together with CHL1-Fc, the peptide blocked the pro-survival effect of CHL1-Fc. Furthermore, the CHL1-derived peptide slightly reduced cell death when applied alone in the culture. Considering this results I conclude that CHL1 binds to the first extracellular loop of patched via its amino acids 1007-1027 in the fourth FNIII repeat, activates smoothened and inhibits apoptosis.

If CHL1 triggers the patched-smoothened pathway, it is crucial to elucidate which other downstream molecules are involved in this signaling cascade. Activated smoothened was

shown to trigger two different pathways: one GLI-dependent “canonical” and one GLI-independent “non-canonical” signaling pathway (Robbins, 2012). Since I could show that CHL1-Fc application to dissociated cerebellar neurons did not change transcription levels of GLI but lead to RhoA activation, it can be concluded that CHL1 activates RhoA in a smoothened-dependent manner and that CHL1 stimulates the “non-canonical” rather than the “canonical” hedgehog signaling pathways. Furthermore, the pro-survival effect of CHL1-Fc application in both dissociated and organotypic cerebellar cultures is blocked by application of RhoA and ROCK inhibitors. From this result it can be suggested that the CHL1-induced activation of “non-canonical” hedgehog signal transduction pathways via RhoA and ROCK promotes cell survival of post-mitotic cerebellar neurons via anti-apoptotic pathways during the second week of postnatal development. The literature shows that inhibition of RhoA/ROCK1 signaling enhances the phosphorylation of Erk1/2 and induces apoptosis of leukemia cells (Li et al., 2013). When applying in the cerebellar culture medium the inhibitors of smoothened, RhoA and ROCK together with CHL1-Fc, apoptosis is significantly higher than when applying CHL1-Fc alone. This result suggests that the pro-survival effect of CHL1-Fc is blocked when smoothened, RhoA and ROCK are inhibited. The pro-survival effect of CHL1 is conducted via smoothened, RhoA and ROCK activation.

Here, in dissociated cerebellar cultures, the CHL1Fc-induced reduction of caspase-3 activity is smoothened-dependent, while its inhibition of caspase-9 activity is smoothened-independent. This partly fits with previous results demonstrating that both caspase-3 and caspase-9 activities induced by patched are smoothened-independent (Thibert et al., 2003; Mille at al., 2009). According to the hypothesis of “non-canonical” type I signaling, patched recruits a pro-apoptotic complex, including caspase-9, on its C-terminus, followed by activation of caspase-9 and caspase-3, which then cleave the C-terminus of patched and induce apoptosis (Robbins et al., 2012). However, my results suggest that CHL1 binds to patched and inhibits caspase-3 in a smoothened dependent way. Besides, CHL1 inhibition of cell death depends on smoothened, RhoA and ROCK activation. Taken together my results and current data from the literature (Robbins et al., 2012; Li et al., 2013), it is possible that CHL1 binds to patched and activates smoothened, which in turn activates RhoA and ROCK signaling leading to the inhibition of caspase-3 activity and inhibition of apoptosis. Thus, when the RhoA- and ROCK-dependent pathway is blocked, caspase-3 activity increases and apoptosis starts. I propose that caspase-3 could be activated both by the “non-canonical” type I signaling independent of smoothened and by the “non-canonical” type II signaling dependent on smoothened. It is likely that CHL1-mediated inhibition of caspase-3 activity is smoothened-dependent, involving the “non-canonical” type II signaling which includes RhoA/ROCK activation. However, other members of the “non-canonical” type II signaling and a precise mechanism of this signaling cascade have to be thoroughly investigated.

It was suggested that CHL1 ablation influences premature differentiation of granule cell precursors and delays their radial migration into the internal granular layer. Based on the results discussed in the previous section, I hypothesize that the prematurely differentiated post-migratory neurons are eliminated by apoptosis, resulting in a loss of granule cells in the internal granule layer in 2-month-old CHL1-deficient mice (Jakovcevski et al., 2009). Here, histological slices of two-weeks-old CHL1-deficient and wild-type cerebellum stained with markers for apoptosis (caspase-3 and TUNEL) and markers for granule and Purkinje cells, show differences in apoptosis between genotypes. Enhanced apoptosis of post-migratory neurons takes place in the internal granule layer of CHL1-deficient mice during the second postnatal week, suggesting that prematurely differentiated granule neurons are eliminated after their migration into the internal granule layer. However, the apoptosis of granule cells precursors from the external granule layer seems not to be dependent on CHL1. Apoptosis of post-migratory granule cells from the internal granule layer is considered to depend on the establishment of proper synapses with Purkinje cells, while the apoptosis of granule cell precursors from the external granule layer does not depend on synapse formation but on whether precursors manage to exit mitosis (Lossi et al., 2002; Cheng et al., 2011). CHL1-ablation induces atrophy of axon terminals and loss of Purkinje cells in the first postnatal week of cerebellar development (Ango et al., 2006; Jakovcevski et al., 2009). The atrophy of axon terminals and the loss of Purkinje cells in CHL1-deficient mice result in a lower number of potential synapses with granule cells. All those granule cells that fail to establish synapses with Purkinje cells undergo apoptosis. Our results suggest that CHL1 ablation induces synapse-dependent apoptosis of granule cells from the internal granule layer during the second postnatal week.

Increased apoptosis of Purkinje and granule cells was observed in organotypic cerebellar cultures from CHL1-deficient mice. This enhanced apoptosis was reduced by application of CHL1-Fc in a smoothened- and RhoA-dependent manner, suggesting that binding of CHL1 to patched activates smoothened and triggers the “non-canonical” type II signaling pathway which prevents apoptosis of Purkinje and granule cells. I confirmed *in vivo* that granule cells from 10- and 14-day old cerebellum undergo apoptosis as a result of CHL1-ablation, while the number of apoptotic Purkinje cells remains the same. This can be explained with the fact that CHL1-ablation induces apoptosis of Purkinje cells during the earlier stages of cerebellar development, namely the first postnatal week (Jankowski et al., 2009). Here, no enhanced apoptosis of Purkinje cells was seen later in development in cerebellar sections from 10- or 14-day old CHL1-deficient mice. However, CHL1 expression reduces apoptosis of Purkinje cells in cerebellar slices of wild-type mice during the first postnatal week of cerebellar development (Jakovcevski et al., 2009).

The results in this thesis show that CHL1 interacts both with patched and vitronectin and thereby regulates development of granule cells, while literature data demonstrate an interaction of the patched ligand sonic hedgehog with vitronectin during granule cell development. Sonic hedgehog promotes proliferation and induces differentiation of granule cell precursors synergistically with vitronectin (Pons et al., 2001; Komada, 2012; Álvarez-Buylla and Ihrie, 2014). In contrast, CHL1 inhibits proliferation and delays differentiation of neural precursor cells (Chapter 6.3; Huang et al., 2011). These observations are compatible with the view that the patched ligands CHL1 and sonic hedgehog have opposite functions in proliferation and differentiation in the early postnatal cerebellar development. Since sonic hedgehog levels are high and CHL1 levels are low in the outer external granule layer (Pons et al., 2001; Jakovcevski et al., 2007) where proliferation occurs, predominant binding of sonic hedgehog to patched triggers proliferation in a smoothened-dependent pathway. Moreover, enhanced proliferation of granule cell precursor in the external granular layer of five-day-old CHL1-deficient mice compared to wild-type mice can be observed (Chapter 6.3), which leads to the suggestion that CHL1 has an anti-proliferative effect during postnatal cerebellar development. Sonic hedgehog promotes differentiation of granule precursor cells in the inner external granular layer, while homophilic CHL1 *trans*-interactions induce a delay in their differentiation (Jakovcevski et al., 2007). Absence of CHL1 therefore leads to enhanced proliferation and differentiation of granule cells by sonic hedgehog. Our observations indicate that an interplay between CHL1, smoothened and patched triggers major morphogenetic activities during postnatal cerebellar development, such as neuritogenesis and migration during the first and cell survival during the second postnatal week. This conclusion was supported by the finding that CHL1 co-localizes with patched and smoothened on the granule cell bodies and along their axons in histological sections of cerebellum, both at the end of the first and during the second postnatal week (Figs. 5.44 and 5.45).

6.5 Functional consequences of CHL1 ablation in the cerebellum

In summary, here presented data shed light on CHL1-dependent processes that regulate proliferation, differentiation, migration and cell death during the development of neurons in the cerebellar cortex. Although CHL1 deficiency does not cause severe structural abnormalities in the cerebellum and the layer thickness is normal (Montag-Sallaz et al., 2002), I could show that CHL1-deficient mice display a higher proliferation rate, impaired migration and immature differentiation of granule cells and a higher apoptosis rate of granule and Purkinje cells. However, CHL1-deficient mice do not show motor deficits, their motor coordination and motor learning abilities are unchanged when compared to the abilities of wild-type mice (Montag-Sallaz et al., 2002; Jakovcevski et al., 2007; Morellini et al., 2007).

The cerebellum is engaged not only in locomotor activities but also in procedural learning, exploratory behavior, emotional or higher cognitive functions (Caston et al., 1998; Bigelow et al., 2006; Ito, 2008). Furthermore, some authors presume a link between early postnatal stress, such as maternal deprivation, and impaired motor performance of CHL1-deficient mice (Jakovcevski et al., 2009), suggesting that CHL1 abaltion causes a disturbed response of the cerebellum on early emotional stress which leads to altered behaviour. CHL1-deficient mice show reduced reactivity to novel stimuli and abnormalities in exploratory behavior (Kleene et al., 2015), which can be explained by disrupted cerebellum-basal ganglia interactions. Moreover, disruptions of cerebellum-basal ganglia interactions, which are responsible for procedural learning, have been reported for schizophrenia patients (Bigelow et al., 2006). In addition, several groups suggest a possible link between a missense polymorphism in the CHL1 gene and the susceptibility to develop schizophrenia (Sakurai et al., 2002; Chen et al., 2005). Thus, CHL1-ablation in the cerebellum might disturb cerebellar connections with basal ganglia leading to impaired procedural learning abilities characteristic in schizophrenia. However, further behavioral studies on CHL1-deficient animals are necessary to understand the role of CHL1 ablation on cerebellar functions during the procedural learning or in emotional functions. Additionally, more refined functional assays such as blink reflex conditioning are required to study the impact of CHL1 ablation on cerebellar functions.

6.6 General conclusions

The cell adhesion molecule CHL1 induces granule cell migration and neurite outgrowth most likely via two independent mechanisms: either by binding to the extracellular matrix molecules vitronectin and plasminogen activator inhibitor-2 or by binding to patched which activates smoothened and the GTPase RhoA. These mechanisms are involved in CHL1-induced inward granule cell migration that occurs in the cerebellar cortex at the end of the first postnatal week. CHL1 also inhibits proliferation and delays differentiation or granule cell precursors prior to their inward radial migration. It regulates dendritic arborization and survival of Purkinje cells. Granule cells that migrate from the external to the internal granule layer establish synaptic contacts with Purkinje cells and survive as a result of CHL1 signaling during the second postnatal week. I identify mechanisms involved in CHL1-induced cell survival: CHL1 binds to patched and activates smoothened, RhoA and the RhoA associated kinase ROCK, which inhibit apoptosis of both Purkinje and granule cells. Granule cells from CHL-deficient mice differentiate earlier, migrate slower and accumulate in the molecular layer during the first postnatal week, they reach the internal granule layer later than granule cells from wild-type mice, fail to make contacts with Purkinje cells and, as a result of that, undergo apoptosis during the second postnatal week.

However, we cannot claim that the role of CHL1 and its interaction partners in neural development is exclusively limited to the cerebellum. Different studies confirm that CHL1, patched, smoothened, vitronectin and PAI-2 are also expressed in other brain regions such as cerebral cortex, hippocampus and striatum, regulating neural development, migration and survival. So far, their mutual interactions in other brain regions apart from the cerebellum were not studied.

Furthermore, CHL1 is not the only cell adhesion molecule involved in cerebellar development. Previous work has indicated the involvement of other members of the L1 family in cerebellar development. Neurofascin is required for specific targeting of GABAergic synapses originating from basket cell axons to the initial segment of Purkinje axons (Ango et al., 2004). L1- or Nr-CAM deficient mice display deficits in the size of cerebellar vermis (Dahme et al., 1997; Sakurai et al., 2001), while the simultaneous ablation of L1 and Nr-CAM impairs the development of granule cells leading to a reduced thickness of the internal granule layer (Sakurai et al., 2001). Having in mind their homology and the similar expression pattern, CHL1, L1 and/or Nr-CAM could have overlapping functions during cerebellar development. Thus, additional studies on CHL1/L1- or CHL1/Nr-CAM-double mutant mice are required to understand potential overlapping functions of the L1 family molecules in development of the cerebellum.

7 REFERENCES

Alavez S, Blancas S, Moran J (2006) Effect of N-methylD-aspartate receptor blockade on Caspase activation and neuronal death in the developing rat cerebellum. Neurosci Lett 404:176-181.

Altman J, Bayer SA (1978) Prenatal development of the cerebellar system in the rat. I. Cytogenesis and histogenesis of the deep nuclei and the cortex of the cerebellum. J Comp Neurol 179:23-48.

Altman J, Bayer SA (1997) Developmentof the Cerebellar System in Relation to Its Evolution, Structure, and Function. CRC Press, Inc., Boca Raton, FL.

Amoureux MC, Cunningham BA, Edelman GM, Crossin KL (2000) N-CAM binding inhibits the proliferation of hippocampal progenitor cells and promotes their differentiation to a neuronal phenotype. J Neurosci 20:3631-3640.

Angeloni D, Lindor NM, Pack S, Latif F, Wei MH, Lerman MI (1999) CALL gene is haploinsufficient in a 3p-syndrome patient. Am J Med Genet 86:482-485.

Ango F, Wu C, Van der Want JJ, Wu P, Schachner M, Huang ZJ (2008) Bergmann glia and the recognition molecule CHL1 organize GABAergic axons and direct innervation of Purkinje cell dendrites. PLoS Biol 6:e103.

Ango F, di Cristo G, Higashiyama H, Bennett V, Wu P, Huang ZJ (2004) Ankyrin-based subcellular gradient of neurofascin, an immunoglobulin family protein, directs GABAergic innervation at Purkinje axon initial segment. Cell 119:257-272.

Archinti M, Britto M, Eden G, Furlan F, Murphy R, Degryse B (2011) The urokinase receptor in the central nervous system. CNS Neurol Disord Drug Targets 10:271-294.

Avilés EC, Wilson NH, Stoeckli ET (2013) Sonic hedgehog and Wnt: antagonists in morphogenesis but collaborators in axon guidance. Front Cell Neurosci 7:86.

Bae HB, Tadie JM, Jiang S, Park DW, Bell CP, Thompson LC, Peterson CB, Thannickal VJ, Abraham E, Zmijewski JW (2013) Vitronectin inhibits efferocytosis through interactions with apoptotic cells as well as with macrophages. J Immunol 190:2273–2281.

Barnes DW, Reing JE, Amos B (1985) Heparin-binding properties of human serum spreading factor. J Biol Chem 260(16):9117-22.

Belgacem YH, Borodinsky LN.Sonic hedgehog signaling is decoded by calcium spike activity in the developing spinal cord. PNAS 108(11):4482-7.

Bieber AJ, Snow PM, Hortsch M, Patel NH, Jacobs JR, Traquina ZR, Schilling J, Goodman CS (1989) Drosophila neuroglian: a member of the immunoglobulin superfamily with extensive homology to the vertebrate neural adhesion molecule L1. Cell 59:447-460.

Bigelow NO, Turner BM, Andreasen NC, Paulsen JS, O'Leary, HO BC (2006) Prism adaptation in schizophrenia. Brain Cogn 61:235–242.

Bolte S, Cordelieres FP (2006) A guided tour into subcellular colocalization analysis in light microscopy. J Microsc 224:213–232.

Bouslama-Oueghlani L, Wehrlé R, Doulazmi M, Chen XR, Jaudon F, Lemaigre-Dubreuil Y, Rivals I, Sotelo C, Dusart I (2012) Purkinje cell maturation participates in the control of oligodendrocyte differentiation: role of sonic hedgehog and vitronectin. PLoS One 7(11):e49015.

Brackenbury R, Thiery JP, Rutishauser U, Edelman GM (1977) Adhesion among neural cells of the chick embryo. I. An immunological assay for molecules involved in cell-cell binding. J Biol Chem 252:6835-6840.

Brennan D, Chen X, Cheng L, Mahoney M, Riobo NA (2012) Noncanonical Hedgehog Signaling. Vitam Horm 88:55-72.

Briscoe J, Chen Y, Jessell T, Struhl G (2001) A Hedgehog-insensitive form of Patched provides evidence for direct long-range morphogen activity of Sonic hedgehog in the neural tube. Mol Cell 7:1279-1291.

Briscoe J, Thérond PP (2013) The mechanisms of Hedgehog signalling and its roles in development and disease. Nat Rev Mol Cell Biol 14:418-431.

Briscoe J, Chen Y, Jessell TM, Struhl GA (2001) hedgehog-insensitive form of patched provides evidence for direct long-range morphogen activity of sonic hedgehog in the neural tube. Mol Cell 7:1279-1291.

Brümmendorf T, Kenwrick S, Rathjen FG (1998) Neural cell recognition molecule L1: from cell biology to human hereditary brain malformations. Curr Opin Neurobiol 8: 87-97.

Brümmendorf T, Lemmon V (2001) Immunoglobulin superfamily receptors: cis-interactions, intracellular adapters and alternative splicing regulate adhesion. Curr Opin Cell Biol 13:611-618.

Bruneau N, Szepetowski P (2011) The role of the urokinase receptor in epilepsy, in disorders of language, cognition, communication and behavior, and in the central nervous system. Curr Pharm Des 17:1914-1923.

Buhusi M, Midkiff BR, Gates AM, Richter M, Schachner M, Maness PF (2003) Close homolog of L1 is an enhancer of integrin-mediated cell migration. J Biol Chem 278:25024-25031.

Butts T, Chaplin N, Wingate RJT (2011) Can Clues from Evolution Unlock the Molecular Development of the Cerebellum? Mol Neurobiol 43:67-76.

Campbell DB, Li C, Sutcliffe JS, Persico AM, Levitt P (2008) Genetic evidence implicating multiple genes in the MET receptor tyrosine kinase pathway in autism spectrum disorder. Autism Res 1:159-168.

Caston J, Chianale C, Delhaye-Bouchaud N, Mariani J (1998) Role of the cerebellum in exploration behavior. Brain Res 808:232-237.

Cerminara NL, Lang EJ, Sillitoe RV, Apps R (2015) Redefining the cerebellar cortex as an assembly of non-uniform Purkinje cell microcircuits. Nat Rev Neurosci 16(2):79-93.

Chaisuksunt V, Campbell G, Zhang Y, Schachner M, Lieberman AR, Anderson PN (2000) The cell recognition molecule CHL1 is strongly upregulated by injured and regenerating thalamic neurons. J Comp Neurol 425:382-392.

Charrier JB, Lapointe F, Le Douarin NM, Teillet MA. 2001. Anti-apoptotic role of Sonic hedgehog protein at the early stages of nervous system organogenesis. Development 128: 4011–4020.

Petralia RS, Wang XY, Mattson MP, Yao PJ (2012) Subcellular distribution of patched and smoothened in the cerebellar neurons. Cerebellum 11(4):972-81.

Charron F, Tessier-Lavigne M (2005) Novel brain wiring functions for classical morphogens: A role as graded positional cues in axon guidance. Development 132:2251-2262.

Chédotal A (2010) Should I stay or should I go? Becoming a granule cell. Trends Neurosci 33(4):163-72.

Chen JK, Taipale J, Young KE, Maiti T, Beachy PA (2002) Small molecule modulation of Smoothened activity. Proc Natl Acad Sci USA 99:14071-14076.

Chen QY, Chen Q, Feng GY, Lindpaintner K, Chen Y, Sun X, Chen Z, Gao Z, Tang J, He L (2005) Case-control association study of the close homologue of L1 (CHL1) gene and schizophrenia in the Chinese population. Schizophr Res 73:269-274.

Chen S, Mantei N, Dong L, Schachner M (1999) Prevention of neuronal cell death by neural adhesion molecules L1 and CHL1. J Neurobiol 38:428-439.

Cheng XS, Li MS, Du J, Jiang QY, Wang L, Yan SY, Yu DM, JB Deng (2011) Neuronal apoptosis in the developing cerebellum. Anat Histol Embryol 40(1):21-7.

Cho E, Lee KJ, Seo JW, Byun CJ, Chung SJ, Suh DC, Carmeliet P, Koh JY, Kim JS, Lee JY (2012) Neuroprotection by urokinase plasminogen activator in the hippocampus. Neurobiol Dis 46:215-224.

Chu T; Hullinger H, Schilling K, Oberdick J (2000) Spatial and temporal changes in natural and target deprivation-induced cell death in the mouse inferior olive. J Neurobiol 43:18-30.

Chu TT, Liu Y (2010) An integrated genomic analysis of gene-function correlation on schizophrenia susceptibility genes. J Hum Genet 55:285-292.

Chuong CM, Crossin KL, Edelman GM (1987) Sequential expression and differential function of multiple adhesion molecules during the formation of cerebellar cortical layers. J Cell Biol 104:331-342.

Cooper MA (2002) Optical biosensors in drug discovery. Nat Rev Drug Discovery, 1: 515–28.

Corrales JD, Blaess S, Mahoney EM, Joyner AL (2006) The level of sonic hedgehog signaling regulates the complexity of cerebellar foliation. Development 133:1811-21.

Crossin KL, Krushel LA (2000) Cellular signaling by neural cell adhesion molecules of the immunoglobulin superfamily. Dev Dyn 218(2):260-79.

Cunningham BT, Li P, Schulz S, Lin B, Baird C, Gerstenmaier J et al. (2004) Label-free assays on the BIND system. J Biomol Screen 9:481– 90.

Cuoco C, Ronchetto P, Gimelli S, Bena F, Divizia MT, Lerone M, Mirabelli-Badenier M, Mascaretti M, Gimelli G (2011) Microarray based analysis of an inherited terminal 3p26.3 deletion, containing only the CHL1 gene, from a normal father to his two affected children. Orphanet J Rare Dis 6:12.

Dahm LM, Bowers CW (1988) Vitronectin regulates smooth muscle contractility via alphav and beta1 integrin. J Cell Sci 111(9):1175-83.

Dahmane N, Ruiz I, Altaba A (1999) Sonic hedgehog regulates the growth and patterning of the cerebellum. Development 126:3089-100.

Dahme M, Bartsch U, Martini R, Anliker B, Schachner M, Mantei N (1997) Disruption of the mouse L1 gene leads to malformations of the nervous system. Nat Genet 17:346-349.

Demyanenko GP, Schachner M, Anton E, Schmid R, Feng G, Sanes J, Maness PF (2004) Close homolog of l1 modulates area-specific neuronal positioning and dendrite orientation in the cerebral cortex. Neuron 44:423-437.

Dijkhuizen T, van Essen T, van der Vlies P, Verheij JB, Sikkema-Raddatz B, van der Veen AY, Gerssen-Schoorl KB, Buys CH, Kok K (2006) FISH and array-CGH analysis of a complex

chromosome 3 aberration suggests that loss of CNTN4 and CRBN contributes to mental retardation in 3pter deletions. Am J Med Genet A 140:2482-2487.

Eagleson KL, Gravielle MC, Schlueter McFadyen-Ketchum LJ, Russek SJ, Farb DH, Levitt P (2010) Genetic disruption of the autism spectrum disorder risk gene PLAUR induces GABAA receptor subunit changes. Neuroscience 168:797-810.

Echelard Y, Epstein DJ, St-Jacques B, Shen L, Mohler J, McMahon JA, McMahon AP (1993) Sonic hedgehog, a member of a family of putative signaling molecules, is implicated in the regulation of CNS polarity. Cell 75:1417-1430.

Ellis V, Behrendt N, Dano K (1991) Plasminogen activation by receptor-bound urokinase. A kinetic study with both cell-associated and isolated receptor. J Biol Chem 266:12752-12758.

Espinosa JS, Luo L (2008) Timing neurogenesis and differentiation: insights from quantitative clonal analyses of cerebellar granule cells. J Neurosci 28(10):2301–2312.

Felding-Habermann B, Cheresh DA (1993) Vitronectin and its receptors. Curr Opin Cell Biol 5(5):864-8.

Fischer G, Kunemund V, and Schachner M (1986) Neurite outgrowth in cerebellar microexplant cultures are affected by antibodies to the cell surface glycoprotein L1. J Neurosci 6: 605–612

Fombonne J, Bissey PA, Guix C, Sadoul R, Thibert C, Mehlen P (2012) Patched dependence receptor triggers apoptosis through ubiquitination of caspase-9. Proc Natl Acad Sci USA 109:10510-10515.

Fransen E, Lemmon V, Van Camp G, Vits L, Coucke P, Willems PJ (1995) CRASH syndrome: clinical spectrum of corpus callosum hypoplasia, retardation, adducted thumbs, spastic paraparesis and hydrocephalus due to mutations in one single gene, L1. Eur J Hum Genet 3:273-284.

Fredriksson S, Gullberg M, Jarvius J, Olsson C, Pietras K, Gustafsdottir SM, Östman A, and Landegren U (2002) Protein detection using proximity-dependent DNA ligation assays. Nat Biotechnol 20: 473-77.

Frints SG, Marynen P, Hartmann D, Fryns JP, Steyaert J, Schachner M, Rolf B, Craessaerts K, Snellinx A, Hollanders K, D'Hooge R, De Deyn PP, Froyen G (2003) CALL interrupted in a patient with non-specific mental retardation: gene dosage-dependent alteration of murine brain development and behavior. Hum Mol Genet 12:1463-1474.

Frotscher M (1998) Cajal-Retzius cells, Reelin, and the formation of layers. Curr Opin Neurobiol 8(5):570-5.

Gebhart AL, Petersen SE, Thach WT (2002) Role of the posterolateral cerebellum in language. Ann NY Acad Sci 978:318–333.

Gil JE, Woo DH, Shim JH, Kim SE, You HJ, Park SH, Paek SH, Kim SK, Kim JH (2009) Vitronectin promotes oligodendrocyte differentiation during neurogenesis of human embryonic stem cells. FEBS Lett 583(3):561-7.

Gilman S, Bloedel J, Lechtenberg R (1981) The symptoms and signs of cerebellar disease. In Disorders of the Cerebellum. Gilman S, Bloedel J, Lechtenberg R, Eds:189-221. Philadelphia F.A. Davis.

Gogolla N, Galimberti I, DePaola V, Caroni P (2006) Staining protocol for organotypic hippocampal slice cultures. Nat Protoc 1:2452–2456.

Goodrich LV, Johnson R L, Milenkovic L, McMahon JA, Scott MP (1996) Conservation of the hedgehog /patched signaling pathway from flies to mice: induction of a mouse patched gene by Hedgehog. Genes Dev. 10, 301-312

Goodrich LV, Milenković L, Higgins KM, Scott MP (1997) Altered neural cell fates and medulloblastoma in mouse patched mutants. Science 277:1109-1113.

Gould BB (1979) The organization of afferents to the cerebellar cortex in the cat: projections from the deep cerebellar nuclei. J Comp Neurol 184:27-42.

Gould BB (1980) Organization of afferents from the brain stem nuclei to the cerebellar cortex in the cat. Adv Anat Embryol Cell Biol 62:1-90.

Grumet M, Mauro V, Burgoon MP, Edelman GM, Cunningham BA (1991) Structure of a new nervous system glycoprotein, Nr-CAM, and its relationship to subgroups of neural cell adhesion molecules. J Cell Biol 113:1399-1412.

Grüsser-Cornehls U, Bäurle J (2001) Mutant mice as a model for cerebellar ataxia. Prog Neurobiol 63(5):489-540.

Gundersen HJ (1986) Stereology of arbitrary particles. A review of unbiased number and size estimators and the presentation of some new ones, in memory of William R. Thompson. J Microsc 143 (Pt 1): 3–45.

Gupta SK, Meiri KF, Mahfooz K, Bharti U, Mani S (2010) Coordination between extrinsic extracellular matrix cues and intrinsic responses to orient the centrosome in polarizing cerebellar granule neurons. J Neurosci 30(7):2755-66.

Hack I, Bancila M, Loulier K, Carroll P, Cremer H (2002) Reelin is a detachment signal in tangential chain-migration during postnatal neurogenesis. Nat Neurosci 5(10):939-45.

Hall H, Liu L, Schachner M and Schmitz B (1993) The L2/HNK-I carbohydrate mediates adhesion of neural cells to laminin. Eul J Neurosci 5:34-42.

Harwell CC, Parker PR, Gee SM, Okada A, McConnell SK, Kreitzer AC, Kriegstein AR (2012) Sonic hedgehog expression in corticofugal projection neurons directs cortical microcircuit formation. Neuron 73(6):1116-26.

Hashimoto M, Hibi M (2012) Development and evolution of cerebellar neural circuits. Dev Growth Differ 54(3):373-89.

Hatten ME, Roussel MF (2011) Development and cancer of the cerebellum. Trends Neurosci 34:134-42.

Hatten ME (1999) Central nervous system neuronal migration. Annu Rev Neurosci 22:511-39.

Higgins JJ, Rosen DR, Loveless JM, Clyman JC, Grau MJ (2000) A gene for nonsyndromic mental retardation maps to chromosome 3p25-pter. Neurology 55:335-340.

Hillenbrand R., Molthagen M., Montag D., Schachner M. (1999) The close homologue of the neural adhesion molecule L1 (CHL1): patterns of expression and promotion of neurite outgrowth by heterophilic interactions. Eur J Neurosci 11:813-826.

Hitt B, Riordan SM, Kukreja L, Eimer WA, Rajapaksha TW, Vassar R (2012) β-Site amyloid precursor protein (APP)-cleaving enzyme 1 (BACE1)-deficient mice exhibit a close homolog of L1 (CHL1) loss-of-function phenotype involving axon guidance defects. J Biol Chem 287(46):38408-25.

Holm J, Hillenbrand R, Steuber V, Bartsch U, Moos M, Lubbert H, Montag D, Schachner M (1996) Structural features of a close homologue of L1 (CHL1) in the mouse: a new member of the L1 family of neural recognition molecules. Eur J Neurosci 8:1613-1629.

Holmes G (1939) The cerebellum of man. Brain 62:1-30.

Huang X, Zhu LL, Zhao T, Wu LY, Wu KW, Schachner M, Xiao ZC, Fan M (2011) CHL1 negatively regulates the proliferation and neuronal differentiation of neural progenitor cells through activation of the ERK1/2 MAPK pathway. Mol Cell Neurosci 46:296-307.

Huang Y, Jellies J, Johansen KM, Johansen J (1997) Differential glycosylation of tractin and LeechCAM, two novel Ig superfamily members, regulates neurite extension and fascicle formation. J Cell Biol 138:143-157.

Huang ZJ, Di Cristo G, Ango F (2007) Development of GABA innervation in the cerebral and cerebellar cortices. Nat Rev Neurosci 8:673-686.

Hynes M, Ye W, Wang K, Stone D, Murone M, Sauvage F, Rosenthal A (2000) The seven-transmembrane receptor smoothened cell-autonomously induces multiple ventral cell types. Nat Neurosci 3:41-46.

Hynes RO (1992) Integrins: versatility, modulation, and signaling in cell adhesion. Cell 69: 11-25.

Ingham PW, McMahon AP (2001) Hedgehog signaling in animal development: paradigms and principles. Genes Dev 15(23):3059-87.

Irintchev A, Koch M, Needham LK, Maness P, Schachner M (2004) Impairment of sensorimotor gating in mice deficient in the cell adhesion molecule L1 or its close homologue, CHL1. Brain Res 1029:131-134.

Ito M (2008) Control of mental activities by internal models in the cerebellum. Nat Rev Neurosci 9:304–313.

Iyer AM, Zurolo E, Boer K, Baayen JC, Giangaspero F, Arcella A, Di Gennaro GC, Esposito V, Spliet WG, van Rijen PC, Troost D, Gorter JA, Aronica E (2010) Tissue plasminogen activator and urokinase plasminogen activator in human epileptogenic pathologies. Neuroscience 167:929-945.

Jaffe AB and Hall A (2005) Rho GTPases: Biochemistry and Biology. Annu Rev Cell Dev Biol 21:247–69.

Jakovcevski I, Siering J, Hargus G, Karl N, Hoelters L, Djogo N, Yin S, Zecevic N, Schachner M, Irintchev A (2009) Close homologue of adhesion molecule L1 promotes survival of Purkinje and granule cells and granule cell migration during murine cerebellar development. J Comp Neurol 513: 496-510.

Jakovcevski I, Wu J, Karl N, Leshchyns'ka I, Sytnyk V, Chen J, Irintchev A, Schachner M (2007) Glial scar expression of CHL1, the close homolog of the adhesion molecule L1, limits recovery after spinal cord injury. J Neurosci 27:7222-7233.

Jankowski J, Miething A, Schilling K, Baader SL (2009) Physiological Purkinje cell death is spatiotemporally organized in the developing mouse cerebellum. Cerebellum 8: 277-290.

Jenkins D (2009) Hedgehog signalling: emerging evidence for non-canonical pathways. Cell Signal 21:1023-1034.

Jensen AM, Wallace VA (1997) Expression of Sonic hedgehog and its putative role as a precursor cell mitogen in the developing mouse retina. Development 124:363-371.

Jensen PH (1997) Structure and function of plasminogen activator inhibitor-2: An intracellular serine proteinase inhibitor modulating apoptosis. Int J Oncol 11:557-570.

Jessell T (2000) Neuronal specification in the spinal cord: In ductive signals and transcriptional codes. Nat Rev Genet 1:20-29.

Jessell TM (1988) Adhesion molecules and the hierarchy of neural development. Neuron 1988 1(1):3-13.

Johnson RL, Rothman AL, Xie J, Goodrich LV, Bare JW, Bonifas JM, Quinn AG, Myers RM, Cox DR, Epstein EH Jr, Scott MP (1996) Human homolog of patched, a candidate gene for the basal cell nevus syndrome. Science 272(5268):1668-71.

Kamiguchi H, Hlavin ML, Lemmon V (1998) Role of L1 in neural development: what the knockouts tell us. Mol Cell Neurosci 12:48-55.

Kamiguchi H, Lemmon V (1997) Neural cell adhesion molecule L1: signaling pathways and growth cone motility. J Neurosci Res 49:1-8.

Kanse SM, Kost C, Wilhelm OG, Andreasen PA, Preissner KT (1996) The urokinase receptor is a major vitronectin-binding protein on endothelial cells. Exp Cell Res 224(2):344-53.

Kasai K, Takahashi M, Osumi N, Sinnarajah S, Takeo T, Ikeda H, Kehrl JH, Itoh G, Arnheiter H (2004) The G12 family of heterotrimeric G proteins and Rho GTPase mediate Sonic hedgehog signalling. Genes Cells 9:49-58.

Katic J, Loers G, Kleene R, Karl N, Schmidt C, Buck F, Zmijewski JW, Jakovcevski I, Preissner KT, Schachner M (2014) Interaction of the Cell Adhesion Molecule CHL1 with Vitronectin, Integrins, and the Plasminogen Activator Inhibitor-2 Promotes CHL1-Induced Neurite Outgrowth and Neuronal Migration. J Neurosci 34(44):14606-14623.

Kemler R, Ozawa M (1989) Uvomorulin-catenin complex: cytoplasmic anchorage of a Ca2+-dependent cell adhesion molecule. Bioessays 11:88-91.

Kjoller L, Hall A (2001) Rac mediates cytoskeletal rearrangements and increased cell motility induced by urokinase-type plasminogen activator receptor binding to vitronectin. J Cell Biol 152:1145-1158.

Kleene R, Chaudhary H, Karl N, Katic J, Kotarska A, Guitart K, Loers G, Schachner M (2015) Interaction between CHL1 and serotonin receptor 2c regulates signal transduction and behavior in mice. J Cell Sci 128(24):4642-52.

Kolata S, Wu J, Light K, Schachner M, Matzel LD (2008) Impaired working memory duration but normal learning abilities found in mice that are conditionally deficient in the close homolog of L1. J Neurosci 28:13505-13510.

Kunemund V, Jungalwala FB, Fischer G, Chou DKH, Keilhauer, G. and Schachner, M. (1988) The L2/HNK-I carbohydrate of neural cell adhesion molecules is involved in cell interactions. J Cell Biol 106:213-223.

Kyrylkova K, Kyryachenko S, Leid M, Kiossi C (2012) Detection of apoptosis by TUNEL assay. Methods Mol Biol 887:41-7.

Lahtinen L, Huusko N, Myöhänen H, Lehtivarjo AK, Pellinen R, Turunen MP, Ylä-Herttuala S, Pirinen E, Pitkänen A (2009) Expression of urokinase-type plasminogen activator receptor is increased during epileptogenesis in the rat hippocampus. Neuroscience 163:316-328.

Lemkey-Johnston N, Larramendi LM (1968) Types and distribution of synapses upon basket and stellate cells of the mouse cerebellum: an electron microscopic study. J Comp Neurol 134:73-112.

Leshchyns'ka I, Sytnyk V, Richter M, Andreyeva A, Puchkov D, Schachner M (2006) The adhesion molecule CHL1 regulates uncoating of clathrincoated synaptic vesicles. Neuron 52:1011-1025.

Leshchyns'ka I, Sytnyk V (2016) Reciprocal Interactions between Cell Adhesion Molecules of the Immunoglobulin Superfamilyand the Cytoskeleton in Neurons. Front Cell Dev Biol 16;4:9.

Levitt P (2005) Disruption of interneuron development. Epilepsia 46 [Suppl 7]:22-28.

Lewis PM, Gritli-Linde A, Smeyne R, Kottmann A, McMahon AP (2004) Sonic hedgehog signaling is required for expansion of granule neuron precursors and patterning of the mouse cerebellum. Dev Biol 270:393-410.

Li F, Jiang Q, Shi KJ, Luo H, Yang Y, Xu CM (2013) RhoA modulates functional and physical interaction between ROCK1 and Erk1/2 in selenite-induced apoptosis of leukaemia cells .Cell Death and Disease 4:e708.

Liao JK, Seto M, Noma K (2007) Rho Kinase (ROCK) Inhibitors. J Cardiovasc Pharmacol 50(1): 17–24.

Lindner J, Rathjen FG, Schachner M (1983) L1 mono- and polyclonal antibodies modify cell migration in early postnatal mouse cerebellum. Nature 305:427-430.

Lipinski RJ, Bijlsma MF, Gipp JJ, Podhaizer DJ, Bushman W (2008) Establishment and characterization of immortalized Gli-null mouse embryonic fibroblast cell lines. BMC Cell Biol 9:49.

Liu B, Zhang B, Wang T, Liang QC, Jing XR, Zheng J, Wang C, Meng Q, Wang L, Wang W, Guo H, You Y, Zhang H, Gao GD (2010) Increased expression of urokinase-type plasminogen activator receptor in the frontal cortex of patients with intractable frontal lobe epilepsy. J Neurosci Res 88: 2747-2754.

Livak KJ and Schmittgen TD (2001) Analysis of Relative Gene Expression Data Using Real-Time Quantitative PCR and the 2-[Delta][Delta]CT Method. Methods 25(4):402–408.

Lobov S, Ranson M (2011) Molecular competition between plasminogen activator inhibitors type -1 and -2 for urokinase: implications for cellular proteolysis and adhesion in cancer. Cancer Lett 303:118-127.

Lobov S, Wilczynska M, Bergström F, Johansson LB, Ny T (2004) Structural bases of the redox-dependent conformational switch in the serpin PAI-2. J Mol Biol 344:1359-1368.

Lodish H, Berk A, Zipursky SL, et al. Molecular Cell Biology. 4th edition. New York: W. H. Freeman; 2000. Section 22.1, Cell-Cell Adhesion and Communication.

Lossi L, Mioletti S, Merighi A (2002) Synapse-independent and synapse-dependent apoptosis of cerebellar granule cells in postnatal rabbits occur at two subsequent but partly overlapping developmental stages. Neuroscience 112(3):509-23.

Lossi L, Zagzag D, Greco MA, Merighi A (1998) Apoptosis of undifferentiated progenitors and granule cell precursors in the postnatal human cerebellar cortex correlates with expression of BCL-2, ICE, and CPP32 proteins. J Comp Neurol 28;399(3):359-72.

Lum L, Yao S, Mozer B, Rovescalli A, Von Kessler D, Nirenberg M, Beachy PA (2003) Identifi cation of Hedgehog pathway components by RNAi in Drosophila cultured cells. Science 299:2039-2045.

Lüthi A, Laurent JP, Figurov A, Muller D, Schachner M (1994) Hippocampal long-term potentiation and neural cell adhesion molecules L1 and NCAM. Nature 372:777-779.

Makhina T, Loers G, Schulze C, Ueberle B, Schachner M, Kleene R (2009) Extracellular GAPDH binds to L1 and enhances neurite outgrowth. Mol Cell Neurosci 41:206 –218
Marín O, Rubenstein JL (2003) Cell migration in the forebrain. Annu Rev Neurosci 26:441-83.

Marshall GM, Carter DR, Cheung BB, Liu T, Mateos MK, Meyerowitz JG, Weiss WA (2014) The prenatal origins of cancer. Nat Rev Cancer 14(4):277-89.

Marti E, Bumcrot DA, Takada R, McMahon AP (1995) Requirement of 19K form of Sonic hedgehog for induction of distinct ventral cell types in CNS explants. Nature 375:322-325.

Martínez-Morales J, Barbas JA, Martí E, Bovolenta P, Edgar D, Rodríquez-Tébar A (1997) Vitronectin is expressed in the ventral region of the neural tube and promotes the differentiation of motor neurons. Development 24:5139-5147.

Marzban H, Sillitoe RV, Hoy M, Chung SH, Rafuse VF, Hawkes R (2004) Abnormal HNK-1 expression in the cerebellum of an N-CAM null mouse. J Neurocytol 33(1):117-30.

Matsushita M, Hosoya Y, Ikeda M (1979) Anatomical organization of the spinocerebellar system in the cat, as studied by retrograde transport of horseradish peroxidase. J Comp Neurol 184: 81-106.

Miale IL, Sidman RL (1961) An autoradiographic analysis of histogenesis in the mouse cerebellum. Expl Neurol 4:277-296.

Mille F, Thibert C, Fombonne J, Rama N, Guix C, Hayashi H, Corset V, Reed JC, Mehlen P (2009) The Patched dependence receptor triggers apoptosis through a DRAL-caspase-9 complex. Nat Cell Biol 11:739-746.

Montag-Sallaz M, Schachner M, Montag D (2002) Misguided axonal projections, neural cell adhesion molecule 180 mRNA upregulation, and altered behavior in mice deficient for the close homolog of L1. Mol Cell Biol 22:7967-7981.

Morag A, Pasmanik-Chor M, Oron-Karni V, Rehavi M, Stingl JC, Gurwitz D (2011) Genome-wide expression profiling of human lymphoblastoid cell lines identifies CHL1 as a putative SSRI antidepressant response biomarker. Pharmacogenomics 12:171-184.

Morellini F, Lepsveridze E, Kahler B, Dityatev A, Schachner M (2007) Reduced reactivity to novelty, impaired social behavior, and enhanced basal synaptic excitatory activity in perforant path projections to the dentate gyrus in young adult mice deficient in the neural cell adhesion molecule CHL1. Mol Cell Neurosci 34:121-136.

Murase S, Hayashi Y (1998) Concomitant expression of genes encoding integrin alpha v beta 5 heterodimer and vitronectin in growing parallel fibers of postnatal rat cerebellum: a possible role as mediators of parallel fiber elongation. J Comp Neurol 397(2):199-212.

Nagai N, Okada K, Kawao N, Ishida C, Ueshima S, Collen D, Matsuo O (2008) Urokinase-type plasminogen activator receptor (uPAR) augments brain damage in a murine model of ischemic stroke. Neurosci Lett 432:46-49.

Naus S, Richter M, Wildeboer D, Moss M, Schachner M, Bartsch JW (2004) Ectodomain shedding of the neural recognition molecule CHL1 by the metalloprotease-disintegrin ADAM8 promotes neurite outgrowth and suppresses neuronal cell death. J Biol Chem 279(16):16083-90.

Nikonenko AG, Sun M, Lepsveridze E, Apostolova I, Petrova I, Irintchev A, Dityatev A, Schachner M (2006) Enhanced perisomatic inhibition and impaired long-term potentiation in the CA1 region of juvenile CHL1- deficient mice. Eur J Neurosci 23:1839-1852.

Owensby DA, Morton PA, Wun TC, Schwartz ALwensby (1991) Binding of plasminogen activator inhibitor type-1 to extracellular matrix of Hep G2 cells. Evidence that the binding protein is vitronectin. J Biol Chem 266(7):4334-40.

Placzek M (1995) The role of the notochord and floor plate in inductive interactions. Curr. Opin Genet Dev 5:499-506.

Polizio AH, Chinchilla P, Chen X, Kim S, Manning DR, Riobo NA (2011a) Heterotrimeric Gi proteins link Hedgehog signaling to activation of Rho small GTPases to promote fibroblast migration. J Biol Chem 286:19589-19596.

Polizio AH, Chinchilla P, Chen X, Manning DR, Riobo NA (2011b) Sonic Hedgehog activates the GTPases Rac1 and RhoA in a Gli-independent manner through coupling of smoothened to Gi proteins. Sci Signal 4:pt7.

Pons S, Martí E (2000) Sonic hedgehog synergizes with the extracellular matrix protein vitronectin to induce spinal motor neuron differentiation. Development 127:333-342.

Pons S, Trejo JL, Martinez-Morales HR, Marti E (2001) Vitronectin regulates Sonic hedgehog activity during cerebellum development through CREB phosphorylation. Development 128: 1481-1492.

Powell EM, Campbell DB, Stanwood GD, Davis C, Noebels JL, Levitt P (2003) Genetic disruption of cortical interneuron development causes region- and GABA cell type-specific deficits, epilepsy, and behavioral dysfunction. J Neurosci 23:622-631.

Pratte M, Jamon M (2009) Impairment of novelty detection in mice targeted for the Chl1 gene. Physiol Behav 97:394-400.

Pratte M, Rougon G, Schachner M, Jamon M (2003) Mice deficient for the close homologue of the neural adhesion cell L1 (CHL1) display alterations in emotional reactivity and motor coordination. Behav Brain Res 147:31-39.

Prince JT, Alberti L, Healy PA, Nauman SJ, Stallcup WB (1991) Molecular cloning of NILE glycoprotein and evidence for its continued expression in mature rat CNS. J Neurosci Res 30:567-581.

Raff MC, Barres BA, Burne JF, Coles HSR, Ishizaki Y, Jacobson MD (1994) Programmed cell death and the control of cell survival. Phil. Trans. R. Soc. London Ser. B 345:265-268.

Rakic P (1971) Neuron-glia relationship during granule cell migration in developing cerebellar cortex. A Golgi and electronmicroscopic study in Macacus Rhesus. J Comp Neurol 141:283-312.

Rathjen FG, Schachner M (1984) Immunocytological and biochemical characterization of a new neuronal cell surface component (L1 antigen) which is involved in cell adhesion. EMBO J 3:1-10.

Reichardt LF, Tomaselli KJ (1991) Extracellular matrix molecules and their receptors: functions in neural development. Annu Rev Neurosci 14:531-570.

Riobo NA, Saucy B, Dilizio C, Manning DR (2006) Activation of heterotrimeric G proteins by Smoothened. Proc Natl Acad Sci USA 103:12607-12612.

Robbins DJ, Fei DL, Riobo NA (2012) The Hedgehog signal transduction network. Sci Signal 5:re6.

Roelink H, Porter JA, Chiang C, Tanabe Y, Chang DT, Beachy PA, Jessell TM (1995) Floor plate and motor neuron induction by different concentrations of the amino-terminal cleavage product of sonic hedgehog autoproteolysis. Cell 81:445-455.

Rominger CM, Bee WL, Copeland RA, Davenport EA, Gilmartin A, Gontarek R, Hornberger KR, Kallal LA, Lai Z, Lawrie K, Lu Q, McMillan L, Truong M, Tummino PJ, Turunen B, Will M, Zuercher WJ, Rominger DH (2009) Evidence for allosteric interactions of antagonist binding to the smoothened receptor. J Pharmacol Exp Ther 329:995-1005.

Ruiz i Altaba A, Sánchez P, Dahmane N (2002) Gli and hedgehog in cancer: tumours, embryos and stem cells. Nat Rev Cancer 2(5):361-72.

Saghatelyan A, de Chevigny A, Schachner M, Lledo PM (2004) Tenascin-R mediates activity-dependent recruitment of neuroblasts in the adult mouse forebrain. Nat Neurosci 7(4):347-56.

Sakurai K, Migita O, Toru M, Arinami T (2002) An association between a missense polymorphism in the close homologue of L1 (CHL1, CALL) gene and schizophrenia. Mol Psychiatry 7:412-415.

Sakurai T, Lustig M, Babiarz J, Furley AJ, Tait S, Brophy PJ, Brown SA, Brown LY, Mason CA, Grumet M (2001) Overlapping functions of the cell adhesion molecules Nr-CAM and L1 in cerebellar granule cell development. J Cell Biol 154:1259-1273.

Salyakina D, Cukier HN, Lee JM, Sacharow S, Nations LD, Ma D, Jaworski JM, Konidari I, Whitehead PL, Wright HH, Abramson RK, Williams SM, Menon R, Haines JL, Gilbert JR, Cuccaro ML, Pericak-Vance MA (2011) Copy number variants in extended autism spectrum disorder families reveal candidates potentially involved in autism risk. PLoS One 6:e26049.

Sambrook J, Fritsch EF, Maniatis T (1989) Molecular Cloning: A Laboratory Manual. New York: Cold Spring Harbor Laboratory Cold Spring Harbor.

Sanes JR (1989) Extracellular matrix molecules that influence neural development. Annu Rev Neurosci 12:491-516.

Sanes JR, Yamagata M (1999) Formation of lamina-specific synaptic connections. Curr Opin Neurobiol 9:79-87.

Schmalbach B, Lepsveridze E, Djogo N, Papashvili G, Kuang F, Leshchyns'ka I, Sytnyk V, Nikonenko AG, Dityatev A, Jakovcevski I,Schachner M (2015) Age-dependent loss of parvalbumin-expressing hippocampal interneurons in mice deficient in CHL1, a mental retardation and schizophrenia susceptibility gene. J Neurochem 135(4):830-44.

Schnitzer J and Schachner M (1981) Developmental expression of cell type-specific markers in mouse cerebellar cells in vitro. J Neuroimmunol 1:471-487.

Scholey AB., Mileusnic R, Schachner M, Rose SP (1995) A role for a chicken homolog of the neural cell adhesion molecule L1 in consolidation of memory for a passive avoidance task in the chick. Learn Mem 2:17-25.

Seiffert D, Iruela-Arispe ML, Sage EH, Loskutoff DJ (1995) Distribution of vitronectin mRNA during murine development. Dev.Dyn 203:71-79.

Shanga X, Marchionia F, Evelyna CR, Sipesa N, Zhoua X, Seibelb W, Wortmanb M , Zhenga Y (2013) Small-molecule inhibitors targeting G-protein–coupled Rho guanine nucleotide exchange factors. PNAS 8:3155–3160

Sharon R, Abramovitz R, Miskin R (2002) Plasminogen mRNA induction in the mouse brain after kainate excitation: codistribution with plasminogen activator inhibitor-2 (PAI-2) mRNA. Brain Res Mol Brain Res 104:170-175.

Shen F, Cheng L, Douglas AE, Riobo NA, Manning DR (2013) Smoothened is a fully competent activator of the heterotrimeric G protein G(i). Mol Pharmacol 83:691-697.

Shoukier M, Fuchs S, Schwaibold E, Lingen M, Ga ¨rtner J, Brockmann K, Zirn B (2013) Microduplication of 3p26.3 in nonsyndromic intellectual disability indicates an important role of CHL1 for normal cognitive function. Neuropediatrics 44:268-271.

Silverman GA, Bird PI, Carrell RW, Church FC, Coughlin PB, Gettins PG et al. (2001) The serpins are an expanding superfamily of structurally similar but functionally diverse proteins. Evolution, mechanism of inhibition, novel functions, and a revised nomenclature. J Biol Chem 276:33293-33296.

Smith HW, Marshall CJ (2010) Regulation of cell signaling by uPAR. Nat Rev Mol Cell Biol 11:23–36.

Sotelo C (2004) Cellular and genetic regulation of the development of the cerebellar system. Prog Neurobiol 72:295–339.

Stanton BZ, Peng LF (2010) Small-molecule modulators of the Sonic Hedgehog signaling pathway. Mol Biosyst 6:44-54.

Stone DM, Hynes M, Armanini M, Swanson TA, Gu Q, Johnson RL, et al.: The tumour-suppressor gene patched encodes a candidate receptor for Sonic hedgehog. Nature 1996, 384:129-134

Stoppini L, Buchs PA, Muller D (1991) A simple method for organotypic cultures of nervous tissue. J Neurosci Methods 37:173–182.

Street CA, Bryan BA (2011) Rho kinase proteins - pleiotropic modulators of cell survival and apoptosis. Anticancer Res 31:3645-3657.

Sugihara I (2006) Organization and remodeling of the olivocerebellar climbing fiber projection. Cerebellum 5:15-22.

Swanson DJ, Tong Y, Goldowitz D (2005) Disruption of cerebellar granule cell development in the Pax6 mutant, Sey mouse. Brain Res Dev Brain Res 160(2):176-193.

Takeichi M (1991) Cadherin cell adhesion receptors as a morphogenetic regulator. Science 251:1451-1455.

Tam GW, van de Lagemaat LN, Redon R, Strathdee KE, Croning MD, Malloy MP, Muir WJ, Pickard BS, Deary IJ, Blackwood DH, Carter NP, Grant SG (2010) Confirmed rare copy number variants implicate novel genes in schizophrenia. Biochem Soc Trans 38:445-451.

Tenzen T, Allen BL, Cole F, Kang JS, Krauss RS, McMahon AP (2006) The cell surface membrane proteins Cdo and Boc are components and targets of the Hedgehog signaling pathway and feedback network in mice. Dev Cell 10:647-656.

Thibert C, Teillet MA, Lapointe F, Mazelin L, Le Douarin NM, Mehlen P (2003) Inhibition of neuroepithelial patched-induced apoptosis by sonic hedgehog. Science 301:843-846.

Tomasini BR, Mosher DF (1988) Conformational states of vitronectin: preferential expression of an antigenic epitope when vitronectin is covalently and noncovalently complexed with thrombin-antithrombin III or treated with urea. Blood 72(3):903-12.

Tongiorgi E, Bernhardt RR, Schachner M (1995) Zebrafish neurons express two L1-related molecules during early axonogenesis. J Neurosci Res 42:547-561.

Traiffort E, Charytoniuk D, Watroba L, Faure H, Sales N, Ruat M (1999) Discrete localizations of hedgehog signalling components in the developing and adult rat nervous system. Eur J Neurosci 11:3199-214.

Traiffort E, Charytoniuk DA, Faure H, Ruat M (1998) Regional distribution of Sonic Hedgehog, patched, and smoothened mRNA in the adult rat brain. J Neurochem 70:1327-30.

Trifilieff P, Rives M, Urizar E, Piskorowski RA, Vishwasrao HD, Castrillon J, Schmauss C, Slättman M, Gullberg M, Javitch JA (2011) Detection of antigen interactions ex vivo by proximity ligation assay: endogenous dopamine D2-adenosine A2A receptor complexes in the striatum. BioTechniques 50:111-118.

Tsai NP, Wei LN (2010) RhoA/ROCK1 signaling regulates stress granule formation and apoptosis. Cell Signal 22(4):668-75.

Vaillant C, Monard D (2009) SHH pathway and cerebellar development. Cerebellum. 8:291-301.

Varjosalo M, Taipale J (2008) Hedgehog: functions and mechanisms. Genes Dev 22:2454-72.

Vetter IR, Wittinghofer A (2001) The guanine nucleotide-binding switch in three dimensions. Science 294(5545):1299-304.

Volkmer H, Hassel B, Wolff JM, Frank R, Rathjen FG (1992) Structure of the axonal surface recognition molecule neurofascin and its relationship to a neural subgroup of the immunoglobulin superfamily. J Cell Biol 118:149-161.

von Heijne G, Liljestro P, Mikus P, Andersson H, Ny TJ (1991) The efficiency of the uncleaved secretion signal in the plasminogen activator inhibitor type 2 protein can be enhanced by point mutations that increase its hydrophobicity. J Biol Chem 266:15240-15243.

Wallace VA (1999) Purkinje-cell-derived Sonic hedgehog regulates granule neuron precursor cell proliferation in the developing mouse cerebellum. Curr Biol 9:445-8.

Walsh FS, Doherty P (1997) Neural cell adhesion molecules of the immunoglobulin superfamily: role in axon growth and guidance. Annu Rev Cell Dev Biol 13:425-456.

Washbourne P, Dityatev A, Scheiffele P, Biederer T, Weiner JA, Christopherson KS, El-Husseini A (2004) Cell adhesion molecules in synapse formation. J Neurosci 42:9244-9249.

Wei MH, Karavanova I, Ivanov SV, Popescu NC, Keck CL, Pack S, Eisen JA, Lerman MI (1998) In silico-initiated cloning and molecular characterization of a novel human member of the L1 gene family of neural cell adhesion molecules. Hum Genet 103:355-364.

Weisheit G, Gliem M, Endl E, Pfeffer PL, Busslinger M, Schilling K (2006) Postnatal development of the murine cerebellar cortex: formation and early dispersal of basket, stellate and Golgi neurons. Eur J Neurosci 24(2):466-78.

Williams AF, Barclay AN (1988) The immunoglobulin superfamily--domains for cell surface recognition. Annu Rev Immunol 6:381-405.

Wingate RJ (2001) The rhombic lip and early cerebellar development. Curr Opin Neurobiol 11:82–88.

Wood KA, DipasqualeB, Youle RJ (1993) In situ labeling of granule cells for apoptosis-associated DNA fragmentation reveals different mechanisms of cell loss in developing cerebellum. Neuron 11:621-632.

Wright AG, Demyanenko GP, Powell A, Schachner M, Enriquez-Barreto L, Tran TS, Polleux F, Maness PF (2007) Close homolog of L1 and neuropilin 1 mediate guidance of thalamocortical axons at the ventral telencephalon. J Neurosci 27:13667-13679.

Yam PT, Langlois SD, Morin S, Charron F (2009) Sonic hedgehog guides axons through a noncanonical, Src-family-kinase-dependent signaling pathway. Neuron 62:349-362.

Yamagata M, Sanes JR, Weiner JA (2003). Synaptic adhesion molecules. Curr Opin Cell Biol 5:621-632.

Yamanaka H, Yanagawa Y, Obata K (2004) Development of stellate and basket cells and their apoptosis in mouse cerebellar cortex. Neurosci Res 50:13-22.

Yamasaki T, Kawaji K, Ono K, Bito H, Hirano T, Osumi N, Kengaku M (2001) Pax6 regulates granule cell polarization during parallel fiber formation in the developing cerebellum. Development 128:3133-3144.

Ye S, Goldsmith EJ (2001) Serpins and other covalent protease inhibitors. Curr Opin Struct Biol 11:740-745.

Zhang SJ, Zou M, Lu L, Lau D, Ditzel DA, Delucinge-Vivier C, Aso Y, Descombes P, Bading H (2009) Nuclear calcium signaling controls expression of a large gene pool: identification of a gene program for acquired neuroprotection induced by synaptic activity. PLoS Genet 5(8):e1000604.

Zhang Y, Roslan R, Lang D, Schachner M, Lieberman AR, Anderson PN (2000) Expression of CHL1 and L1 by neurons and glia following sciatic nerve and dorsal root injury. Mol Cell Neurosci 16:71-86.

Zheng X, Mann RK, Sever N, Beachy PA (2010) Genetic and biochemical definition of the Hedgehog receptor. Genes Dev 24:57-71.

Zhou L, Barão S, Laga M, Bockstael K, Borgers M, Gijsen H, Annaert W, Moechars D, Mercken M, Gevaert K, De Strooper B (2012) The neural cell adhesion molecules L1 and CHL1 are cleaved by BACE1 protease in vivo. J Biol Chem 287(31):25927-40.

Zmuda JF and Rivas RJ (1998) The Golgi apparatus and the centrosome are localized to the sites of newly emerging axons in cerebellar granule neurons in vitro. Cell Motil Cytoskeleton 41:18-38.

8 ABSTRACT

Cell adhesion molecules of the immunoglobulin superfamily are expressed in a well-coordinated temporospatial pattern during nervous system development and are important for cerebellar histogenesis and formation of specific synaptic contacts. The close homologue of L1 (CHL1) is a member of the immunoglobulin superfamily and is abundantly expressed both in the developing and in the adult cerebellum. It is required for normal cerebellar cytoarchitecture and constitutive ablation of CHL1 in mice causes impaired cerebellar development. Stellate axons and Purkinje cell dendrites from CHL1-deficient mice show aberrant branching and reduced synapse formation which leads to progressive atrophy of axon terminals and loss of Purkinje cells during the first postnatal week. Moreover, granule cell migration seems to be impaired leading to the accumulation of this cells within the molecular layer of 7-day-old CHL1-deficient mice. Significant loss of Purkinje and granule cells has been reported in the adult CHL1-deficient mice suggesting that CHL1-ablation during development has consequences in the adult cerebellum. Therefore, it is of great interest to identify CHL1 interaction partners and mechanisms involved in granule and Purkinje cell development.

In previous experiments the extracellular matrix molecule vitronectin was identified as novel binding partner of CHL1 using biochemical cross-linking, while the plasminogen activator inhibitor-2 (PAI-2) and patched, a receptor for hedgehog morphogens, were identified as novel binding partners of CHL1 using phage display. In this study binding of vitronectin, PAI-2 and patched to CHL1 was verified by co-immunoprecipitation, ELISA and label-free binding assay. The co-localization of these proteins was confirmed in histological sections of postnatal cerebellum using immunohistochemistry and proximity ligation assay. Vitronectin and PAI-2 proved to bind to the extracellular part of CHL1 and induce neurite outgrowth and cell migration in cultures of cerebellar neurons. A PAI-2-derived peptide, antibodies against vitronectin, PAI-2, urokinase type plasminogen activator (uPA) and uPA receptor reduced granule cell migration. Interestingly, in 5-day-old mice interaction of vitronectin and CHL1 led to reduced proliferation and delayed differentiation of granule cell precursors, while their mutual interaction enhanced radial migration of granule cells two days later. Moreover, the *trans*-interaction of CHL1 with patched promoted neuritogenesis as well as neuronal migration and survival in cultures of cerebellar neurons. A sequence stretch in the extracellular CHL1 domain showing similarity to sonic hedgehog sequences mediated the binding of CHL1 to the first extracellular loop of patched. Patched- and CHL1-derived peptides, patched antibodies, the smoothened inhibitor SANT-1 and inhibitors of RhoA and Rho-associated kinase (ROCK) reduced CHL1-triggered neuritogenesis, migration and survival in cultures of dissociated cerebellar neurons. Inhibitors of smoothened, RhoA and ROCK prevented CHL1-triggered survival of cerebellar granule and Purkinje cells in organotypic cerebellar cultures. In histological sections from 10-

and 14-day-old CHL1-deficient mice enhanced apoptosis of granule cells from the internal granule layer, but not of Purkinje cells, was observed, indicating that CHL1 regulates apoptosis of granule cells during the second postnatal week.

In the present thesis novel binding partners of CHL1 and pathways that contribute to morphogenesis during postnatal cerebellar development were identified and characterized. Furthermore, I showed that CHL1 regulates proliferation and differentiation of granule cell precursors and that CHL1 induces neuritogenesis and migration of granule cells during the first postnatal week by binding to vitronectin, PAI-2 and patched. CHL1-ablation induces retarded migration of granule cells and their accumulation in the molecular layer. Additionally, CHL1 activates RhoA and RhoA-associated kinase via patched and smoothened-dependent signal transduction pathways. Triggering of these pathways contributes to the granule cell survival during the second postnatal week. CHL1-ablation induces apoptosis of granule cells from the internal granule layer during development, which consequentially leads to granule cell loss in the adult CHL1-deficient cerebellum. CHL1 and its novel interaction partners stongly influence the development of the cerebellar cortex cytoarchitecture by regulating different developmental stages of cerebellar neurons within a well-defined time window.

9 ZUSAMMENFASSUNG

Zelladhäsionsmoleküle der Immunglobulin-Superfamilie spielen eine wichtige Rolle während der Entwicklung des Nervensystems und werden in gut organisierten temporospatialen Muster exprimiert. Sie spielen eine wichtige Rolle bei der Entwicklung des Kleinhirns und der Bildung synaptischer Kontakte. Ein Mitglied der Immunglobulin-Superfamilie und enger Verwandter des Zelladhäsionsmoleküls L1, ist das Zelladhäsionsmolekül CHL1 (close homologue of L1), welches in vielen verschiedenen Zellen während der Entwicklung und im adulten Kleinhirn exprimiert wird. Da CHL1 eine wichtige Funktion beim Aufbau und der Ausbildung der Architektur des Kleinhirns in Mäusen übernimmt, wirkt sich die Entfernung von CHL1 störend auf die Gehirnentwicklung aus. Die Axone der Sternzellen und Dendriten der Purkinje-Zellen CHL1-defizienter Mäuse weisen ein abnormales Verzweigungsmuster und eine reduzierte Synapsen-Bildung auf, was zu einer progressiven Atrophie der Axonendigungen und nachfolgend zum Absterben von Purkinje-Zellen wärend der ersten postnatalen Woche führt. Außerdem scheint die Zellmigration der Körnerzellen von sieben Tage alten CHL1-defizienten Mäusen beeinträchtigt zu sein, was eine Akkumulation der Zellen in der Molekularschicht zur Folge hat. Das signifikante Absterben der Purkinje-Zellen in adulten CHL1-defizienten Mäusen wird als Konsequenz der Ablation von CHL1 während der Entwicklung des Kleinhirns gesehen. Aus diesem Grund ist es von großem Interesse neue Interaktionspartner von CHL1 zu finden und die Mechanismen, welche bei der Entwicklung von Körnerzellen und Purkinje- Zellen eine Rolle spielen, zu erforschen. In vorausgegangenen biochemischen cross-linking Experimenten konnte das Transmembranprotein Vitronektin als neuartiger Bindungspartner von CHL1 identifiziert werden. Weiterhin wurden der Plasminogen-Aktivator-Inhibitor (plasminogen activator inhibitor-2; PAI-2) und der Hedgehog Rezeptor patched mit Hilfe von phage-display als Interaktionspartner ermittelt.

In meiner Arbeit konnte ich die direkte Interaktion von CHL1 mit Vitronektin, PAI-2 und patched mittels Ko-Immunopräzipitation, im Enzyme Linked Immunosorbent Assay (ELISA) und Label Free Binding Assay verifizieren. Durch immunhistologische Experimente und Proximity Ligation Assay (PLA) an histologischen Schnitten von frühem postnatalen Kleinhirngewebe konnte die Ko-Lokalisation mit diesen Proteinen bestätigt werden. Ich konnte zeigen, dass Vitronektin und PAI-2 an den extrazellulären Teil von CHL1 binden und dass CHL1 durch Interaktion mit Vitronektin und PAI-2 das Neuritenwachstum und die Zellmigration von kultivierten Kleinhirnneuronen induziert. Darüber hinaus reduziert die Applikation eines PAI-2 abgeleiteten Peptids und von Antikörpern welche an Vitronektin, PAI-2, Urokinase-Typ Plasminogen Aktivator (uPA) oder uPA Rezeptor die Migration von Kleinhirnneuronen.

Interessanterweise führt die Interaktion von Vitronektin mit CHL1 zu einer reduzierten Proliferation und verzögerten Differenzierung von Vorläuferzellen der Körnerzellen, wobei die

radiale Migration der Körnerzellen zwei Tage später durch diese Interaktion erhöht wird. Zudem konnte in Kulturen von Kleinhirnneuronen gezeigt werden, dass die trans-Interaktion von CHL1 und patched sowohl die Neuritogenese als auch die Migration und das Überleben von Körnerzellen begünstigt. Die Bindung von CHL1 an die erste extrazelluläre Schleife von patched erfolgt durch eine extrazelluläre Aminosäuresequenz in CHL1 die einer Aminosäuresequenz von sonic hedgehog sehr stark ähnelt. Patched - oder von CHL1-abgeleitete Peptide, patched Antikörper, der smoothened Inhibitor SANT-1 sowie von RhoA- oder ROCK-Inhibitoren reduzieren die CHL1-vermittelte Neuritogenese, Migration sowie das Überleben von dissoziierten Körnerzellen in Kultur. In organotypischen Kulturen von Kleinhirnneuronen wird das CHL1-induzierte Zellüberleben von Körnerzellen und Purkinje-Zellen durch Zugabe von Inhibitoren gegen smoothened, RhoA und ROCK reduziert. Histologische Untersuchungen von 10 und 14 Tage alten CHL1-deffizienten Mäusen zeigten eine erhöhte Apoptose von Körnerzellen der internen Körnerzellschicht, jedoch konnte keine vermehrte Apoptose bei Purkinje-Zellen festgestellt werden. Diese Ergebnisse weisen auf eine regulatorische Funktion von CHL1 bei der Apoptose von Körnerzellen während der zweiten postnatalen Woche hin.

In dieser Forschungsstudie wurden neue Bindungspartner von CHL1 sowie Signalwege, die bei der Morphogenese während der postnatalen Entwicklung des Kleinhirns mitwirken, identifiziert und charakterisiert. Zudem konnte ich zeigen, dass die Proliferation und Differenzierung von Vorläuferzellen der Körnerzellen durch CHL1 reguliert werden. Die Bindung von CHL1 mit Vitronektin, PAI-2 und patched führt zu einer vermehrten Neuritogenese und Migration von Körnerzellen während der ersten postnatalen Woche. Außerdem führt die Abwesenheit von CHL1 zu einer verzögerten Migration von Körnerzellen und deren Akkumulation in der Molekularzellschicht. Weiterhin werden RhoA und die RhoA-assoziierte Kinase durch patched und smoothend anhängige Signalübertragungswege aktiviert. Durch das Einleiten dieser Signalwege wird das Zellüberleben in der zweiten postnatalen Woche gesteuert.

In adulten CHL1-defizienten Mäusen induziert die Abwesenheit von CHL1 während der Entwicklung die Apoptose von Körnerzellen aus der internen Körnerzellschicht des Kleinhirns, was folglich zum Verlust der Körnerzellen führt. Es wurde untersuchend belegt dass CHL1 und seine Bindungspartner einen definierten regulatorischen Effekt auf die verschiedenen Entwicklungsstadien von Kleinhirnneuronen und einen Einfluss auf die Zytoarchitektur der Großhirnrinde haben.

10 STATEMENT OF CONTRIBUTION

The first part of this work is published in The Journal of Neurocience as:

Katic J, Loers G, Kleene R, Karl N, Schmidt C, Buck F, Zmijewski JW, Jakovcevski I, Preissner KT, Schachner M (2014) Interaction of the Cell Adhesion Molecule CHL1 with Vitronectin, Integrins, and the Plasminogen Activator Inhibitor-2 Promotes CHL1-Induced Neurite Outgrowth and Neuronal Migration. J Neurosci 34(44):14606-14623.

Contributions of the authors to this work are indicated in the Chapter 5.1.

11 ACKNOWLEDGEMENTS

I first have to heartily thank Prof. Dr. Melitta Schachner for the great opportunity to write this thesis in her lab, for proposing and guiding me into interesting research projects, for all those fruitful discussions and support to finish and publish my work. It was a great privilege to be thought from one of the leading experts in the field. Moreover, I am grateful both to Prof. Dr. Melitta Schachner and Prof. Dr. Christian Lohr for agreeing to co-supervise this thesis.

I specially thank Dr. Ralf Kleene for his supervision during my entire work, for clear planning and insightful discussion of each step during the experiments described in this thesis. I am also grateful to Ralf for including me in other interesting projects and giving me the opportunity to learn so much. During the years of my PhD, he was always very supportive and patient with the best intention to teach me how to properly conduct my experiments and to write my thesis.

I am grateful to Dr. Gabriele Loers who helped me to learn different experimental techniques and who has always had a smart advice on how to overcome any problem that emerged in the everyday work. I have to thank her for creative suggestions during the writing which helped me to complete this thesis.

I would like to thank Dr. David Lutz, Dr. Alexander Drakew and Urban Maier for teaching me organotypic slice culture and being eager to share with me their knowledge and their useful advices. I am grateful to Dr. Lars Fester and Dr. Sabine Fleischer from the ZMNH PhD program for their support and interesting discussions we had.

Many thanks also go to the German Academic Exchange Service/ Deutscher Akademischer Austauschdienst DAAD that granted me with a one-year scholarship during my PhD studies.

My dear colleagues from Prof. Schachner's lab have been extremely supportive and helpful during all these years. Dear Nina, Kristina, Agnieszka, Jelena, Gaston and Mina, it was a great pleasure to work with you, thank you for your support and friendship. I am grateful to Jelena Tosic who helped me with stereological analysis, to Ute Bork for excellent technical assistance and to all the co-authors from the paper we published for their help and contribution.

Last but not least, my beloved parents, brother and boyfriend have been the power engine behind me. One "thank you" is not nearly enough to express my gratitude for all the support, love and courage you have been giving me. Mon Grand, ce n'aurait pas été possible sans toi.